THESIS

POLYSACCHARIDE-BASED NANOSTRUCTURES FOR GROWTH FACTOR

DELIVERY AND MESENCHYMAL STEM CELL ACTIVATION

Submitted by

Jorge Luis Almodóvar Montañez

Department of Chemical and Biological Engineering

In partial fulfillment of the requirements

For the Degree of Doctor of Philosophy

Colorado State University

Fort Collins, Colorado

Summer 2011

Doctoral Committee:

    Advisor: Matt J. Kipper

    Travis S. Bailey
    John D. Kisiday
    Ashok Prasad

ABSTRACT

POLYSACCHARIDE-BASED NANOSTRUCTURES FOR GROWTH FACTOR
DELIVERY AND MESENCHYMAL STEM CELL ACTIVATION

Mesenchymal stem cells (MSCs) are very promising in tissue engineering and regenerative medicine because of their ability to differentiate into different type of cells including bone and cartilage. MSCs differentiation can be modulated using both chemical (i.e. proteins) and physical cues (i.e. topography). This thesis presents work performed evaluating polysaccharide-based nanostructures for growth factor delivery and MSCs activation. Different polysaccharide-based nanostructures were developed and characterized including polyelectrolyte multilayers (PEMs) and electrospun nanofibers.

On flat gold-coated glass surfaces, PEMs were constructed using the polycations chitosan and *N,N,N*-trimethyl chitosan, and the polyanions hyaluronan, chondroitin sulfate, and heparin. An exhaustive spectroscopic study was performed on all of the PEMs pairs to investigate the effects of polyelectrolyte charge density on thickness, swelling, composition, and ion-pairing. The results demonstrated that hydrophilicity and swelling are reduced when one polyelectrolyte is strong and the other is weak, while ion pairing is increased. The stability of adsorbed proteins to PEMs was also investigated using IR spectroscopy.

Construction of PEMs and adsorption of basic fibroblast growth factor (FGF-2) was evaluated on heparin-chitosan PEMs constructed on gold-coated glass, tissue culture

polystyrene (TCPS), and titanium. In vitro testing of the FGF-2-loaded PEM constructed on TCPS and titanium was performed using ovine bone marrow-derived MSCs. It was noted that FGF-2 activity is enhanced, with regards to MSCs proliferation, when delivered from PEMs compared to delivery in solution.

Chitosan nanofibers were successfully electrospun from a trifluoroacetic acid and dichloromethane solution. A new technique was developed to modify electrospun chitosan nanofibers with polyelectrolyte multilayers using *N,N,N*-trimethyl chitosan and heparin. Controlled release of bioactive FGF-2, complexed with heparin-chitosan polyelectrolyte complex nanoparticles, from electrospun chitosan nanofiber mats was achieved with zero-order kinetics over a period of 27 days. When the nanofibers are further modified with a single PEM bilayer (PEM, composed of *N,N,N*-trimethyl chitosan and heparin), the release is completely prevented. The mitogenic activity of the released FGF-2 was also evaluated, with respect to the proliferation of ovine bone marrow-derived MSCs.

The effect on osteogenic differentiation of bone marrow-derived ovine and equine MSCs seeded on electrospun chitosan nanofibers versus flat TCPS was investigated. The effect of dexamethasone on osteogenic differentiation was also investigated. We found that we can successfully grow and maintain both equine and ovine MSCs on electrospun chitosan nanofibers. Also, both MSCs exhibit higher differentiation markers (alkaline phosphatase activity) when cultured on chitosan nanofibers compared to flat TCPS surfaces.

This work demonstrates new systems for stabilizing and controlling the delivery of heparin-binding growth factors for the activation of bone marrow-derived MSCs, using polysaccharide-based nanomaterials. These novel materials have potential applications in musculoskeletal tissue regeneration.

ACKNOWLEDGMENTS

As I reach the final stepping stone toward obtaining my graduate degree from Colorado State University (CSU) I wish to acknowledge the countless people who, in one way or another, were vital in this achievement.

First, I wish to acknowledge my advisor, Dr. Matt J. Kipper, for his outstanding role as an advisor, mentor, colleague, and friend. Throughout the years, we have had many insightful conversations and shared many experiences that have expanded my knowledge in research and science. I decided to attend CSU as a result of his inspiring work, and I am confident this decision was the best I ever made during my academic career. I am honored to be his student.

Thanks to my committee members Dr. John D. Kisiday, Dr. Travis S. Bailey, and Dr. Ashok Prasad. Dr. Kisiday and his former student Ben Hale for training me in cell culture techniques, and answering all my questions about cells. Dr. Bailey for all of his intuitive exchanges, and his availability to answer questions from polymers to MacBook issues. Dr. Prasad for stepping in as a last-minute committee member replacement.

I appreciate the help obtained from different staff and faculty members at CSU, who trained me in different techniques and instruments or allowed me to use their facilities. These include: Dr. Pat McCurdy and Dr. Sandeep Kohli from the Central Instrument Facility in the Department of Chemistry; Dr. Simon Turner and Kimberly Menges from the College of

TABLE OF CONTENTS

APPENDIX

Chapter 1

Introduction

1.1 Motivation

Musculoskeletal conditions are a major burden worldwide with diseases such as osteoarthritis which affect 9.6% of men and 18% of women of ages greater than 60.[1] Osteoarthritis is characterized by the loss of articular cartilage in synovial joints.[1] Articular cartilage has limitations for self repair because of its restricted amount of vascular supply and there is a limited supply of cells for repair.[2] Articular cartilage is one of the many tissues in need of biomaterials that will supply cells and the nutrients necessary for tissue repair.

Biomaterials for articular cartilage repair generally are polymeric with modifiable mechanical and chemical properties. Bulk properties of biomaterials for the regeneration of soft tissue should satisfy the requirements of being able to withstand mechanical load, degrade with appropriate kinetics, and not induce an immune response.[3] However, properties in smaller scales (micro- and nano-) are also crucial for tissue repair, having strong effects in cell attachment, alignment, recruitment, growth and differentiation.[4] Thus in the design of biomaterials for articular cartilage repair it is crucial to evaluate them from the macro- to the nano-scale. Tissue repair also requires biochemical cues for the recruitment, growth, and differentiation of cells. These chemical cues are generally available as cytokines and growth factors; however, biochemists can also isolate specific peptide sequences which

can be incorporated into biomaterials.[3] Lastly, cells are crucial in tissue repair, and biomaterials can be designed to recruit cells or could have cells incorporated in them.

Fundamental studies of material properties (from macro- to nano-scale), interactions between bio-molecules and materials, and cell-material interactions are necessary for the proper engineering of biomaterials. The combined effect of materials, biochemical cues, and cells along with proper engineering could lead to novel treatments in regenerative medicine.

1.2 Tissue Engineering

As mentioned in the motivation section above, tissue engineering of articular cartilage involves materials, cells, and biochemical cues. In this work polysaccharide-based nano materials will be evaluated as possible biomaterials for tissue engineering. The interactions between cells, materials, and growth factors will be studied. The three subsections below will provide a brief introduction on polysaccharides, mesenchymal stem cells, and growth factors used in this work.

1.2.1 Polysaccharides

Polysaccharides are carbohydrate polymers found in nature with a wide variety of biochemical and biomechanical functions. In mammalian tissue, many polysaccharides are assembled in complex nanostructures (e.g. aggrecan aggregate) giving biomedical engineers a template to develop biomimetic biomaterials.[5] In this work we engineered an array of biomaterials using the polysaccharides hyaluronic acid, chondroitin sulfate, heparin, chitosan and *N,N,N*-trimethyl chitosan. Their chemical structures are presented in Figure 1.1 and a brief overview of each follows in the next few paragraphs. An excellent review, by Boddohi and Kipper, in the engineering of nanoassemblies of polysaccharides is recommended for more information about polysaccharides.[5]

2
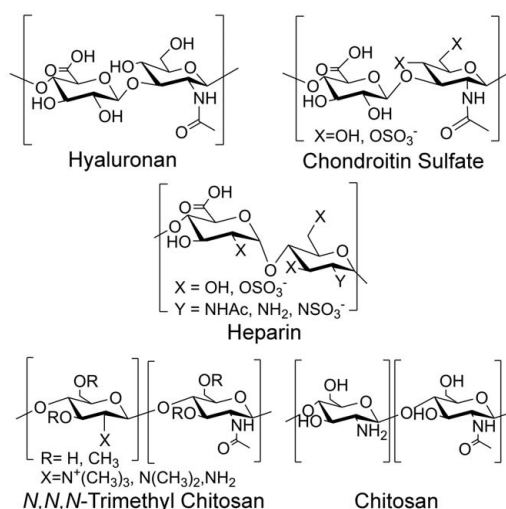
Figure 1.1 Chemical structures for the polysaccharides used in this work.

Heparin is a glycosaminoglycans (GAG) with the highest negative charge density of any biological macromolecule.[6] It is obtained from animal tissues (porcine intestinal mucosa, and/or bovine lung) and is used in medicine as an antithrombotic drug.[6] One of heparin's roles in the extracellular matrix is a protective GAG because of its multiple binding sites for many of the transforming growth factor beta (TGF-β) superfamily and fibroblast growth factor (FGF) family proteins.[7, 8] Binding of TGF-β proteins by heparin is isoform specific[9] and has been shown to protect both TGF-β1 and FGF-2 from proteolytic and chemical inactivation.[10] Binding FGF to heparin also increases its half life almost six fold.[11] Heparin bound TGF-β1[12] and TGF-β3[13, 14] enhances chondrogenesis, while heparin bound bone morphonogenic protein 2 (BMP-2)[15] and FGF-2[16] promote osteogenesis in vitro and in vivo.

Chondroitin sulfate is a weaker sulfated GAG, containing one sulfate group per disaccharide either in the 4-carbon or the 6-carbon of the *N*-acetyl-D-glucosamine residue. It is an important structural component of all connective tissues and is a key component of skin.[17] It is also used in the treatment of the symptoms of osteoarthritis.[18]

3

Hyaluronic acid is the only non-sulfonated GAG, making it a weak polyanion of great biological interest. It serves as a lubricant in cartilage, participates in the control of tissue hydration and water transport, and in the control of the inflammatory response after trauma.[19, 20] It is used in the construction of polyelectrolyte multilayers[21] and hydrogels[22] for mammalian cell culture.

Chitosan is a GAG-like weak polycation derived from the *N*-deacetylation of chitin, the most abundant naturally occurring polysaccharide.[22] Chitosan is widely used in both the packaging industry[23, 24] and the construction of vascular grafts[25, 26] due to its antimicrobial activity. Chitosan-based scaffolds support mammalian cell growth and is also an attractive material for wound healing applications.[27, 28] Chitosan based materials are widely used for tissue regeneration because it promotes wound healing.[29]

N,N,N-trimethyl chitosan is a chemical modification of chitosan where the amine is methylated creating a quaternary ammonium. Different methylating agents are available including dimethylsulfate[30] and methyl iodide.[31] *N,N,N*-trimethyl chitosan is soluble at pH higher than 5 (which chitosan is not). It also has antimicrobial properties even at higher pH[31] and it is investigated as a potential material for drug delivery.[32]

1.2.2 Mesenchymal Stem Cells

Bone marrow derived mesenchymal stem cells (MSC) are pluripotent cells capable of differentiating into different lineages (chondrogenic, osteogenic, myogenic, marrow stromal, tendongenic/ligamentagenic, adipogenic and other connective tissue cells) given proper stimuli.[33] They are suitable candidates for osteochondral tissue repair since they can differentiate into osteoblasts and/or chondrocytes depending on factors such as biochemical and biomechanical cues.[34, 35] MSCs can be isolated from bone marrow of small mammals

including rats[36] and rabbits,[37] or large mammals such as sheep[38] and horses.[39] Bone marrow harvest is relatively easy and repeatable yielding millions of cells from a small amount of marrow aspirate (4-17 ml).[38] In this work both ovine (sheep) and equine (horse) cells were evaluated. The ovine cells were harvested from 4-5 year old female sheep that had been recently euthanized for other studies at the Colorado State University Veterinary Teaching Hospital under the supervision of Dr. Simon Turner. The bone marrow is aspirated from the iliac crest of the sheep (Figure 1.2) using a biopsy needle. Equine cells were donated from Dr. John Kisiday from the Department of Clinical Sciences at Colorado State University.

Procedures for culture expansion of MSCs from different animal models have been published.[35, 38, 39] Reports characterizing bone marrow-derived MSCs support the use of cryo-preserved cells and give detailed procedures for MSC isolation. [38, 39] Rhodes et al. investigated ovine-derived MSCs and demonstrated the age of the sheep, sheep breed, and freeze-thaw of MSCs had no significant difference in proliferation rate.[38, 39] Bruder et al. showed that the osteogenic potential of bone marrow-derived MSCs is conserved even after 15 passages.[40] These studies show the robust characteristics that MSCs have making them suitable candidates for tissue engineering applications. A significant number of cells can be obtained and culture-expanded, and then after undergoing a few passages, they can be cryo-preserved for further studies while maintaining their proliferation and differentiation capabilities. MSCs behave differently depending on the topographical features present in their environment. Cell adhesion of both chondrocytes and osteoblasts has been shown to improve with the addition of nanoscale features.[41, 42]

Figure 1.2 Bone marrow harvest from the iliac crest of sheep.

1.2.3 Growth Factors

Growth factors are proteins with great potential in tissue engineering because of their involvement in many signaling pathways that regulate healing, cell processes, and maintenance of healthy tissue. Growth factors, including members from the fibroblast growth factor family and the transforming growth factor superfamily, affect MSC attachment, migration, and differentiation. Specifically, TGF-β1 and FGF-2 promote chondrogenesis[43] and osteogenesis,[16] respectively. The TGF-β superfamily consists of more than 25 proteins including the three mammalian TGF-β isoforms 1, 2, and 3 which are 60-80% homologues, and bone morphogenetic proteins, all of which are crucial in articular tissue repair.[44] TGF-β1 is a 26 kDa protein with an iso-electric point of 8.9, involved in cell migration, proliferation, extracellular matrix synthesis and degradation, and the immune response.[10] During the re-epithelialization phase of wound healing, high levels of TGF-β1 will act to decrease the inflammatory response by increasing extracellular matrix deposition.[45] TGF-β1 and its

6

isoform TGF-β3 are particularly important in tissue engineering due to their ability to induce chondrogenesis[13, 37, 43] of MSCs and differentiation of myofibroblasts from fibroblasts.[46] TGF-β1 is also involved in angiogenesis.[3, 44] Basic FGF-2 is a 18 kDa protein with an iso-electric point of 9.6, involved in cellular proliferation, differentiation, angiogenesis and ossification.[47] The FGF family includes 22 proteins, sharing up to 55% of their amino acid sequence, and is highly conserve among species.[16, 47] FGF-2 is involved in both osteogenesis[16, 36] and chondrogenesis[48] of MSCs. FGF-2 is also involved in angiogenesis.[49] The heparin-binding domains of TGF-β1 and FGF-2 are homologues, thus FGF-2 serves as a good model for heparin-binding proteins. These growth factors are very promising candidates to be use in regenerative medicine; however, their delivery poses a challenge. Growth factors, when delivered in solution, are susceptible to degradation to the point where 24 hours of incubation can significantly decrease their bioactivity.[50] Also, growth factors have short plasma half-lives (1.5 min for FGF-2, and 11-160 min for TGF-β1).[3] These growth factors delivered in solution are susceptible to proteolytic degradation as soon as they enter the body.

For successful growth factor therapies, biomaterials could be engineered to protect them from degradation. Some biomaterials have been developed for the delivery of growth factors but fail to protect them from degradation. One study demonstrated controlled release of FGF-2 from ceramic materials, but the FGF-2 was degraded after the second day.[51] Other biomaterials developed for the delivery of FGF-2 include sulfonated silk fibroin,[52] chitosan/hydroxyapatite scaffolds,[53] heparin conjugated fibrin gels,[54] and GAG-containing polyelectrolyte multilayers.[55, 56] Some of these studies demonstrate control release of FGF-2 but do not attempt to investigate whether the protein retains its activity.[53] Others show promising FGF-2 delivery results using sulfated synthetic or natural materials.[52, 54-56] Sulfated

7

molecules, such as heparin and chondroitin sulfate, are very promising as biomaterials because they protect growth factor from degradation and enhance their activity. This thesis will show how polysaccharide-based materials (which include sulfated GAGs) can be used for the delivery of FGF-2 and demonstrate that the FGF-2 bioactivty is retained or enhanced.

1.3 Biomaterials

In this work, a combination of polysaccharide-based biomaterials will be explored for the delivery of growth factors. These materials include polyelectrolyte multilayers, polyelectrolyte complex nanoparticles, and electrospun nanofibers. A brief summary of polyelectrolyte multilayers (PEMs) and electrospun nanofibers follows and more information about them can be found in chapters 2, 3, and 6 of this thesis. No characterization was performed on the polyelectrolyte complex nanoparticles in this work; rather they were used as a method of delivery of growth factor. For the interested, an exhaustive characterization of these polysaccharide-based polyelectrolyte complex nanoparticles has been previously performed in our lab correlating mixing ratio to the morphology, yield, zeta potential and hydrodynamic radius of the nanoparticles.[57, 58]

1.3.1 Polyelectrolyte multilayers

Polyelectrolyte multilayers are thin films formed by the electrostatic interactions of polyelectrolytes. A charged substrate is exposed to an oppositely charged polyelectrolyte (e.g. a polycation) solution, which allows for the polyelectrolyte to be deposited in the substrate changing the overall charge of the surface. This allows for the substrate to be modified with another polyelectrolyte (e.g. a polyanion) layer with a charge opposite to that of the initial layer. This process is continued until the desired number of layers is reached. PEMs can be constructed form synthetic polymers such as poly(styrene sulfonate),[59]

poly(allylamine hydrochloride),[59] and poly(acrylic acid);[60] and natural polymers including polypeptides (e.g. poly(L-lysine)),[61] DNA,[62] and polysaccharides.[58, 61, 63, 64] Many parameters affect PEM thickness, including solution pH, solution ionic strength, and charge density of one or both polyelectrolytes.[63] The focus in this thesis; however, involves the use of PEMs as a platform for growth factor delivery. Nonetheless, chapter 3 will give some details on the construction and characterization of different polysaccharide-based PEMs while chapter 4 investigates protein-PEM interactions. An excellent review by Picart highlights different properties (physical and chemical) in PEMs which are important to control cellular processes.[65]

1.3.2 Electrospun nanofibers

Electrospinning is performed by dispensing a polymer solution through a capillary and applying a high voltage between the capillary tip and a collector as displayed in Figure 1.3. At the point when the electrostatic force overcomes surface tension and the viscosity of the solution, the droplet at the needle tip changes from a meniscus to a cone (Taylor cone). A polymer jet is ejected from the Taylor cone as the electric field exceeds the surface tension of the polymer solution.[66] The solvent evaporates as the polymer jet travels in air, following the electric field path, and it is eventually deposited in a grounded collector.
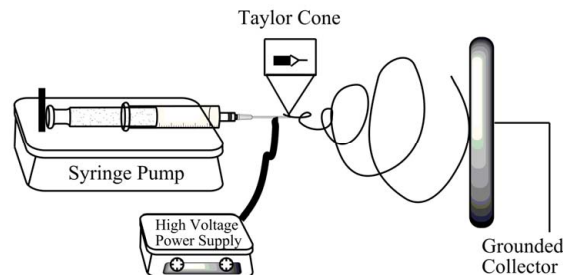
Figure 1.3 Electrospinning apparatus schematic. (Adapted from Biomaterials, 29/13, T.J. Sill, H.A. von Recum, Electrospinning: Applications in drug delivery and tissue engineering, 1989-2006, Copyright 2008, with permission from Elsevier)

Fiber diameter ranges from the nano- to the micro-scale. As simple as the process looks, the number of variables that influence fiber diameter and morphology is great. It has been noted that fiber diameter depends on tip-to-collector distance, voltage, position of syringe, humidity, temperature and solution properties such as viscosity, and concentrations.[66] Moreover, electrospinning of polysaccharides is difficult due to their inability to form entanglements and their limited solubility.[5] However, we have successfully electrospun chitosan and we use this material as a platform for growth factor delivery and MSC activation. Chapters 6, 7, and 8 of this thesis utilize electrospun nanofibers and more information can be found there. Also, a review by Sill and von Recum is highly recommended, in which they discuss the history, the process, and the applications of electrospun fibers in drug delivery and tissue engineering.[66]

1.4 Research Aims

Recent demonstration that polysaccharides protect growth factors from degradation in the extracellular matrix of multiple tissues has led researchers to pursue the development of polysaccharide-based materials for the delivery of growth factors. Moreover, nanostructured features in native tissue has been demonstrated to be of great importance in cell modulation and tissue repair. Thus, the hypothesis which will be investigated in this thesis is that nanostructured polysaccharide-based biomaterials will enhance the delivery and efficacy of growth factors from the FGF family by protecting them from enzymatic degradation. Further, it is hypothesized that the nanoscale features in these polysaccharide-based biomaterials will provide mesenchymal stem cells with an environment similar to that of their native extracellular matrix, which will promote tissue repair or regeneration. An exhaustive

literature review is presented in chapter 2, to support these hypotheses. The rest of the chapters are dedicated to testing these hypotheses.

The goal of this work is to develop novel polysaccharide-based biomaterials for the stabilization and delivery of growth factors for bone marrow derived mesenchymal stem cell activation. The goal of this work will be accomplished through five specific aims:

I.   Investigate spectroscopically the layer-by-layer assembly of polysaccharide-based multilayers using chitosan and *N,N,N*-trimethyl chitosan as polycations and hyaluronan, chondroitin sulfate, and heparin as the polyanions.

II. Investigate how polysaccharide-based surfaces affect the structure and stability of proteins using IR spectroscopy.

III. Demonstrate the ability of polysaccharide-based PEMs to stabilize the growth factor FGF-2 and therefore enhance MSC proliferation on flat surfaces.

IV. Develop methods for the coating of electrospun chitosan nanofibers using PEMs, and use them as a substrate for the adsorption and controlled release of FGF-2.

V.   Demonstrate the ability of the electrospun chitosan nanofibers to support MSC growth, and investigate how nanoscale features affect osteogenic differentiation.

1.5 Organization of Dissertation

Each of the previously mentioned specific aims is addressed in the subsequent chapters of this thesis. A brief description of each chapter is given below.

Chapter 2. *"Engineering Soft Nanostructures for Guided Cell Response"* A literature review is provided in this chapter with a focus on soft nanostructured materials for guided cell response. This chapter provides an overview of biological soft nanostructures and

nanoscale features of the extracellular matrix. It then mentions how these biological nanostructures serve as templates for the engineering of soft nanostructures. It provides details of different methods for the engineering of soft nanostructures such as nanoparticles (emulsions and self-assembled), surface structures (polyelectrolyte multilayers, cell membrane-mimetic thin films, polymer brushers and soft lithography), and nanofibers (electrospun and molecular self-assembled). The chapter finalizes with speculations on what the future of engineering soft nanostructures will be for guided cell response.

Chapter 3. *"Layer-by-Layer Assembly of Polysaccharide-Based Multilayers: A Spectroscopic Study of Hydrophilicity, Composition, and Ion Pairing"* This chapter will focus on the layer-by-layer assembly of polysaccharide-based polyelectrolyte multilayers. PEMs of different polyelectrolyte pairs, were constructed using the polycations chitosan and *N,N,N*-trimethyl chitosan and the polyanions hyaluronan, chondroitin sulfate, and heparin. An exhaustive spectroscopic study was performed on all of the PEM pairs to investigate the effects of polyelectrolyte charge density on thickness, swelling, composition, and ion-pairing. X-ray photoelectron spectroscopy (XPS), Fourier transform surface plasmon resonance (FT-SPR), polarization-modulation infrared reflection adsorption spectroscopy (PM-IRRAS), variable-angle spectroscopic ellipsometry, and water contact angle experiments were performed on all of the PEM pairs. The results demonstrate that hydrophilicity and swelling are reduced when one polyelectrolyte is strong and the other is weak, while ion pairing is increased. This chapter fulfills research aim I.

Chapter 4. *"FT-IR Studies on Stability of Proteins Adsorbed to Polysaccharide-Based Polyelectrolyte Multilayers"* The focus of this chapter is to address the stability of proteins adsorbed to polysaccharide-based polyelectrolyte multilayers using Fourier transform

infrared spectroscopy. IR spectroscopy gives relative information of the secondary structure of the protein, which relates to the stability of the protein. PEMs were constructed using chitosan, heparin, and hyaluronan. The model proteins, lysozyme and bovine serum albumin, were adsorbed onto either negative (heparin- or hyaluronan-terminated) or neutral surfaces (chitosan terminated) surfaces. FT-SPR was used to monitor protein adsorption while PM-IRRAS was used to obtain IR spectra of the adsorbed protein to analyze its secondary structure. Hydrogen-deuterium exchange was also performed to investigate the stability of the adsorbed protein (unfolding). This chapter demonstrates techniques that can be applied to analyze growth factors and other important protein interactions with PEMs. The results from this chapter satisfy research aim II.

Chapter 5. *"Polysaccharide-Based Polyelectrolyte Multilayer Surface Coatings can Enhance Mesenchymal Stem Cell (MSC) Response to Adsorbed Growth Factors"* This chapter demonstrates the ability of polysaccharide-based PEMs to protect and deliver growth factors to enhance mesenchymal stem cell activity. Construction of PEMs and adsorption of FGF-2 was evaluated on heparin-chitosan PEMs constructed on gold-coated glass, tissue culture polystyrene (TCPS), and titanium. XPS, FT-SPR, and PM-IRRAS were used to evaluate PEM construction on the different substrates and growth factor adsorption. In vitro testing of the FGF-2-loaded PEM constructed on TCPS and titanium was performed using ovine bone marrow-derived MSCs. MSC proliferation was enhanced on the FGF-2-loaded PEMs versus the controls. Chapter 5 address research aim III.

Chapter 6. *"Coating Electrospun Chitosan Nanofibers with Polyelectrolyte Multilayer Using the Polysaccharides Heparin and* N,N,N-*Trimethyl Chitosan"* A new technique was developed for coating electrospun chitosan nanofibers with polyelectrolyte multilayers in this

13

chapter. Chitosan was successfully electrospun from a trifluoroacetic acid and dichloromethane solution. A new technique was developed to modify electrospun chitosan nanofibers with polyelectrolyte multilayers using the *N,N,N*-trimethyl chitosan and heparin. PEM construction on the fibers was confirmed using Alcian blue staining, XPS, and FT-IR. Moreover, FGF-2 was successfully adsorbed on the modified chitosan nanofibers.

Chapter 7. *"Controlled Release of Bioactive FGF-2 from Electrospun Chitosan Nanofibers Using Polysaccharide-Based Nanostructures"* In this chapter a nanostructure polysaccharide-based material was developed using chitosan nanofibers, PEMs, and polyelectrolyte complex nanoparticles (PCNs) for the delivery of FGF-2. FGF-2 was first adsorbed onto PCN and these modified FGF-PCNs were then adsorbed onto chitosan nanofibers with and without PEMs. FGF-PCNs were released in vitro for a period of 27 days. After 27 days the bioactivity of the released FGF-2 was assessed using MSCs. These polysaccharide structures also protect and enhance FGF-2 similar to the results from chapter 5. Both chapters 6 and 7 fulfill research aim IV.

Chapter 8. *"Osteogenic Ovine and Equine Mesenchymal Stem Cell Differentiation on Electrospun Chitosan Nanofibers with and without Dexamethasone"* The effect of nanostructured substrates on the differentiation of mesenchymal stem cells towards the osteogenic lineage was investigated in this chapter using chitosan nanofibers. Ovine and equine MSCs were seeded on chitosan nanofibers or TCPS and the production of alkaline phosphatase and calcium deposition was monitored. It was noted that the nanostructure of the chitosan fibers alone was enough to induce cell differentiation. The effect of the chemical cue dexamethasone was also investigated. Research aim V is accomplished through this chapter.

Chapter 9. *"Conclusion and Future work"* In this chapter the conclusion of all the work

done in this thesis will be presented along with possible future studies.

1.6 References

1. Woolf, A. D.; Pfleger, B., *Bulletin of the World Health Organization* **2003,** *81* (9), 646-656.
2. McPherson, J. M.; Tubo, R., Articular Cartilage Injury. In *Principles of Tissue Engineering*, Second Edition ed.; Lanza, R. P.; Langer, R.; Vacanti, J., Eds. Elsevier: San Diego, CA, 2000; pp 697-709.
3. Tessmar, J. K.; Gopferich, A. M., *Advanced Drug Delivery Reviews* **2007,** *59* (4-5), 274-291.
4. Martínez, E.; Engel, E.; Planell, J. A.; Samitier, J., *Annals of Anatomy - Anatomischer Anzeiger* **2009,** *191* (1), 126-135.
5. Boddohi, S.; Kipper, M. J., *Advanced Materials* **2010,** *22* (28), 2998-3016.
6. Salmivirta, M.; Lidholt, K.; Lindahl, U., *Faseb Journal* **1996,** *10* (11), 1270-1279.
7. Rider, C. C. In *Heparin/heparan sulphate binding in the TGF-beta cytokine superfamily*, **2006**; pp 458-460.
8. Maccarana, M.; Casu, B.; Lindahl, U., *Journal of Biological Chemistry* **1993,** *268* (32), 23898-23905.
9. Lyon, M.; Rushton, G.; Gallagher, J. T., *Journal of Biological Chemistry* **1997,** *272* (29), 18000-18006.
10. McCaffrey, T. A.; Falcone, D. J.; Du, B. H., *Journal of Cellular Physiology* **1992,** *152* (2), 430-440.
11. Damon, D. H.; Lobb, R. R.; Damore, P. A.; Wagner, J. A., *Journal of Cellular Physiology* **1989,** *138* (2), 221-226.
12. Sato, M.; Ishihara, M.; Kaneshiro, N.; Mitani, G.; Nagai, T.; Kutsuna, T.; Asazuma, T.; Kikuchi, M.; Mochidal, J., *Journal of Biomedical Materials Research Part B-Applied Biomaterials* **2007,** *83B* (1), 181-188.
13. Park, J. S.; Park, K.; Woo, D. G.; Yang, H. N.; Chung, H. M.; Park, K. H., *Biomacromolecules* **2008,** *9* (8), 2162-2169.
14. Park, J. S.; Woo, D. G.; Yang, H. N.; Lim, H. J.; Chung, H. M.; Park, K. H., *Transplantation* **2008,** *85* (4), 589-596.
15. Zhao, B. H.; Katagiri, T.; Toyoda, H.; Takada, T.; Yanai, T.; Fukuda, T.; Chung, U. I.; Koike, T.; Takaoka, K.; Kamijo, R., *Journal of Biological Chemistry* **2006,** *281* (32), 23246-23253.
16. Lee, J. Y.; Choo, J. E.; Choi, Y. S.; Lee, K. Y.; Min, D. S.; Pi, S. H.; Seol, Y. J.; Lee, S. J.; Jo, I. H.; Chung, C. P.; Park, Y. J., *Journal of Biomedical Materials Research Part A* **2007,** *83A* (4), 970-979.
17. Machens, H. G.; Berger, A. C.; Mailaender, P., *Cells Tissues Organs* **2000,** *167* (2-3), 88-94.
18. Ronca, F.; Palmieri, L.; Panicucci, P.; Ronca, G., *Osteoarthritis and Cartilage* **1998,** *6*, 14-21.

19. Lapcik, L.; De Smedt, S.; Demeester, J.; Chabrecek, P., *Chemical Reviews* **1998,** *98* (8), 2663-2684.
20. Laurent, T. C.; Fraser, J. R. E., *Faseb Journal* **1992,** *6* (7), 2397-2404.
21. Richert, L.; Lavalle, P.; Payan, E.; Shu, X. Z.; Prestwich, G. D.; Stoltz, J. F.; Schaaf, P.; Voegel, J. C.; Picart, C., *Langmuir* **2004,** *20* (2), 448-458.
22. Suh, J. K. F.; Matthew, H. W. T., *Biomaterials* **2000,** *21* (24), 2589-2598.
23. Durango, A. M.; Soares, N. F. F.; Benevides, S.; Teixeira, J.; Carvalho, M.; Wobeto, C.; Andrade, N. J., *Packaging Technology and Science* **2006,** *19* (1), 55-59.
24. Lee, C. H.; An, D. S.; Park, H. F.; Lee, D. S., *Packaging Technology and Science* **2003,** *16* (3), 99-106.
25. Fujita, M.; Kinoshita, M.; Ishihara, M.; Kanatani, Y.; Morimoto, Y.; Simizu, M.; Ishizuka, T.; Saito, Y.; Yura, H.; Matsui, T.; Takase, B.; Hattori, H.; Kikuchi, M.; Maehara, T., *Journal of Surgical Research* **2004,** *121* (1), 135-140.
26. Hu, S. G.; Jou, C. H.; Yang, M. C., *Journal of Applied Polymer Science* **2002,** *86* (12), 2977-2983.
27. Sechriest, V. F.; Miao, Y. J.; Niyibizi, C.; Westerhausen-Larson, A.; Matthew, H. W.; Evans, C. H.; Fu, F. H.; Suh, J. K., *Journal of Biomedical Materials Research* **2000,** *49* (4), 534-541.
28. Raghunath, J.; Rollo, J.; Sales, K. M.; Butler, P. E.; Seifalian, A. M., *Biotechnology and Applied Biochemistry* **2007,** *46*, 73-84.
29. Muzzarelli, R.A.A., *Carbohydrate Polymers* **2009,** 76, 167-182.
30. de Britto, D.; Assis, O. B. G., *Carbohydrate Polymers* **2007,** *69* (2), 305-310.
31. Runarsson, O. V.; Holappa, J.; Nevalainen, T.; Hjalmarsdottir, M.; Jarvinen, T.; Loftsson, T.; Einarsson, J. M.; Jonsdottir, S.; Valdimarsdottir, M.; Masson, M., *European Polymer Journal* **2007,** *43* (6), 2660-2671.
32. Mourya, V. K.; Inamdar, N. N., *Journal of Materials Science-Materials in Medicine* **2009,** *20* (5), 1057-1079.
33. Lanza, R. P.; Langer, R.; Vacanti, J., *Principles of Tissue Engineering*. Second ed.; Academic Press: San Diego, 2000; p 697-708.
34. Pittenger, M. F.; Mackay, A. M.; Beck, S. C.; Jaiswal, R. K.; Douglas, R.; Mosca, J. D.; Moorman, M. A.; Simonetti, D. W.; Craig, S.; Marshak, D. R., *Science* **1999,** *284* (5411), 143-147.
35. Caplan, A. I., *Journal of Orthopaedic Research* **1991,** *9* (5), 641-650.
36. Hanada, K.; Dennis, J. E.; Caplan, A. I., *Journal of Bone and Mineral Research* **1997,** *12* (10), 1606-1614.
37. Roostaeian, J.; Carlsen, B.; Simhaee, D.; Jarrahy, R.; Huang, W. B.; Ishida, K.; Rudkin, G. H.; Yamaguchi, D. T.; Miller, T. A., *Journal of Surgical Research* **2006,** *133* (2), 76-83.
38. Rhodes, N. P.; Srivastava, J. K.; Smith, R. F.; Longinotti, C. In *Heterogeneity in proliferative potential of ovine mesenchymal stem cell colonies*, Kluwer Academic Publ: **2004**; pp 397-402.
39. Arnhold, S. J.; Goletz, I.; Klein, H.; Stumpf, G.; Beluche, L. A.; Rohde, C.; Addicks, K.; Litzke, L. F., *American Journal of Veterinary Research* **2007,** *68* (10), 1095-1105.
40. Bruder, S. P.; Jaiswal, N.; Haynesworth, S. E., *Journal of Cellular Biochemistry* **1997,** *64* (2), 278-294.

41. Khang, D.; Lu, J.; Yao, C.; Haberstroh, K. M.; Webster, T. J., *Biomaterials* **2008,** *29* (8), 970-983.
42. Li, W. J.; Jiang, Y. J.; Tuan, R. S., *Tissue Engineering* **2006,** *12* (7), 1775-1785.
43. Worster, A. A.; Nixon, A. J.; Brower-Toland, B. D.; Williams, J., *American Journal of Veterinary Research* **2000,** *61* (9), 1003-1010.
44. Okane, S.; Ferguson, M. W. J., *International Journal of Biochemistry & Cell Biology* **1997,** *29* (1), 63-78.
45. Shah, M.; Revis, D.; Herrick, S.; Baillie, R.; Thorgeirson, S.; Ferguson, M.; Roberts, A., *American Journal of Pathology* **1999,** *154* (4), 1115-1124.
46. Metzger, W.; Grenner, N.; Motsch, S. E.; Strehlow, R.; Pohlemann, T.; Oberringer, M., *Tissue Engineering* **2007,** *13* (11), 2751-2760.
47. De Luca, F.; Baron, J., *Trends in Endocrinology and Metabolism* **1999,** *10* (2), 61-65.
48. Vincent, T.; Hermansson, M.; Bolton, M.; Wait, R.; Saklatvala, J., *Proceedings of the National Academy of Sciences of the United States of America* **2002,** *99* (12), 8259-8264.
49. Zamora, P. O.; Tsang, R.; Pena, L. A.; Osaki, S.; Som, P., *Bioconjugate Chemistry* **2002,** *13* (5), 920-926.
50. Ziegler, J.; Anger, D.; Krummenauer, F.; Breitig, D.; Fickert, S.; Guenther, K. P., *Journal of Biomedical Materials Research Part A* **2008,** *86A* (1), 89-97.
51. Ziegler, J.; Mayr-Wohlfart, U.; Kessler, S.; Breitig, D.; Gunther, K. P., *Journal of Biomedical Materials Research* **2002,** *59* (3), 422-428.
52. Wenk, E.; Murphy, A. R.; Kaplan, D. L.; Meinel, L.; Merkle, H. P.; Uebersax, L., *Biomaterials* **2010,** *31* (6), 1403-1413.
53. Tigli, R. S.; Akman, A. C.; Gumusderelioglu, M.; Nohutcu, R. M., *Journal of Biomaterials Science-Polymer Edition* **2009,** *20* (13), 1899-1914.
54. Jeon, O.; Kang, S. W.; Lim, H. W.; Chung, J. H.; Kim, B. S., *Biomaterials* **2006,** *27* (8), 1598-1607.
55. Almodóvar, J.; Bacon, S.; Gogolski, J.; Kisiday, J. D.; Kipper, M. J., *Biomacromolecules* **2010,** *11* (10), 2629-2639.
56. Macdonald, M. L.; Rodriguez, N. M.; Shah, N. J.; Hammond, P. T., *Biomacromolecules* **2010,** *11* (8), 2053-2059.
57. Boddohi, S.; Moore, N.; Johnson, P. A.; Kipper, M. J., *Biomacromolecules* **2009,** *10* (6), 1402-1409.
58. Boddohi, S.; Almodóvar, J.; Zhang, H.; Johnson, P. A.; Kipper, M. J., *Colloids and Surfaces B-Biointerfaces* **2010,** *77* (1), 60-68.
59. Ramos, J. J. I.; Stahl, S.; Richter, R. P.; Moya, S. E., *Macromolecules* **2010,** *43* (21), 9063-9070.
60. Muller, M.; Kessler, B.; Houbenov, N.; Bohata, K.; Pientka, Z.; Brynda, E., *Biomacromolecules* **2006,** *7* (4), 1285-1294.
61. Crouzier, T.; Picart, C., *Biomacromolecules* **2009,** *10* (2), 433-442.
62. Cai, K. Y.; Hu, Y.; Wang, Y. L.; Yang, L., *Journal of Biomedical Materials Research Part A* **2008,** *84A* (2), 516-522.
63. Boddohi, S.; Killingsworth, C. E.; Kipper, M. J., *Biomacromolecules* **2008,** *9* (7), 2021-2028.
64. Almodóvar, J.; Kipper, M. J., *Macromolecular Bioscience* **2011,** *11* (1), 72-76.
65. Picart, C., *Current Medicinal Chemistry* **2008,** *15* (7), 685-697.
66. Sill, T. J.; von Recum, H. A., *Biomaterials* **2008,** *29* (13), 1989-2006.

Chapter 2

Engineering Soft Nanostructures for Guided Cell Response

- Kipper M., Almodóvar J. "Engineering Soft Nanostructures for Guided Cell Response" in *Nanotechnology in Tissue Engineering and Regenerative Medicine*, Ed. Popat K., Boca Raton, FL: CRC, **2011**. Print.

2.1 Biological Soft Nanostructures

Tissue engineering involves applying the principles of engineering and the life sciences towards the development of biological replacements that restore, maintain, or improve tissue function.[1] Investigators have attempted to engineer many mammalian tissues using a variety of approaches. Broadly, these can be classified as in vitro approaches and in vivo approaches.[2] In the former approaches cells are cultured on a scaffold in vitro, where they form functional tissue for future transplantation. In the latter approaches scaffolds are designed such that after implantation they recruit native tissue cells that are guided to create new tissue or enhance wound healing. In both approaches, it has been demonstrated that cells respond to a vast array of cues provided by scaffolds and culture conditions, including chemical, biochemical, electrical, mechanical, and topographical stimuli. Thus, in order to achieve predictable cell responses, materials for tissue engineering are often engineered to mimic the structure and properties of natural tissue, both at their surfaces and in the bulk. Surface properties that dictate the interactions between the material and its environment,

where the environment consists of cells and important biomolecules, are by nature nanoscale properties.[3] Bulk properties are also dependent upon the nanoscale organization of materials. This is because natural tissues are designed and assembled in controlled ways, at a hierarchy of length scales ranging from the macro to the nano scale.

Cartilage serves as a perfect example to demonstrate the hierarchy of tissue structure across multiple length scales (See Figure 2.1). On the macroscopic scale, articular cartilage can be described as a tissue. On the microscopic scale, one observes the organization of a material sparsely populated with cells (chondrocytes) and a relatively small amount of blood vessels. Here the extracellular matrix (ECM) is organized to contain fibrous structural components in a fluid phase. At the nanoscale the molecules which make up the ECM are organized into complex nanoassemblies. The ECM in cartilage mostly consists of collagen but many other proteins and polysaccharides are present, which form a complex nano scale matrix that controls both mechanical properties and cell behavior (Figure 2.1). The protein collagen forms a triple helix with nanometer dimensions. Many of these helices assemble to form long fibrils with diameters ranging from about 20 to 200 nm.[4] These complex nanoassemblies provide tensile strength to connective tissues. The alignment of fibers can result in anisotropic mechanical properties appropriate for the particular biomechanics of the tissue in question. Compressive strength and tribological prosperities are imparted to tissues like cartilage through another soft nanoassembly – the aggrecan aggregate.[5, 6] Aggrecan is a proteoglycan that carries about 100 highly sulfated polysaccharide chains (chondroitin sulfate and keratan sulfate).[7] The very high negative charge density results in electrostatic repulsion causing aggrecan to adopt a rigid bottle-brush conformation in solution, several tens of nanometers in diameter and 200 to 400 nm in length. Many aggrecans bind to another

19

polysaccharide, hyaluronic acid, to form a complex nanoassembly called the aggrecan aggregate in cartilage and other tissues (Figure 2.1). This dense, rigid nanoassembly with high negative charge density imparts a high osmotic pressure to the tissues in which it is found providing compressive strength.[8] Polysaccharide containing assemblies such as the aggrecan aggregate also facilitate the assembly of collagen fibrils[8] and protect them from biochemical modes of degradation.[9]
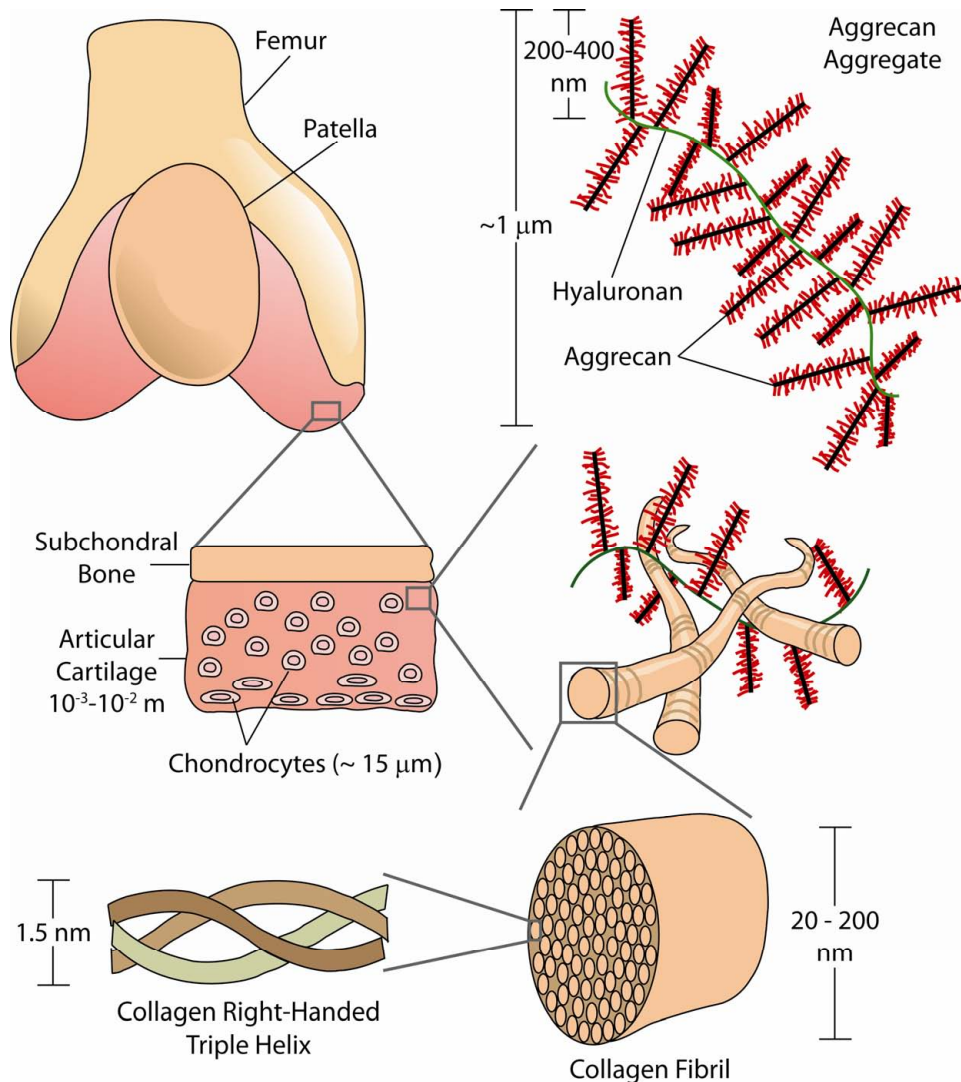
Figure 2.1 Structural hierarchy of articular cartilage. In the macro scale, articular cartilage spans about 0.5-15 cm. On the micro scale chondrocytes (around 15 μm in diameter) are the main component in articular cartilage. On the nano scale cartilage is composed of extracellular matrix proteoglycan aggregates embedded within collagen fibers. (Adapted from Biomaterials, 13/2, V.C Mow, A. Ratcliffe, Cartilage and diarthrodial joints as paradigms for hierarchical materials and structures, 67-97, Copyright 1991, with permission from Elsevier.)

The hierarchical arrangement of materials at multiple length scales illustrated by cartilage is one of the hallmarks of what condensed matter physicists refer to as "soft materials." Soft materials generally have relatively high molecular kinetic energy and relatively low intermolecular bonding energy compared to "hard materials."[10] This combination allows them to explore the configurational space necessary to find local free energy minima that result in self-assembly into hierarchical structures over multiple length scales. These structures are then stabilized by the multiplicity of relatively weak forces whose combined effect holds the structure together, while still allowing for local structural changes. Because soft materials are characterized by a variety of molecular interactions with different energies and dynamics, their multi-scale organization, results in physical properties that can vary with the length scales and time scales of experiments. This feature of soft materials is also exhibited by cartilage, as illustrated in Figure 2.2, where its elastic modulus is a function of loading rate over physiologically relevant ranges.[11]

The relatively weak attractive interactions that stabilize structures in soft materials are often van der Waals interactions, which arise from the Coulombic forces between permanent and/or inducible dipoles (dipole-dipole, dipole-induced dipole, and induced dipole-induced dipole).[12] In aqueous solutions in particular, hydrogen bonds and electrostatic forces between formally charged groups can also become very important. These typically have higher energies than the van der Waals interactions.[12] The typical lipid bilayers that compartmentalize cells and intracellular structures and organize membrane-associated proteins exemplify how these forces combine to result in a soft nanoscale assembly.[13] The hydrophobic core of the lipid bilayers is dominated by van der Waals interactions, while at the surfaces ion-dipole, ion-ion, and hydrogen bond interactions dominate. Differences in the

packing density in these two regions tend to frustrate the structure of lipid bilayers, potentially introducing additional fluidity.[14]
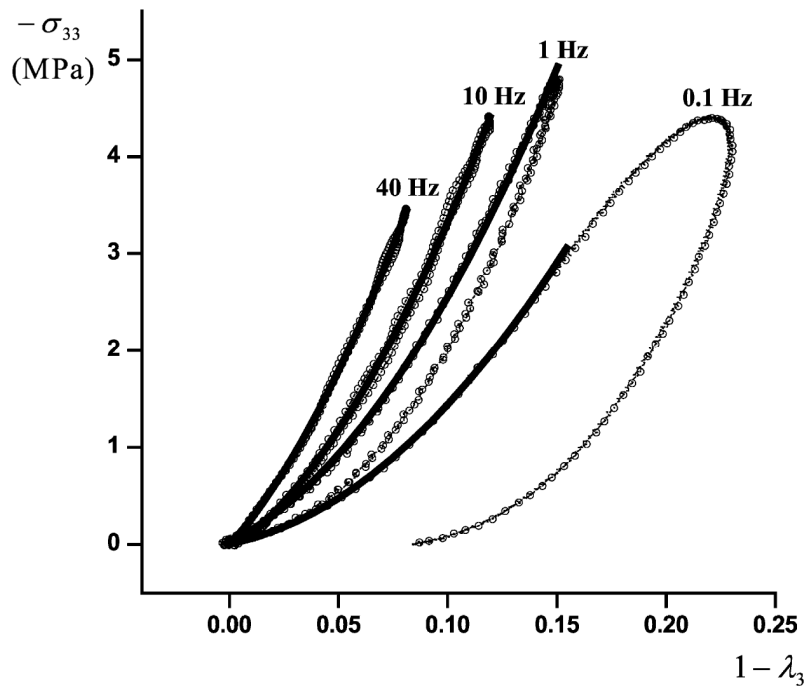
Figure 2.2 Stress-strain response for bovine articular cartilage at various loading frequencies. (Reprinted from Osteoarthritis and Cartilage, 12/1, S. Park, C.T. Hung, G.A Ateshian, Mechanical response of bovine articular cartilage under dynamic unconfined compression loading at physiological stress levels, 65-73, Copyright 2004, with permission from Elsevier.)

The nanoscale organization of the soft materials illustrated by the biological examples discussed above suggests that the design of biomaterials for the repair and/or regeneration of mammalian tissue by mimicking tissue properties require that materials be engineered from the nanoscale up. In many cases, this can be done by a judicious manipulation of the non-covalent interactions that govern soft material interactions and assembly. Such approaches can be described as "bottom-up" assembly. In other cases, "top-down" approaches are used to introduce nanoscale features into materials that do not otherwise form nanostructures. This chapter will focus on nanoscale soft materials in mammalian tissues and recent research efforts in manipulating nanoscale properties of soft materials to guide cell

and tissue responses. We begin with a brief description of the nanoscale organization of the ECM, followed by a review of the current understanding of cell response to nanoscale features of soft biomaterials, and the techniques used to tailor biomaterials at the nanometer scale.

2.2 Nanoscale Features of the Extracellular Matrix

Cells, which are 10 to 100 μm in diameter, respond differently to topographical features from the macro down to the molecular size.[15] At the very low end of this range (a few nanometers) are found features such as proteins, polysaccharides, and small protein complexes. Proteoglycans, enzymes, cadherins, growth factors, and other proteins have dimensions on the nanometer scale, and are all crucial determinants of cell response to materials. At larger length scales (tens to hundreds of nanometers) these components are organized into more complex assemblies that decorate cell surfaces and form the structural building blocks of the ECM in tissues. Many of these biomolecules can be isolated or produced via biomolecular techniques which can then be used for biomaterials. By tailoring the interactions that govern the organization of these building blocks, biomaterials scientists have the opportunity to explore how the nanoscale structure and organization of these biologically derived materials influences their biochemical and biomechanical functions.

The ECM is the material underlying the epithilia and endothelia, and surrounds all connective tissue cells providing mechanical support and strength to the tissue.[16] The ECM not only provides mechanical support to cells, but it also influences their behavior (e.g., adhesion, spreading, migration, and differentiation). The components of the ECM also have important biochemical activity, and can play major roles in growth factor signaling, by

23

sequestering, releasing, and activating growth factors.[15] Thus, the composition of the ECM strongly affects stem cell differentiation and the maintenance of healthy tissue. The ECM is composed of a variety of molecules depending upon the organism and tissue. Connective tissues in mammals have an ECM with fibers composed of mostly the proteins collagen and elastin, and soluble molecules including glycosaminoglycans and proteins (Table 2.1).

Table 2.1 Components of the ECM along with their relative native size and structure

Molecule	Size
Collagen	Fibrillar protein approximately 300 nm in length and 1.4 nm in diameter, organized into larger fibrils and fibers.[16]
Aggrecan	Bottlebrush proteoglycan with a length of 400 nm and a radius between 20–60 nm[5]
Elastin	Fibrillar protein approximately 10–20 nm in diameter[21]
Fibronectin	Rod-like protein approximately 60 nm long and 2.5 nm wide[101]
Hyaluronic acid	Stiff random coil with radius of gyration about 200 nm[38]
Heparan sulfate	Extended helical structure with 40–160 nm in length[124]
Chondroitin sulfate	Semiflexible coil with intrinsic persistence length in the range of 4.5–5.5 nm[41]
Growth Factors (e.g. BMP-2)	BMP-2 is a globular protein 7 x 3.5 x 3 nm in size[36]

Naturally derived polymers found in the ECM, such as proteins and glycosaminoglycans are attractive biomaterials due to their biological, mechanical, and physical properties. Many of these materials are soluble in aqueous solutions, avoiding the need of organic solvents that are often required to process synthetic polymers. Many of these biopolymers also act as polyelectrolytes. Their polyelectrolyte properties can be exploited in the assembly of nanostructured materials by using their water solubility and electrostatic interactions to tune nanoscale assembly. Because naturally derived polymers have biochemical function, their successful incorporation into engineered ECM provides a bioactive material for the guidance of cell responses.

Proteins are biological polymers composed of amino acids which define their structure and function. Collagen, gelatin (denatured collagen), elastin, and fibrinogen, among others are ECM proteins that form structural networks, and that can also be fabricated into biomaterials with nanoscale structure. Collagens are a class of glycoproteins consisting of at least 19 genetically distinct types and are the most abundant protein in mammals, accounting for 20–30% of total protein content.[17] Collagens type I, II, and III are the most abundant fibril-forming molecules in mammalian tissue.[16] They are a primary structural component of the ECM of many tissues, and is an essential building block in the musculoskeletal system.[19] They are synthesized intracellularly as large precursor procollagens forming a continuous triple helix (Figure 2.1). This triple helix is approximately 300 nm in length and 1.5 nm in diameter.[16] This triple helix structure assembles into fibrils tens of nanometers in diameter. In some tissues, these fibrils further assemble into larger fibers. Collagens can be easily isolated for the construction of nanostructured biomaterials. Collagen sponges, nanoparticles, nanofibers, ultra thin films, and hydrogels have been constructed as wound dressings, for the repair of tendon and cartilage, and for studying cell response to nanomaterials.[17, 18] Collagen constructs support mammalian cell growth and are biodegradable. Elastin is a major protein component of lung and vascular tissue responsible for their elastic properties.[20] Elastin is found naturally in the form of fibers approximately 10-20 nm in diameter.[21] It has been used in coatings for vascular grafts due to its minimal interactions with platelets.[20] Fibrinogen is a fibrous protein that polymerizes to form fibrin – the primary structural component of blood clots. Fibrin forms the structure which supports the early stages of the wound healing process, and is therefore supportive of key cellular functions during tissue repair. Fibrin is one of the earliest biopolymers used as a biomaterial due to its biodegradability and

injectability.[20] Aside from structural applications, proteins are crucial in modulating cell behavior. Growth factors comprise several protein families, present in every mammalian tissue, which influences cell adhesion, recruitment, proliferation, differentiation, and apoptosis.

Polysaccharides are polymeric carbohydrate structures typically composed of repeating units of mono- or di-saccharides bonded via glycosidic bonds. Polysaccharides widely used as biomaterials include those from non-mammalian sources, such as cellulose, chitosan, chitin, alginate, and dextran. They also include glycosaminoglycans (GAGs), often from mammalian tissues, such as heparin, heparan sulfate, hyaluronic acid, chondroitin sulfate, and keratan sulfate. Chitin and chitosan behave as polycations, while alginate and the GAGs behave as polyanions. In fact, heparin, which carries a high number of substituent sulfate groups, has the highest negative charge density of any biological macromolecule.[22] Chitosan is a GAG-like weak polycation derived from the *N*-deacetylation of chitin, the most abundant naturally occurring polysaccharide.[23] Chitosan has been widely used in both the packaging industry[24] and the construction of vascular grafts[25] due to its antimicrobial activity. Chitosan supports mammalian cell growth and is also an attractive material for wound healing applications.[26, 27] The GAGs are usually obtained from animal tissues, where their biological functions range from potentiation of enzyme activity in the blood coagulation cascade to influencing the biomechanics of joint tissues. Heparin is used therapeutically as an antithrombotic drug.[22] Heparin and other GAGs also influence the activities of growth factors by binding them in the extracellular matrix, sequestering them, stabilizing them with respect to enzymatic degradation, and mediating their binding to growth factor receptors.[22, 28] For example, binding of transforming growth factor beta (TGF-β) proteins by heparin is isoform

specific[29] and has been shown to protect TGF-β1 from proteolytic and chemical inactivation.[28] Binding fibroblast growth factor (FGF) to heparin also increases its half life almost six fold.[30] Heparin bound TGF-β1[31] and TGF-β3[32, 33] enhances chondrogenesis, while heparin-bound bone morphogenetic protein (BMP-2)[34] and FGF-2[35] promote osteogenesis in vitro and in vivo. Chondroitin sulfate is the major component of aggrecan, a complex ECM nanoassembly (Figure 2.1). Chondroitin sulfate can stimulate metabolic response of cartilage and has anti-inflammatory properties.[20] Hyaluronic acid is the only non-sulfated GAG, making it a weak polyanion of great biological interest. It serves as a lubricant in cartilage, participates in the control of tissue hydration, water transport, and inflammatory response, and organizes the nanostructure of other components of the ECM.[37, 38] It has been used for the construction of polyelectrolyte multilayers[39] and hydrogels[23] for mammalian cell culture. Chondroitin sulfate has been used in biomaterials, and it has been shown to support mammalian cell growth when used in hydrogels[20] or polyelectrolyte multilayers.[40] Chondroitin sulfate forms a semiflexible coil in solution with an intrinsic persistence length in the range of 4.5-5.5 nm.[41] All of these polysaccharides are biodegradable; degrading into inert products such as di- and mono-saccharides (carbohydrates).

Naturally derived polymers are attractive for the construction of tissue engineered constructs due to their biocompatibility, biodegradability, and ability to bind and stabilize important biomolecules such as growth factors. One of the key features of natural polymers in their native biological environments is their nanoscale assembly, as illustrated by the components of the ECM illustrated in Figure 2.1. This native nanoscale assembly can be exploited to create constructs which mimic the native ECM and control cell response. The next section, will review a series of current techniques available to create nanostructured soft

materials. It will be divided into three main sections including nanoparticles, surface structures, and nanofibers.

2.3 Engineering Soft Material Nanostructures

There are many techniques currently being investigated for the construction of soft nanostructures. In the following section a brief review of different nanostructures is presented. We discuss both how the properties of soft materials can be used to engineer their nanostructure and how these nanostructures can be used to tune cell responses. Engineering of these structures can be applied to both naturally derived and synthetic polymers. The nanostructure of synthetic polymers (or combinations of naturally derived and synthetic polymers) has been engineered to tune the biological response to non-natural soft biomaterials. These include, most notably, polyesters such as poly(ε-caprolactone) and poly(L-lactic acid), which have been successfully used for constructs dedicated to the regeneration of bone and cartilage.[20] Natural polymers can also be blended with synthetic polymers to change their chemical, physical, or mechanical properties.[42]

2.3.1 Nanoparticles

Nanoparticles have a wide range of applications in biomedicine, as vehicles for delivery of therapeutics (via topical, oral, parenteral, and pulmonary administration), as means of introducing topographical features on smooth surfaces, and contrast agents for imaging. Nanoparticles (NP) are very attractive as drug delivery vehicles because their size alone can be engineered to influence cellular behavior such as cellular uptake.[42] For example, Desai et al. investigated the effect of particle size in gastrointestinal uptake using biodegradable particles made from poly(lactic-co-glycolic)acid.[43] The particles were formulated using an emulsion technique, and they investigated the uptake of the particles in the intestinal loop in

rat with particles diameter ranging from 100 nm to 10 µm. They discovered that the uptake of

the nanoparticles (100 nm in diameter) was from 15-fold to 250-fold higher compared to the

larger microparticles (10 µm in diameter). Size differences in the nanometer scale also

greatly affect blood circulation time and availability of the particles in the body.[44] Particles

with diameters less than 10 nm are quickly removed from the body through renal clearance

and extravasation.[42] Particles with diameter between 100-200 nm demonstrate the most

prolonged blood circulation times.[45] While particles greater than 200 nm are sequestered in

the spleen and eventually removed via phagocytosis.[46]

Several methods for creating soft nanoparticles have been investigated (Table 2.2) which

are applicable to both biological and synthetic polymers. In the following two sub-sections,

emulsions and self-assembly methods are discussed.

Table 2.2 Reference list of soft nanostructured nanoparticles discussed in this section

Soft Nanostructure Nanoparticles	References
Emulsions	48, 125
Self-Assembled	
Amphiphiles	58, 59
Polyelectrolytes	61, 126

2.3.1.1 Emulsions

An emulsion is a mixture of two or more immiscible fluids, one making up a dispersed

phase, and the other a bulk phase. One technique available to create nanoparticles through

emulsions is the oil-in-water method. Oil-in-water (O/W) emulsions consists of small lipid

(oil) droplets dispersed in aqueous medium.[47] The emulsion is created by mechanical

agitation of the heterogeneous mixture with the addition of a surfactant. The surfactant is

added to stabilize the droplets against molecular diffusion, degradation, and against

coalescence by collisions.[48] Molecules dissolved in the oil phase can then be precipitated,

29

creating nanoparticles. These molecules could be proteins,[49] polymers or monomers to induce polymerization (emulsion polymerization),[50] drugs,[51] inorganics[52] and others. The technique used for mechanical agitation will have an effect on particle size. Low-energy techniques (such as stirring) will results in large particles with a non-homogenous size distributions, while high-energy techniques (such as ultrasonication) result in small particles with a homogenous size distribution.[48] Agitation time also has been shown to have an effect on particle size.[53] Surfactants lower the interfacial tension, and improve the stability of smaller particles resulting in reduced particle size.[54] Both the type of surfactant and amount of surfactant used will have a great effect on particle size. Landfester et al. investigated the effect of amount of surfactant (sodium dodecyl sulfate) on latex particles prepared via an O/W emulsion polymerization.[53] They noticed that particle size decreased with increasing concentration of surfactant. Mun et al. investigated the effect of using either sodium dodecyl sulfate or Tween 20 as surfactants for O/W droplets coated with chitosan.[47] They found that more stable emulsions were created using Tween 20 for their system. Variations in the amount of the dispersed phase (volume fraction) also affect the size of the emulsion. An increase in diameter was noted on O/W emulsions when the solid content was increased from 5% to 25%.[48] The O/W method creates particles in solvents, which are often toxic. Thus, in order to use the resultant nanoparticles in biological applications the solvent must be removed, usually by drying or solvent extraction. Several factors have been identified which affect the efficiency of these processes including: including entrapped particle solubility, internal morphology, solvent type, diffusion rate, temperature, solvent viscosity, solvent vapor pressure, and particulate loading.[55] Many types of nanoparticles have been created

through the O/W emulsion and solvent removal method to study cell response; a few of them will be discussed bellow.

Recently, heparin-conjugated poly(L-lactide-*co*-glycolide) (PLGA) nanospheres were constructed for the delivery of the growth factor FGF-2 through the O/W emulsion and solvent evaporation method.[49] The nanospheres with FGF-2 were loaded on a fibrin gel and the bioactivity of the growth factor was assessed using human umbilical vein endothelial cells (HUVECs). The nanospheres allowed for a controlled released of FGF-2, and proliferation of the HUVECs was enhance when they where in contact with the nanospheres in comparison to delivery of soluble FGF-2 (Figure 2.3). The nanospheres not only allowed for controlled release of the drugs, but may also have influenced the cell response by introduction of nano-scale topographical features.

bFGF daily injection   **bFGF/Fibrin**   **bFGF /HCPNs /Fibrin**
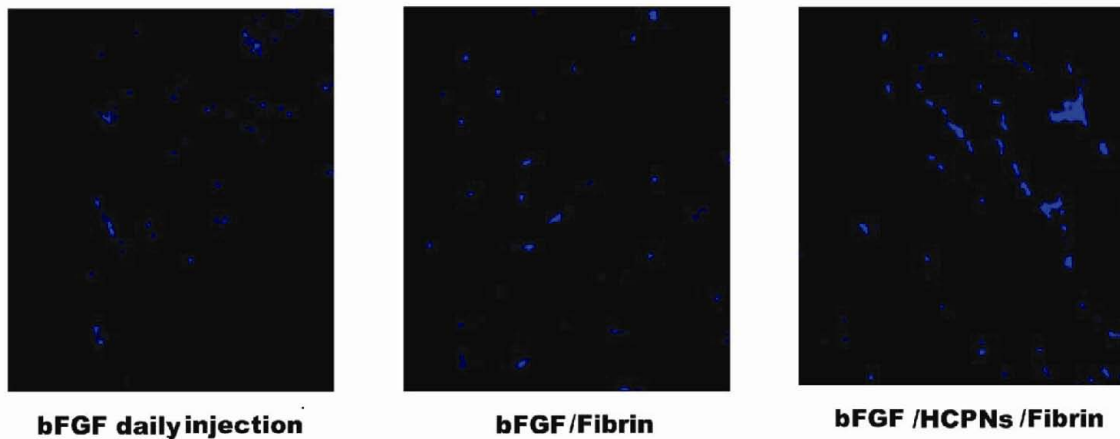
Figure 2.3 Immunohistochemical analysis of mouse ischemic limbs 4 weeks after treatment with FGF loaded nanoparticles. The specimens were stained with cyanine-conjugated vWF antibodies, which binds specifically to endothelial cells. Note that the delivery of FGF through the heparin modified nanoparticles induce higher growth of endothelial cell when compared to FGF delivered in solution or through a fibrin gel. HCPNs = Heparin-conjugated PLGA nanospheres. (Reprinted from Biomaterials, 27/8, O. Jeon, S. Kang, H. Lim, J.H. Chung, B. Kim, Long-term and zero-order release of basic fibroblast growth factor from heparin-conjugated poly(L-lactide-co-glycolide) nanospheres and fibrin gel, 1598-1607, Copyright 2006, with permission from Elsevier.)

Other investigators have studied similar nanospheres with different cell types yielding similar results.[56] Yilgor et al.[57] created PLGA and poly(3-hydroxybutyrate-*co*-3-hydroxyvalerate) (PHBV) nanocapsules loaded with BMP-2 and BMP-7 respectively. These nanocapsules were incorporated onto a 3-D chitosan fiber mesh and cell response studies were performed using bone marrow-derived rat mesenchymal stem cells (MSCs). The incorporation of the nanocapsules onto the fiber mesh yielded a higher alkaline phosphatase (ALP), a specific marker for osteogenesis, activity over the fiber mesh without the nanocapsules (Figure 2.4).
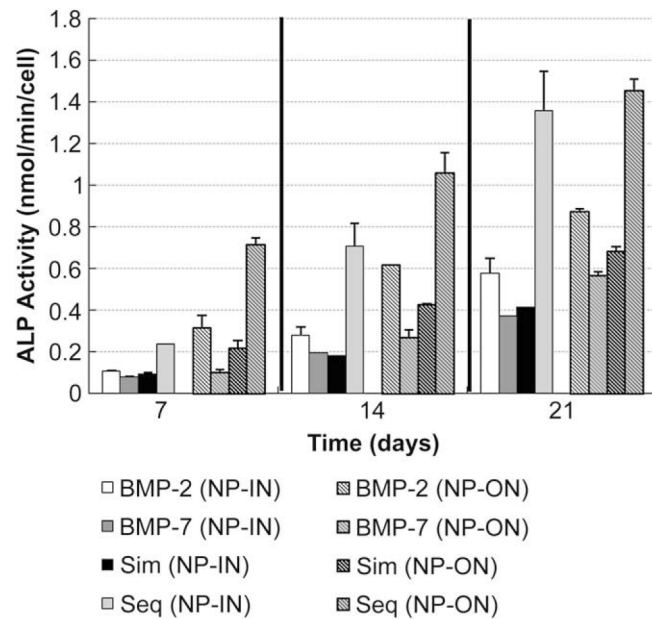
Figure 2.4 Specific ALP activity on BMP-loaded particles incorporated chitosan fiber mesh scaffolds. "Sim" denotes simultaneous delivery of BMP-2 and BMP-7, "seq" denotes sequential delivery of BMP-2 and BMP-7, "NP-IN" denotes for nanoparticles that were incorporated into the fibers by allowing them to mix in the chitosan solution before electrospinning, "NP-ON" denotes nanoparticles which were applied on the fibers after electrospinning by a series of vacuum-pressure cycles. (Reprinted from Biomaterials, 30/21, P. Yilgor, K. Tuzlakoglu, R.L. Reis, N. Hasirci, V. Hasirci, Incorporation of a sequential BMP-2/BMP-7 delivery system into chitosan-based scaffolds for bone tissue engineering, 3551-3559, Copyright 2009, with permission from Elsevier.)

2.3.1.2 Self-Assembled

Self-assembled nanoparticles are formed when the materials themselves phase separate to form nanoparticles, as opposed to the solvent/non-solvent induced phase separation used in emulsion-based techniques described above. Self-assembled nanoparticles can be engineered by controlling the intermolecular forces responsible for their assembly. These forces are tuned by altering the chemistry of the constituent molecules, and by adjusting the assembly conditions, such as temperature and solution pH.

Peptide amphiphiles (PA) are nanometer-sized molecules with a peptide "head group" covalently linked to a hydrophobic "tail." The peptide head group forms a distinct structural element and may introduce some useful biochemical functionality (Figure 2.5). The hydrophobic tail serves to align the peptide strands and induce secondary (α-helices and β-sheets)[58] and tertiary structure ($\beta/\alpha/\beta$ motif, hairpin, α-helical-coiled coil, α-helical bundle, Jelly Roll, and the Greek Key).[58] The tail also provides a hydrophobic surface for self-association and/or interaction with other surfaces. Some PA are a promising class of nanoscale biomaterials which can be tuned to promote or inhibit behaviors such as cell proliferation. PA can form nanospheres and nanofibers.
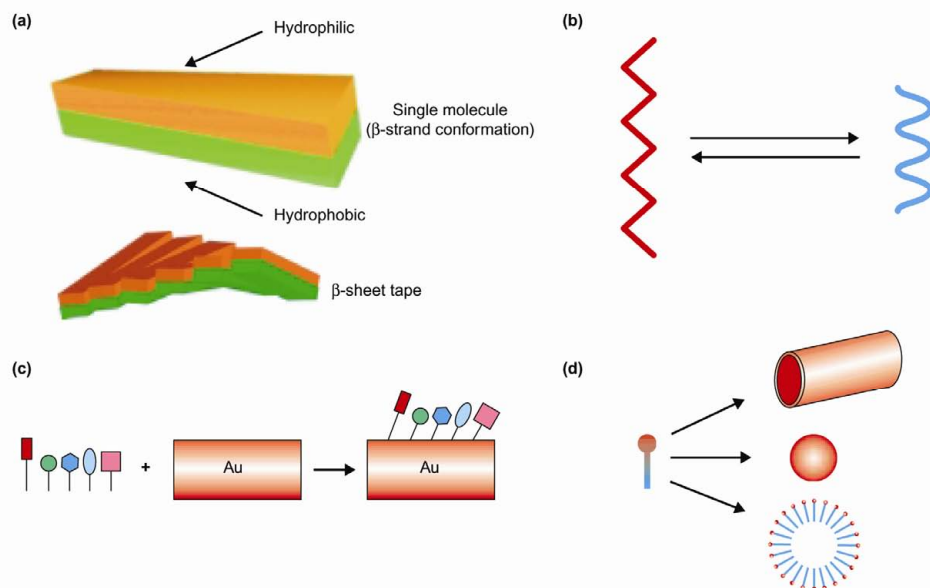
Figure 2.5 Various type of self-assembling peptide systems. (a) Amphiphilic peptides in β-strand conformation are chiral objects. As a consequence, they self-assemble into twisted tapes. (b) Helical dipolar peptides can undergo a conformational change between α-helix and β-sheet, much like a molecular switch. (c) Surface-binding peptides can form monolayers covalently bound to a surface. (d) Surfactant-like peptides can form vesicles and nanotubes. (Reprinted from Current Opinion in Chemical Biology, 6, S. Zhang, D. Marini, W. Hwang, S. Santoso, Design of nanostructured biological materials through self-assembly of peptides and proteins, 865-871, Copyright 2002, with permission from Elsevier.)

Fields et al. developed peptide amphiphiles with a collagen-like structural motif comprised of a dialkyl ester lipid tail with a collagen model peptide head group with a cell-binding sequence that promotes cell spreading.[59] Using human melanoma cells they demonstrated that the PA promotes cell adhesion and spreading. Recently, Aulisa et al. developed a PA which self-assembles into micelles and shows inhibition of pancreatic cancer cells, leukemia cells, and melanoma cells while non-cancerous fibroblast are less affected.[60] The small size of the PA along with a specific gene added to promote cell uptake of the PA allowed for the cancerous cells to absorb the PA to inhibit their proliferation.

The electrostatic interactions of polyelectrolytes can also be exploited to yield different types of assemblies. The complexation of oppositely charged polyelectrolytes to form soluble polyelectrolyte complex nanoparticles (PCNs) has been studied for over 30 years.[61, 62]

Nonetheless, the application of this technology to form nanoparticles of soft biomaterials remains an active area of research. The complexation of oppositely charged polyelectrolytes in solution can lead to the formation of colloidally stable nanoparticles by several mechanisms. Generally, one of the charged polymer chains must be in excess. As the polyelectrolyte in default complexes with the polyelectrolyte in excess, some charge neutralization occurs, forming hydrophobic regions along portions of the polymer chains that are complexed. The hydrophobic regions of these primary complexes tend to aggregate, forming a hydrophobic core, surrounded by a charged, hydrophilic corona. However, some residual surface charge is required to ensure the colloidal stability of the particles. Thus, as the condition of one-to-one charge complexation is approached, the complexes begin to aggregate, forming larger particles and may completely precipitate from solution.

The size distribution of PCNs tends to be relatively broad. The mean particle size is influenced by a number of factors related to the mechanism of particle formation. Both the complexation between the oppositely charged groups responsible for PCN formation, and the repulsion between the PCN that keeps them from aggregating are due to electrostatic forces. Thus the same conditions that promote the growth of PCN also tend to stabilize the smaller particles. Any system parameter that promotes the complexation to form larger particles by influencing the electrostatics might also tend to favor the stabilization of smaller ones. For instance, as more of the polyelectrolyte in default is added, the particles may initially collapse to smaller diameters as the magnitude of the charge density in the corona is reduced.[63] However, at higher contents of the excess charged group, the stability of smaller particles is increased, while at lower contents of the excess charged group, the smaller particles tend to be less stable and form aggregates.[64] If the charge density is reduced

sufficiently, the smallest particles lose their colloidal stability altogether, and larger particles or aggregates are favored near the one-to-one charge mixing ratio. Similarly, solution ionic strength can also influence the sizes of the particles formed by affecting the charge screening length, thereby influencing the electrostatic interactions responsible for the attractive forces and stabilization of PCNs. Solution ionic strength can also influence the osmotic pressure within the complexes. Thus, increasing ionic strengths can lead to both disintegration of the particles and aggregation, depending upon the system.[65] For weak polyelectrolytes, the pH of the solutions in which the PCN are formed can also be used to tune the electrostatic interactions.[66]

Our lab and others have studied the formation of polyelectrolyte complex nanoparticles using polysaccharides.[64, 67] In these studies, tuning of the composition and particle size have been demonstrated by changing the charge mixing ratios and polymer molecular weights. The complexation between proteins and synthetic polyelectrolytes has also been studied.[68] In one such study, the aggregation of these complexes was shown to depend only on the mixing ratios of the polymer and protein, and not on their concentrations.[69]

PCN can be used to decorate surfaces to induce topographical changes, and for localized delivery of important molecules such as proteins. In fact, chitosan/dextran sulfate polyelectrolyte nanoparticles have been developed for the delivery FGF-10[70] and vascular endothelial growth factor.[71] Hartig et al. recently reported that positively charged PCN containing polysaccharides are rapidly taken up by microvascular endothelial cells, probably by micropinocytosis,[72] suggesting that nanoparticles are an effective means of delivering payloads to the intracellular space. In these studies, the particle size and surface chemistry are key parameters that must be tuned in order to elicit the desired cellular response.

2.3.2 Surface Structures

One of the ongoing challenges in creating biomaterials for tissue repair is their biocompatibility. In particular, many metals and other hard materials are currently being used as biomaterials with limited biocompatibility. To improve the biocompatibility of these materials, researchers have been investigating different surface modifications which could promote or inhibit cell and protein adhesion, ultimately influencing the behaviors of native tissue cells, immune cells, and pathogenic microorganisms such as bacteria and fungi. Soft materials are currently being used to decorate the surfaces of biomaterials with the end of improving wound healing, influencing the inflammation response, preventing thrombosis, and delivering therapeutic proteins and other molecules. Table 2.3 lists a few techniques available to modify surfaces using soft materials. These techniques allow the modification of both hard and soft surfaces. The surface techniques discussed in this section include polyelectrolyte multilayers, cell membrane-mimetic thin films, polymer brushes, and soft-lithography.

Table 2.3 Reference list of soft nanostructured surfaces discussed in this section

Soft Nanostructure surfaces	References
Self-Assembled	
Polyelectrolyte multilayers	73, 76, 82, 83
Cell membrane-mimetic thin films	87-89
Polymer brushes	92, 93
Soft-Lithography	103, 127
Electron beam	102, 104

2.3.2.1 Self-Assembled

Layer-by-layer (LBL) assembly of polyelectrolyte multilayers (PEM) was first introduced by Decher and coworkers.[73] This technology has gained attention as an attractive method of surface coating for a broad range of applications due to its simplicity and the control over coating thickness and composition that can be obtained at the nanometer length scale. The LBL assembly consists of successively adsorbing layers of a polyanion and polycation (or other asymmetrically interacting pair, such as a hydrogen-bond donor/acceptor pair) from solution onto charged substrates (Figure 2.6).

PEM have been constructed using bio-molecules such as DNA,[74] collagen,[75] the polysaccharides chitosan,[76] heparin,[76] hyaluronic acid,[77] chondroitin sulfate,[77] and synthetic polymers such as poly(styrene sulfonate) and poly(allylamine hydrochloride).[73] PEM assemblies can be used to mimic key features of ECM by using biopolymers and embedding important peptides and proteins. The growth factors BMP-2,[74] TGF-β3[32] and FGF-2[77] are a few of the many proteins that have been successfully delivered to cells using PEM retaining or enhancing their function. PEM have been constructed to deliver other types of molecules such as nanoparticles,[32] plasmid vectors[78] and drugs for cancer treatment.[79]
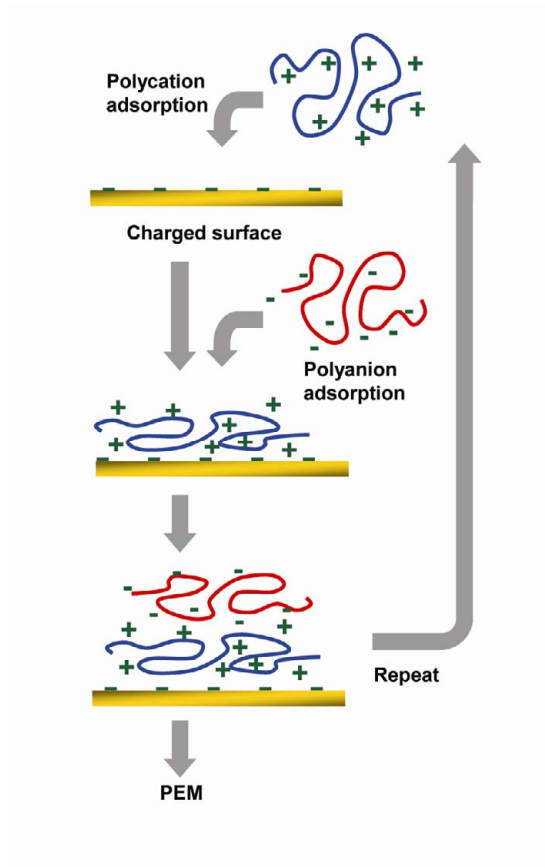
Figure 2.6 Construction of polyelectrolyte multilayers. A charged surface is exposed to a solution of an oppositely charged polyelectrolyte, resulting in polyelectrolyte adsorption and inversion of the surface charge. The charge inversion prevents additional adsorption of the polyelectrolyte, limiting the layer thickness. The surface is then rinsed and exposed to a polyelectrolyte with a charge opposite to that of the first polyelectrolyte. The surface charge is again inverted and the process can be repeated.

Engineering of PEM consists in being able to predictively tune their properties that will induce changes in cell behavior. PEM thickness, surface chemistry, stiffness, and surface roughness are just a few of the properties that researchers are investigating. The thickness of PEM can be tuned at the nanometer scale by adjusting the number of adsorbed monolayers, and the pH and ionic strength of the polyelectrolyte solution.[76] The effect of solution pH on the thickness of PEM has been investigated for weak,[80, 81] strong,[82] synthetic[81] and natural[76] polyelectrolytes. The thickness of PEM constructed using weak polyelectrolytes can be tuned with great control over a wide range of values in the nanometer scale. The pH dependence on

39

thickness for the polyanion/polycation pair of poly(acrylic acid)/poly(allylamine hydrochloride) was investigated by Shiratori et al., who noted that the thickness of an adsorbed polycation or polyanion layer can be tuned from 0.5 to 8 nm by adjusting the pH of the polymer solution.[80] Boddohi et al. investigated the change in thickness with increasing solution pH and ionic strength for the weak polycation/strong polyanion chitosan/heparin pair.[76] They determined that the PEM thickness could be increased from less than 2 nm per bilayer to more than 4 nm per bilayer with increasing solution pH and ionic strength.[76] At relatively high values of the solution ionic strength; however, pH had a greatly reduced affect on the layer thickness, presumably because of enhanced electrostatic screening effects. Both of these studies show how PEM thickness can increase as charge density on weak polyelectrolytes is decreased (by increasing pH or increasing ionic strength). This could be related to the conformation of the polyelectrolytes in solution, in addition to their interactions at the adsorbing surface. Polyelectrolytes with high charge densities tend to form a more stiff/extended conformation whereas those with a low charge density adopt a more coiled/globular conformation.[83] Strong polyelectrolytes, such as heparin, tend to be in a stiffer state forming thinner monolayers upon adsorption.

Cell behavior as a function of PEM thickness has also been investigated. Li et al. investigated the effect of PEM thickness on smooth muscle cell attachment using poly(allylamine hydrochloride)/poly(sodium 4-styrenesulfonate).[84] They observed that the roundness (and thus attachment) of the cells is greatly affected by the number of monolayers, with cells having a less-rounded, more natural morphology on the thicker films.[84] The interactions of photoreceptor cells and PEM was investigated by Tezcaner et al.[77] The viability of the photoreceptor cells varied with number of monolayer and terminated layer in

the poly(L-lysine)/chondroitin sulfate system.[77] In that system, the 20-monolayer films terminated with chondroitin sulfate were superior to 2-, 21-, and 41- monolayer PEM.[77]

The stiffness of PEM can also be tuned to control cell response.[85, 86] Ren et al. prepared PEM using the weak polycation/weak polyanion poly(L-lysine)/hyaluronan pair with stiffness values ranging between 3 kPa to 400 kPa by cross-linking the films using the 1-ethyl-3-(3-dimethylamino-propyl)carbodiimide (EDC) chemistry to modulate myoblast cell differentiation.[85] Myoblast adhesion, proliferation, and differentiation were strongly affected by PEM stiffness. On soft films, the myotubes exhibited a short and thick morphology, whereas on stiffer films the cells formed elongated and thin striated myotubes.

One of the most active areas of research involving PEMs is their use as coatings to enhance biocompatibility and/or deliver proteins or particles at the surface of metallic implants. Coronary stents,[75] dental screws, and orthopedic implants have all been coated with PEMs to enhance their biocompatibility both in vitro and in vivo. PEMs have also been used in the coating of soft materials such as microspheres.[32] Coating a smooth surface with a PEM will add nano-scale features which have been shown to enhance cell adhesion and proliferation. Recently, Yan et al.[78] investigated the plasmid uptake response of mesenchymal stem cells for differentiation on titanium films modified with PEMs. They compared smooth unmodified titanium surfaces (with plasmid delivered in solution) with those modified with a chitosan/plasmid DNA PEM. The modified titanium surfaces showed higher cell transfection, which led to high production of both alkaline phosphatase and osteocalcin, two differentiation markers (Figure 2.7)
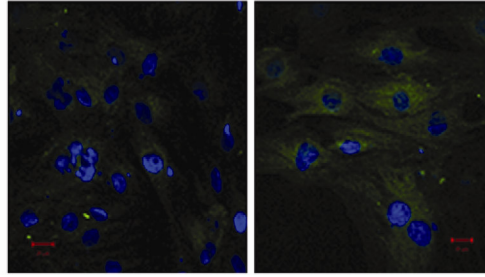
Figure 2.7 Expression of green fluorescence protein (GFP) of cells adhered on titanium surfaces 3 days after culture. (Left) Unmodified titanium surface with GFP plasmid vector delivered in solution with lipofectamine 2000. (Right) Titanium surface modified with chitosan/plasmid LBL assembly. The higher expression of GFP denotes a higher plasmid uptake by the cells. (Reprinted from Biomaterials, 30/21, Y. Hu, K. Cai, Z. Luo, R. Zhang, L. Yang, L. Deng, K.D. Jandt, Surface mediated in situ differentiation of mesenchymal stem cells on gene-functionalized titanium films fabricated by layer-by-layer technique, 3626-3635, Copyright 2009, with permission from Elsevier.)

A major factor to consider when designing biomaterials is their hemocompatibility. Hemocompatibility of implants can be enhanced by engineering surface coatings from different materials which can be modulated at the nano scale. Moreover, several groups have engineered biologically inert surfaces which mimic a blood cell membrane using polymeric phospholipids (Figure 2.8).[87-89] Plasma cell membranes consist of a combination of proteins and glycoproteins embedded on a lipid bilayer.[87] Over 100 different types of lipids are present in the hydrophobic and hydrophilic portion of the lipid bilayer.[87] The hydrophilic polar head groups are in contact with water, and thus are the main contributor to the interfacial properties of cell surfaces. The major phospholipid head group present in the cell outer membrane is phosphorylcholine.[88] Thus, researchers are investigating using phosphorylcholine-like molecules to coat surfaces to induce non-thrombogenic characteristics on potential biomedical implants. Gong et al. studied the adhesion of human macrophages onto different modified polypropylene surfaces.[90] Different types of plasma-treated polypropylene surfaces (ammonia, nitrogen, and oxygen) were investigated along with a phosphorylcholine-coated surface. The macrophages did not adhere to any of the

42

surfaces except for the phosphorylcholine-coated surface.[90] Their results provide new surfaces on which macrophages can be culture expanded and the interactions between macrophage and cell membrane can be investigated. Wilson et al. coated alginate microcapsules with a phospholipid layer and studied its biocompatibility in vivo.[91] The microcapsules were implanted into the peritoneal cavity of mice and removed after 4 weeks of implantation. The phospholipid-coated microcapsules demonstrated an improved biocompatibility since they were free of cell adhesion and fibrotic overgrowth compared to the non-coated capsule controls.
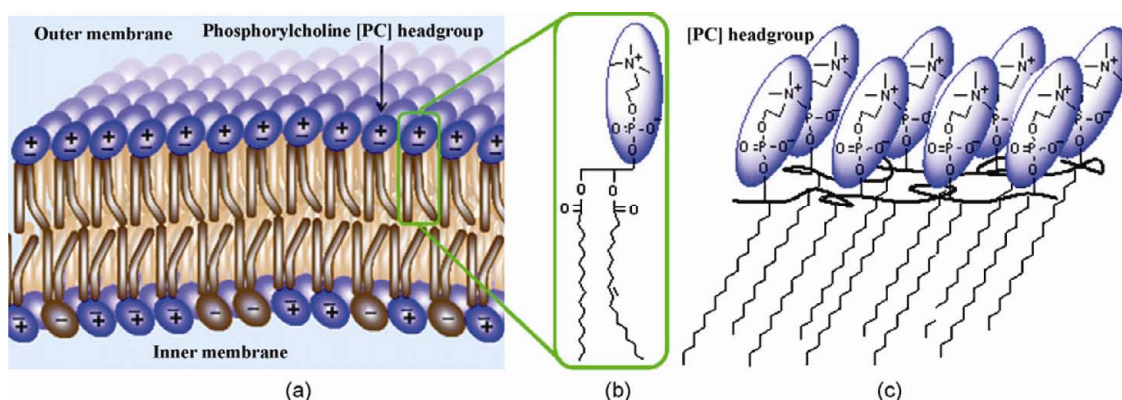
Figure 2.8 Schematic structures of the cell membrane and the outer membrane mimetic polymeric assembly: (a) lipid bilayer of cell membrane; (b) phosphatidylcholine; (c) cell membrane mimetic assembly with PC head group and synthetic polymer tails. (Reprinted from Applied Surface Science, 255/2, M. Gong, S. Yang, J. Ma, S. Zhang, F.M. Winnik, Y. Gong, Tunable cell membrane mimetic surfaces prepared with a novel phospholipid polymer, 555-558, Copyright 2008, with permission from Elsevier.)

2.3.2.2 Polymer Brushes

Polymer brushes are an assembly of polymer chains which are closely packed and anchored by one end to a surface.[92] The proximity of the polymer chains forces them to stretch away from the surface with a length significantly higher than the radius of gyration that the molecule would ordinarily adopt in solution.[92] These stretched configurations occur under equilibrium conditions, avoiding the need of a confining geometry or an external

43

field.[93] Polymer brushes can be applied in several systems including polymer micelles, block copolymers at fluid-fluid interfaces, grafted polymers on a solid surface, and diblock copolymers and graft copolymers at fluid-fluid interfaces. In general, there are two ways to create surfaces with polymer brushes, physisorption and covalent attachment.[93] In physisorption, the polymer chain adsorbs onto a surface with one end interacting strongly with the surface. Covalent attachment can be accomplished using either the "grafting to" or "grafting from" approaches. In the "grafting to" approach, a functionalized end of the chain reacts with an appropriate molecule on the surface to form the brushes. This approach generally yields low grafting densities and low film thickness. In the "grafting from" approach, an initiator is bounded to a surface, and polymer brushes are created through polymerization. The "grafting from" method generally yields high grafting density.[93] The type of initiator used and the method of polymerization are the two important adjustable parameters to control the characteristics of the brushes.

Physisorption is a reversible process achieved by the self-assembly of polymeric surfactants or end-functionalized polymers on a solid surface.[93] The several characteristic dimensions of the brushes, including surface grafting density, are controlled by thermodynamic equilibrium.[94] Physisorption of polymers occurs in the presence of selective solvents or selective surfaces, which gives selective solvation and selective adsorption, respectively. The structure of the brushes depends upon the selectivities of these media and the nature of the polymer (e.g. the architecture of the polymer, the length of the polymer, and the interaction between the polymer end and the surface).[93] Ideal solvents for physisorption are ones which act like a precipitant for one end of the polymer chain to permit it to anchor to the surface, while acting as a good solvent for the other end to form brushes in solution.

44

Physisorption interactions are in most cases van der Waals forces or hydrogen bonding. Desorption easily occurs upon exposure to other solvents or other harsh conditions.[93]

Polymer brushes make interesting systems to control cell behavior. Several types of cells have been successfully cultured in polymer brush systems including HUVECs,[95] neurons,[96] osteoblasts,[97] and fibroblasts.[98] Several groups are investigating the effect of brush thickness on cell adhesion using thermoresponsive polymer brushes.[98, 99] Using the "graft from" technique, Li et al. prepared a poly(*N*-isopropylacrylamide) gradient of polymer brushes on a silicon substrate with linear variation of thickness to study cell attachment and detachment by changes in temperature.[99] The variation in thickness was performed by changing the polymerization time. They used HepG2 cells, and discovered that cells could adhere at 37 °C and could be detached at 24 °C when the polymer brush thickness was in the range of 20–45 nm.[99] Wischerhoff et al. performed a similar study in which the thickness of the brushes was varied and cell adhesion experiments were performed using thermoresponsive polymers.[98] They tuned the thickness of their polymer brush by using the "graft from" approach on a PEM. The thickness of the underlying PEM was varied to yield a variation of polymer brush thickness. They studied fibroblast adhesion at 37 °C and detachment at 22 °C using systems with different thicknesses. They noticed that when the underlying PEM had 4 bilayers, which accounts for a brush thickness between 20 and 40 nm, the cells could attach at 37 °C and be detached at 22 °C.[98] Mei et al. prepared polymer brush surfaces using poly(2-hydroxyethyl methacrylate) to create a gradient substrate to modulate cell adhesion using fibronectin.[100] The gradient ranged from 2 to 8 nm and from a high graft density to a low graft density region. The substrate was coated with fibronectin, and fibroblasts were allowed to attach. They noticed that protein adsorption and cell adhesion was higher on the low grafting density

region. However, the trend is not linear since between 2 and 3 nm of film thickness the amount of protein adsorbed drops significantly while the cell density remains constant (Figure 2.9).[101]
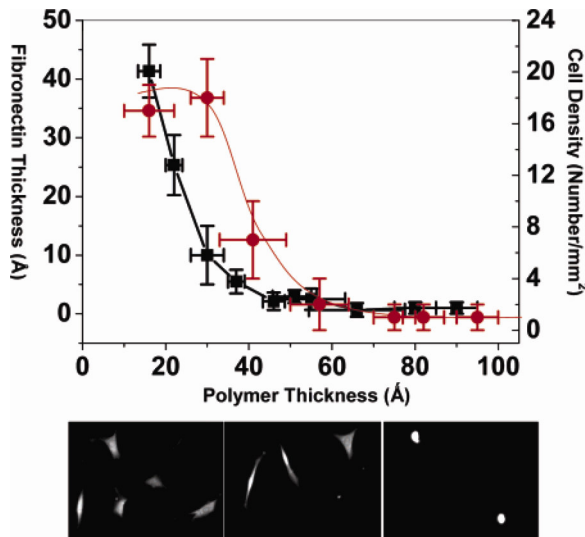
Figure 2.9 The effect of polymer brush thickness on the amount of adsorbed fibronectin, cell density, and cell morphology. The black and red lines represent the fibronectin thickness and cell density, respectively. The error bars are the standard from uncertainties from triplicate runs. The lines are to aid the reader's eye. (Reprinted with permission from Mei, Y.; Wu, T.; Xu, C.; Langenbach, K. J.; Elliott, J. T.; Vogt, B. D.; Beers, K. L.; Amis, E. J.; Washburn, N. R., Tuning cell adhesion on gradient poly(2-hydroxyethyl methacrylate)-grafted surfaces. *Langmuir* **2005,** *21* (26), 12309-12314. Copyright 2005 American Chemical Society.)

2.3.2.3 Soft-Lithography

Lithography encompasses a number of techniques which allow for the modification of the surfaces of materials. These modifications include adding topographical features at the microscale and nanoscale, such as pits, wells, arrays; and chemical and biochemical surface modifications. Lithographic methods are available for both soft and hard surfaces, in this section we will discuss several lithographic methods applied on soft surfaces. There are several lithographic methods to create patterns from the micrometer to the nanometer scale. These methods can be divided into several groups including: accelerated particle beam lithography, scanning probe lithography, photolithography, and contact printing. Accelerated

particle beam lithography involves using charged particles which are accelerated by electric fields and focused into a beam by magnets to strike a surface with high accuracy and nano-scale resolution.[102] One technique which falls in this category is electron beam lithography (EBL) which has a resolution of 10 nm. In scanning probe lithography, a probe, such as an atomic force microscope (AFM) tip, is used to alter surfaces to create features down to 20 nm.[102] Dip-pen lithography uses an AFM tip, which is dipped into a solution of biomolecules or other chemicals, and scans along the surface depositing the inked molecules.[102] In contact printing a pattern stamp is used to transfer material onto a surface. Micro-contact printing uses a flexible stamp to form patterns of self-assembled monolayers onto surfaces with a resolution of 35 nm.[103] In photolithography a structure is deposited onto a photoresist surface using UV light. It has a resolution of about 250 nm, but depends upon the wavelength of light used.[103] Each technique has a limitation on resolution, and on price. For example, EBL has excellent resolution (10 nm) but is an expensive technique and only allows for small area printing. Photolithography on the other hand is fairly inexpensive, allows for large area printing, but has a resolution of 250 nm and requires specific photoresist surfaces. All of these techniques can be used to modify surfaces to study cell responses to nanometer scale features on soft materials.

Recently, EBL was used to create nano-patterned surfaces onto poly(methylmethacrylate) to investigate the effect of symmetric and disordered patterns on MSC differentiation.[104] The behavior of the MSCs greatly differs between highly ordered patterns and random topographies. Indeed cells on the random topographies exhibited higher cell adhesion and enhancement in cell differentiation (Figure 2.10). Figure 2.10 demonstrates that not only cell behavior can be controlled by topographical features, but also by the spatial arrangement of

47

these features. Lithography may provide efficient tools for studying the interactions between cells and soft nanostructured materials
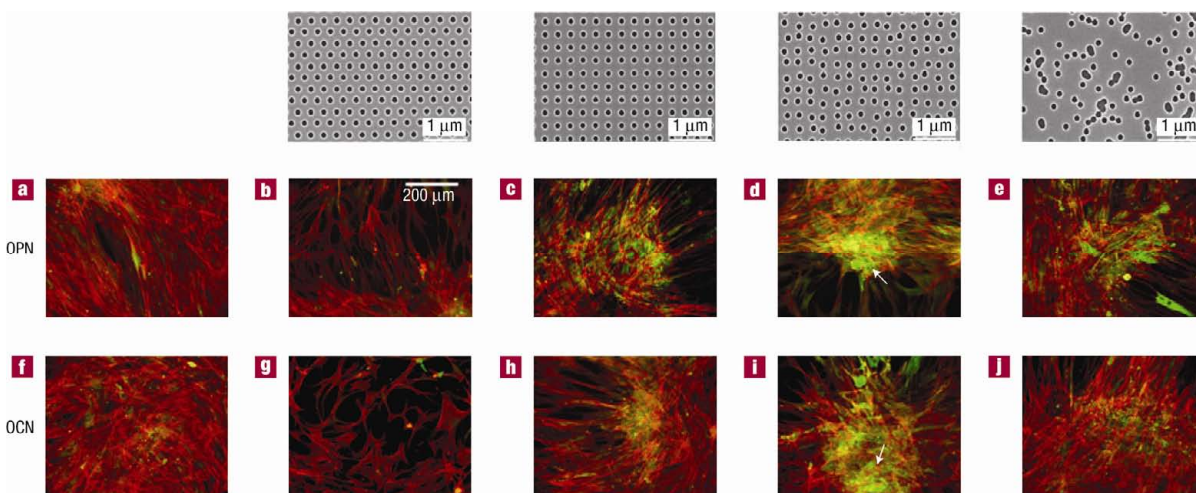
Figure 2.10 Osteopontin (OPN) and osteocalcin (OCN) staining of osteoprogenitor cells after 21 days of culture. The top row shows images of nanotopographies fabricated by EBL. All have 120-nm-diamter pits (100 nm deep, absolute or average 300 nm centre-centre spacing) with hexagonal, square, displaced square 50 (±50 nm from true centre) and random placements. **a-j**, Osteoprogenitors cultured on the control (**a,f**), note the lack of positive OPN and OCN stain; HEX (**b,g**), note the loss of cell adhesion; SQ (**c,h**), note reduced cell numbers compared with the control, but some OPN and OCN positive cells; DSQ50 (**d,i**), note bone nodule formation (arrows); RAND (**e,j**), note good cell populations with cells expressing OPN and OCN. Actin = red, OPN/OCN = green. (Reprinted by permission from Macmillan Publishers Ltd: Nature Materials, 6, M.J. Dalby, N. Gadegaard, R. Tare, A. Andar, M.O. Riehle, P. Herzyk, C.D.W Wilkinson, R.O.C. Oreffo, The control of human mesenchymal cell differentiation using nanoscale symmetry and disorder, 997-1003, Copyright 2007)

2.3.3 Nanofibers

Soft nanofibers are a very attractive class of biomaterials due to their simple preparation methods, which can provide an environment with features similar to those found in the native ECM. Indeed, nanofibers can be constructed form both biological and synthetic polymers to mimic the ECM of different hard and soft tissues. Different methods are available to create nanofibers (Table 2.4).

Table 2.4 Reference list of soft nanostructured nanofibers discussed in this section

Soft Nanostructure nanofibers	Reference
Electrospun	105, 106
Molecular Self-Assembled	119, 121, 128

2.3.3.1 Electrospun

Electrospinning is a simple and inexpensive method to create fiber meshes with diameters varying from 3 nm to more than 5 μm.[105] Electrospun nanofibers are formed when a polymer solution is drawn into a thin jet by a strong (~ 1 kV cm^{-1}) electrostatic field, concurrent with evaporation of the solvent and precipitation of the polymer. This is done in practice by slowly pumping a polymer solution through a needle set a controlled distance from a collector, with a voltage applied between the needle and the collector.[106] Although the apparatus is relatively simple to assemble and use, the process is very complex.[85] There are many adjustable experimental parameters and multiple kinetic processes occurring simultaneously. The flow of the polymer jet is occurring along with both conduction and advection of electrical current. Elongation of the jet occurs along with alignment of the polymer chains and evaporation of the solvent. Mechanical and electrical forces acting on the polymer solution jet result in a whipping instability that leads to further elongation of the jet as the solution approaches the collector. The simple spinning geometry uses a stationary flat plate as the collection electrode and results in a non-woven mat of fibers that have a random orientation of their axes in the plane of the collection electrode surface. Alignment of nanofibers can be achieved by altering the geometry of the electric field, and/or the grounded collector. This can permit axial alignment of fibers[107], and materials with anisotropic mechanical properties.[108]

Several different biological and synthetic polymers have been successfully electrospun including gelatin,[109] hyaluronic acid,[109] chitosan,[110] poly(ε-caprolactone) (PCL),[106] poly(L-lactic acid) (PLLA),[111] and others. The electrospinning process can be manipulated by a number of variables yielding fibers with different diameters. These variables include:

solution viscosity, solution charge density, solution surface tension, polymer molecular weight, dipole moment and dielectric constants, flow rate, electric field strength, distance between tip and collector, needle tip design and placement, collector composition and geometry, and ambient parameters such as temperature and humidity.[105] While complete descriptions of the electrospinning process would be quite complex, several theoretical approaches have enabled successful engineering of the electrospinning process. For example by assuming that the fiber forms as a purely viscous fluid jet, Fridrikh et al. derive a model for the terminal fiber diameter, which predicts that the fiber diameter should scale as the 2/3 power of the ratio of the solution flow rate to the electric current.[112] This model, although simplified, is parameterized by measurable properties of the polymer solution and correctly predicts the trend in fiber diameter for electrospun PCL from a few hundred nanometers to several microns.

Various researchers have investigated the effect of fiber diameter in cell behavior using several cell types. Cell morphology and proliferation of fibroblasts may not be sensitive to PLGA fiber diameter.[113] However, many other cell types have been demonstrated to exhibit significant functional responses to nanofiber size. Osteoprogenitor cells cultured on PLLA fibers had an increase of cell density with increasing fiber diameter.[114] However, decreasing nanofiber diameter has been demonstrated to enhance matrix production by chondrocytes,[115] cell spreading of rat marrow stromal cells,[116] and adhesion and proliferation of both HUVECs[117] and neural stem/progenitor cells (NSCs).[118] Reducing fiber diameter also results in a positive effect on cell differentiation of NSC into oligodendrocytes (Figure 2.11).[118] Adding particles to electrospun fibers is another modification which researchers have used to enhance bioactivity. Electrospun PLLA nanofibers grafted with hydroxyapatite (HA) have

been evaluated in response to human MSCs[118] and osteoblasts.[111] Cell adhesion and growth was enhanced for osteoblasts (Figure 2.12), while differentiation of human MSCs into chondrocytes was enhanced with the presence of hydroxyapatite nanoparticles in the fiber. The enhanced bioactivity with the presence of nanoparticles is most likely due to the topographical changes induced in the fibers making them structurally similar to native ECM.
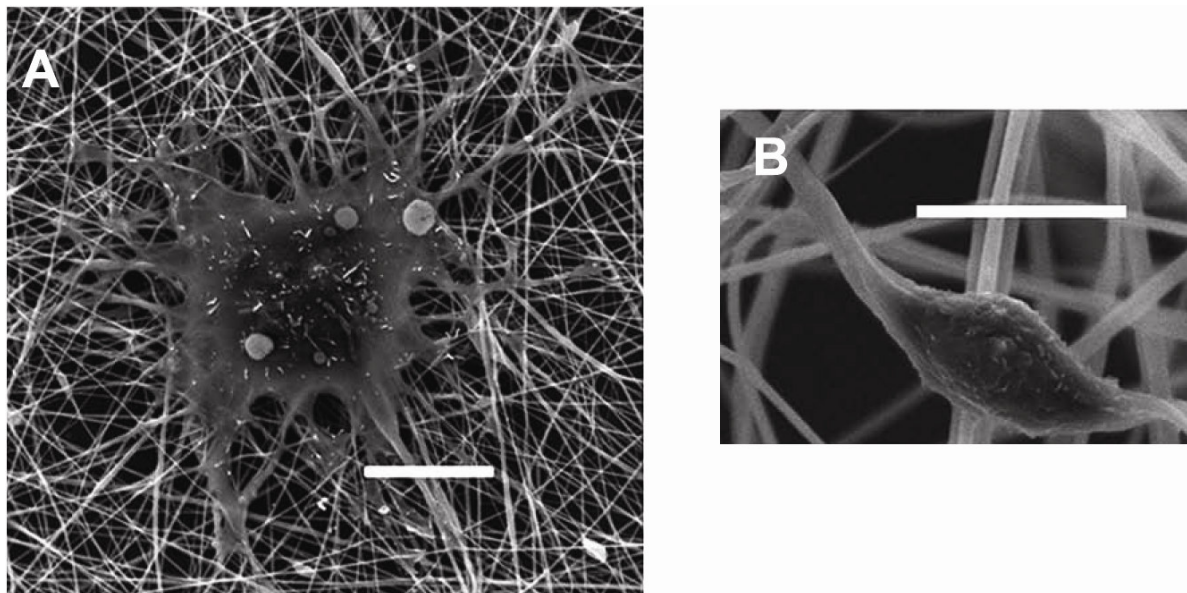
Figure 2.11 SEM images of rat NSCs cultured on polyethersulfone fiber meshes of varying fiber diameter. (A) Cells cultured on fiber mesh of 283 nm in diameter. (B) Cells cultured on fiber mesh of 746 nm in diameter. Note the improvement on cell spreading with the lower diameter meshes. Scale bar is 10 µm. (Reprinted from Biomaterials, 30/4, G.T. Christopherson, H. Song, H. Mao, The influence of fiber diameter of electrospun substrates on neural stem cell differentiation and proliferation, 556-564, Copyright 2009, with permission from Elsevier.)
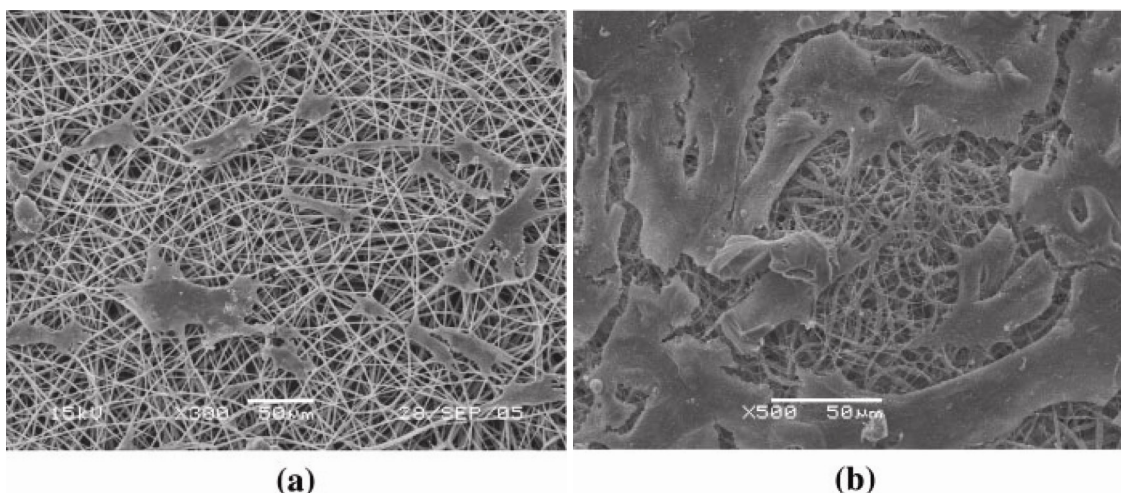
Figure 2.12 SEM images of osteoblast cell adhesion and growth on (a) PLLA and (b) PLLA/HA hybrid membranes. (Reprinted from Journal of Biomedical Materials Research Part A, 82A, G. Sui, X. Yang, F. Mei, X. Hu, G. Chen, X. Deng, S. Ryu, Poly-L-lactic acid/hydroxyapatite hybrid membrane for bone tissue regeneration, 445-454, Copyright 2007, Wiley)

2.3.3.2 Molecular Self-Assembly

Molecular self-assembly is controlled by weak non-covalent bonds (hydrogen bonds, electrostatic interactions, hydrophobic interactions, van der Walls, water-mediated hydrogen bonds, etc.), which may be relatively small in isolation, but when combined together govern the structure of all biological macromolecules.[119] Self-assembled peptide-based nanofiber scaffolds are a class of self-assembled nanostructures that are attractive for regenerative medicine. These nanofibers are created using the "bottom-up" approach beginning with an alternating sequence of amino acids that contains charged residues. Due to hydrophilic and hydrophobic interactions, these peptides form β-sheets structure spontaneously. Finally these β-sheet structures are ion screened, by varying the pH of the solution, to form 3-D scaffolds of nanofibers of ~10 nm in diameter.[120] Self-assembled peptides are very attractive because they can be designed at the single amino acid level, which can be tailored to specific amino acid sequences that change cell behavior. Also, they can be formed in the presence of cells to encapsulate cells in a 3-D environment. Indeed, Horii et al. prepared peptide nanofibers

52

designed specifically for osteoblasts.[121] Their peptide scaffolds contained osteoblast-specific motifs including: osteogenic growth peptides, bone-cell secreted-signal peptides, osteopontin cell adhesion motifs, and RGD binding sequences. They seeded pre-osteoblast cells on the specific osteogenic peptide scaffold and on a non-specific peptide scaffold. The osteogenic specific scaffold demonstrated significant improvement in cell proliferation (Figure 2.13) and osteogenic differentiation. Others have developed peptide self-assembled scaffolds to tune the adhesion and spreading of fibroblasts using the RGD sequence.[122] Peptide nanofibers have also been used as delivery vehicles for important growth factors. Stendahl et al. conducted an in vivo study using heparin-binding peptide amphiphile nanofibers to deliver VEGF and FGF-2.[123] They implanted their scaffolds in the omentum of mice with induced diabetes. Their scaffolds induced significant increases in blood vessel density over the control scaffold with no growth factor. Their results pave the way for new therapies for controlling diabetes.
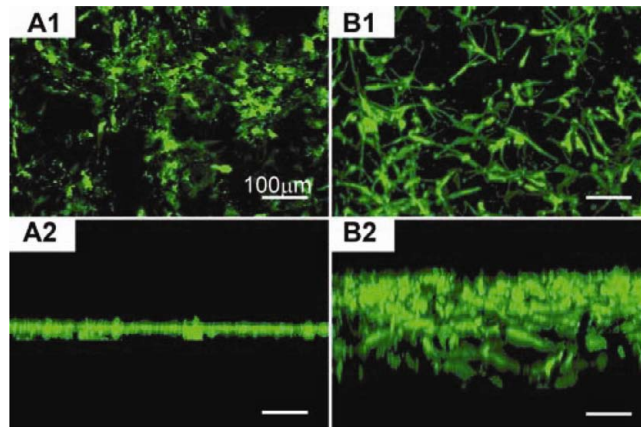
Figure 2.13. Reconstructed image of 3-D confocal micrographs of culturing on the different scaffolds consisting of different mix ratio of RADA16 1% (w/v) and PRG 1% (w/v) using calcein-AM staining. The bar represents 100 μm. A1 and A2: 10% of the 2-unit RGD binding sequence PRG and B1&B2: PRG 70%. A1 and B1 are vertical view and A2 and B2 are horizontal view. In the case of 10% PRG scaffold, the cells were attached on the surface of the scaffold whereas the cells were migrated into the scaffold in the case of 70% PRG scaffold. There is a drastic cell migration into the scaffold with higher concentration of PRG motif. (Reprinted from Horii A, Wang X, Gelain F, Zhang S (Copyright 2007) Biological Designer Self-Assembling Peptide Nanofiber Scaffolds Significantly Enhance Osteoblast Proliferation, Differentiation and 3-D Migration. PLoS ONE 2(2): e190. doi:10.1371/journal.pone.0000190)

2.4 The Future of Engineering Soft Nanostructures for Guided Cell Response

In the past two decades there has been an explosion in the development of nanostructured soft materials for biomedical technologies, fueled in no small part by advances in techniques for synthesizing and characterizing materials with features at the nanometer length scale. These advances have enabled us to begin understanding how biochemical and biomechanical properties emerge from the organization of organs and tissues at multiple length scales. Our ability to control and engineer these soft nanostructures is maturing to the point where dimensions can be tuned with sub-nanometer, and in some cases molecular resolution. Nanostructures of varying geometries can be reproducibly created, including ultra-thin films, fibers, and spherical particles, using a variety of materials that range from those with potent biochemical activity to the biologically inert. With this repertoire of building blocks at our disposal, we are now exploring the construction of more complex nanoassemblies,[126] and one can begin to imagine the reconstruction of at least some features of the exquisite hierarchy found in natural tissues.

Transformative advancements in this field will be realized when we move from describing cell behavior, to developing predictive theories of the mechanisms by which cells respond to the myriad stimuli provided by soft nanostructures. To begin with, well-defined and validated nanostructures can be used as platforms to catalog the influence of nanoscale features on cell adhesion, cell proliferation, cell migration, protein transcription and cell-cell communication. In many cases, the current observations of cell response to nanostructures produce as many or more questions as they have answered. While the questions that have been answered are often, "What will the response be?", the questions that are left unanswered are often of a more mechanistic nature, such as "Why do the cells respond this way?" and

"What if this parameter is varied?" These are the types of questions that can be answered by predictive models of cell-nanomaterial interactions. Engineered nanostructures will then provide the realm in which to test and refine these theories.

From predictive theories describing the cell responses to biomaterials, engineering design principles can be developed whereby biomaterials scientists can design novel nanostructures for new biomedical applications. Furthermore, theoretical limits defining upper and lower bounds of cell response functions can be defined, which can guide the development of solutions to new problems. This exciting field offers the opportunity for biomaterials scientist to also make contributions to the biological sciences, by providing new tools and theories to study cellular and molecular biology. The application of materials science to biological materials has already revealed much about the behavior of biomolecules, cells, and tissues, by viewing them as soft nanostructures. Future developments along the lines of predictive theories of cell-nanomaterial interactions will enable realization of the great promise of engineered soft nanostructures for biomaterials.

2.5 References

1. Langer, R.; Vacanti, J. P., TISSUE ENGINEERING. *Science* **1993,** *260* (5110), 920-926.
2. Howard, D.; Buttery, L. D.; Shakesheff, K. M.; Roberts, S. J., Tissue engineering: strategies, stem cells and scaffolds. *J Anat* **2008,** *213* (1), 66-72.
3. Crouzier, T.; Ren, K.; Nicolas, C.; Roy, C.; Picart, C., Layer-By-Layer Films as a Biomimetic Reservoir for rhBMP-2 Delivery: Controlled Differentiation of Myoblasts to Osteoblasts. *Small* **2009,** *5* (5), 598-608.
4. Mow, V. C.; Ratcliffe, A.; Poole, A. R., Cartilage and Diarthrodial Joints as Paradigms for Hierarchical Materials and Structures. *Biomaterials* **1992,** *13* (2), 67-97.
5. Horkay, F.; Basser, P. J.; Hecht, A. M.; Geissler, E., Gel-like behavior in aggrecan assemblies. *Journal of Chemical Physics* **2008,** *128* (13), 7.

6. Lee, S. H.; Shin, H., Matrices and scaffolds for delivery of bioactive molecules in bone and cartilage tissue engineering. *Adv. Drug. Deliver. Rev.* **2007,** *59* (4-5), 339-359; Roughley, P. J.; Melching, L. I.; Heathfield, T. F.; Pearce, R. H.; Mort, J. S., The structure and degradation of aggrecan in human intervertebral disc. *Eur Spine J* **2006,** *15*, S326-S332.

7. Papagiannopoulos, A.; Waigh, T. A.; Hardingham, T.; Heinrich, M., Solution structure and dynamics of cartilage aggrecan. *Biomacromolecules* **2006,** *7* (7), 2162-2172.

8. Dudhia, J., Aggrecan, aging and assembly in articular cartilage. *Cell Mol Life Sci* **2005,** *62* (19-20), 2241-2256.

9. Pratta, M. A.; Yao, W. Q.; Decicco, C.; Tortorella, M. D.; Liu, R. Q.; Copeland, R. A.; Magolda, R.; Newton, R. C.; Trzaskos, J. M.; Arner, E. C., Aggrecan protects cartilage collagen from proteolytic cleavage. *J. Biol. Chem.* **2003,** *278* (46), 45539-45545.

10. Hamley, I. W., *Introduction to Soft Matter: Synthetic and Biological Self-Assembling Materials*. Wiley: Chichesteer, 2007; Dutcher, J. R.; Marangoni, A. G., *Soft Materials: Structure and Dynamics*. Marcel Dekker: New York, **2005**.

11. Park, S.; Hung, C. T.; Ateshian, G. A., Mechanical response of bovine articular cartilage under dynamic unconfined compression loading at physiological stress levels. *Osteoarthritis and Cartilage* **2004,** *12* (1), 65-73.

12. Atkins, P. W., *Physical Chemistry*. 4th ed.; W.H. Freeman and Company: New York, 1990.

13. Hanshaw, R. G.; Stahelin, R. V.; Smith, B. D., Noncovalent keystone interactions controlling biomembrane structure. *Chemistry-a European Journal* **2008,** *14* (6), 1690-1697.

14. Brannigan, G.; Brown, F. L. H., Solvent-free simulations of fluid membrane bilayers. *J Chem Phys* **2004,** *120* (2), 1059-1071.

15. Stevens, M. M.; George, J. H., Exploring and engineering the cell surface interface. *Science* **2005,** *310* (5751), 1135-1138.

16. Shirley, A.; P., B.-H. R.; J., H. M.; E., K. K.; Adrian, S. C., *The Extracellular Matrix FactsBook*. Academic Press: San Diego, **1998**.

17. Lee, C. H.; Singla, A.; Lee, Y., Biomedical applications of collagen. *International Journal of Pharmaceutics* **2001,** *221* (1-2), 1-22.

18. Aigner, T.; Stove, J., Collagens - major component of the physiological cartilage matrix, major target of cartilage degeneration, major tool in cartilage repair. *Advanced Drug Delivery Reviews* **2003,** *55* (12), 1569-1593

19. Thierry, B.; Winnik, F. M.; Merhi, Y.; Silver, J.; Tabrizian, M., Bioactive coatings of endovascular stents based on polyelectrolyte multilayers. *Biomacromolecules* **2003,** *4* (6), 1564-1571.

20. Christenson, E. M.; Anseth, K. S.; van den Beucken, J. J. J. P.; Chan, C. K.; Ercan, B.; Jansen, J. A.; Laurencin, C. T.; Li, W.-J.; Murugan, R.; Nair, L. S.; Ramakrishna, S.; Tuan, R. S.; Webster, T. J.; Mikos, A. J., Nanobiomaterial applications in orthopedics. *J Orthop Res* **2007,** *25*, 11-22.

21. Kanai, A.; Kaufman, H. E., ELECTRON-MICROSCOPIC STUDIES OF ELASTIC FIBER IN HUMAN SCLERA. *Investigative Ophthalmology* **1972,** *11* (10), 816-&.

22. Salmivirta, M.; Lidholt, K.; Lindahl, U., Heparan sulfate: A piece of information. *Faseb Journal* **1996,** *10* (11), 1270-1279.

23. Suh, J. K. F.; Matthew, H. W. T., Application of chitosan-based polysaccharide biomaterials in cartilage tissue engineering: a review. *Biomaterials* **2000,** *21* (24), 2589-2598.

24. Durango, A. M.; Soares, N. F. F.; Benevides, S.; Teixeira, J.; Carvalho, M.; Wobeto, C.; Andrade, N. J., Development and evaluation of an edible antimicrobial film based on yam starch and chitosan. *Packaging Technology and Science* **2006,** *19* (1), 55-59;

25. Fujita, M.; Kinoshita, M.; Ishihara, M.; Kanatani, Y.; Morimoto, Y.; Simizu, M.; Ishizuka, T.; Saito, Y.; Yura, H.; Matsui, T.; Takase, B.; Hattori, H.; Kikuchi, M.; Maehara, T., Inhibition of vascular prosthetic graft infection using a photocrosslinkable chitosan hydrogel. *Journal of Surgical Research* **2004,** *121* (1), 135-140

26. Sechriest, V. F.; Miao, Y. J.; Niyibizi, C.; Westerhausen-Larson, A.; Matthew, H. W.; Evans, C. H.; Fu, F. H.; Suh, J. K., GAG-augmented polysaccharide hydrogel: A novel biocompatible and biodegradable material to support chondrogenesis. *Journal of Biomedical Materials Research* **2000,** *49* (4), 534-541; Raghunath, J.; Rollo, J.; Sales, K. M.; Butler, P. E.; Seifalian, A. M., Biomaterials and scaffold design: key to tissue-engineering cartilage. *Biotechnology and Applied Biochemistry* **2007,** *46*, 73-84.

27. Pusateri, A. E.; McCarthy, S. J.; Gregory, K. W.; Harris, R. A.; Cardenas, L.; McManus, A. T.; Goodwin, C. W., Effect of a chitosan-based hemostatic dressing on blood loss and survival in a model of severe venous hemorrhage and hepatic injury in swine. *Journal of Trauma-Injury Infection and Critical Care* **2003,** *54* (1), 177-182.

28. Mccaffrey, T. A.; Falcone, D. J.; Du, B. H., Transforming Growth Factor-Beta-1 Is a Heparin-Binding Protein - Identification of Putative Heparin-Binding Regions and Isolation of Heparins with Varying Affinity for Tgf-Beta-1. *J Cell Physiol* **1992,** *152* (2), 430-440.

29. Lyon, M.; Rushton, G.; Gallagher, J. T., The interaction of the transforming growth factor-beta s with heparin heparan sulfate is isoform-specific. *Journal of Biological Chemistry* **1997,** *272* (29), 18000-18006.

30. Damon, D. H.; Lobb, R. R.; Damore, P. A.; Wagner, J. A., HEPARIN POTENTIATES THE ACTION OF ACIDIC FIBROBLAST GROWTH-FACTOR BY PROLONGING ITS BIOLOGICAL HALF-LIFE. *Journal of Cellular Physiology* **1989,** *138* (2), 221-226.

31. Sato, M.; Ishihara, M.; Kaneshiro, N.; Mitani, G.; Nagai, T.; Kutsuna, T.; Asazuma, T.; Kikuchi, M.; Mochidal, J., Effects of growth factors on heparin-carrying polystyrene-coated atelocollagen scaffold for articular cartilage tissue engineering. *Journal of Biomedical Materials Research Part B-Applied Biomaterials* **2007,** *83B* (1), 181-188.

32. Park, J. S.; Park, K.; Woo, D. G.; Yang, H. N.; Chung, H. M.; Park, K. H., PLGA microsphere construct coated with TGF-beta 3 loaded nanoparticles for neocartilage formation. *Biomacromolecules* **2008,** *9* (8), 2162-2169.

33. Park, J. S.; Woo, D. G.; Yang, H. N.; Lim, H. J.; Chung, H. M.; Park, K. H., Heparin-bound transforming growth factor-beta 3 enhances neocartilage formation by rabbit mesenchymal stem cells. *Transplantation* **2008,** *85* (4), 589-596.

34. Zhao, B. H.; Katagiri, T.; Toyoda, H.; Takada, T.; Yanai, T.; Fukuda, T.; Chung, U. I.; Koike, T.; Takaoka, K.; Kamijo, R., Heparin potentiates the in vivo ectopic bone formation induced by bone morphogenetic protein-2. *Journal of Biological Chemistry* **2006,** *281* (32), 23246-23253.

35. Lee, J. Y.; Choo, J. E.; Choi, Y. S.; Lee, K. Y.; Min, D. S.; Pi, S. H.; Seol, Y. J.; Lee, S. J.; Jo, I. H.; Chung, C. P.; Park, Y. J., Characterization of the surface immobilized synthetic heparin binding domain derived from human fibroblast growth factor-2 and its effect on osteoblast differentiation. *Journal of Biomedical Materials Research Part A* **2007,** *83A* (4), 970-979.

36. Scheufler, C.; Sebald, W.; Hulsmeyer, M., Crystal structure of human bone morphogenetic protein-2 at 2.7 angstrom resolution. *Journal of Molecular Biology* **1999,** *287* (1), 103-115.

37. Lapcik, L.; Lapcik, L.; De Smedt, S.; Demeester, J.; Chabrecek, P., Hyaluronan: Preparation, structure, properties, and applications. *Chem Rev* **1998,** *98* (8), 2663-2684.

38. Laurent, T. C.; Fraser, J. R. E., HYALURONAN. *Faseb Journal* **1992,** *6* (7), 2397-2404.

39. Richert, L.; Lavalle, P.; Payan, E.; Shu, X. Z.; Prestwich, G. D.; Stoltz, J. F.; Schaaf, P.; Voegel, J. C.; Picart, C., Layer by layer buildup of polysaccharide films: Physical chemistry and cellular adhesion aspects. *Langmuir* **2004,** *20* (2), 448-458.

40. Jia, Y. T.; Gong, J.; Gu, X. H.; Kim, H. Y.; Dong, J.; Shen, X. Y., Fabrication and characterization of poly (vinyl alcohol)/chitosan blend nanofibers produced by electrospinning method. *Carbohydr. Polym.* **2007,** *67* (3), 403-409.

41. Rodriguez-Carvajal, M. A.; Imberty, A.; Perez, S., Conformational behavior of chondroitin and chondroitin sulfate in relation to their physical properties as inferred by molecular modeling. *Biopolymers* **2003,** *69* (1), 15-28.

42. Goldberg, M.; Langer, R.; Jia, X. Q., Nanostructured materials for applications in drug delivery and tissue engineering. *Journal of Biomaterials Science-Polymer Edition* **2007,** *18* (3), 241-268.

43. Desai, M. P.; Labhasetwar, V.; Amidon, G. L.; Levy, R. J., Gastrointestinal uptake of biodegradable microparticles: Effect of particle size. *Pharmaceutical Research* **1996,** *13* (12), 1838-1845.

44. Vinogradov, S. V.; Bronich, T. K.; Kabanov, A. V., Nanosized cationic hydrogels for drug delivery: preparation, properties and interactions with cells. *Advanced Drug Delivery Reviews* **2002,** *54* (1), 135-147.

45. Ishida, O.; Maruyama, K.; Sasaki, K.; Iwatsuru, M., Size-dependent extravasation and interstitial localization of polyethyleneglycol liposomes in solid tumor-bearing mice. *International Journal of Pharmaceutics* **1999,** *190* (1), 49-56.

46. Stolnik, S.; Illum, L.; Davis, S. S., LONG CIRCULATING MICROPARTICULATE DRUG CARRIERS. *Advanced Drug Delivery Reviews* **1995,** *16* (2-3), 195-214.

47. Saehun, M.; A., D. E.; Julian, M. D., Effect of molecular weight and degree of deacetylation of chitosan on the formation of oil-in-water emulsions stabilized by surfactant–chitosan membranes. *Journal of Colloid and Interface Science* **2005,** *296* (2).

48. Antonietti, M.; Landfester, K., Polyreactions in miniemulsions. *Progress in Polymer Science* **2002,** *27* (4), 689-757.

49. Jeon, O.; Kang, S. W.; Lim, H. W.; Chung, J. H.; Kim, B. S., Long-term and zero-order release of basic fibroblast growth factor from heparin-conjugated poly(L-lactide-co-glycolide) nanospheres and fibrin gel. *Biomaterials* **2006,** *27* (8), 1598-1607.

50. El-Aasser, M. S.; Sudol, E. D. In *Miniemulsions: Overview of research and applications*, Federation Soc Coatings Technology: **2004**; pp 21-31.

51. Prankerd, R. J.; Stella, V. J., THE USE OF OIL-IN-WATER EMULSIONS AS A VEHICLE FOR PARENTERAL DRUG ADMINISTRATION. *Journal of Parenteral Science and Technology* **1990,** *44* (3), 139-149.

52. Pileni, M. P., Nanosized particles made in colloidal assemblies. *Langmuir* **1997,** *13* (13), 3266-3276.

53. Landfester, K.; Bechthold, N.; Tiarks, F.; Antonietti, M., Formulation and stability mechanisms of polymerizable miniemulsions. *Macromolecules* **1999,** *32* (16), 5222-5228.

54. Tadros, T.; Izquierdo, R.; Esquena, J.; Solans, C. In *Formation and stability of nano-emulsions*, Elsevier Science Bv: **2004**; pp 303-318.

55. Odonnell, P. B.; McGinity, J. W., Preparation of microspheres by the solvent evaporation technique. *Advanced Drug Delivery Reviews* **1997,** *28* (1), 25-42.

56. Kim, S. E.; Jeon, O.; Lee, J. B.; Bae, M. S.; Chun, H. J.; Moon, S. H.; Kwon, I. K., Enhancement of ectopic bone formation by bone morphogenetic protein-2 delivery using heparin-conjugated PLGA nanoparticles with transplantation of bone marrow-derived mesenchymal stem cells. *Journal of Biomedical Science* **2008,** *15* (6), 771-777.

57. Yilgor, P.; Tuzlakoglu, K.; Reis, R. L.; Hasirci, N.; Hasirci, V., Incorporation of a sequential BMP-2/BMP-7 delivery system into chitosan-based scaffolds for bone tissue engineering. *Biomaterials* **2009,** *30* (21), 3551-3559.

58. Yu, Y. C.; Berndt, P.; Tirrell, M.; Fields, G. B., Self-assembling amphiphiles for construction of protein molecular architecture. *Journal of the American Chemical Society* **1996,** *118* (50), 12515-12520.

59. Fields, G. B.; Lauer, J. L.; Dori, Y.; Forns, P.; Yu, Y. C.; Tirrell, M., Proteinlike molecular architecture: Biomaterial applications for inducing cellular receptor binding and signal transduction. *Biopolymers* **1998,** *47* (2), 143-151.

60. Aulisa, L.; Forraz, N.; McGuckin, C.; Hartgerink, J. D., Inhibition of cancer cell proliferation by designed peptide amphiphiles. *Acta Biomaterialia* **2009,** *5* (3), 842-853.

61. Tsuchida, E., Formation of Polyelectrolyte Complexes and Their Structures. *J Macromol Sci Pure Appl Chem* **1994,** *A31* (1), 1-15.

62. Tsuchida, E.; Osada, Y.; Sanada, K., Interaction of poly(styrene sulfonate) with polycations carrying charges in the chain backbone. *J Polym Sci Polym Chem Ed* **1972,** *10*, 3397-3404.

63. Schatz, C.; Lucas, J. M.; Viton, C.; Domard, A.; Pichot, C.; Delair, T., Formation and properties of positively charged colloids based on polyelectrolyte complexes of biopolymers. *Langmuir* **2004,** *20* (18), 7766-7778.

64. Boddohi, S.; Moore, N.; Johnson, P. A.; Kipper, M. J., Polysaccharide-Based Polyelectrolyte Complex Nanoparticles from Chitosan, Heparin, and Hyaluronan. *Biomacromolecules* **2009,** *10* (6), 1402-1409.

65. Dautzenberg, H.; Jaeger, W., Effect of charge density on the formation and salt stability of polyelectrolyte complexes. *Macromol Chem Phys* **2002,** *203* (14), 2095-2102.

66. Hartig, S. M.; Carlesso, G.; Davidson, J. M.; Prokop, A., Development of improved nanoparticulate polyelectrolyte complex physicochemistry by nonstoichiometric mixing of polyions with similar molecular weights. *Biomacromolecules* **2007,** *8* (1), 265-272.

67. Schatz, C.; Domard, A.; Viton, C.; Pichot, C.; Delair, T., Versatile and efficient formation of colloids of biopolymer-based polyelectrolyte complexes. *Biomacromolecules* **2004,** *5* (5), 1882-1892.

68. Ball, V.; Winterhalter, M.; Schwinte, P.; Lavalle, P.; Voegel, J. C.; Schaaf, P., Complexation mechanism of bovine serum albumin and poly(allylamine hydrochloride). *Journal of Physical Chemistry B* **2002,** *106* (9), 2357-2364.

69. Schwinte, P.; Ball, V.; Szalontai, B.; Haikel, Y.; Voegel, J. C.; Schaaf, P., Secondary structure of proteins adsorbed onto or embedded in polyelectrolyte multilayers. *Biomacromolecules* **2002,** *3* (6), 1135-1143.

70. Huang, M.; Berkland, C., Controlled Release of Repifermin (R) from Polyelectrolyte Complexes Stimulates Endothelial Cell Proliferation. *Journal of Pharmaceutical Sciences* **2009,** *98* (1), 268-280.

71. Huang, M.; Vitharana, S. N.; Peek, L. J.; Coop, T.; Berkland, C., Polyelectrolyte complexes stabilize and controllably release vascular endothelial growth factor. *Biomacromolecules* **2007,** *8* (5), 1607-1614.

72. Hartig, S. M.; Greene, R. R.; Carlesso, G.; Higginbotham, J. N.; Khan, W. N.; Prokop, A.; Davidson, J. M., Kinetic analysis of nanoparticulate polyelectrolyte complex interactions with endothelial cells. *Biomaterials* **2007,** *28* (26), 3843-3855.

73. Decher, G., Fuzzy nanoassemblies: Toward layered polymeric multicomposites. *Science* **1997,** *277* (5330), 1232-1237.

74. van den Beucken, J.; Walboomers, X. F.; Boerman, O. C.; Vos, M. R. J.; Sommerdijk, N.; Hayakawa, T.; Fukushima, T.; Okahata, Y.; Nolte, R. J. M.; Jansen, J. A., Functionalization of multilayered DNA-coatings with bone morphogenetic protein 2. *Journal of Controlled Release* **2006,** *113* (1), 63-72.

75. Peterson, S.; Frick, A.; Liu, J., Design of biologically active heparan sulfate and heparin using an enzyme-based approach. *Nat. Prod. Rep.* **2009,** *26* (5), 610-627.

76. Boddohi, S.; Killingsworth, C. E.; Kipper, M. J., Polyelectrolyte multilayer assembly as a function of pH and ionic strength using the polysaccharides chitosan and heparin. *Biomacromolecules* **2008,** *9*, 2021-2028.

77. Tezcaner, A.; Hicks, D.; Boulmedais, F.; Sahel, J.; Schaaf, P.; Voegel, J. C.; Lavalle, P., Polyelectrolyte multilayer films as substrates for photoreceptor cells. *Biomacromolecules* **2006,** *7* (1), 86-94.

78. Yan, H.; Kaiyong, C.; Zhong, L.; Rui, Z.; Li, Y.; Linhong, D.; D., J. K., Surface mediated in situ differentiation of mesenchymal stem cells on gene-functionalized titanium films fabricated by layer-by-layer technique. *Biomaterials* **2009,** *30*.

79. Kim, T. G.; Lee, H.; Jang, Y.; Park, T. G., Controlled Release of Paclitaxel from Heparinized Metal Stent Fabricated by Layer-by-Layer Assembly of Polylysine and Hyaluronic Acid-g-Poly(lactic-co-glycolic acid) Micelles Encapsulating Paclitaxel. *Biomacromolecules* **2009,** *10* (6), 1532-1539.

80. Shiratori, S. S.; Rubner, M. F., pH-dependent thickness behavior of sequentially adsorbed layers of weak polyelectrolytes. *Macromolecules* **2000,** *33* (11), 4213-4219.

81. Choi, J.; Rubner, M. F., Influence of the degree of ionization on weak polyelectrolyte multilayer assembly. *Macromolecules* **2005,** *38* (1), 116-124.

82. Dubas, S. T.; Schlenoff, J. B., Factors controlling the growth of polyelectrolyte multilayers. *Macromolecules* **1999,** *32* (24), 8153-8160.

83. Morgan, S. E.; Jones, P.; Lamont, A. S.; Heidenreich, A.; McCormick, C. L., Layer-by-layer assembly of pH-responsive, compositionally controlled (co)polyelectrolytes synthesized via RAFT. *Langmuir* **2007**, *23* (1), 230-240.

84. Li, M. Y.; Mills, D. K.; Cui, T. H.; McShane, M. J., Cellular response to gelatin- and fibronectin-coated multilayer polyelectrolyte nanofilms. *Ieee Transactions on Nanobioscience* **2005**, *4* (2), 170-179.

85. Reneker, D. H.; Yarin, A. L., Electrospinning jets and polymer nanofibers. *Polymer* **2008**, *49*, 2387-2445.

86. Schneider, A.; Vodouhe, C.; Richert, L.; Francius, G.; Le Guen, E.; Schaaf, P.; Voegel, J. C.; Frisch, B.; Picart, C., Multifunctional polyelectrolyte multilayer films: Combining mechanical resistance, biodegradability, and bioactivity. *Biomacromolecules* **2007**, *8* (1), 139-145.

87. Hayward, J. A.; Chapman, D., BIOMEMBRANE SURFACES AS MODELS FOR POLYMER DESIGN - THE POTENTIAL FOR HEMOCOMPATIBILITY. *Biomaterials* **1984**, *5* (3), 135-142.

88. Gong, M.; Yang, S.; Ma, J. N.; Zhang, S. P.; Winnik, F. M.; Gong, Y. K. In *Tunable cell membrane mimetic surfaces prepared with a novel phospholipid polymer*, Elsevier Science Bv: **2008**; pp 555-558.

89. Nakabayashi, N.; Williams, D. F., Preparation of non-thrombogenic materials using 2-methacryloyloxyethyl phosphorylcholine. *Biomaterials* **2003**, *24* (13), 2431-2435.

90. Gong, Y. K.; Mwale, F.; Wertheimer, M. R.; Winnik, F. M. In *Promotion of U937 cell adhesion on polypropylene surfaces bearing phosphorylcholine functionalities*, Vsp Bv: **2004**; pp 1423-1434.

91. Wilson, J. T.; Cui, W. X.; Sun, X. L.; Tucker-Burden, C.; Weber, C. J.; Chaikof, E. L., In vivo biocompatibility and stability of a substrate-supported polymerizable membrane-mimetic film. *Biomaterials* **2007**, *28* (4), 609-617.

92. Senaratne, W.; Andruzzi, L.; Ober, C. K., Self-assembled monolayers and polymer brushes in biotechnology: Current applications and future perspectives. *Biomacromolecules* **2005**, *6* (5), 2427-2448.

93. Zhao, B.; Brittain, W. J., Polymer brushes: surface-immobilized macromolecules. *Progress in Polymer Science* **2000**, *25* (5), 677-710.

94. Halperin, A.; Tirrell, M.; Lodge, T. P., TETHERED CHAINS IN POLYMER MICROSTRUCTURES. *Advances in Polymer Science* **1992**, *100*, 31-71.

95. Chang, B. J.; Prucker, O.; Groh, E.; Wallrath, A.; Dahm, M.; Ruhe, J. In *Surface-attached polymer monolayers for the control of endothelial cell adhesion*, Elsevier Science Bv: **2002**; pp 519-526.

96. Ruhe, J.; Yano, R.; Lee, J. S.; Koberle, P.; Knoll, W.; Offenhausser, A., Tailoring of surfaces with ultrathin polymer films for survival and growth of neurons in culture. *Journal of Biomaterials Science-Polymer Edition* **1999**, *10* (8), 859-874.

97. Navarro, M.; Benetti, E. M.; Zapotoczny, S.; Planell, J. A.; Vancso, G. J., Buried, covalently attached RGD peptide motifs in poly(methacrylic acid) brush layers: The effect of brush structure on cell adhesion. *Langmuir* **2008**, *24* (19), 10996-11002.

98. Wischerhoff, E.; Glatzel, S.; Uhlig, K.; Lankenau, A.; Lutz, J. F.; Laschewsky, A., Tuning the Thickness of Polymer Brushes Grafted from Nonlinearly Growing Multilayer Assemblies. *Langmuir* **2009**, *25* (10), 5949-5956.

99. Li, L. H.; Zhu, Y.; Li, B.; Gao, C. Y., Fabrication of Thermoresponsive Polymer Gradients for Study of Cell Adhesion and Detachment. *Langmuir* **2008,** *24* (23), 13632-13639.

100. Mei, Y.; Wu, T.; Xu, C.; Langenbach, K. J.; Elliott, J. T.; Vogt, B. D.; Beers, K. L.; Amis, E. J.; Washburn, N. R., Tuning cell adhesion on gradient poly(2-hydroxyethyl methacrylate)-grafted surfaces. *Langmuir* **2005,** *21* (26), 12309-12314.

101. Meinel, L.; Hofmann, S.; Betz, O.; Fajardo, R.; Merkle, H. P.; Langer, R.; Evans, C. H.; Vunjak-Novakovic, G.; Kaplan, D. L., Osteogenesis by human mesenchymal stem cells cultured on silk biomaterials: Comparison of adenovirus mediated gene transfer and protein delivery of BMP-2. *Biomaterials* **2006,** *27* (28), 4993-5002.

102. Laurencin, C. T.; Nair, L. S., *Nanotechnology and Tissue Engineering: The Scaffold.* Taylor and Francis: Boca Raton, **2008**.

103. Xia, Y. N.; Whitesides, G. M., Soft lithography. *Annual Review of Materials Science* **1998,** *28*, 153-184.

104. Dalby, M. J.; Gadegaard, N.; Tare, R.; Andar, A.; Riehle, M. O.; Herzyk, P.; Wilkinson, C. D. W.; Oreffo, R. O. C., The control of human mesenchymal cell differentiation using nanoscale symmetry and disorder. *Nature Materials* **2007,** *6* (12), 997-1003.

105. Pham, Q. P.; Sharma, U.; Mikos, A. G., Electrospinning of polymeric nanofibers for tissue engineering applications: A review. *Tissue Engineering* **2006,** *12* (5), 1197-1211.

106. Sill, T. J.; Recum, H. A. v., Electrospinning: Applications in drug delivery and tissue engineering. *Biomaterials* **2008,** *29*, 1989-2006.

107. Ishii, Y.; Sakai, H.; Murata, H., A new electrospinning method to control the number and a diameter of uniaxially aligned polymer fibers. *Materials Letters* **2008,** *62* (19), 3370-3372.

108. Mathew, G.; Hong, J. P.; Rhee, J. M.; Leo, D. J.; Nah, C., Preparation and anisotropic mechanical behavior of highly-oriented electrospun poly(butylene terephthalate) fibers. *J. Appl. Polym. Sci.* **2006,** *101* (3), 2017-2021.

109. Li, J. X.; He, A. H.; Zheng, J. F.; Han, C. C., Gelatin and gelatin-hyaluronic acid nanofibrous membranes produced by electrospinning of their aqueous solutions. *Biomacromolecules* **2006,** *7* (7), 2243-2247.

110. Zhang, Y. Z.; Su, B.; Ramakrishna, S.; Lim, C. T., Chitosan nanofibers from an easily electrospinnable UHMWPEO-doped chitosan solution system. *Biomacromolecules* **2008,** *9* (1), 136-141.

111. Sui, G.; Yang, X. P.; Mei, F.; Hu, X. Y.; Chen, G. Q.; Deng, X. L.; Ryu, S., Poly-L-lactic acid/hydroxyapatite hybrid membrane for bone tissue regeneration. *Journal of Biomedical Materials Research Part A* **2007,** *82A* (2), 445-454.

112. Fridrikh, S. V.; Yu, J. H.; Brenner, M. P.; Rutledge, G. C., Controlling the fiber diameter during electrospinning. *Phys Rev Lett* **2003,** *90* (14).

113. Bashur, C. A.; Dahlgren, L. A.; Goldstein, A. S., Effect of fiber diameter and orientation on fibroblast morphology and proliferation on electrospun poly(D,L-lactic-co-glycolic acid) meshes. *Biomaterials* **2006,** *27* (33), 5681-5688.

114. Badami, A. S.; Kreke, M. R.; Thompson, M. S.; Riffle, J. S.; Goldstein, A. S., Effect of fiber diameter on spreading, proliferation, and differentiation of osteoblastic cells on electrospun poly(lactic acid) substrates. *Biomaterials* **2006,** *27* (4), 596-606.

115. Li, W.-J.; Jiang, Y. J.; Tuan, R. S., Chondrocyte phenotype in engineered fibrous matrix is regulated by fiber size. *Tissue Eng* **2006,** *12* (7), 1775-7285.

116. Pham, Q. P.; Sharma, U.; Mikos, A. G., Electrospun poly(epsilon-caprolactone) microfiber and multilayer nanofiber/microfiber scaffolds: Characterization of scaffolds and measurement of cellular infiltration. *Biomacromolecules* **2006,** *7* (10), 2796-2805.

117. Kwon, I. K.; Kidoaki, S.; Matsuda, T., Electrospun nano- to microfiber fabrics made of biodegradable copolyesters: structural characteristics, mechanical properties and cell adhesion potential. *Biomaterials* **2005,** *26* (18), 3929-3939.

118. Christopherson, G. T.; Song, H.; Mao, H. Q., The influence of fiber diameter of electrospun substrates on neural stem cell differentiation and proliferation. *Biomaterials* **2009,** *30* (4), 556-564.

119. Li, J. L.; Pan, J. L.; Zhang, L. G.; Guo, X. J.; Yu, Y. T., Culture of primary rat hepatocytes within porous chitosan scaffolds. *J. Biomed. Mater. Res. A* **2003,** *67A* (3), 938-943.

120. Gelain, F.; Horii, A.; Zhang, S. G., Designer self-assembling peptide scaffolds for 3-D tissue cell cultures and regenerative medicine. *Macromolecular Bioscience* **2007,** *7* (5), 544-551.

121. Horii, A, X. Wang, F. Gelain, and S. Zhang, Biological Designer Self-Assembling Peptide Nanofiber Scaffolds Significantly Enhance Osteoblast Proliferation, Differentiation and 3-D Migration. *PLoS ONE* **2007,** *2* (2).

122. Zhou, M.; Smith, A. M.; Das, A. K.; Hodson, N. W.; Collins, R. F.; Ulijn, R. V.; Gough, J. E., Self-assembled peptide-based hydrogels as scaffolds for anchorage-dependent cells. *Biomaterials* **2009,** *30* (13), 2523-2530.

123. Stendahl, J. C.; Wang, L. J.; Chow, L. W.; Kaufman, D. B.; Stupp, S. I., Growth factor delivery from self-assembling nanofibers to facilitate islet transplantation. *Transplantation* **2008,** *86* (3), 478-481.

124. Rabenstein, D. L., Heparin and heparan sulfate: structure and function. *Natural Product Reports* **2002,** *19* (3), 312-331.

125. Solans, C.; Izquierdo, P.; Nolla, J.; Azemar, N.; Garcia-Celma, M. J., Nano-emulsions. *Current Opinion in Colloid & Interface Science* **2005,** *10* (3-4), 102-110.

126. Boddohi S., Almodóvar J. Zhang H. Johnson P. Kipper M; "Layer-by-layer assembly of polysaccharide based nanostructured surfaces containing polyelectrolyte complex nanoparticles", *Colloids and Surfaces B:Biointerfaces*, 77 (2010) 60-68

127. Whitesides, G. M.; Ostuni, E.; Takayama, S.; Jiang, X. Y.; Ingber, D. E., Soft lithography in biology and biochemistry. *Annual Review of Biomedical Engineering* **2001,** *3*, 335-373.

128. Zhang, S. G.; Marini, D. M.; Hwang, W.; Santoso, S., Design of nanostructured biological materials through self-assembly of peptides and proteins. *Current Opinion in Chemical Biology* **2002,** *6* (6), 865-871.

Chapter 3

Layer-by-Layer Assembly of Polysaccharide-Based Multilayers: a Spectroscopic Study of Hydrophilicity, Composition, and Ion Pairing

3.1 Abstract

Polyelectrolyte multilayers using the polycations chitosan and *N,N,N*-trimethyl chitosan, and the polyanions hyaluronan, chondroitin sulfate, and heparin are studied. Chitosan and hyaluronan behave as a weak polycation and weak polyanion, respectively, while *N,N,N*-trimethyl chitosan, chondroitin sulfate, and heparin behave as strong polyelectrolytes. Hydrophilicity is determined by water contact angle measurements and by comparing wet and dry film thickness measurements. Wet thickness is obtained using Fourier transform surface plasmon resonance while dry thickness is obtained through ellipsometry. For the very thin PEMs studied here, the surface hydrophilicity and swelling in water are highly correlated. The multilayer chemistry is assessed by FT-IR and X-ray photoelectron spectroscopy (XPS). FT-IR and XPS provide information about the composition, degree of ionization, and by inference, the ion pairing. We find that hydrophilicity and swelling are reduced when one polyelectrolyte is strong and the other is weak, while ion pairing is

increased. By this combination of techniques we are able to compose a unified description of how the PEM swelling is dictated by the ion pairing in thin polysaccharide-based PEMs.

3.2 Introduction

The layer-by-layer (LbL) assembly of polyelectrolyte multilayers (PEMs) is typically achieved by the electrostatic adsorption of alternating layers of a polycation and polyanion from aqueous solutions. Polysaccharide-based PEMs have gained considerable attention as functional surface coatings for biomaterials.[1, 2] Such PEMs have been used to impart biological properties of polysaccharides to surfaces, including antimicrobial activity, anticoagulant activity, and the binding, stabilization, and delivery of growth factors.[3-6] In addition to the biochemistry of the polysaccharide constituents, the emergent properties of the PEMs themselves can also have strong influences on biological responses. The PEM structure at the molecular level, including the identity of the terminal PEM layer, the bonding between the polyelectrolytes, and the nanomechanical properties that arise from the LbL assembly can all influence biological responses.[3-5, 7, 8] These emergent properties of the PEMs can result from the specific interactions among the constituent polyelectrolytes (e.g. ionic bonding and hydrogen bonding) that occur as a result of the LbL assembly process. For example, films with higher degrees of ion pairing between the polycation and polyanion or covalent cross links might have increased stiffness, decreased macromolecular mobility, and reduced swelling in aqueous environments.[9] These properties in turn influence cell adhesion and spreading, protein adsorption, and the diffusion-controlled release of encapsulated therapeutics.[7, 8, 10-15]

In general, investigations with synthetic polyelectrolytes have revealed that decreasing the charge density on one or more of the polyelectrolytes can lead to much thicker PEMs.[16, 17] This could be due to a combination of many factors, including decreased electrostatic repulsion that otherwise limits each layer thickness, weakly charged polyelectrolytes adsorbing in a more coiled conformation, and reduced solubility of weakly charged polyelectrolytes. Similar studies on the growth of polysaccharide-based PEMs have been performed using in situ techniques, including Fourier transform surface plasmon resonance (FT-SPR),[18] quartz crystal microbalance (QCM),[19, 20] and optical waveguide lightmode spectroscopy (OWLS).[7] These investigations have led to new understanding of the interactions between the polyelectrolytes during the LbL process. Richert et al. demonstrated, using OWLS, that chitosan-hyaluronan (CHI-HA) PEMs exhibit an exponential growth associated with the diffusion of chitosan into and out of the PEM during PEM deposition.[7] This diffusion-enhanced mechanism of PEM growth was further investigated by Lavalle et al. using the poly(L-lysine)-hyaluronan (PLL-HA) system.[21] They demonstrated, using fluorescently-labeled polyelectrolytes, that the PLL (but not the HA) could diffuse throughout the entire film. Lundin et al. used fluorescence resonance energy transfer to measure the diffusion coefficient of CHI, in the direction normal to the surface, in very thin chitosan-heparin (CHI-HEP) PEMs.[22] They also confirmed diffusion of chitosan throughout the PEMs on time scales comparable to time scale of the LbL assembly.[22] This high degree of mobility within polysaccharide-based PEMs suggests that the electrostatic adsorption responsible for the LbL assembly can result in a loosely-associated network of mobile complexes, rather than a glassy, stratified multilayer, tightly bound together by a preponderance of obdurate ionic cross links.

Boddohi et al. investigated (CHI-HEP) PEM construction using FT-SPR, X-ray photoelectron spectroscopy (XPS), and ellipsometry, to discern how the composition and layer thickness could be controlled by changing the pH and ionic strength of the polysaccharide solutions.[18] These observations were related to the modulation of the solubility and charge density on chitosan by changing the pH, and the mediation of electrostatic interactions by electrostatic screening.[18] To investigate the ion pairing and its potential effects on film thickness and hydration, PEMs using PLL as the polycation and HA, HEP, and chondroitin sulfate (CS) as the polyanion were investigated by Crouzier et al.[23] Carboxylate-ammonium ion pairs were then covalently cross linked, and changes in the infrared spectra upon cross linking were used to infer the ion pairing stoichiometry.[23] This work concluded that increasing polyanion strength (HA < CS < HEP) resulted in PEMs with reduced hydration and reduced amount of "free" ammonium, defined as ammonium complexed to a small molecular weight counterion.[23] Based on these reports, one can conclude that the mechanism of film growth, the polycation-polyanion interactions, and PEM hydration are closely related. Tuning these properties is essential for controlling the emergent biological properties of polysaccharide-based PEMs.

We have previously studied the polyelectrolyte complexation using several polysaccharides, including CHI, *N,N,N*-trimethyl chitosan (TMC), HA, and HEP.[5, 6, 18, 19, 24] Our group has previously investigated CHI-HEP,[18] CHI-HA,[19] and TMC-HEP[6] PEMs on flat surfaces such as gold-coated glass,[18] tissue culture polystyrene,[19] and titanium,[5] and 3-D surfaces such as electrospun chitosan nanofibers.[6] In the present work, we study PEM formation using the six polycation-polyanion pairs that can be made using the polycations CHI and TMC, and the polyanions HEP, CS, and HA (Figure 3.1). Chitosan is a weak

polycation with a pKa of the amine groups between 6.0 and 6.5. Chitosan has antimicrobial activity and promotes wound healing through a number of mechanisms.[2, 25, 26] Partial methylation of the CHI to form TMC is used here to produce an analogous polysaccharide containing strong cationic groups. HEP, a sulfated glycosaminoglycan (GAG), is a strong polyanion containing in average 2.5 sulfate groups per disaccharide. CS is a weaker sulfated GAG, containing one sulfate group per disaccharide either in the 4-carbon or the 6-carbon of the N-acetyl glucosamine residue. HA is a non-sulfated GAG, which behaves as a weak polyanion. The pKa of the carboxylate group is approximately 2.9.[27] Collectively, these GAGs have a host of biochemical activities that have been exploited to develop functional surface coatings. These include anticoagulant activity, the binding and stabilization of growth factors and growth factor receptors, and serving as ligands for cell surface receptors.[2, 5, 28]
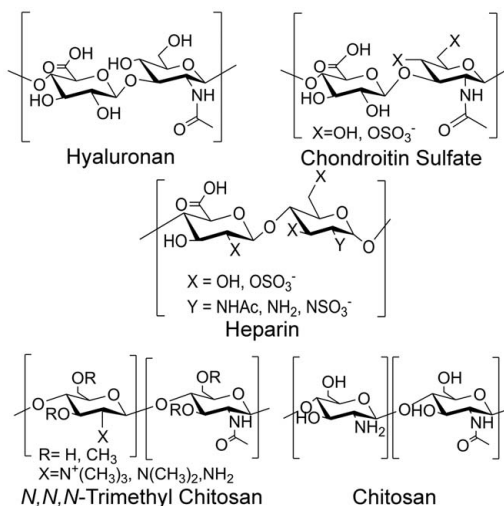
Figure 3.1 Chemical structure of each polysaccharide used in this study. Counterions are not shown.

This work is a detailed spectroscopic study of polysaccharide-based PEM formation using XPS, polarization-modulation infrared reflection absorption spectroscopy (PM-IRRAS), in situ FT-SPR, variable-angle spectroscopic ellipsometry, and water contact

angle measurements. LbL assembly of TMC-HA PEMs to form microcapsules around a sacrificial template was recently reported.[29] We recently reported on the modification of chitosan nanofibers with TMC-HEP PEMs.[6] However, to our knowledge, this is the first thorough study of the composition of PEMs formed from TMC and GAGs. PM-IRRAS and XPS are complementary techniques that we use to determine the stoichiometry of the PEMs as well as quantitative information regarding the polycation charge density. FT-SPR and spectroscopic ellipsometry provide information about the wet and dry film thickness, respectively. Water contact angle measurements are used to provide further insights into the physical chemistry of the PEM surfaces. We have proposed using such PEMs for the stabilization and delivery of growth factors to mammalian cells from biomaterial surfaces. Thus, in this work, all of the PEMs were polyanion-terminated because our previous experiments have shown that mammalian cells interact more favorably with GAG-terminated PEMs than with chitosan-terminated PEMs.[5]

3.3 Experimental Section

3.3.1 Materials

Chitosan (CHI) was purchased from Novamatrix (Protosan UP B 90/20, 5% acetylated determined by ^{1}H NMR, 80 kDa; Sandvika, Norway). Heparin sodium (HEP) was purchased from Celsus Laboratories (from porcine intestinal mucosa, 12.5% sulfur, 14.4 kDa; Cincinnati, OH). Chondroitin sulfate (CS) sodium salt (from shark cartilage, 6% sulfur, 6-sulfate:4-sulfate = 1.24, 84.3 kDa), hyaluronic acid (HA) sodium salt (743 kDa), and 11-mercaptoundecanoic acid (MUA) were purchased from Sigma-Aldrich (St. Lois, MO). *N,N,N*-Trimethyl chitosan (TMC) was synthesized following the procedure described by de

Britto and Assis.[30] A detailed TMC synthesis procedure and its characterization by ^{1}H-NMR

can be found in the supporting information (Appendix). Degree of quaternarization of TMC

was 18%. The methylation procedure also results in some *O*-methylation, as described in the

supporting information. Glacial acetic acid and ethanol (200 proof 99.5%) were purchased

from Acros Organics (Geel, Belgium). SF-10 glass chips (18 mm × 18 mm) were purchased

from GWC Technologies Inc. (Madison, WI). Gold shot, used for coating glass chips by

evaporation, was purchased from Alfa-Aesar (Ward Hill, MA). A Millipore Synthesis water

purification unit (Millipore, Billerica, MA) was used to obtain 18.2 MΩ water, used for

making all aqueous solutions.

3.3.2 Construction of polyelectrolyte multilayers (PEMs) on gold-coated glass and in situ

Fourier-transform surface plasmon resonance (FT-SPR).

Construction of polysaccharide-based PEMs on gold-coated SF-10 glass substrates has

been previously studied in our laboratory, and a detailed procedure can be found in

reference 18. Briefly, gold surfaces were cleaned and then modified with a self-assembled

monolayer (SAM) of MUA, by adsorption from a 1 mM ethanolic solution overnight. CHI,

TMC, HEP, CS, and HA solutions with concentrations of 0.01 M (on a saccharide unit basis)

were prepared in acetate buffer (sodium acetate/acetic acid, 0.2 M, pH 5.0). All

polysaccharide and rinse solutions were filtered with a 0.22 μm polyvinylidene fluoride

(PVDF) syringe filters (Fisher Scientific). Construction of the PEMs was performed in the

flow cell of an SPR-100 module, equipped with an InGaAs detector, coupled to a Nicolet

8700 FT-IR spectrometer (Thermo-Electron, Madison, WI), at a flow rate of 1.3 mL/min.

Data were collected using the Omnic 7.3 software (Thermo Electron), at 8 cm^{-1} resolution

over the range from 6000 to 12,000 cm^{-1}. A total of 16 scans were co-added at each time

point to produce an FT-SPR spectrum every 4.7 s during PEM construction. PEMs were constructed by alternating five-minute adsorption steps of the polyelectrolytes with five-minute acidified water rinses between adsorption steps (pH 4.0, acidified with acetic acid). PEMs were constructed from each of the six possible polycation-polyanion pairs using either CHI or TMC as the polycation and either HEP, CS, or HA as the polyanion. 10-layer "thin" PEMs were constructed for characterization by in situ FT-SPR and ellipsometry. However, 10-layer PEMs were too thin to reliably characterize by ellipsometry to obtain both the thickness and the refractive index. Hence, "thick" PEMs (20 layers for the CHI-HA pair and 30 layers for all other polyelectrolyte pairs) were constructed for characterization by ellipsometry. The use of these data to interpret the ellipsometry and FT-SPR experiments from the thin PEMs is described below. These thick PEMs were also characterized by X-ray photoelectron spectroscopy, polarization-modulation infrared reflection absorption spectroscopy, and water contact angle measurements.

3.3.3 Variable-angle spectroscopic ellipsometry

Ellipsometry data for the thin (10-layer) and thick (20- or 30-layer) PEMs were acquired using JA Woollam VASE ellipsometer in the wavelength range 400-1200 nm at two angles of incidence 65° and 75°. Optical modeling and data analysis were done using the J. A. Woollam WVASE32 software package. Data were first collected for the gold layer on a clean gold-coated SF-10 glass chip which had no polysaccharide. The preloaded optical properties for gold, SF-10 glass, and the chromium adhesion layer were used to obtain the gold thickness (~50 nm). Data were then obtained for the thick PEMs constructed on the previously characterized gold-coated SF-10 glass. For each of the thick PEM samples, the MUA-SAM and the PEM were modeled as a single Cauchy layer, to obtain the thickness and

the Cauchy equation parameters. The Cauchy parameters for each PEM sample were then used to model the ellipsometry data from the thin PEMs to obtain their respective thicknesses. The thickness of the MUA-SAM (1.7 nm) was subtracted to obtain the thickness of the PEM. The Cauchy parameters were also used to obtain PEM thickness from FT-SPR data, by including the wavelength dependence of the refractive index of the film, as described in the results section. More explanation on fitting ellipsometry data can be found in the supporting information.

3.3.4 Polarization-modulation infrared reflection absorption spectroscopy (PM-IRRAS) and transmission FT-IR

FT-IR spectroscopy was used in polarization modulation mode to confirm construction of PEMs and investigate the chemistry of the thick (20- or 30-layer) PEMs as described in reference 18. Experiments were conducted using a Nicolet 8700 FT-IR (Thermo-Electron) spectrometer configured with a Tabletop Optics Module equipped with a PEM-90 photo elastic modulator (Hinds Instruments, Hillsboro, OR) to provide polarization of the incident infrared light, grazing angle sampling optics (86° for gold substrate), a liquid nitrogen-cooled MCT-A detector, and a demodulator (GWC Technologies) to process the *s-* and *p*-polarized reflection spectra. PM-IRRAS spectra were collected at 2 cm^{-1} resolution with 1000 scans for each sample in the range of 800-4000 cm^{-1} with a modulation frequency of 1500 cm^{-1}. Each spectrum was corrected by determining a cubic spline function from a defined set of spline points and dividing it into the PM-IRRAS spectrum to correct for the Bessel function background. The 2nd-order 9-point Savitzky-Golay algorithm was used to smooth all spectra. The spectroscopy analysis software IgorPro (Version 5.0.5.7, Wave Metrics, Inc., Portland, OR) was used for background correction, smoothing, and spectral math. Transmission FT-IR

was used to obtain the IR spectrum of the polysaccharide powders. KBr (IR grade, Acros Organics) pellets were prepared for all five polysaccharides, and a blank KBr pellet was used as the background. Data were collected at 2 cm^{-1} resolution with 160 scans in the range of 400-8000 cm^{-1} using a DTGS detector.

3.3.5 X-ray photoelectron spectroscopy (XPS)

XPS experiments were performed on thick (20- or 30-layer) PEMs using a Physical Electronics 5800 spectrometer (Chanhassen, MN). This system has a monochromatic Al Kα X-ray source (hν = 1486.6 eV), hemispherical analyzer, and multichannel detector. The binding energy scales for the samples were referenced to either the Au1 peak at 84 eV, or to the carbon peak at 285 eV. High resolution spectra of the C1s, O1s, N1s and S2p envelopes were acquired at analyzer pass energy of 23.5 eV, with 0.1 eV steps, and an X-ray spot size of 800 μm. All XPS analyses were performed at a photoelectron takeoff angle of 45°. XPS spectra for HEP was collected from dry powder taped to double sided carbon tape. Enough powder was used in order to cover the surface of the tape. TMC, HA, CS and CHI were film cast from water (acidified water for CHI) at a concentration of 5 mg/mL on gold-coated glass, dried in ambient conditions, and then further dried in a vacuum oven at room temperature. XPS spectra were analyzed using the XPSPEAK41 free software. For curve fitting of all spectra, a Shirley background was used and Gaussian peaks were fit according to the expected chemistry (minimizing χ^2). For the N1s peak, three peaks were assigned and fixed near their expected positions (amine at 399, amide at 400, and ammonium at 401.5 eV) and their full width at half max (FWHM) was also fixed. The area of each peak was fit first, then the FWHM, and finally, the position. FWHM was not allowed to go above 1.7.

3.3.6 Water contact angle

Static contact angles were measured by the sessile drop method with a contact angle goniometer (Krüss DSA 10, Hamburg, Germany) equipped with video capture. The automatic dosing feature of the DSA 10 dispenses a water drop (2 µL) on the PEM surfaces and the needle is manually withdrawn. An image was taken within two seconds of the placement of the drop on the surface. Contact angle measurements are analyzed by the circle fitting profile available with the DSA 10 imaging software. Three separate measurements were made on each PEM at different locations. All of the contact angle values for the different PEMs are available in table form in the supporting information.

3.4 Results

3.4.1 FT-SPR, ellipsometry, and water contact angle measurements

FT-SPR was used to monitor layer deposition of the PEMs in situ. PEMs were constructed with either CHI or TMC as the polycation and with HA, CS, or HEP as the polyanion. FT-SPR spectra were collected over a range from 6000 to 12,000 cm^{-1} at a fixed angle of incidence. (Small adjustments in the incident angle, approximately 53°, were made so that the initial FT-SPR minimum was near 9000 cm^{-1}.) Incident light with energy in resonance with surface plasmons in the gold film produces a broad minimum in the reflectance spectrum. The position of this minimum is sensitive to changes in the thickness and refractive index of the layer on the surface of the gold film (i.e. the PEM). Thus, when the solution is changed and/or layers are adsorbed to the surface there is a shift in the position of the minimum.[31] Figure 3.2 A shows representative FT-SPR spectra obtained during construction of a CHI-HEP PEM. Figure 3.2 B shows the position of the minimum as a

function of time during PEM construction. The first five minutes (gray arrow) represents an acidified water rinse on the gold-coated and MUA SAM-modified glass chip. The next five-minute interval (black arrow) represents the peak position during the first CHI adsorption step. The large drop in the FT-SPR during this time is due to the adsorption of CHI to the surface, and to the difference in refractive index between the rinse and CHI solutions. The third five-minute interval corresponds to the acidified water rinse following the CHI adsorption. The FT-SPR peak occurs at a different frequency than during the first acidified water rinse, due to deposition of CHI on the surface. This process is continued, by alternating HEP and CHI deposition solutions with acidified water rinse steps. At each rinse step the peak position does not return to the position of the previous rinse, indicating layer deposition. FT-SPR data were obtained for thin films (10-layers) for all of the polyanion-polycation combinations (CHI-HA, CHI-CS, CHI-HEP, TMC-HA, TMC-CS, and TMC-HEP) in duplicate.
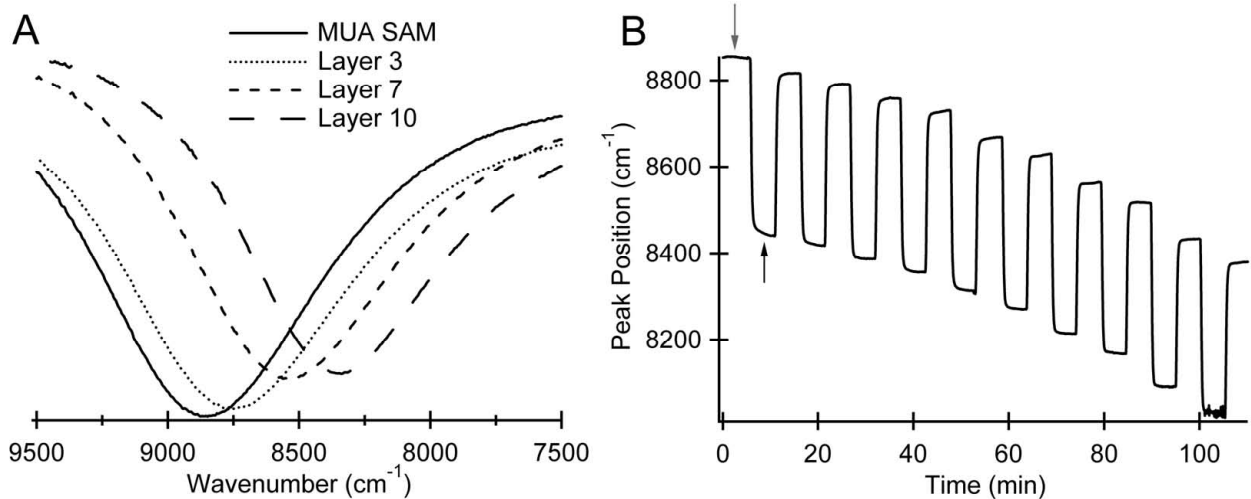
Figure 3.2 (A) In situ FT-SPR spectra during construction of a CHI-HEP PEM. FT-SPR peaks are shown for the rinses after the MUA-SAM, and after layers 3, 7, and 10. (B) FT-SPR peak position as a function of time for the entire construction of the PEM. The gray arrow indicates the initial five-minute acidified water rinse; the black arrow indicates the first polysaccharide (CHI) adsorption step. Five-minute intervals associated with deposition and rinse steps can be clearly discerned.

FT-SPR curves can be predicted using multi-phase Fresnel calculations, which requires the refractive index of each layer (glass, gold, PEM, and rinse solution), the thicknesses of gold and the PEM, and the angle of incidence.[31] An algorithm was written using the spectral software IgorPro, which predicts the FT-SPR curves using multi-phase Fresnel calculations. More information is available in the supporting information (Appendix). These predicted curves can be compared to the experimental data in order to obtain unknown parameters. For modeling the FT-SPR data, the angle of incidence was fixed at 53°, and the wavelength dependence of the refractive index of the SF-10 glass and gold were used. The refractive index of the rinse solution was assumed to be that of water, and its wavelength dependence was accounted for using the Cauchy equation. (See supporting information.) The thickness of gold and the (wavelength-dependent) refractive indices of the PEMs were obtained from ellipsometry. Thus, the only adjustable parameter is the PEM thickness. FT-SPR curves (reflectance versus frequency) were then predicted using PEM thickness as an independent variable. Figure 3.3A shows such FT-SPR predictions generated through the Fresnel calculations using the parameters for the CHI-HEP pair, by varying the film thickness from 0 to 35 nm. For all polycation-polyanion pairs, the position of the FT-SPR minimum is approximately linear (R^2 > 0.99) over the range of thicknesses evaluated (Figure 3.3B). The slopes obtained from similar predictions were then used to compute the thickness for each polycation-polyanion pair from the changes in the FT-SPR peak position during rinse steps.
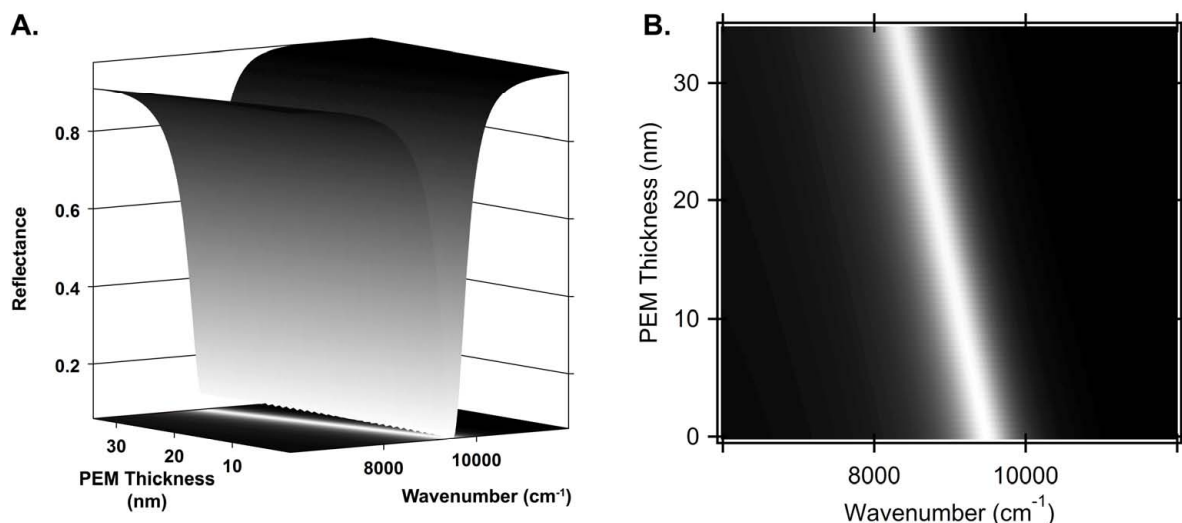
Figure 3.3 (A) Reflected light intensity from predicted FT-SPR curves as a function of PEM thickness and frequency using the parameters for the CHI-HEP PEMs. FT-SPR curves were predicted for PEM thicknesses ranging between 0 and 35 nm in 0.5 nm increments. The gray scale in A. and B. correspond to the reflected intensity. (B) Predicted FT-SPR reflected light intensity as a function of wavelength and PEM thickness.

Plots of film thickness as a function of deposited layer number for all PEM combinations are shown in Figure 3.4. Note that the thickness range in Figure 3.4A is more than twice the range in Figure 3.4B. The growth of all six PEMs appears linear over the range investigated.
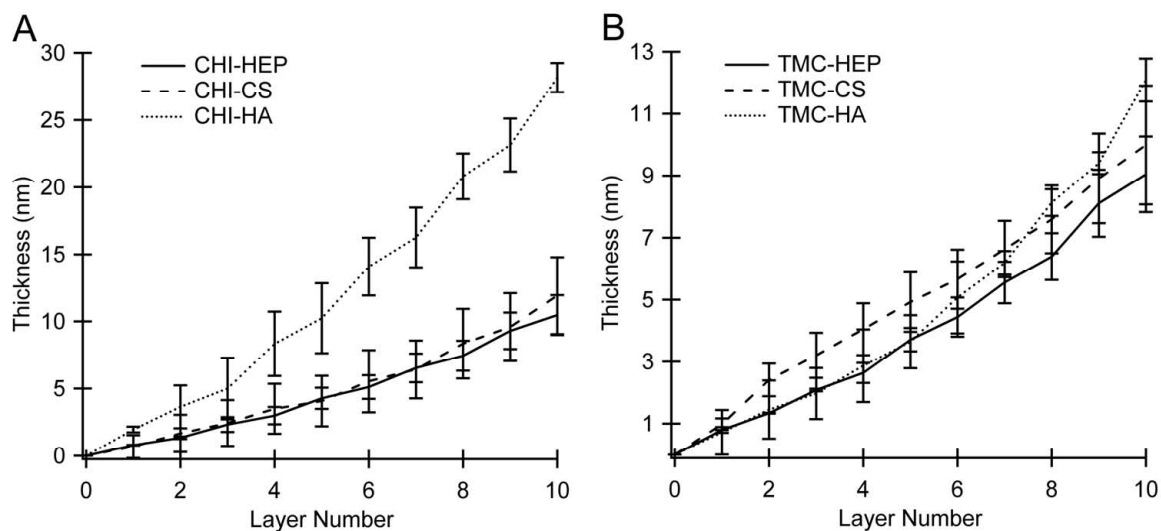
Figure 3.4 PEM thicknesses obtained from in situ FT-SPR data for (A) CHI-based PEMs, and (B) TMC-based PEMs. Note that the thickness range plotted in (A) is more than twice the range plotted in (B). Uncertainties represent the range of duplicate samples for each condition.

77

Ellipsometry was conducted on dry thin films within one week of PEM construction, in order to obtain the dry thickness along with the Cauchy parameters necessary for the refractive index calculations of the PEMs. However, the very small thickness of 10-layer PEMs made it impossible to obtain reasonable fits for the ellipsometry data. Thus, thick, 30-layer PEMs (20-layers for CHI-HA) were assembled to obtain better fits for the ellipsometry data. The optical parameters obtained for the thick layers were used to fit the ellipsometry data for the thin layers and the thickness was obtained (Figure 3.5).

The final FT-SPR thickness and the thickness measured by ellipsometry are shown in Figure 3.5. The PEM thickness increases with increasing molecular weight of the polyanions, which also corresponds to decreasing polyanion strength. Comparing the CHI PEMs to the TMC PEMs, we find that in general, the strong polycation (TMC) results in thinner layers.

Figure 3.5 also shows the water contact angle and the swelling percent of the PEMs as

$$\% Swelling = \frac{d_{SPR} - d_{Ellipsometry}}{d_{Ellipsometry}} \times 100 \qquad (1)$$

were d_{spr} and $d_{Ellipsometry}$ represent the PEM thickness obtained using FT-SPR and ellipsometry respectively. For thick PEMs the charge density and hydrophilicity of the surface may be very different from the bulk of the film. However, in our experiments the PEMs are very thin. Therefore, we expect that the surface hydrophilicity (measured by water contact angle) to be highly correlated to the swelling of the PEMs.[32] Hydrophilic PEMs will absorb water and swell, exhibiting thicker layers when wet (i.e. during FT-SPR measurements). When these hydrophilic PEMs are dried, they collapse resulting in reduced thickness measurements from ellipsometry. The CHI-HA PEMs were found to be the most hydrophilic, with a contact angle of 35°. These PEMs also had the largest collapse after drying of the CHI-based PEMs. TMC-HEP and TMC-CS had similar contact angles, near

40°. These two PEMs also exhibit a comparable amount of collapse. CHI-HEP, CHI-CS, and TMC-HA resulted in similar contact angles, near 54°, the largest and most hydrophobic contact angle observed, and exhibited less collapse upon drying. These results show that when the weak polycation is paired with a weak polyanion (CHI-HA) and when the strong polycation is paired with strong polyanions (TMC-CS and TMC-HEP), the most hydrophilic PEMs result. However, when a weak and a strong polyelectrolyte are paired (CHI-CS, CHI-HEP, and TMC-HA) more hydrophobic PEMs are obtained.
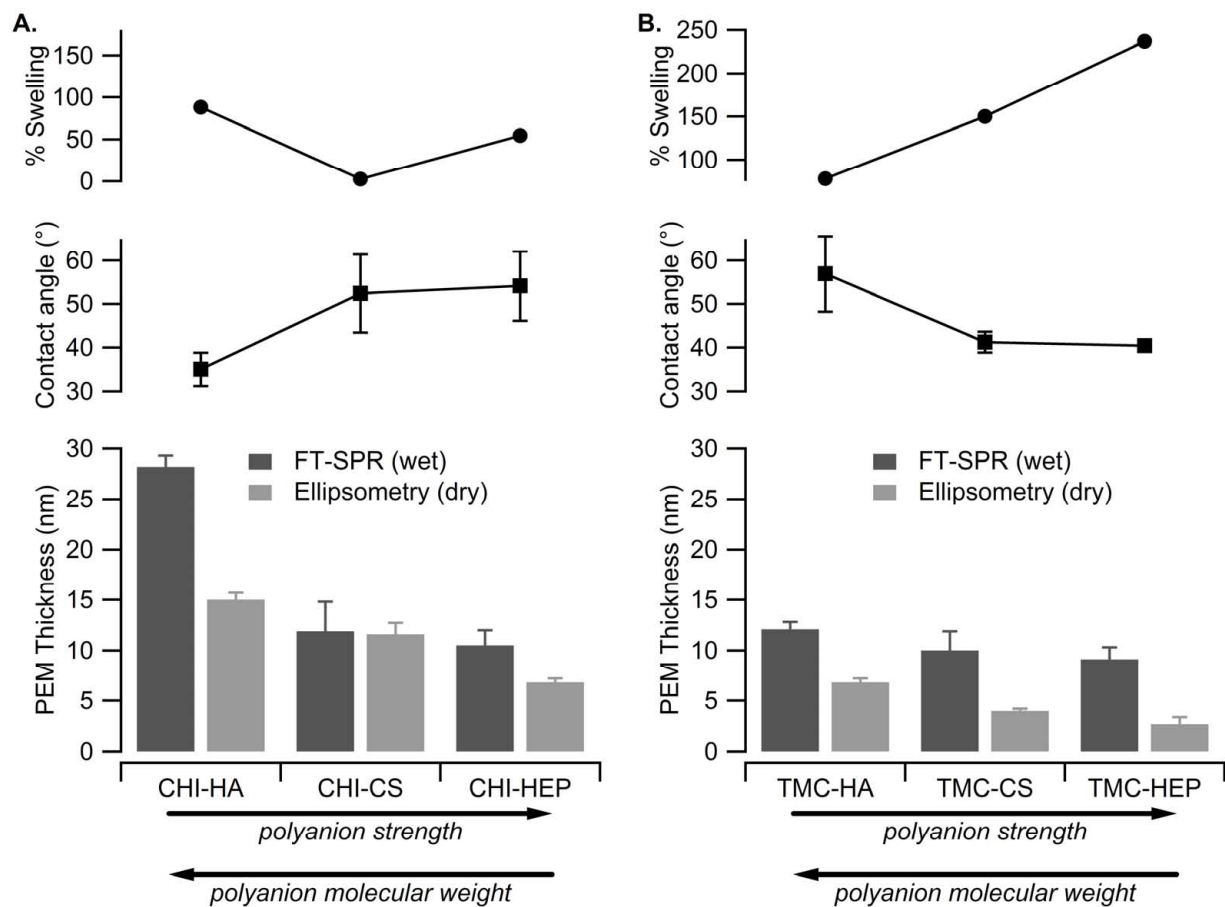
Figure 3.5 (Bottom) PEM thickness measured by both FT-SPR and ellipsometry, (Middle) water contact angle, and (Top) % swelling of PEMs as calculated from equation 1, for (A) CHI-based PEMs and (B) TMC-based PEMs.

3.4.2 Transmission FT-IR and PM-IRRAS

FT-IR in transmission mode was used to obtain spectra of the polysaccharide powders using a KBr pellet. FT-IR spectra for all of the different polysaccharide-based PEMs were obtained using PM-IRRAS to investigate their chemistry. The IR spectrum for each of the neat polysaccharides is displayed in Figure 3.6, and the characteristic absorptions are summarized in Table 3.1. All of the polysaccharides exhibit a broad absorption between 1733 and 1600 cm^{-1}. The asymmetric stretch of the amide carbonyl groups (i.e. the amide I vibration) should occur between 1700 and 1600 cm^{-1}. In the polyanions, this peak should also contain the asymmetric carbonyl stretch in the carboxylate groups around 1610 cm^{-1}. Hyaluronan is the only neat polysaccharide that contains a discernable absorption above 1700 cm^{-1} (1733), which corresponds to the carbonyl stretch in the (protonated) carboxylic acid. This suggests that the carboxylate groups in heparin and chondroitin sulfate are deprotonated, and associated with a counterion (Na$^+$) in the neat polysaccharides. In CHI and TMC there are no carboxylic acids and only 8% of the saccharide residues are acetylated. So in CHI, the additional strong absorption at 1600 cm^{-1} is attributed to –NH$_2$ scissoring vibrations from the amine groups.[33] (Asymmetric –NH$_3^+$ deformations would also appear in this region, but the corresponding symmetric –NH$_3^+$ vibration, expected around 1530 cm^{-1} is lacking. The neat CHI polymer is supplied as free base, with little or no ammonium.) This assignment of the peak at 1600 cm^{-1} in CHI is confirmed by comparison to the TMC spectrum. In TMC the absorbance at 1600 cm^{-1} is reduced significantly, as a fraction of primary amines have been converted to secondary, tertiary, and quaternary amines by methylation. The N–H in-plane bending vibration in the amide groups (amide II) also occurs below 1600 cm^{-1}. This amide II vibration is apparent in the HA and CS spectra at 1559 cm^{-1},

but does not appear as a strong peak in the other three polysaccharides. TMC is the only polysaccharide exhibiting a peak at 1457 cm^{-1}, which can be attributed to the methyl groups. All of the polysaccharides also exhibit absorptions between 1420 and 1418 cm^{-1}. This is attributed to the CH_2 scissoring (at the 6-carbon of the glucosamine residues), and might also contain contributions from carboxylate ion ($-COO^-$) symmetric stretch for the polyanions.[7] In TMC, the peak in this region is obscured by the very strong absorption from the methyl groups. The weaker peak at 1379 cm^{-1} can be attributed to the $-OH$ in-plane bending vibration. In HEP, the $-OH$ in-plane bending is reduced due to sulfation of many of the hydroxyl groups. Comparing TMC to CHI, the 1379 peak is also reduced in TMC, as some of the hydroxyl groups are methylated. Both HEP and CS have a strong adsorption band between 1300 and 1200 cm^{-1} due to the sulfate group (at about 1260 cm^{-1}) and the C–O stretch in the carboxylic acid (at about 1240 cm^{-1}). All of the polysaccharides exhibit a peak between 1161 and 1132 cm^{-1}, which is attributed to the ether bonds. The remaining broad absorption band between 1100 and 1000 cm^{-1} is due to vibrational modes associated with the saccharide rings and to C–N stretching. The C−O−S stretching vibration is also expected to occur at about 1000 cm^{-1} and appears as a shoulder on this broad absorption in CS and HEP.[23]
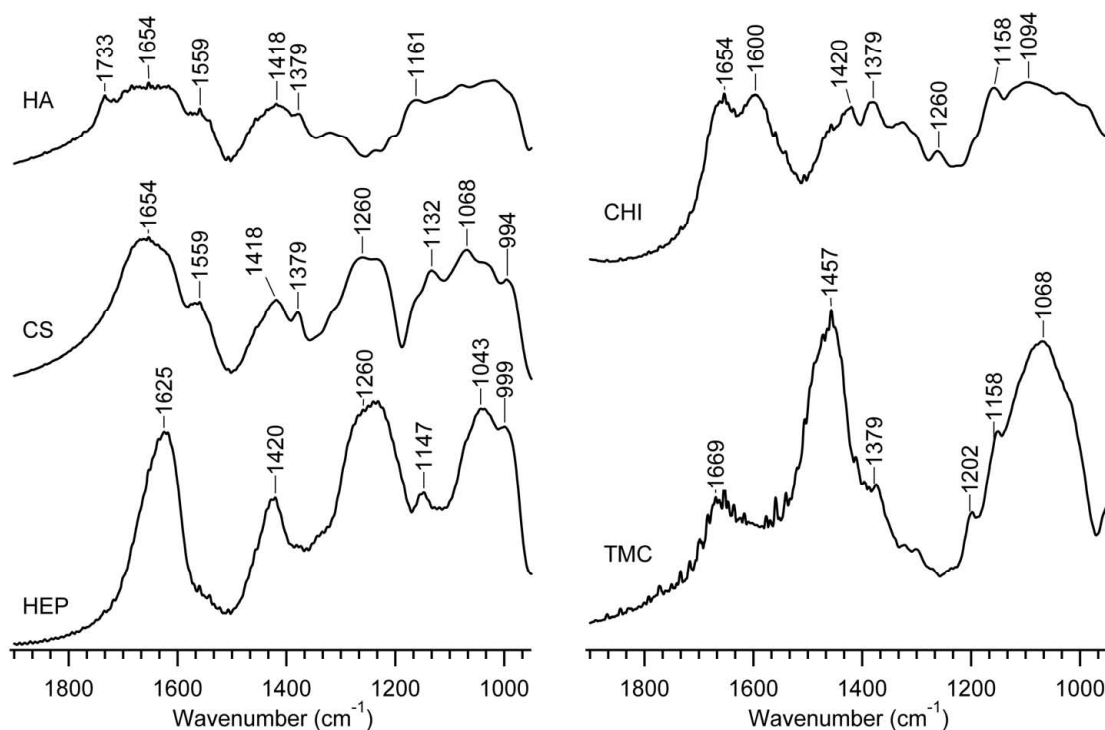
Figure 3.6 Transmission FT-IR for all of the polysaccharide powders used in this study using a KBr pellet.

Table 3.1 Characteristic absorptions in the pure polysaccharide spectra shown in Figure 3.6.

Absorption (cm^{-1})	Peak assignment
1733	–COOH carbonyl stretch (HA)
1700 – 1600	Amide asymmetric carbonyl stretch (C=O ν_{as})
1600	NH$_2$ scissoring (CHI)
1559	Amide N–H in-plane bend (HA and CS)
1457	CH$_3$ deformation (TMC)
1420 – 1418	CH$_2$ scissoring, COO$^-$ symmetric stretch
1379	–OH bending
1260	–OSO$_3^-$ ν_{as} (CS and HEP)
1239	C–O stretch in carboxylic acid
1161 – 1132	C–O–C ν_{as}
1100 – 1000	Saccharide ring vibrations and C–N stretch
999 – 994	C–O–S stretch (CS and HEP)

PM-IRRAS spectra for all PEM combinations are displayed in Figure 3.7, and the principle absorptions are summarized in Table 3.2. The left panel of Figure 3.7 has PEMs with CHI as the polycation and the right panel has PEMs with TMC as the polycation. Interestingly, both HEP and CS exhibit protonated carboxylic acid peaks above 1700 cm^{-1} that are not present in the neat polymers. When this carbonyl oxygen participates in hydrogen bonding as an H-bond acceptor, this stretching vibration is shifted to lower frequency. The relatively high frequency of these vibrations in the CHI-HEP, TMC-CS, and TMC-HEP PEMs indicates that these are not participating in H-bond networks. In CHI-HA, CHI-CS, and TMC-HA PEMs, this absorption occurs at a distinctly lower frequency, suggesting that the carbonyl oxygen of the carboxylic acid groups is acting as an H-bond acceptor.[34] These three PEMs also have distinct shoulders or peaks between 1611 and 1603 cm^{-1}. The asymmetric carbonyl stretch from carboxylate groups and the NH_3^+ bending vibrations might both occur here. Comparing the two HA PEMs, there is more carboxylic acid (1709 cm^{-1}) in the CHI-HA PEM, and potentially more carboxylate (1611 cm^{-1}) in the TMC-HA PEM. All CHI PEMs contain a peak between 1538 and 1530 cm^{-1} corresponding to the symmetric NH_3^+ deformation. The intensity of this peak increases with increasing charge density of the polyanion (HA < CS < HEP), indicating that the strength of the polyanion influences the charge density on the CHI. This peak is weaker or absent in the TMC PEMs due to methylation of the amine groups in TMC. All TMC-containing PEMs exhibit the methyl group deformations at higher frequency (1477 – 1486 cm^{-1}) and reduced intensity than in the neat TMC. The bands between 1422 – 1400 cm^{-1} contain contributions from the symmetric $-COO^-$ stretch for all polyanions, as well as CH_2 scissoring and –OH bending for all polysaccharides. The bands near 1379 cm^{-1} for all PEMs correspond to –OH

bending. The peak between 1263 and 1252 cm^{-1} is attributed to the asymmetric sulfate stretch in HEP- and CS-containing PEMs. The strong peak at 1239 cm^{-1} in the CHI-HA PEM is only very weakly present in the neat HA (Figure 3.6). This could be due to strong C–O stretching in the protonated carboxylic acid, which changes upon complexation with chitosan. Both HEP- and CS-containing PEMs also exhibit peaks at about 1227 and 1155 cm^{-1}. Others have attributed absorptions in this range to interactions between sulfates and amines.[35] However, they could also be due to the carboxylic acid C–O stretch and the ether C–O–C stretch, respectively. The shoulder near 1000 cm^{-1} due to C–O–S stretching can be seen in the CHI-HEP, TMC-CS, and TMC-HEP spectra.
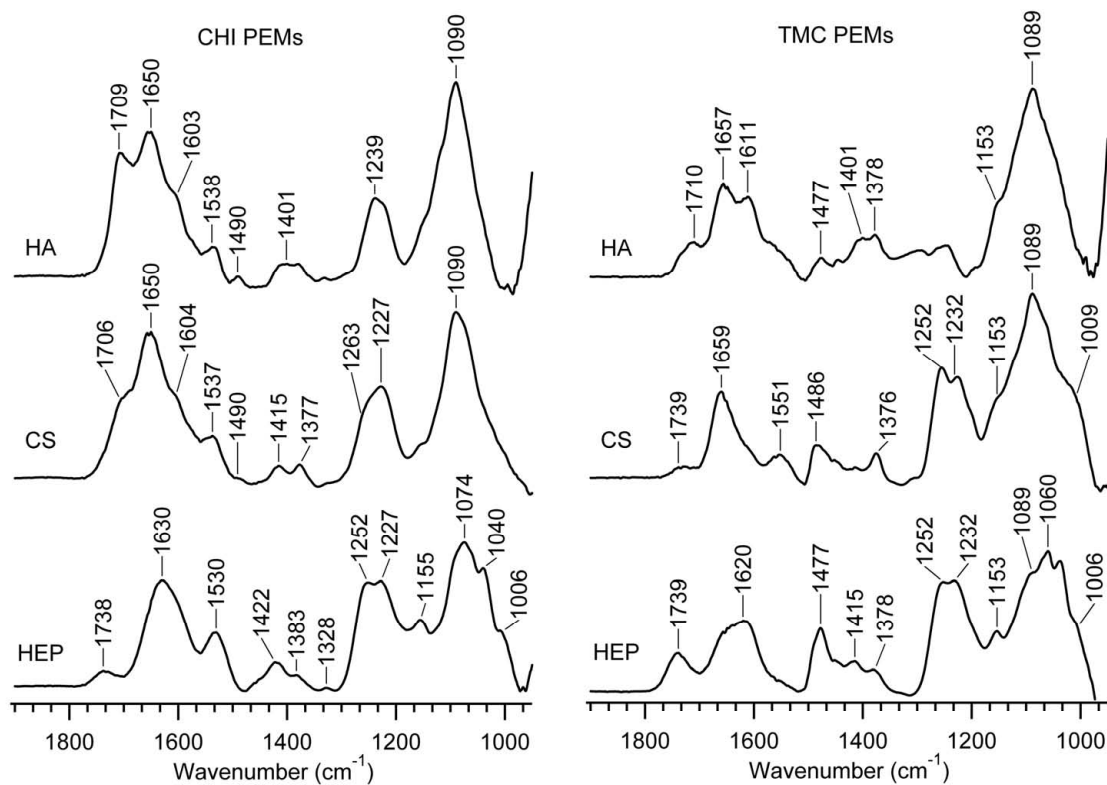
Figure 3.7 PM-IRRAS spectra for all PEMs combination.

Table 3.2 Characteristic absorptions in PEM spectra shown in Figure 3.7.

Absorption (cm^{-1})	Peak assignment
1739 – 1738	–COOH carbonyl stretch
1710 – 1706	–COOH carbonyl stretch (H-bonded)
1700 – 1600	Amide carbonyl asymmetric stretch (C=O ν_{as})
1611 – 1600	–COO$^-$ (C=O ν_{as}), NH$_2$ scissoring, –NH$_3^+$ asymmetric deformation
1538 – 1530	–NH$_3^+$ symmetric deformation
1486 – 1477	CH$_3$ deformation
1422 – 1400	CH$_2$ scissoring, COO$^-$ symmetric stretch
1383 – 1376	–OH bending
1263 – 1252	–OSO$_3^-$ ν_{as}
1239 – 1227	C–O stretch in carboxylic acid, and perhaps sulfate – amine interactions
1155 – 1153	C–O–C ν_{as}, and perhaps sulfate – amine interactions
1100 – 1000	Saccharide ring vibrations and C–N stretch
1009 – 1006	C–O–S stretch

3.4.3 XPS

High-resolution XPS spectra were obtained for all of the pure polysaccharides and all PEM combinations. The C1s and the O1s envelopes of both the pure components and the PEMs contain contributions from several different specific species (ether, hydroxyl, amide, carboxyl, carboxylate, and sulfate oxygens, for example), making their de-convolution difficult and uncertain. These are archived in the supporting information (Appendix) for the interested reader. The S2p envelopes contain the expected contributions from the sulfate substituents in chondroitin sulfate and heparin. These are also provided in the supporting information (Appendix). The high-resolution spectra in the region of the N1s envelopes are shown for the pure components and all PEM combinations in Figure 3.8. The N1s envelope contains contributions from primary, secondary, and tertiary amine groups (−NH$_2$, −NHCH$_3$,

$-N(CH_3)_2$) at nominally 399.6 eV, amide at nominally 400.7 eV, and primary, secondary, tertiary, and quaternary ammonium ($-N^+H_3$, $-N^+H_2CH_3$, $-N^+H(CH_3)_2$, $-N^+(CH_3)_3$) at nominally 402 eV. The fractional contributions from amine, amide, and ammonium can be used to estimate the composition of the PEMs and to discern the degree of ionization of the glucosamine residues in the polycations. These calculations were performed assuming that each polyanion contains 0.5 amide nitrogens per disaccharide, and that the polycations have 0.05 amide groups per saccharide and 0.95 amine or ammonium groups per saccharide. The polycation to polyanion ratio in the PEMs is reported on a saccharide unit basis. These data are summarized in Table 3.3 for the pure polycations and Table 3.4 for the PEMs. All of the polyanions exhibited only the amide peak (Figure 3.8). Note that neither the C1s, nor the N1s envelopes can be used to distinguish amine and ammonium groups with different degrees of methylation in TMC. Though, in general, the ammonium peak in TMC tends to be centered at a higher binding energy than the ammonium group in chitosan, probably due to methylation.
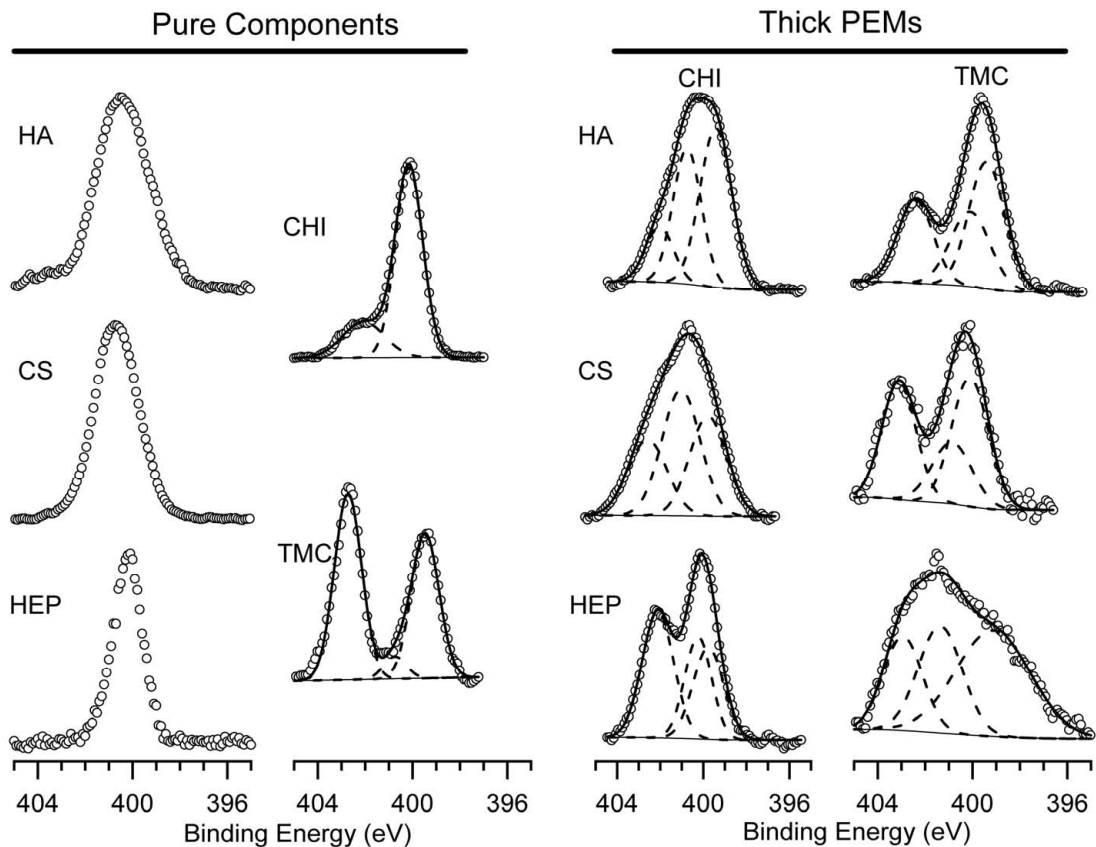
Figure 3.8 N1s envelopes for each of the polysaccharides (left) and each of the PEMs (right). Circles correspond to raw data, broken line correspond to fitted Gaussian peaks, thick solid line is the sum of the Gaussian peaks, and thin solid line is the background curve.

Table 3.3 Components of the N1s envelope for pure polycations.[†]

	Amine		Amide		Ammonium	
	Position	% of	Position	% of	Position	% of
Sample	(eV)	N1s	(eV)	N1s	(eV)	N1s
CHI[‡]	399.7	77.6			401.6	22.4
TMC	399.5	41.5	400.7	5.5	402.7	53.0

[†]The polyanions HA, CS, and HEP showed only the expected amide peak at 400.4, 400.7, and 400.2 respectively.

[‡]Only two peaks were fit to the N1s spectrum for CHI. Since CHI is 95% deacetylated, the peak at 401.6 was assigned to ammonium with small contributions from the amide.

Table 3.4 Components of the N1s envelope for PEMs, and computed molar compositions.

PEM	Amine Position (eV)	% of N1s	Amide Position (eV)	% of N1s	Ammonium Position (eV)	% of N1s	Composition Cat:An Ratio	N^+:N in cation
CHI-HA	399.4	48.5	400.8	36.7	402.1	14.8	50:50	23:77
CHI-CS	399.6	32.3	400.8	41.9	402.2	25.8	44:56	44:56
CHI-HEP	399.8	29.5	400.2	28.7	402.1	41.8	60:40	59:41
TMC-HA	399.4	43.4	400.1	28.5	402.4	28.1	60:40	39:61
TMC-CS	400.1	42.0	400.9	22.1	403.1	35.9	70:30	46:54
TMC-HEP	399.1	48.6	401.4	28.9	402.9	22.5	60:40	32:68

When CHI is used as the polycation, the ratio of ammonium to amine groups in the chitosan increases with increasing charge density of the polyanion (from 23% for CHI-HA to 59% for CHI-HEP). This suggests that the chitosan charge density is partially controlled by complexation with the polyanion. This is consistent with the observed increase in the symmetric NH_3^+ vibration (1538 – 1530 cm^{-1}) with increasing polyanion charge density, seen in Figure 3.7. Comparing the CHI PEMs formed with the two strong polyanions (CHI-CS and CHI-HEP), the ratio of chitosan in these films is also increased with increasing charge density. Nonetheless, the total number of ammonium groups in the CHI-CS and CHI-HEP PEMs is sufficient to neutralize only about 70% of the sulfate groups, based on the calculated stoichiometry. Thus, these films likely contain significant quantities of small counterions, and are not formed by one-to-one complexation of the charged groups in the polycation and polyanion pairs.

When TMC is used as the polycation, the PEMs formed from HA and CS contains significantly more polycation than the similar PEMs formed with CHI as the polycation. However, there is no clear correlation between the anion charge density and the fraction of charged groups in the TMC, as there is for CHI. Thus the polyanion charge density does not control the charge density on TMC as it does for CHI.

3.5. Discussion

In a recent study by Crouzier and Picart, ion pairing in PEMs using PLL as the polycation and HA, CS, and HEP as the polyanions was studied.[23] In their work FT-IR spectra were quantitatively evaluated before and after cross linking with a carbodiimide and *N*-hydroxysulfosuccinimidyl ester chemistry to form stable amide bonds between interacting ammonium and carboxylate groups. Their analysis permitted the determination of the carboxylate ion pairing in the films by assuming: (1) The cross linking was 100% efficient at forming covalent amide bonds between ammonium-carboxylate ion pairs. (2) The cross linking did not introduce additional amide bonds between otherwise non-interacting ammonium and carboxylate groups. And (3) the remaining carboxylate groups were complexed to a small molecular weight counterion (Na^+). Next, the ion pairing of the ammonium groups in PLL was determined by assuming: (4) All pendent amines in PLL are protonated. (5) Ammonium groups not covalently cross linked to form amide bonds prefer to form ion pairs with sulfate groups in the CS or HEP. (6) Excess ammonium groups then form complexes with counterions (Cl^-) only after the sulfate groups have been completely consumed. Based on these six assumptions, the authors demonstrate that the ion pairing between the polycation (PLL) increases with increasing charge density of the polyanion (HA < CS < HEP). They also demonstrate that this increase in ion pairing within the film is associated with a decrease in the film hydration.

In the present work, we cannot use the cross linking method proposed by Crouzier and Picart, since we cannot assume that all of the amine groups are protonated (the pK_{aCHI} = 6.0-6.5, while the pK_{aPLL} = 10-10.5). Also, the methylation of amine groups in TMC would complicate the assumptions associated with the cross linking reaction. In an investigation of

the chitosan-alginate system (CHI-ALG) Lawrie et al. provide a very thorough interpretation of the FT-IR spectra and suggest that FT-IR cannot be used to unambiguously determine the ion pairing when chitosan is used as the polycation, since the carboxylate and ammonium groups do not absorb at different frequencies when complexed.[33] They also employ high-resolution XPS spectra of the N1s envelope to determine the composition of the nitrogen species in films and PEMs.

In general, we find that the PEM thickness increases with increasing molecular weight of the polyanion. The PEM thickness and hydrophilicity are also very different depending upon which polyelectrolyte pairs are used. The CHI-HA PEM is composed of the two weak polyelectrolytes used in this study. In the CHI-HA PEM, a significant fraction of the carboxylic acid peaks are protonated (as evidenced by the peak at 1709 cm^{-1} in the CHI-HA PM-IRRAS spectrum in Figure 3.7). Therefore, we can conclude that these two polysaccharides are not tightly bound by many ionic bonds. The CHI-HA PEM is also the thickest, the most hydrophilic, and has the largest change in thickness upon drying of the CHI PEMs (comparing the SPR and ellipsometry data). The position of the carboxylic acid peak in this PEM also indicates a high degree of hydrogen bonding compared to the neat HA spectrum. We conclude from all of these observations that the CHI and HA are only loosely associated in the PEM, which has a high water content. This is consistent with previous reports suggesting that CHI-HA multilayers formed under similar conditions might have significant diffusion of the CHI during PEM assembly.[7] When HA is replaced by the strong polyanions CS and HEP, the PEMs are much thinner, have significantly reduced hydrophilicity, and have less thickness loss upon drying. This is also consistent with

observations made using synthetic weak polyelectrolytes, suggesting that reducing charge density results in thicker PEMs.[16]

When the weak polycation, CHI, is replaced by a stronger polycation, TMC, all of the PEMs have reduced thickness. This is most dramatic for the HA PEM, and within the thickness uncertainty for the other two PEMs. But, the HEP and CS PEMs are significantly more hydrophilic than their CHI-containing counterparts, and exhibit a greater loss of thickness on drying. The most hydrophilic PEMs are formed from the weak polycation-weak polyanion pair (CHI-HA) and the strong polycation-strong polyanion pairs (TMC-CS and TMC-HEP). The most hydrophobic PEMs are formed when one of the polyelectrolytes is weak and the other is strong (CHI-CS, CHI-HEP, and TMC-HA).

Figure 3.9 summarizes these observations and illustrates possible explanations based on our understanding of the ion pairing from the spectroscopic data presented above. When the two weak polyelectrolytes are paired, the charge density on CHI is relatively weak. There is also a substantial amount of protonated carboxylic acid with H-bonded carbonyl groups present, suggesting a relatively weak charge density on the HA as well. Thus there is reduced ion pairing between the two constituent polyelectrolytes, which allows the PEMs to swell significantly when wet. Figure 3.9 shows one of the carboxylic acid groups from HA H-bonded to water, but these could also be H-bonded to other carboxylic acids.

Increasing the charge density on the polyanion by incorporation of sulfate groups results in increased charge density on CHI, causing increased ion pairing between the constituent polyelectrolytes. This is evidenced by the increase in the $-NH_3^+$ symmetric stretch between 1538 and 1530 cm^{-1} and by the increase in the component of the XPS peak corresponding to the ammonium nitrogen at about 402 eV. This increase in the complexation between the

polyelectrolytes reduces the ability of the CHI-CS and CHI-HEP to swell. The increased electrostatic complexation also makes these PEMs more hydrophobic.
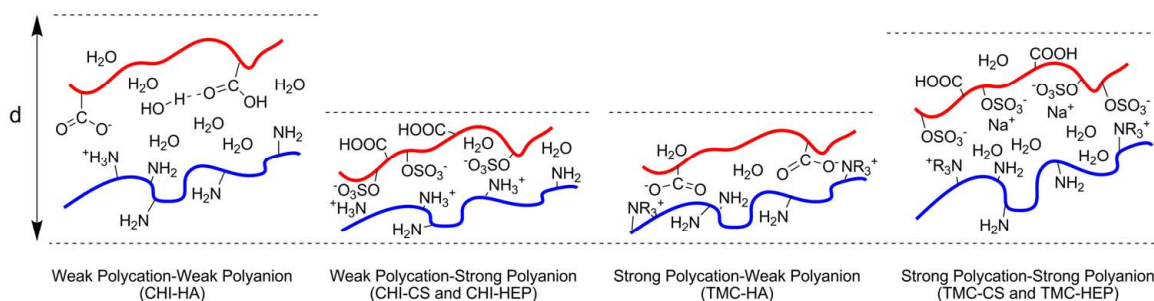
Figure 3.9 Schematic illustrating interactions that govern PEM wet thickness for different polyelectrolyte combinations.

Conversion of CHI to TMC by partial methylation of the amine groups does not significantly increase the pK_a of *N,N*-dimethyl glucosamine residues.[36] However, it does introduce strong cationic *N,N,N*-trimethyl glucosamine residues at fixed locations along the chitosan chains. PEM formation using TMC and the weak polyanion HA causes an increase in the charge density of the HA, compared to complexation with CHI, as evidenced by the change in the carboxylic acid ($1711 - 1710$ cm^{-1}) and carboxylate peaks ($1611 - 1603$ cm^{-1}), seen in Figure 3.7.

When a strong polycation (CS or HEP) is paired with TMC, the charge density on the TMC is not significantly increased, as it was in the case of CHI. This could be because the strong cationic *N,N,N*-trimethyl glucosamine groups are at fixed locations along the chain, thereby decreasing the ability of TMC to conform its charge distribution to optimally complex with the sulfate groups in the polyanion. The result is that the TMC has a relatively low charge density. This also requires that a significant amount of positive counterion (Na$^+$) must be present in the PEM, to achieve charge neutrality. The large amount of sulfate and sodium ions in these PEMs imparts significant osmotic pressure, which in turn causes these

PEMs to swell and exhibit relative hydrophilicity, compared to the corresponding CHI-containing PEMs.

The PEM hydrophilicity and water uptake due to excess ions has been extensively investigated by Schlenoff et al. using the synthetic polycations poly(allylamine hydrochloride) (PAH) and poly(diallyldimethylammonium chloride) (PDADMAC), and the polyanion poly(styrene sulfonate) PSS, using a ClO_4^- salt that is detectable by FT-IR.[32, 37] PAH is a weak polycation, PDADMAC is a strong (quaternary ammonium) polycation, and PSS is a strong sulfonated polyanion. In general they observe that the small molecular weight counterion intake and water intake in the PAH-PSS (weak-strong) system is relatively low compared to the PDADMAC-PSS (strong-strong) system.[32] Based on this observation they conclude that the weak polycation-strong polyanion pair has increased ion pairing between the two polyelectrolytes, compared to the strong polycation-strong polyanion pair.[32] They explain that the low water uptake in the PAH-PSS (weak-strong) PEMs is due to higher ion pairing between the polyelectrolytes.[32] This is similar to our observations for the CHI-CS, CHI-HEP, and TMC-HA PEMs (weak-strong and strong-weak pairs) compared to the TMC-CS and TMC-HEP PEMs (strong-strong pairs) (Figure 3.9). Furthermore, when two strong polyelectrolytes are paired in PEMs, at low salt concentrations the PEMs may de-swell as salt is added, due to the "polyelectrolyte effect", while at higher salt concentrations the PEMs swell (the "antipolyelectrolyte effect").[32, 37] Although our study did not investigate the effects of salt concentration, we suggest that under the conditions at which the PEMs are deposited (0.2 M acetate buffer) there is sufficient Na^+ to induce the antipolyelectrolyte effect in the TMC-CS and TMC-HEP PEMs. In our experiments, the PEM wet thickness is actually measured during the rinsing step. At this point, the PEM is being exposed to a very

low concentration of small molecular weight counterions. However, the requirement of charge neutrality in the PEM prevents the removal of Na^+ ions during rinsing, and the resulting difference in osmotic pressure between the PEM and the rinse solution causes the PEM to swell, as illustrated in Figure 3.9. This mechanism whereby PEM swelling is enhanced when two strong polyelectrolytes are combined has not been previously described for polysaccharide-based PEMs.

3.6. Conclusions

This work is the first to provide composition details of PEMs based on TMC and glycosaminoglycans. Here, we compare polysaccharide-based PEMs formed from the polycations CHI and TMC, and the polyanions HA, CS, HEP. By a combination of spectroscopic techniques that measure the wet and dry thickness (FT-SPR and spectroscopic ellipsometry, respectively), the PEM chemistry (PM-IRRAS and XPS), and water contact angle measurements, this work provides an understanding of how the charge density on the polysaccharides affects their hydrophilicity and swelling. By comparison of water contact angle and thickness measurements, we found that the most hydrophilic PEMs were formed from the weak polycation-weak polyanion (i.e. the CHI-HA PEMs) and strong polycation-strong polyanion pairs (i.e. TMC-CS and TMC-HEP PEMs); the most hydrophobic PEMs were formed when one polyelectrolyte was strong and the other was weak (i.e. CHI-CS, CHI-HEP, and TMC-HA PEMs). PM-IRRAS and XPS provided details of the PEM composition that allow us to make conjectures that explain these observations. When both polyelectrolytes are weak, there is reduced ion pairing, enabling the PEMs to swell. When a strong polyelectrolyte is combined with a weak polyelectrolyte, the strong

polyelectrolyte controls the charge density on the weak polyelectrolyte, effectively enforcing increased ion pairing that compacts the PEM and reduces the swelling. Finally, when both polyelectrolytes are strong, the TMC only has a fraction of strong cationic groups at fixed locations along the polymer chain. Thus the strong polyanions do not as readily influence the charge density on TMC, and instead pair with some small molecular weight counterions. This increases the osmotic pressure in the PEMs, causing them to swell.

3.7 Acknowledgment

3.8 References

1. Picart, C., *Current Medicinal Chemistry* **2008**, 15 (7), 685-697.
2. Boddohi, S.; Kipper, M. J., *Advanced Materials* **2010**, 22 (28), 2998-3016.
3. Fu, J. H.; Ji, J.; Yuan, W. Y.; Shen, J. C., *Biomaterials* **2005**, 26 (33), 6684-6692.
4. Serizawa, T.; Yamaguchi, M.; Akashi, M., *Biomacromolecules* **2002**, 3 (4), 724-731.
5. Almodóvar, J.; Bacon, S.; Gogolski, J.; Kisiday, J. D.; Kipper, M. J., *Biomacromolecules* **2010**, 11 (10), 2629-2639.
6. Almodóvar, J.; Kipper, M. J., *Macromolecular Bioscience* **2011**, 11 (1), 72-76.
7. Richert, L.; Lavalle, P.; Payan, E.; Shu, X. Z.; Prestwich, G. D.; Stoltz, J. F.; Schaaf, P.; Voegel, J. C.; Picart, C., *Langmuir* **2004**, 20 (2), 448-458.
8. Schneider, A.; Francius, G.; Obeid, R.; Schwinte, P.; Hemmerle, J.; Frisch, B.; Schaaf, P.; Voegel, J. C.; Senger, B.; Picart, C., *Langmuir* **2006**, 22 (3), 1193-1200.
9. Crouzier, T.; Boudou, T.; Picart, C., *Current Opinion in Colloid & Interface Science* **2010**, 15 (6), 417-426.
10. Boudou, T.; Crouzier, T.; Nicolas, C.; Ren, K.; Picart, C., *Macromolecular Bioscience* **2011**, 11 (1), 77-89.
11. Ren, K. F.; Crouzier, T.; Roy, C.; Picart, C., *Advanced Functional Materials* **2008**, 18 (9), 1378-1389.
12. Ren, K. F.; Fourel, L.; Rouviere, C. G.; Albiges-Rizo, C.; Picart, C., *Acta Biomaterialia* **2010**, 6 (11), 4238-4248.
13. Wood, K. C.; Chuang, H. F.; Batten, R. D.; Lynn, D. M.; Hammond, P. T., *Proceedings of the National Academy of Sciences of the United States of America* **2006**, 103 (27), 10207-10212.
14. Hillberg, A. L.; Holmes, C. A.; Tabrizian, M., *Biomaterials* **2009**, 30 (27), 4463-4470.

15. Mendelsohn, J. D.; Yang, S. Y.; Hiller, J.; Hochbaum, A. I.; Rubner, M. F., *Biomacromolecules* 2003, 4 (1), 96-106.
16. Choi, J.; Rubner, M. F., *Macromolecules* **2005**, 38 (1), 116-124.
17. Schoeler, B.; Kumaraswamy, G.; Caruso, F., *Macromolecules* **2002**, 35 (3), 889-897.
18. Boddohi, S.; Killingsworth, C. E.; Kipper, M. J., *Biomacromolecules* **2008**, 9 (7), 2021-2028.
19. Boddohi, S.; Almodóvar, J.; Zhang, H.; Johnson, P. A.; Kipper, M. J., *Colloids and Surfaces B-Biointerfaces* **2010**, 77 (1), 60-68.
20. Kujawa, P.; Moraille, P.; Sanchez, J.; Badia, A.; Winnik, F. M., *Journal of the American Chemical Society* **2005**, 127 (25), 9224-9234.
21. Lavalle, P.; Picart, C.; Mutterer, J.; Gergely, C.; Reiss, H.; Voegel, J. C.; Senger, B.; Schaaf, P., *Journal of Physical Chemistry B* **2004**, 108 (2), 635-648.
22. Lundin, M.; Blomberg, E.; Tilton, R. D., *Langmuir* **2010**, 26 (5), 3242-3251.
23. Crouzier, T.; Picart, C., *Biomacromolecules* **2009**, 10 (2), 433-442.
24. Boddohi, S.; Moore, N.; Johnson, P. A.; Kipper, M. J., *Biomacromolecules* **2009**, 10 (6), 1402-1409.
25. Senel, S.; McClure, S. J., *Adv. Drug Deliver. Rev.* 2004, *56*, 1467-1480.
26. Muzzarelli, R. A. A., *Carbohydr. Polym.* 2009, *76*, 167-182.
27. Picart, C.; Lavalle, P.; Hubert, P.; Cuisinier, F. J. G.; Decher, G.; Schaaf, P.; Voegel, J. C., *Langmuir* **2001**, 17 (23), 7414-7424.
28. Crouzier, T.; Ren, K.; Nicolas, C.; Roy, C.; Picart, C., *Small* **2009**, 5 (5), 598-608.
29. Cui, D.; Szarpak, A.; Pignot-Paintrand, I.; Varrot, A.; Boudou, T.; Detrembleur, C.; Jerome, C.; Picart, C.; Auzely-Velty, R., *Advanced Functional Materials* **2010**, 20 (19), 3303-3312.
30. de Britto, D.; Assis, O. B. G., *Carbohydr. Polym.* **2007**, 69, 305-310.
31. Frutos, A. G.; Weibel, S. C.; Corn, R. M., *Anal. Chem.* **1999**, 71 (18), 3935-3940.
32. Jaber, J. A.; Schlenoff, J. B., *Langmuir* **2007**, 23 (2), 896-901.
33. Lawrie, G.; Keen, I.; Drew, B.; Chandler-Temple, A.; Rintoul, L.; Fredericks, P.; Grondahl, L., *Biomacromolecules* **2007**, 8 (8), 2533-2541.
34. ElMiloudi, K.; Benygzer, M.; Djadoun, S.; Sbirrazzuoli, N.; Geribaldi, S., *Macromolecular Symposia* **2005**, 230, 39-50.
35. Rana, V.; Tiwary, A. K.; Jain, S.; Singh, D., *Iranian Journal of Pharmaceutical Research* **2007**, 6 (4), 231-242.
36. Amidi, M.; Romeijn, S. G.; Borchard, G.; Junginger, H. E.; Hennink, W. E.; Jiskoot, W., *Journal of Controlled Release* **2006**, 111 (1-2), 107-116.
37. Schlenoff, J. B.; Rmaile, A. H.; Bucur, C. B., *Journal of the American Chemical Society* **2008**, 130 (41), 13589-13597.

Chapter 4

FT-IR Studies on Stability of Proteins Adsorbed to

Polysaccharide-Based Polyelectrolyte Multilayers

4.1 Introduction

Polyelectrolyte/protein interactions have been shown to enhance stability of a protein's secondary structure.[1] Furthermore, it has been demonstrated that polysaccharides play an important role in the stability and activation of important growth factors used to induce mesenchymal stem cell differentiation.[2-5] In this study, we are interested in using IR spectroscopy to study the adsorption and stability of model proteins onto polyelectrolyte multilayers films. Three naturally derived polyelectrolytes are used in this study: heparin, hyaluronan and chitosan. Heparin, a strong polyanion, is a sulfated polysaccharide that binds and activates many important growth factors, including members of the fibroblast growth factor (FGF) family[3] and the transforming growth factor beta (TGF-β) superfamily.[4,5] Chitosan, a weak polycation, has demonstrated antimicrobial activity,[6-10] and supports mammalian cell growth.[11,12] Polyelectrolyte multilayers made from these polysaccharides may serve as surface coatings for tissue engineering scaffolds and orthopedic implants.

Several recent studies have investigated adsorption of proteins onto polyelectrolyte multilayers (PEM).[1,13-16] These PEM are created by alternating deposition of a polycation and polyanion on a charged substrate. These studies demonstrated that electrostatic interactions are primarily responsible for stabilizing bound proteins. Several studies have observed that proteins adsorb to PEM regardless of the charge of the final layer. Schwinté et al.[1] explains that this happens because even though proteins carry an overall charge, pendent groups whose charge is different from the net charge of the protein are sufficient to stabilize adsorption.

Infrared spectroscopy has been widely used to study the secondary structure of proteins.[17-18] The IR spectra of proteins contains three regions that can be used to discern protein secondary structure: amide I (1700-1600 cm^{-1}), amide II (1600-1500 cm^{-1}), and amide III (1350-1200 cm^{-1}).[17-18] The amide I and II regions are favorable in IR studies due to their high absorbance even at low protein concentrations. Secondary structural features can be discerned in the amide I region.[17-18] Resolving the principle component bands from the amide I peak provides relative amounts of the secondary structural features of the proteins.[17-21,23] Different methods for resolving the amide I region in a protein spectrum in solution or adsorbed onto a surface have been reported including: Fourier self-deconvolution,[17-21] second derivative,[17-19,21-24] and partial least squares.[17,25] All of these methods show reasonable results of protein secondary structure when compared to other methods such as X-ray crystallography and circular dichroism. Hydrogen-deuterium exchange (HDX) has also been used to study the secondary structure of proteins using FT-IR.[17,18] During HDX, hydrogen atoms are exchanged with heavier deuterium atoms causing a shift to lower wavenumber in the IR spectra (Figure 4.1). When globular proteins

are in a folded state, in which they are stable, they should exchange fewer hydrogen atoms, thus the quantification of the exchange can provide information about the stability of the protein.

In this article we report results obtained from the interactions of model proteins, with surfaces having different net charges at physiological pH, using PEMs constructed from naturally-derived polysaccharides. FT-IR spectroscopy used in polarization modulation mode (PM-IRRAS) is used to analyze the adsorbed proteins on the PEM, while FT-IR in transmission mode is used to investigate the proteins in solution. FT-IR of the amide I regions of the spectra and HDX experiments are used to obtain secondary structural information.
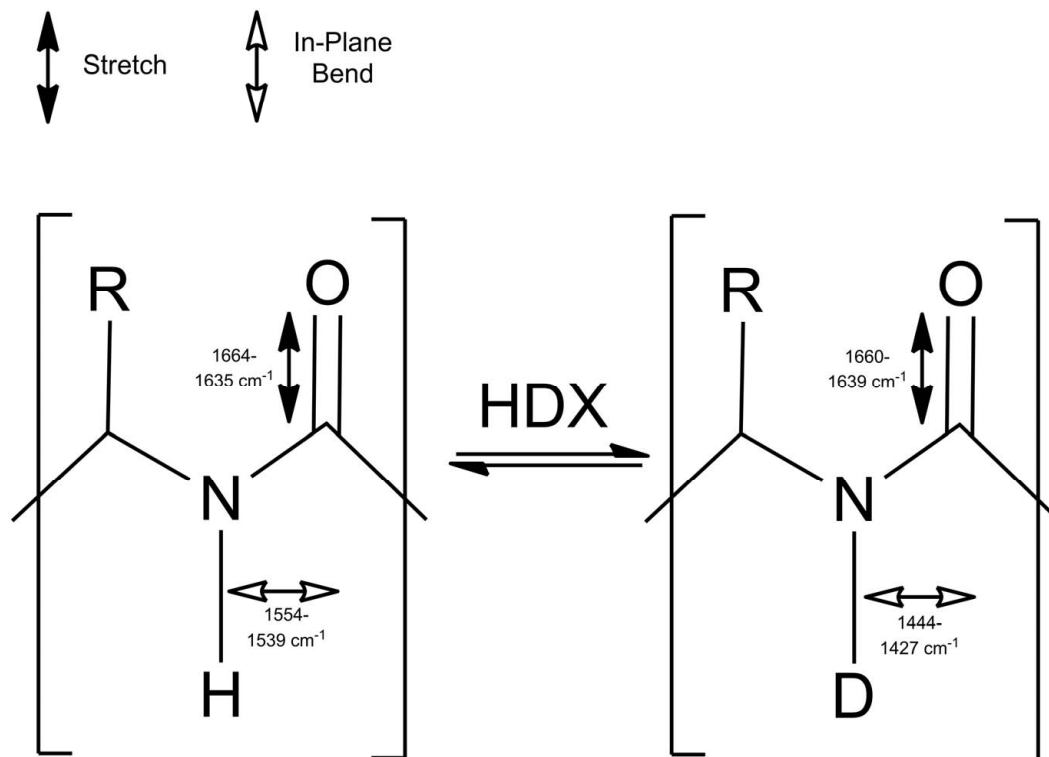
Figure 4.1 Hydrogen-Deuterium exchange schematic.

4.2 Materials and Methods

4.2.1 Materials

Chitosan (poly(β-(1,4)-D-glucosamine-co-*N*-acetyl-D-glucosamine); 4.7% acetylated) was purchased from Biosyntech Inc. (Laval, Canada). Heparin sodium (from porcine intestinal mucosa, 12.5% sulfur) was purchased from Celsus Laboratories (Cincinnati,OH). Hyaluronan and 11-mercaptoundecanioc acid (MUA) 95% were purchased from Sigma-Aldrich (St. Louis, MO). SF10 glass chips (18 mm by 18 mm) were purchased from GWC Technologies Inc. (Madison, WI). Gold was purchased from Alfa Aesar (Ward Hill, MA). Glacial acetic acid and ethanol (200 proof 99.5%) were purchased from Acros Organics (Geel, Belgium). Sodium acetate was purchased from Fisher Scientific. (Pittsburgh, PA). A Millipore Synthesis water purification unit was used to obtain 18.2 MΩ water, used for making all aqueous solutions (Millipore, Billerica, MA).

The polyelectrolytes were dissolved in an acetate buffer solution of pH 5 and a concentration of 0.2 M. Table 4.1 lists some of the key features of the proteins used in this study. Bovine serum albumin was purchased from Sigma. Lysozyme was purchased from Pierce (Rockford, IL). All proteins were used as received, without further purification. Proteins were dissolved in water or phosphate buffered saline (PBS) with pH 7.3 and sodium chloride concentration of 0.137 M. PBS was made from sodium chloride, sodium phosphate dibasic anhydrous, potassium chloride, and potassium phosphate monobasic, all purchased from Fisher Scientific. All solutions were filtered with a 0.22 µm PVDF filter (Fisher Scientific) prior to any experiment.

Table 4.1 Proteins used in this study.

Protein	MW (kDa)	Conformation	pI	Net charge at pH 7.3
BSA	66.4	Globular	4.7	Negative
Lysozyme	14.3	Globular	11.4	Positive

4.2.2 Construction of polyelectrolytes multilayers (PEMs) and protein adsorption

PEM construction has been extensively studied in our laboratory, and a detailed procedure can be found in reference 26. In brief, an SF-10 glass chip was coated with gold (~45 nm) using chromium as an adhesion layer (~5 nm). A self-assembled monolayer of MUA was deposited on the gold substrate by adsorption from a 1 mM ethanolic solution. The MUA-coated gold substrate was mounted on the flow cell of an SPR-100 module of a Nicolet 8700 FT-IR (Thermo-Electron, Madison, WI). The SPR module was used to monitor the construction of the PEM by alternating 5-minute adsorption steps of the polyelectrolytes, with a 5-minute acidified water rinse (pH 4) between adsorption steps (Figure 4.2). Polysaccharide solutions with concentrations of 0.01 M were prepared in acetate buffer (0.2 M, pH 5). Concentrations were calculated on a saccharide unit basis.
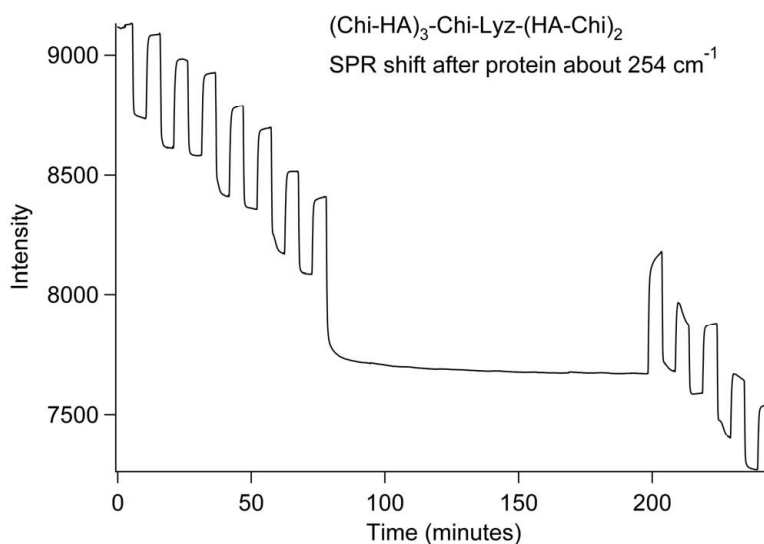
Figure 4.2 FT-SPR peak position during construction of a chitosan-terminated PEM. The five minute deposition and rinse intervals are clearly seen. Lysozyme was adsorbed under constant flow after the 7th layer from a 10 μg/mL solution in water. 4 more PEM layers are added after protein adsorption.

101

Figure 4.2 shows an SPR trace (plasmon resonance peak position versus time), beginning with the initial rinse, and showing the subsequent polyelectrolyte adsorption steps (chitosan, water, hyaluronan, water, etc). The wavenumber shift after deposition of each layer (during water rinse) confirms the construction of the PEM. Two methods were investigated for adsorbing proteins to the PEM – static and constant flow. For static adsorption, the PEM was removed from the SPR flow cell, rinsed with ethanol then with water and placed in a petri dish containing the dissolved protein in water or PBS. The substrate was kept in the solution for 2 hours. For the constant flow adsorption, first PBS or water was allowed to flow through the flow cell for 20 or 5 minutes. Following the rinse, the protein solution was allowed to flow and recycle through the cell for 2 hours. Before completion, the substrate was rinsed to remove any unbound protein.

4.2.3 Polarization-modulation infrared reflection absorption spectroscopy (PM-IRRAS)

FT-IR spectroscopy was used in polarization modulation mode to study protein adsorption. Experiments were conducted using a Nicolet 8700 FT-IR (Thermo-Electron) spectrometer configured with a Tabletop Optics Module equipped with a PEM-90 photo elastic modulator (Hinds Instruments, Hillsboro, OR) to provide polarization of the incident infra-red light with a grazing angle sampling optics (86º for gold substrate), a liquid nitrogen-cooled MCT-A detector and a demodulator (GWC Technologies) to process the *s*- and *p*-polarized reflection spectra. A cubic spline function, with predetermined spline points, was applied to the data to remove the Bessel function background characteristic of PM-IRRAS spectra.[26] PM-IRRAS spectra were collected at 2 cm^{-1} resolution with 1000 scans for each sample in the range of 1000-2000 cm^{-1}.

4.2.4 Transmission Fourier transform infrared (FT-IR) spectroscopy

FT-IR spectroscopy in transmission mode was used to study the native structure of the proteins in solution. Proteins were dissolved in deuterium oxide at a concentration of 10 mg/ml for all transmission FT-IR experiments. D_2O was used as the solvent in order to avoid the water absorption band found in the amide I region. It has been shown that D_2O serves as a good solvent which maintains protein stability while avoiding water absorption.[17-19] Experiments were conducted using a Nicolet 8700 FT-IR (Thermo-Electron) spectrometer with a Spectra-Tech Demountable Pathlength Cell Kit (Thermo-Electron) holder using two 32 mm diameter and 3 mm thick CaF_2 windows and a 25 µm Teflon® spacer. 200 scans were collected at a resolution of 4 cm^{-1}. A liquid nitrogen-cooled MCT-A detector was used to collect the data. The chamber of the FT-IR was purged with CO_2-free dry air prior to and during all experiments. A background spectrum was collected when the sample holder was not present in the chamber. Spectra of the holder with D_2O and protein in D_2O were then collected. The protein spectra were obtained by subtracting the D_2O spectrum from the protein in D_2O spectra.

4.2.5 Hydrogen-deuterium exchange (HDX)

An HDX technique was used to study the secondary structure of the adsorbed proteins. The substrates with the protein adsorbed were put in a chamber humidified with D_2O (95% relative humidity). PM-IRRAS spectra were collected at several time periods until equilibrium was achieved (up to 72 hours).

4.2.6 Spectral analysis

Data for all FT-IR experiments was collected using the OMNIC 7.3 (Thermo-Electron) software. For FT-IR in transmission mode, OMNIC's spectral math feature was used to

obtain the protein spectra. The spectroscopy analysis software IgorPro (Version 5.0.5.7, Wave Metrics, Inc., Portland, OR) was used to perform the Bessel function subtraction for the PM-IRRAS data. IgorPro was also used to subtract the PEM spectra from the PEM substrates with adsorbed protein. To study the secondary structure of the adsorbed proteins, the amide I regions (1600-1700 cm^{-1}) of the spectra were analyzed. The peak resolve procedure in OMNIC was used to fit the Gaussian components of the amide I peak. This algorithm uses a cubic-polynomial 5-point Savitzky-Golay second derivative to identify the positions of component peaks within the amide I band, and then optimizes their intensities, widths and positions to fit a composite spectrum to the original spectrum. The peak positions and the areas of the component bands were recorded. The areas were expressed in percent of the total area of the peaks corresponding to secondary structural features within the amide I band.

4.3 Results and Discussions

In general, we found that constant flow adsorption was more effective than static adsorption when water is used as the protein solvent and the rinse. The opposite is true when PBS is used. The PM-IRRAS spectra of the samples prepared using static adsorption showed more intense peaks, indicating that more protein was adsorbed on the surface when PBS was used as the solvent (data not shown). Figure 4.3 shows the PM-IRRAS spectra of a heparin terminated PEM with (middle) and without (top) protein, and the spectra of the adsorbed proteins with the PEM subtracted (bottom). Figure 4.4 shows similar spectra for a chitosan terminated PEM. IR spectra of proteins are characterized by the presence of the amide I (1700-1600 cm^{-1}) and II (1600-1500 cm^{-1}) regions. For Figures 4.3 and 4.4, the strong presence of the amide I (~1670 cm^{-1}) and amide II (~1550 cm^{-1}) peaks in the spectra

confirms the adsorption of lysozyme onto the PEM. Figures 4.3 and 4.4 shows that lysozyme, positive at physiological pH, adsorbs onto the PEM regardless of whether the final layer carries a negative or neutral charge. The chitosan-terminated PEM carries a neutral charge at physiological pH, while the heparin-terminated surface caries a negative charge at neutral pH. Similar experiments with bovine serum albumin (negative at physiological pH) confirmed that proteins with isoelectric points above and below the solution pH adsorb onto both negative and neutral surfaces (figures not shown). Our results are in agreement with previous reports of protein adsorption onto PEM made from synthetic polymers.[1,13-16] Several mechanisms[1,14-15] have been proposed to explain this phenomenon. Proteins do not behave as point charges; rather globular proteins have a surface characterized by local regions of both positive and negative charges that can interact with surfaces. Thus, the net charge and isoelectric point are not necessarily good predictors of protein adsorption.
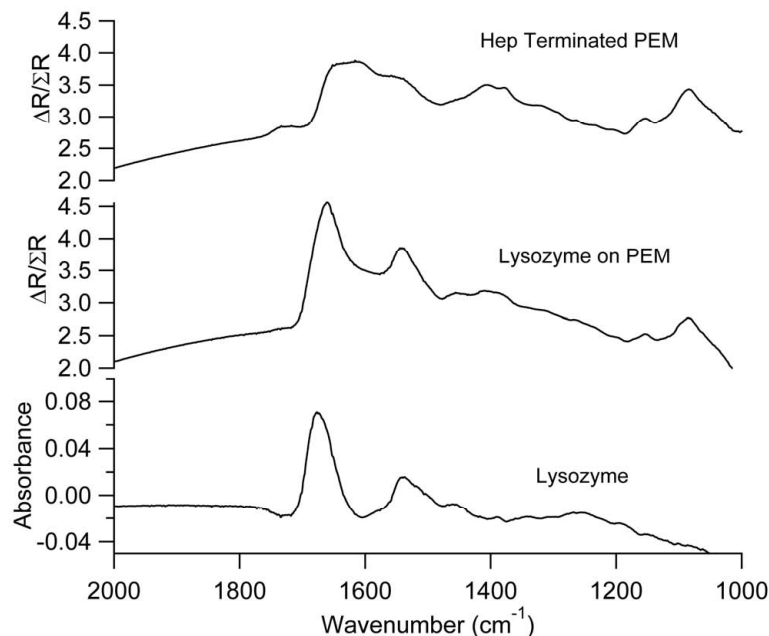
Figure 4.3 IR spectra of a heparin terminated polyelectrolyte multilayers without lysozyme (top), with lysozyme (middle), and subtracted spectrum of lysozyme (bottom). Lysozyme was adsorbed from solution (10 µg/ml) under constant flow for 2 hours.
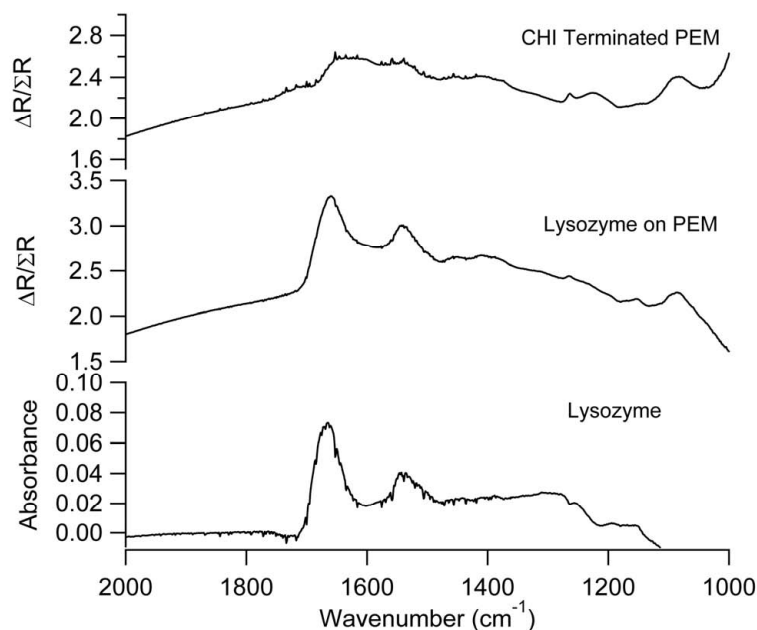
Figure 4.4 IR spectra of a chitosan terminated polyelectrolyte multilayers without lysozyme (top), with lysozyme (middle), and subtracted spectrum of lysozyme (bottom). Lysozyme was adsorbed from solution (10 µg/ml) under constant flow for 2 hours.

Noticeable changes in IR spectra can provide stability information of absorbed proteins. For example, disappearance of the amide peaks over time may indicate protein hydrolysis. In the case of BSA, a decrease α-helix and increases in both β-sheet and β-turn content (obtained by analyzing the amide I region) indicates aggregation.[27]

Protein adsorption studies were performed at two different concentrations, 10 and 250 µg/ml. Adsorption of lysozyme was noted for both concentrations; however, adsorption of BSA was not observed at a concentration of 10 µg/ml. To study the stability of the adsorbed proteins, an analysis of the amide I region of the spectra was performed. It was assumed that the PEM with protein spectra were a linear combination of the spectra of the PEM plus the spectra of the proteins in the form:

$$M(v) = a_1 S_1(v) + a_2 S_2(v) \tag{1}$$

106

were $M(v)$ is the collected spectra, $S_1(v)$ and $S_2(v)$ are the spectra of the PEM and the protein, respectively, as functions of wavenumber (v), and a_1 and a_2 are weight factors. Dividing equation 1 by the PEM spectrum enables one to solve for the value of a_1:[28]

$$\frac{M(v)}{S_1(v)} = a_1 + a_2 \frac{S_2(v)}{S_1(v)} \tag{2}$$

The constant a_1 is found from the ratio $M(v)/S_1(v)$ when $S_2(v)$ equals zero (i.e. in a region where the protein does not adsorb). Once, a_1 is known, equation 1 can be used to find the protein spectrum. Values of a_1 used for all experiments fell within the range of 0.15-1.1. A 15 point Savitzky-Golay smoothing algorithm was performed prior to analysis of spectra. The amide I region from 1600-1700 cm^{-1} was evaluated by fitting a number of Gaussian curves. The number and location of the peaks were estimated by calculating the cubic-polynomial 5-point Savitzky-Golay second derivative of the spectra. The peaks were automatically adjusted to produce a composite spectrum that matches the original. Figure 4.5 shows an example of the corrected spectrum with its second derivative, Gaussian peaks, fitted curve, and residual error.
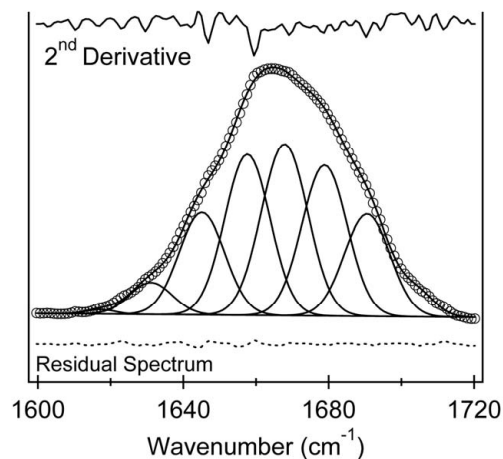
Figure 4.5 IR spectra (middle circles) and calculated curve (middle line) of lysozyme adsorbed onto a heparin-terminated PEM (from a 10 µg/ml solution), its second derivative (top), and its residual (bottom).

107

Figure 4.5 demonstrates that the amide I region of lysozyme adsorbed onto a heparin-terminated PEM can be deconvolved into 8 Gaussian peaks. Six of the eight peaks can be assigned to secondary structural features of the protein, while the other two can be attributed to side chain regions. The peaks at 1631, 1645, 1657, 1667, 1678, and 1691 cm^{-1} were assigned to β-sheet, α-helices, α-helices, α-helices, turns, and turns or β-sheet respectively.[1,17-19,22] Contributions of each peak to the sum of the areas of the secondary structure peaks can be calculated to give the relative percentage of the secondary structural features of the protein. For Figure 4.5 the low frequency β-sheet (1631 cm^{-1}) accounts for 4%, three α-helix peaks (1645, 1657 & 1667 cm^{-1}) add up to 61%, turns (1678 cm^{-1}) account for 21%, and a peak at 1691, which can be assigned to turn or β-sheet, accounts for 14% of the protein's secondary structure. Similar analysis was performed for all the protein and surface combinations, and the Gaussian peak parameters were recorded and compared.

The proteins in solution were also studied. The solution spectra were obtained by dissolving 10 mg/ml of protein in D$_2$O. D$_2$O is a favorable solvent for transmission FTIR of proteins in solution because it preserves the protein structure and avoids the overlapping water band in the amide I region.[17-19] Figure 4.6 shows the deconvolved amide I peak of lysozyme dissolved in D$_2$O (Table 4.2). The deconvolution results in nine peaks, seven of which can be assigned to structural features of the protein.
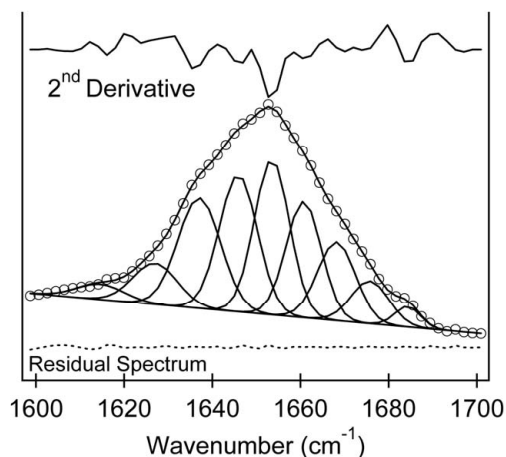
Figure 4.6 IR spectrum (middle circles) and calculated curve (middle line) of lysozyme dissolved in deuterium oxide (10 mg/ml), its second derivative (top), and its residual (bottom).

Hydrogen/deuterium exchange (HDX) consists of exposing a sample to a D_2O rich environment to allow the exposed hydrogen atoms to be exchange with deuterium atoms. The FT-IR spectrum of the exchanged sample typically has adsorption bands with lower wavenumber positions since the deuterium atoms are heavier than hydrogen atoms. (Figure 4.1) HDX causes all of the absorption bands within the amide I region to shift to lower wavenumbers by 2 to 10 cm^{-1}. The amide II region encounters the largest shift, were the region at 1554-1539 cm^{-1} decreases in intensity and a new region appears at 1444-1427 cm^{-1}, generally referred as amide II'.[17-19] The relative intensities of the amide II and amide II' peaks gives information on the stability of the secondary structure of the proteins by indicating the relative number of hydrogen atoms exposed for exchange; proteins in an unfolded state have more protons exposed for greater exchange.

Figure 4.7 shows PM-IRRAS spectra of lysozyme adsorbed to a chitosan-terminated PEM undergoing HDX. Spectra were corrected by subtracting the underlying PEM from each of them. Before HDX (0 hrs) the strong presence of the amide II peak is noticeable in Figure 4.7. HDX is confirmed by the evident reduction of the amide II peak and the

109

formation of the amide II' peak around 1450 cm^{-1}. Previous experiments in our laboratory

confirm that the spectrum of the underlying PEM does not change detectably during the

HDX process, thus it is safe to assume that the protein spectra is the only one affected.
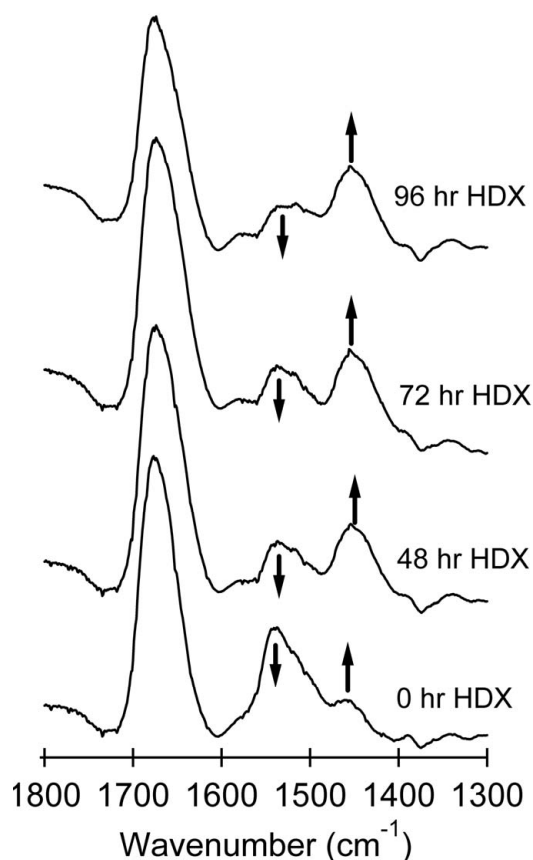
Figure 4.7 Spectra of lysozyme during HDX at different time points, having the underlying PEM (chitosan-terminated) spectrum subtracted. Lysozyme was adsorbed from a 10 µg/ml solution. Arrows indicate the amide II peak which are strongly affected by HDX.

Tables 4.2 and 4.3 summarize the FT-IR studies of lysozyme and BSA, respectively, and

compare the proteins in solution to proteins adsorbed to PEM, both before and after HDX.

When lysozyme is adsorbed to surfaces, in all cases the α-helical content is decreased and

the percentages of higher wavenumber turn and β-sheet structures are increased. Adsorption

from more concentrated solutions, in general, reduces protein stability. On the

heparin-terminated surfaces, the α-helical peaks of lysozyme adsorbed from 250 µg/ml

solution undergo a greater wavenumber shift during HDX than at other conditions. In protonated samples α-helical peaks appear in a range that overlaps with peaks from some unordered regions. Upon HDX, typically, the unordered regions undergo a greater wavenumber shift than the α-helix peaks. Thus, the greater wavenumber shift for these peaks could also indicate some unfolding of lysozyme when adsorbed from concentrated solution onto heparin-terminated PEM. However, this effect is not observed when lysozyme was adsorbed to heparin-terminated surfaces from 10 µg/ml solutions, or when lysozyme was adsorbed to chitosan-terminated surfaces. The results obtained in our lab are in agreement with those found in literature for the composition of BSA and lysozyme.[17]

Table 4.2 Structural analysis of lysozyme adsorbed on a PEM and in solution.

Condition[a]		Secondary Structure Features and their representative IR peaks (cm⁻¹)				
		β-Sheet or Side Chain	β-Sheet	α-Helix[b]	Turn	Turn or β-sheet
Solution 10 mg/ml		1626 (8%)	1636 (18%)	1645-1660 (65%)	1675 (7%)	1684 (2%)
Hep-terminated 250 µg/ml	0 hr of HDX	1622 (3%)	1635 (7%)	1647-1669 (58%)	1681 (22%)	1694 (10%)
Hep-terminated 250 µg/ml	72 hr of HDX	1617 (3%)	1630 (7%)	1643-1663 (57%)	1674 (20%)	1683 (13%)
Chi-terminated 250 µg/ml	0 hr of HDX	1623 (4%)	1633 (9%)	1646-1669 (59%)	1678 (16%)	1690 (12%)
Chi-terminated 250 µg/ml	72 hr of HDX	1625 (6%)	1636 (11%)	1647-1669 (61%)	1680 (15%)	1691 (7%)
Hep-terminated 10 µg/ml	0 hr of HDX	-	1631 (4%)	1645-1667 (61%)	1679 (21%)	1691 (14%)
Hep-terminated 10 µg/ml	72 hr of HDX	-	1632 (9%)	1645-1668 (63%)	1679 (19%)	1691 (9%)
Chi-terminated 10 µg/ml	0 hr of HDX	-	1630 (7%)	1643-1665 (55%)	1676 (21%)	1688 (16%)
Chi-terminated 10 µg/ml	72 hr of HDX	-	1630 (10%)	1643-1665 (61%)	1677 (19%)	1689 (10%)

[a]"Solution" indicates protein spectra obtained in a D₂O solvent at the concentration given. "Hep-terminated" and "Chi-terminated indicate protein adsorbed to a heparin-terminated PEM and chitosan-terminated PEM, respectively, at the indicated concentrations.
[b]Range in the peak positions accounts for multiple peaks that can be assigned to a structural feature;the percentage is the sum of the areas of those peaks. For lysozyme three peaks were obtained that can be assigned to α-Helix.

For BSA adsorbed to surfaces, there is significant loss of α-helical content and an increase in β-sheet structures, compared to the BSA in solution. The β-sheet structures found at 1616 cm^{-1} and 1675 cm^{-1} when BSA is dissolved in D$_2$O occur at slightly elevated wavenumbers when adsorbed to surfaces. This may indicate that the formation of β-sheets upon adsorption result in relatively stable H-bonds that are not susceptible to HDX.

Table 4.3 Structural analysis of BSA adsorbed on a PEM and in solution[a].

Condition		Secondary Structure Features and their representative IR peaks (cm^{-1})				
		β-Sheet or Side Chain	*β-Sheet*	*α-Helix*[b]	*Turn*	*Turn or β-sheet*
Solution 10 mg/ml		1616 (4%)	1637 (22%)	1646-1660 (56%)	1667 (11%)	1675 (7%)
Hep terminated 250 μg/ml	0 hr of HDX	1619 (14%)	1630 (20%)	1644-1657 (41%)	1665 (14%)	1676 (11%)
Hep terminated 250 μg/ml	72 hr of HDX	1619 (18%)	1630 (22%)	1643-1658 (41%)	1666 (11%)	1676 (8%)
Chi terminated 250 μg/ml	0 hr of HDX	1621 (13%)	1634 (15%)	1646-1657 (36%)	1667 (19%)	1677 (17%)
Chi terminated 250 μg/ml	72 hr of HDX	1621 (13%)	1633 (14%)	1643-1655 (42%)	1667 (18%)	1677 (13%)

[a]"Solution" indicates protein spectra obtained in a D$_2$O solvent at the concentration given. "Hep-terminated" and "Chi-terminated indicate protein adsorbed to a heparin-terminated PEM and chitosan-terminated PEM, respectively, at the indicated concentrations.
[b]Range in the peak positions accounts for multiple peaks that can be assigned to a structural feature; the percentage is the sum of the areas of those peaks. In solution there were three peaks assigned to α-Helix. On surfaces, only two α-helix peaks were found in the indicated ranges.

FT-IR spectroscopy can also be used to monitor protein release from PEMs in solution. Preliminary studies have been performed were a heparin-terminated PEM is constructed and lysozyme is adsorbed as the final layer of the protein (Figure 4.8). The sample was incubated at 37ºC and a PM-IRRAS spectrum is obtained every day for a period of 12 days. A noticeable decrease in amide I is noticed throughout the days, and the spectra of the PEM with protein begins to resemble the spectra of a native PEM after 12 days of incubations.

This technique also allows investigating the secondary structure of the adsorbed protein over

time, and might provide information about protein degradation kinetics.
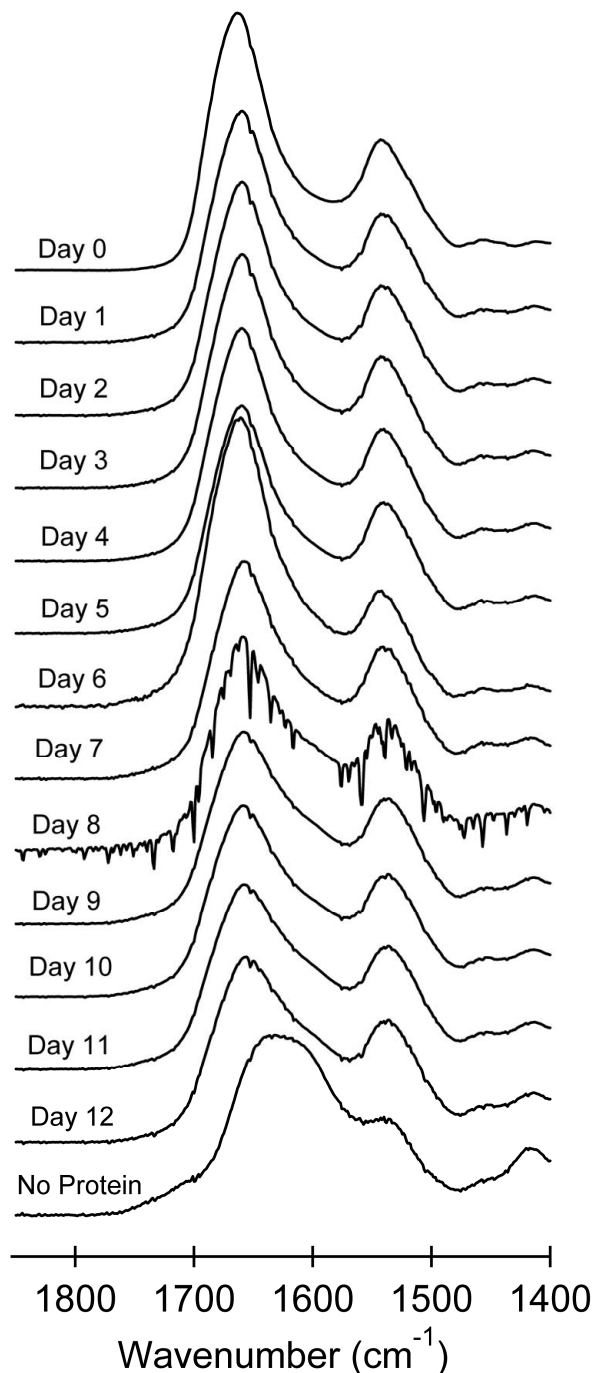
Figure 4.8 PM-IRRAS spectra of a PEM with adsorbed lysozyme incubated for protein release in water at 37°C for a period of 12 days. Every day the PEM was removed, air dried, and a PM-IRRAS spectrum was collected.

4.4 Conclusions

The adsorption and stability of model proteins onto polyelectrolyte multilayers prepared from naturally derived polysaccharides was investigated. It was confirmed via FT-IR that both negatively and positively charged proteins adsorb onto both negatively charged and neutral PEMs. Both lysozyme and BSA undergo changes in their secondary structures when adsorbed to PEMs, characterized by loss of α-helical content and increases in β-sheet structures. For lysozyme, the secondary structure is more stable when it is adsorbed from dilute solution. For BSA, the β-sheet structures that are formed during adsorption are apparently strongly H-bonded, as they undergo a reduced degree of HDX compared to the protein in solution. FT-SPR, PM-IRRAS, and transmission FT-IR along with HDX are shown to be powerful tools for investigating protein adsorption, release, and stability on polysaccharide-based PEMs.

4.5 References

1. P. Schwinte, V. Ball, B. Szalontai, Y. Haikel, J.C. Voegel, P. Schaaf, Secondary Structure of Proteins Adsorbed onto or Embedded in Polyelectrolyte Multilayers *Biomacromolecules* **3**: 1135-1143 (2002).
2. A. Au, A. Polotsky, K. Krzyminski, A. Gutowska, D.S. Hungerford, C.G. Frondoza, Evaluation of thermoreversible polymers containing fibroblast growth factor 9 (FGF-9) for chondrocyte culture, *J Biomed Mater Res A* **69A**: 367-372 (2004).
3. M. Maccarana, B. Casu, U. Lindahl, Minimal Sequence in Heparin Heparan-Sulfate Required for Binding of Basic Fibroblast Growth-Factor, *J Biol Chem* **268**: 23898-23905 (1993).
4. T.A. Mccaffrey, D.J. Falcone, B.H. Du, Transforming Growth Factor-Beta-1 Is a Heparin-Binding Protein - Identification of Putative Heparin-Binding Regions and Isolation of Heparins with Varying Affinity for Tgf-Beta-1, *J Cell Physiol* **152**: 430-440 (1992).
5. C.C. Rider, Heparin/heparan sulphate binding in the TGF-beta cytokine superfamily, *Biochem Soc Trans* **34**: 458-460 (2006).

6. A.M. Durango, N.F.F. Soares, S. Benevides, J. Teixeira, M. Carvalho, C. Wobeto, N.J. Andrade, Development and evaluation of an edible antimicrobial film based on yam starch and chitosan, *Packag Technol Sci* **19**: 55-59 (2006).

7. C.H. Lee, D.S. An, H.F. Park, D.S. Lee, Wide-spectrum antimicrobial packaging materials incorporating nisin and chitosan in the coating, *Packag Technol Sci* **16**: 99-106 (2003).

8. S.G. Hu, C.H. Jou, M.C. Yang, Surface grafting of polyester fiber with chitosan and the antibacterial activity of pathogenic bacteria, *J Appl Polym Sci* **86**: 2977-2983 (2002).

9. M. Fujita, M. Kinoshita, M. Ishihara, Y. Kanatani, Y. Morimoto, M. Simizu, T. Ishizuka, Y. Saito, H. Yura, T. Matsui, B. Takase, H. Hattori, M. Kikuchi, T. Maehara, Inhibition of vascular prosthetic graft infection using a photocrosslinkable chitosan hydrogel, *J Surg Res* **121**: 135-140 (2004).

10. C.K. Peng, S.H. Yu, F.L. Mi, S.S. Shyu, Polysaccharide-based artificial extracellular matrix: Preparation and characterization of three-dimensional, macroporous chitosan and chondroitin sulfate composite scaffolds, *J Appl Polym Sci* **99**: 2091-2100 (2006).

11. V.F. Sechriest, Y.J. Miao, C. Niyibizi, A Westernausen-Larson, H.W. Matthew, C.H. Evans, F.H. Fu, J. Suh, GAG-augmented polysaccharide hydrogel: A novel biocompatible and biodegradable material to support chondrogenesis, *J. Biomed Mater Res,* **49**: 534-541 (2000)

12. J.-K.F. Suh, H.W.T. Matthew, Application of chitosan-based polysaccharide biomaterials in cartilage tissue engineering: a review, *Biomaterials*, **21**: 2589-2598 (2000)

13. G. Ladam, C. Gergely, B. Senger, G. Decher, J.C. Voegel, P. Schaaf, F.J.G Cuisinier, Protein Interactions with Polyelectrolyte Multilayers: Interactions between Human Serum Albumin and Polystyrene Sulfonate/Polyallylamine Multilayers, *Biomacromolecules* **1**: 674-687 (2000)

14. G. Ladam, P. Schaaf, G. Decher, J.C. Voegel, F.J.G Cuisinier, Protein adsorption onto auto-assembled polyelectrolyte films, *Biomolecular Engr.* **19**: 273-280 (2002)

15. D.S. Salloum, J.B. Schlenoff, Protein Adsorption Modalities on Polyelectrolytes Multilayers, *Biomacromolecules* **5**: 1089-1096 (2004)

16. M. Müller, B. Kessler, N. Houbenov, K. Bohatá, Z. Pientka, E. Brynda, pH Dependence and Protein Selectivity of Poly(ethyleneimine)/Poly(acrylic acid) Multilayers Studied by in Situ ATR-FTIR Spectroscopy, *Biomacromolecules* **7**: 1285-1294 (2006)

17. Singh B.R. Basic Aspects of the Technique and Applications of Infrared Spectroscopy of Peptides and Proteins. In *Infrared Analysis of Peptides and Proteins Principles and Applications*; Singh B.R., Ed; ACS Symposium Series 750; American Chemical Society: Washington D.C., 2000; 2-34, Chapter 1

18. A. Barth, C. Zscherp, What vibrations tell us about proteins *Quat. Rev. Biophys.* **35**: 369-430 (2002)

19. H. Susi, D.M. Byler, Resolution-Enhanced Fourier Transform Infrared Spectroscopy of Enzymes, *Methods in Enzymology* **130**: 290-311 (1986)

20. T.F. Kumosinski, J.J. Unruh Quantitation of the global secondary structure of globular proteins by FTIR spectroscopy: comparison with X-ray crystallographic structure, *Talanta* **43**: 199-219 (1996)

21. V. Turula, J.A. Haseth, Evaluation of Particle Beam Fourier Transform Infrared Spectrometry for the Analysis of Globular Proteins: Conformation of β-Lactoglobulin and Lysozyme, *Appl. Spect.* **48**: 1255-1264 (1994)

22. A. Dong, P. Huang, W.S. Caughey, Protein Secondary Structures in Water from Second-Derivative Amide I Infrared Spectra *Biochemistry* **29**: 3303-3308 (1990)

23. S. Luo, C.F. Huang, J.F. McClelland, D.J. Graves, A study of Protein Secondary Structure by Fourier Transform Infrared/Photoacoustic Spectroscopy and Its Application for Recombinant Proteins, *Anal. Biochem.* **216**: 67-76 (1994)

24. M. van de Weert, R. van't Hof, J. van der Weerd, R.M.A. Heeren, G. Posthuma, W.E. Hennink, D.J.A. Crommelin, Lysozyme distribution and conformation in a biodegradable polymer matrix as determined by FTIR techniques, *J. of Control Release*. **68**: 31-40 (2000)

25. A. Wittemann, M. Ballauff, Secondary Structure Analysis of Proteins Embedded in Spherical Polyelectrolyte Brushes by FT-IR Spectroscopy, *Anal. Chem.* **76**: 2813-2819 (2004)

26. S. Boddohi, C. Killingsworth, M.J. Kipper, Polyelectrolyte Multilayer Assembly as a Function of pH and Ionic Strength Using the Polysaccharides Chitosan and Heparin, *Biomacromolecules* **9**: 2021-2028 (2008)

27. K. Murayama, M. Tomida, Heat-Induced Secondary Structure and Conformation Change of Bovine Serum Albumin Investigated by Fourier Transform Infrared Spectroscopy, *Biochemistry*. **43**: 11526-11532 (2004)

28. J.L. Koenig, L. D'Esposito, M.K. Antoon, The Ratio Method for Analyzing Infrared Spectra of Mixtures *Appl. Spect.* **31**: 292-295 (1977)

Chapter 5

Polysaccharide-Based Polyelectrolyte Multilayer Surface Coatings can Enhance Mesenchymal Stem Cell (MSC) Response to Adsorbed Growth Factors

- <u>Almodóvar J.</u>, Bacon S., Gogolski J., Kisiday J.D., Kipper M.J.; "Polysaccharide-based polyelectrolyte multilayer surface coatings can enhance mesenchymal stem cell (MSC) response to adsorbed growth factors", Biomacromolecules, 11 (2010) 2629-2639 http://dx.doi.org/10.1021/bm1005799

5.1 Abstract

It is generally accepted that both surface chemistry and biochemical cues affect mesenchymal stem cell (MSC) proliferation and differentiation. Several growth factors that have strong influences on MSC behavior bind to glycosaminoglycans in interactions that affect their stability and their biochemical activity. The goal of this work was to develop polysaccharide-based polyelectrolyte multilayers (PEMs) to bind and stabilize growth factors for delivery to MSCs. Using the naturally derived polysaccharides chitosan and heparin, PEMs were constructed on gold-coated glass chips, tissue-culture polystyrene (TCPS), and titanium. PEM construction and basic fibroblast growth factor (FGF-2) adsorption to these PEMs were evaluated by Fourier transform surface plasmon resonance, X-ray photoelectron spectroscopy, and polarization modulation infrared reflection absorption spectroscopy. The functional response of bone marrow-derived ovine MSCs to FGF-2 on PEM-coated TCPS

and titanium was evaluated in vitro. The effect of FGF-2 dose and presentation on MSC proliferation was evaluated using low-serum media, over four days. On TCPS, we found that FGF-2 adsorbed to heparin-terminated PEMs induces a stronger proliferative response of MSCs than any of the other conditions tested, including delivery of the FGF-2 in solution, at an optimally mitogenic dose. Cell densities on day four were 1.8 times higher when FGF-2 was delivered by adsorption to the PEM, than when FGF-2 was delivered in solution. This system represents a promising candidate for the development of surface coatings that can stabilize and potentiate the activity of growth factors for therapeutic applications. Interestingly, the same effects were not observed when FGF-2 was delivered by adsorption to PEMs on titanium. When the polysaccharide-based PEMs were formed on titanium the proliferative response of ovine MSCs to adsorbed FGF-2 was not as strong as the response to FGF-2 delivered in solution.

5.2 Introduction

Growth factors are proteins with a wealth of potential for tissue engineering applications, due to their involvement in many signaling pathways that regulate wound healing responses and the maintenance of healthy tissue. Materials designed to modulate cell behavior through growth factor stabilization and delivery may improve outcomes in tissue engineering strategies. However, one of the key challenges of growth factor delivery is that many of the most potent growth factors also exhibit very short plasma half-lives. Basic fibroblast growth factor (FGF-2), for example, has a plasma half-life of about 1.5 minutes.[1] FGF-2 is an 18 kDa protein with an iso-electric point of 9.6, involved in cell proliferation, differentiation, angiogenesis and ossification.[2] FGF-2 has been shown to enhance cell proliferation at low doses for bone marrow-derived human mesenchymal stem cells (MSCs)[3] in media with 10%

118

serum, and for bone marrow-derived ovine MSCs in serum-deprived media.[4] Some biomaterials have been proposed for FGF-2 delivery, but fail to protect it from degradation. For example, one recent study attempted delivery of FGF-2 by adsorption to ceramic materials.[5] This work demonstrated controlled release of FGF-2, but after the second day of release most of the FGF-2 was degraded.[5] Successful delivery of FGF-2 for tissue engineering applications using synthetic and natural polymers and ceramics has been demonstrated in several studies.[6-8] Sulfated materials capable of non-covalently binding and stabilizing FGF-2 are of particular interest, because they may mimic the biochemical function of glycosaminoglycans. Examples include sulfonated silk fibroin films,[9] heparin-conjugated polyester nanospheres,[10] chondroitin sulfate-containing coatings,[11] and heparin-containing microparticles and hydrogels.[12, 13]

Sulfated biopolymers, which include glycosaminoglycans (GAGs), are of particular interest for FGF-2 delivery, as they have shown to be capable of non-covalently binding and stabilizing FGF-2.[9-13] FGF-2 binds to sulfated GAGs, such as heparin and heparan sulfate, in the extracellular and pericellular space, which may protect it from degradation.[14, 15] Heparin has been shown to protect FGF-2 from proteolytic and chemical inactivation.[16] In fact, binding FGF-2 to heparin increases its half life almost six fold.[17] GAG binding also potentiates the activity of FGF-2 via several mechanisms. Specific binding to heparin or heparan sulfate may stabilize a ternary complex between the growth factor and its cell surface receptor, or block this complex formation.[18] Binding sequences for FGF-2 in sulfated GAGs are also believed to promote dimerization or oligomerization of the protein along the GAG chain, and thereby activate the mitogenic activity of FGF-2.[18, 19] GAG-FGF-2 interactions have been implicated in the promotion of angiogenesis and in the response of

chondrocytes to tissue injury in articular cartilage.[20, 21] Heparin-bound FGF-2 has been shown to promote osteogenesis in vitro and in vivo.[22] The ability of heparin to bind, stabilize and potentiate growth factor activity makes heparin a particularly promising material from which to design bioactive materials and surface coatings for growth factor delivery.

Layer-by-layer assembly of polyelectrolyte multilayers (PEM) has been demonstrated to be a simple yet efficient method to modify biologically relevant surfaces by creating nanoscale thin films. The growth mechanisms of polysaccharide-based PEMs have been studied, demonstrating that their thickness and composition can be controlled by polyelectrolyte selection and deposition conditions.[48,49] PEMs are attractive for developing biomaterials surface coatings because they allow the mechanical and chemical properties of the surface to be precisely tuned, by simple, reproducible methods. For example the biological responses to changes in surface hydrophobicity, stiffness, composition, coating thickness, anticoagulant activity, and topography have all been evaluated using PEMs.[23-31] PEM surface coatings might also be used as a tool to precisely tune the presentation of biomolecules in both space and time to mimic key features of the extracellular matrix. Spatial organization in PEMs can be controlled by the layer deposition sequence and the number of layers. Controlled release of therapeutic molecules can also be achieved by altering the PEM biodegradability and by modulating the coating thickness and drug loading.[32, 33]

We have previously characterized the complexation of chitosan and heparin both in nanoparticles and in PEMs.[34-36] The goal of this study was to use polysaccharide-based PEMs to bind, stabilize, and deliver FGF-2 to bone marrow-derived ovine MSCs using the polysaccharides chitosan and heparin. In this work, we characterize chitosan-heparin PEM assembly on gold-coated surfaces and subsequent FGF-2 adsorption using Fourier transform

120

surface plasmon resonance (FT-SPR) and polarization modulation infrared reflection absorption spectroscopy (PM-IRRAS). We then translate the PEM assembly procedure to tissue-culture polystyrene (TCPS) and titanium surfaces. PEM assembly is characterized by X-ray photoelectron spectroscopy (XPS) on these surfaces. FGF-2 adsorption on PEM-modified titanium is also evaluated by PM-IRRAS. Biological responses to polysaccharide-based PEMs might be determined by both bulk properties and terminal surface chemistry.[53] For example, for relatively thick PEMs, cell responses to polysaccharide-based PEMs have been modulated by changing the bulk mechanical properties and total amount of embedded growth factor in PEM volume.[33,54] For thinner PEMs, biological responses, such as blood coagulation, have been shown to be dependent upon the terminal PEM layer.[55] In this work we used PEMs which are 6 or 7 layers thick. This thickness was chosen to obtain complete surface coverage,[35-36] while maintaining relatively thin layers, so that differences in the cell response could be attributed to differences in the terminal PEM layer chemistry. The proliferation of MSCs induced by FGF-2 delivered from PEMs is evaluated on both PEM-coated TCPS and PEM-coated titanium.

5.3 Materials and Methods

5.3.1 Materials

The following were purchased from HyClone (Logan, UT): fetal bovine serum (FBS), 0.25% trypsin with EDTA, low glucose Dulbecco's modified Eagle's medium (D-MEM), minimum essential medium alpha (α-MEM) (supplemented with L-glutamine, ribonucleosides, and deoxyribonucleosides), and Dulbecco's phosphate buffered saline (DPBS) without Ca^{2+} and Mg^{2+}. The following were purchased from Gibco (Grand Island, NY): antibiotic-antimycotic (anti/anti), 1 M HEPES buffer solution, and Dulbecco's

phosphate buffered saline with Ca^{2+} and Mg^{2+}. 4 mM calcein-AM in dimethyl sulfoxide (DMSO) was purchased from Invitrogen (Eugene, OR). 4'6-Diamidino-2-phenylindole-2HCl (DAPI) was purchased from Thermo-Scientific (Rockford, IL). Titanium foil (1 mm thick, 99.2% metal basis) and gold were purchased from Alfa-Aesar (Ward Hill, MA). SF-10 glass chips (18 mm × 18 mm) were purchased from GWC Technologies Inc. (Madison, WI). 11-Mercaptoundecanoic acid (MUA) and 11-phosphonoundecanoic acid (PUA) were purchased from Sigma-Aldrich (St. Lois, MO). Chitosan (poly(β-(1,4)-D-glucosamine-*co-N*-acetyl-D-glucosamine); 4.7% acetylated) used for PEM characterization was purchased from Biosyntech Inc. (Laval, Canada) and for cell culture (5% acetylated, determined by ^{1}H NMR) was purchased from Novamatrix (Sandvika, Norway). Heparin sodium (from porcine intestinal mucosa, 12.5% sulfur) was purchased from Celsus Laboratories (Cincinnati, OH). Recombinant human FGF basic (FGF-2) 146 aa was purchased from R&D Systems (Minneapolis, MN). Human fibronectin (FN) was purchased from BD Biosciences (Bedford, MA). Glacial acetic acid was purchased from Acros Organics (Geel, Belgium). Sodium acetate and DMSO were purchased from Fisher Scientific (Pittsburgh, PA). A Millipore Synthesis water purification unit (Millipore, Billerica, MA) was used to obtain ultrapure, 18.2 MΩ water (DI water), used for making all aqueous solutions.

5.3.2 Construction of polyelectrolytes multilayers (PEMs) and FGF-2 adsorption on gold-coated glass

Construction of polysaccharide-based PEMs on gold-coated SF-10 glass substrates has been previously studied in our laboratory, and a detailed procedure can be found in reference 36. Briefly, gold surfaces were modified with a self-assembled monolayer (SAM) of MUA.[36] Chitosan and heparin solutions with concentrations of 0.01 M (on a saccharide

unit basis) were prepared in acetate buffer (0.2 M, pH 5). FGF-2 was dissolved in DI water at 100 ng mL^{-1}. All polysaccharide, rinse, and FGF-2 solutions were filtered with a 0.22 μm polyvinylidene fluoride (PVDF) syringe filters (Fisher Scientific). Construction of the PEMs was performed in a flow cell by alternating five-minute adsorption steps of the polyelectrolytes with five-minute acidified water rinses (pH 4.0, acidified with acetic acid) between adsorption steps. Heparin-terminated PEMs (PEM$_{Hep}$) were constructed with six layers, chitosan-terminated PEMs (PEM$_{Chi}$) were constructed with seven layers. Surfaces with FGF-2 adsorbed (PEM$_{Hep}$+FGF$_{ad}$ and PEM$_{Chi}$+FGF$_{ad}$) were prepared by exposing surfaces to FGF-2 solution for two hours, after PEM construction. FGF-2 adsorption was followed by a DI water rinse. The nomenclature for these surfaces is summarized in Table 5.1. Construction of PEMs and protein adsorption were monitored using in situ FT-SPR. Details of the FT-SPR experiments are provided in section 5.3.3 below. The chemistry of the surfaces was confirmed using PM-IRRAS. Details of the PM-IRRAS experiments are provided below, in section 5.3.6.

Table 5.1 Sample nomenclature and experimental characterization of polysaccharide-based PEMs.

Substrate	Sample name	Surface coating	Characterization
Gold	PEM$_{Hep}$	Six-layer (heparin-terminated) PEM	All conditions were characterized by FT-SPR (for PEM construction and FGF-2 adsorption), and by PM-IRRAS (for surface chemistry and FGF-2 adsorption).
	PEM$_{Hep}$+FGF$_{ad}$	FGF-2 adsorbed to PEM$_{Hep}$	
	PEM$_{Chi}$	Seven-layer (chitosan-terminated) PEM	
	PEM$_{Chi}$+FGF$_{ad}$	FGF-2 adsorbed to PEM$_{Chi}$	
TCPS	PEM$_{Hep}$	Six-layer (heparin-terminated) PEM	All conditions were characterized by XPS for (PEM construction and surface chemistry).
	PEM$_{Chi}$	Seven-layer (chitosan-terminated) PEM	
Titanium	PEM$_{Hep}$	Six-layer (heparin-terminated) PEM	All conditions were characterized by XPS (for PEM construction and surface chemistry), and by PM-IRRAS (for surface chemistry and FGF-2 adsorption).
	PEM$_{Hep}$+FGF$_{ad}$	FGF-2 adsorbed to PEM$_{Hep}$	
	PEM$_{Chi}$	Seven-layer (chitosan-terminated) PEM	
	PEM$_{Chi}$+FGF$_{ad}$	FGF-2 adsorbed to PEM$_{Chi}$	

5.3.3 Fourier-transform surface plasmon resonance (FT-SPR)

On gold-coated glass surfaces, PEM construction and protein adsorption were conducted in the flow cell of an SPR-100 module coupled to a Nicolet 8700 FT-IR spectrometer (Thermo-Electron, Madison, WI) at a flow rate of 1.3 mL min^{-1}.[36] Data were collected using the Omnic 7.3 software (Thermo Electron), at 8 cm^{-1} resolution over the range from 6000 to 12,000 cm^{-1}. A total of 16 scans were co-added at each time point to produce an FT-SPR spectrum every 4.7 s.[36]

5.3.4 PEM formation on tissue-culture polystyrene (TCPS)

Construction of PEMs on sterile Nuclon Δ TCPS (24-well plates, Nunc ALS, Roskilde, Denmark) has been described previously.[35] Briefly, PEM construction was performed using the solutions described above, with alternating five-minute rinse and adsorption steps, by adding one mL of solution to each well and adsorbing under gentle agitation. Heparin-terminated PEMs (PEM$_{Hep}$) were constructed with six layers, chitosan-terminated PEMs (PEM$_{Chi}$) were constructed with seven layers. The nomenclature for these surfaces is summarized in Table 5.1. XPS was used to characterize construction of PEMs on TCPS. Details of the XPS experiments are provided below, in section 5.3.7. For cell proliferation studies some surfaces were also prepared with adsorbed FGF-2 (PEM$_{Hep}$+FGF$_{ad}$ and PEM$_{Chi}$+FGF$_{ad}$), and with adsorbed FGF-2 and adsorbed FN (PEM$_{Hep}$+FN+FGF$_{ad}$ and PEM$_{Chi}$+FN+FGF$_{ad}$). Preparation of the protein-modified PEMs on TCPS surfaces is described in detail in section 5.3.9.

5.3.5 PEM formation on titanium

Titanium foil was cut using a water saw into either 20 mm × 20 mm square chips or disks of 13 mm in diameter and polished using silicone carbide paper of increasing grit size (1000, 1200, 1500, 2000, 4000) using water to clean between each grit increment. The titanium chips were cleaned and acid-etched by exposing them for 30 minutes to piranha solution (70% sulfuric acid, 30% hydrogen peroxide) under sonication, followed by a ten-minute water sonication step and ten minutes in a Tegal Plasmaline (Petaluma, CA) air plasma chamber set at 50 W and 0.5 Torr. **Caution: piranha solution reacts violently with many organic materials and should be handled with care.** A SAM of PUA was deposited on the titanium substrates by adsorption from a 10 mM solution in DMSO. Six-layer PEMs

(PEM$_{Hep}$) were prepared by placing the titanium surfaces in the wells of multi-well plates, and following the protocol used for PEM construction on TCPS. The nomenclature for these surfaces is summarized in Table 5.1. Some PEMs were subsequently modified with FGF-2 (PEM$_{Hep}$+FGF$_{ad}$), and with FGF-2 and FN (PEM$_{Hep}$+FN+FGF$_{ad}$). The procedure for protein adsorption is described below in section 5.3.9. PM-IRRAS and XPS were used to characterize construction of PEMs on titanium. PM-IRRAS was also used to characterize FGF-2 adsorption. Details of the PM-IRRAS and XPS experiments are provided below, in sections 5.3.6 and 5.3.7, respectively. Because the preparation of the titanium surfaces with the PUA SAMs and the subsequent PEM adsorption have not been previously described in detail, additional characterization of this process is provided in the supporting information (Appendix).

5.3.6 Polarization-modulation infrared reflection absorption spectroscopy (PM-IRRAS)

FT-IR spectroscopy was used in polarization modulation mode to confirm construction of PEMs and protein adsorption on the gold-coated glass and titanium surfaces as described in reference 36. PM-IRRAS spectra were collected at 2 cm^{-1} resolution with 1000 scans for each sample in the range of 1000-2000 cm^{-1}. The modulation frequency was adjusted depending on the type of metal used: gold (1500 cm^{-1}) and titanium (1285 cm^{-1}). Each spectrum was corrected by determining a cubic spline function from a defined set of spline points and dividing it into the PM-IRRAS spectrum to correct for the Bessel function background.[36] The spectrum of the adsorbed protein was obtained by subtracting the polysaccharide PEM spectrum from the spectrum of the surfaces with protein adsorbed, using a weighting factor on the PEM spectrum to achieve the criteria of 0 absorbance beyond 1750 cm^{-1}. The 2nd order 9-point Savitzky-Golay algorithm was used to smooth all spectra.

The spectroscopy analysis software IgorPro (Version 5.0.5.7, Wave Metrics, Inc., Portland, OR) was used for background correction, smoothing, and spectral math.

5.3.7 X-ray photoelectron spectroscopy (XPS)

XPS experiments were performed on a Physical Electronics 5800 spectrometer (Chanhassen, MN). This system has a monochromatic Al Kα X-ray source (hν = 1486.6 eV), hemispherical analyzer, and multichannel detector. The binding energy scales for the samples were referenced to the C1s peak at 284.7 eV. All XPS analyses were performed at a photoelectron takeoff angle of 45°.

5.3.8 Cell harvest and culture

Bone marrow-derived MSCs were obtained from female sheep (four to seven years old). 2-4 mL of marrow was drawn from the iliac crest using a Jamshidi® biopsy needle (Cardinal Health, Dublin, OH) loaded with heparin sodium solution 1000 USP (APP Pharmaceuticals, Schaumburg, IL). The bone marrow aspirate was centrifuged at 200 g for 2-6 minutes and the supernatant containing the nucleated cells was saved. After counting the nucleated cells, the supernatant was mixed with growth media (low-glucose D-MEM with 10% FBS, 1% anti/anti, 2.5% HEPES) and seeded into culture flasks at a nucleated cell density of 2.5×10^5 cells cm^{-2}. After 24 hours, the medium was changed to remove all non-adherent cells. MSC colonies were allowed to develop for at least seven days, at which point the cells were lifted using trypsin media, counted, and re-seeded in culture flasks using maintenance media (α-MEM with 10% FBS, 1% anti/anti, 2.5% HEPES 1 M). To obtain the necessary amount of cells from each donor animal for all experiments, the cells were expanded by seeding them at a density of 10,000 cells cm^{-2} and re-seeding every two days when the cultures were approximately 80% confluent. The MSCs were then cryo-preserved prior to seeding into

experimental conditions. During culture expansion, cell populations proliferated at a rate of approximately one population doubling every two days. Cells were not used beyond the seventh passage.

5.3.9 MSC proliferation response to FGF-2, PEMs, and PEMs with adsorbed FGF-2 and FN

MSCs were seeded at a density of 7000 cells cm^{-2} for all cell proliferation experiments. Low-serum media was used (2.5% FBS) for all FGF-2 response studies since it has been demonstrated that the presence of FBS could suppress the effect of FGF-2 on ovine MSC proliferation.[4] Media was changed every two days during proliferation studies.

The dose response of ovine MSCs to FGF-2 in solution was measured by seeding cells on a 24-well TCPS plate and treating them with 1 mL per well of different concentrations of FGF-2 (0, 0.1, 1, 10, and 100 ng mL^{-1}) using low-serum media. Cultures were maintained for 4 days, with a medium change on day two with the corresponding dose of FGF-2 included in the media change. Cells were counted each day for four days after seeding, using the fluorescence microscopy method described below. One ng mL^{-1} and ten ng mL^{-1} were identified as the FGF-2 doses inducing the greatest proliferative response. Thus, delivery of one ng mL^{-1} of FGF-2 dissolved in the culture medium was used as the positive control FGF-2 dose in all subsequent experiments.

The effect of polysaccharide-based PEMs and PEMs containing adsorbed proteins on MSC proliferation was investigated on TCPS using PEM$_{Hep}$ and PEM$_{Chi}$ surfaces. On each of these two types of PEMs were investigated, as summarized in Table 5.2. For adsorbing FGF-2 to PEMs, the protein was dissolved in DI water at 50 ng mL^{-1}, and 1 mL was placed in each well of the 24-well plates and allowed to adsorb for 2 hours under gentle agitation. The FGF-2 solution was then aspirated off, and the surfaces were rinsed with DI water.

128

For adsorbing FN, the protein was dissolved in DI water at 10 μg mL^{-1}, and 1 mL was placed in each well of the 24-well plate for 1 hour under static conditions. The FN solution was then aspirated off and the surfaces were rinsed with DI water. For preparation of PEM$_x$+FN+FGF$_{ad}$ surfaces, the FGF-2 was adsorbed first, followed by FN.

Based on the results obtained from MSC proliferation on TCPS, several conditions were chosen to evaluate MSC proliferation on Ti with PEM$_{Hep}$ coatings. For these experiments, five conditions were studied, as described in Table 5.2. Protein adsorption to PEMs on titanium was performed following the same protocols used to adsorb the proteins to the PEMs on TCPS, described in the previous paragraph.

All surfaces used for MSC response studies were sterilized by exposing them to 70% ethanol for 15 minutes, and rinsed with Dulbecco's PBS prior to protein adsorption and cell seeding. FGF-2 was included in the media change when FGF-2 was delivered in solution (FGF$_{sol}$, PEM$_x$+FGF$_{sol}$, and PEM$_x$+FN+FGF$_{sol}$). When FGF-2 was delivered by adsorption on the surfaces (PEM$_x$+FGF$_{ad}$ and PEM$_x$+FN+FGF$_{ad}$), no additional FGF-2 was provided at the media change.

Cells were counted on day two and day four after initial seeding. To evaluate cell proliferation, cells were stained with calcein-AM, fixed with 2% glutaraldehyde, and then counterstained with DAPI. Calcein-AM was added to fresh low-serum media (4 mM, 37 °C, 5% CO_2, and 50 minutes) which stains the cytoplasm of live cells. Cell fixation was performed with a 2% solution of glutaraldehyde in DPBS with Ca^{2+} and Mg^{2+} (4 °C, 45 minutes). Nuclei staining were performed with a solution of DAPI in DPBS with Ca^{2+} and Mg^{2+} (room temperature, 1 μg mL^{-1}, 15 minutes). The wells were rinsed with DPBS with Ca^{2+} and Mg^{2+} between each step, and were protected from light. After fixing and staining,

surfaces were stored dry, protected from light, at 4°C until microscopy was performed. Images were obtained using an Olympus IX70 epi-fluorescence microscope (Center Valley, PA) equipped with a QImaging Micropublisher camera and a filter wheel with the wide ultraviolet (WU) and narrow blue (NB) filters for DAPI and calcein-AM respectively. Images for cell counting were obtained using a 4× objective with a preview and capture depth of 8 bit. For experiments on TCPS, images were obtained at five different locations in each well of the 24-well plate, which corresponds to about 25% of total well surface area. For experiments on titanium, images were obtained at five different locations for each sample, which corresponds to about 35% of the total surface area. All images were processed using the ImageJ 1.41o software (National Institutes of Health, USA). The polychromatic images were split into their respective red, green, and blue channels. The blue channel of each image, (nuclei stained with DAPI) was thresholded and automatically counted using the particle analyzer algorithm in the ImageJ software, to obtain cell numbers per area. Population doubling rates between days two and four were computed as the base 2 logarithm of the ratio of cell density on day four to the cell density on day two,

5.3.10 Statistical analysis

Data analysis was performed using SAS (SAS Institute, Inc., Cary, NC, USA) version 9.2. Comparisons between groups were performed via analysis of variance (ANOVA) models with Tukey's multiple comparison tests. Differences with $p < 0.05$ were considered statistically significant. All cell proliferation data were obtained from triplicate samples ($n = 3$) using (non-pooled) MSCs from the same three donor animals, and are expressed as the mean ± standard deviation.

**Table 5.2** Sample nomenclature and description of MSC proliferation experiments.

Substrate	Sample name	Conditions
TCPS	FGF-2 dose response	FGF-2 delivered in solution at 0, 0.1, 1.0, 10, and 100 ng mL^{-1} on day 0 and day 2. Cells counted daily for four days.
	PEM$_{Hep}$	TCPS coated with a six-layer (heparin-terminated) PEM. Cells counted on days 2 and 4.
	PEM$_{Hep}$+FGF$_{sol}$	PEM$_{Hep}$ with 1.0 ng mL^{-1} FGF-2 delivered in solution on days 0 and 2. Cells counted on days 2 and 4.
	PEM$_{Hep}$+FN+FGF$_{sol}$	PEM$_{Hep}$ with adsorbed FN and 1.0 ng mL^{-1} FGF-2 delivered in solution on days 0 and 2. Cells counted on days 2 and 4.
	PEM$_{Hep}$+FGF$_{ad}$	PEM$_{Hep}$ with FGF-2 adsorbed from an initial concentration of 50 ng mL^{-1}. Cells counted on days 2 and 4.
	PEM$_{Hep}$+FN+FGF$_{ad}$	PEM$_{Hep}$ with FGF-2 adsorbed followed by FN adsorption. Cells counted on days 2 and 4.
	PEM$_{Chi}$	TCPS coated with a seven-layer (chitosan-terminated) PEM. Cells counted on days 2 and 4.
	PEM$_{Chi}$+FGF$_{sol}$	PEM$_{Chi}$ with 1.0 ng mL^{-1} FGF-2 delivered in solution on days 0 and 2. Cells counted on days 2 and 4.
	PEM$_{Chi}$+FN+FGF$_{sol}$	PEM$_{Chi}$ with adsorbed FN and 1.0 ng mL^{-1} FGF-2 delivered in solution on days 0 and 2. Cells counted on days 2 and 4.
	PEM$_{Chi}$+FGF$_{ad}$	PEM$_{Chi}$ with FGF-2 adsorbed from an initial concentration of 50 ng mL^{-1}. Cells counted on days 2 and 4.
	PEM$_{Chi}$+FN+FGF$_{ad}$	PEM$_{Chi}$ with FGF-2 adsorbed followed by FN adsorption. Cells counted on days 2 and 4.
Titanium	Ti	Polished, cleaned and oxidized titanium. Cells counted on days 2 and 4.
	Ti+FGF$_{sol}$	Ti with 1.0 ng mL^{-1} FGF-2 delivered in solution on days 0 and 2. Cells counted on days 2 and 4.
	PEM$_{Hep}$	Titanium coated with a six-layer (heparin-terminated) PEM. Cells counted on days 2 and 4.
	PEM$_{Hep}$+FGF$_{ad}$	PEM$_{Hep}$ with FGF-2 adsorbed from an initial concentration of 50 ng mL^{-1}. Cells counted on days 2 and 4.
	PEM$_{Hep}$+FN+FGF$_{ad}$	PEM$_{Hep}$ with FGF-2 adsorbed followed by FN adsorption. Cells counted on days 2 and 4.

5.4 Results

5.4.1 PEM construction and protein adsorption on gold-coated glass, TCPS, and titanium

Construction of polysaccharide-based PEMs has been previously performed in our lab on both gold-coated glass substrates[36] and TCPS.[35] In this work, we first assembled PEMs on gold-coated glass substrates to characterize both PEM assembly and the adsorption of FGF-2 using in situ FT-SPR. In FT-SPR, p-polarized near-IR light is reflected off of a thin (~45 nm) gold film at a fixed angle of incidence. An interferometer is used to scan wavelengths. A broad absorption peak is observed at the wavelength that excites surface plasmon polaritons in the gold film. This absorption wavelength is sensitive to the thickness and refractive index of the media on the opposite side of the gold film, which enables measurements of surface adsorption events. The FT-SPR peak shifts observed during the rinse following each of the adsorption steps during construction of a six-layer, heparin-terminated PEM (PEM_{Hep}), and a seven-layer, chitosan-terminated PEM (PEM_{Chi}) are shown in Figure 5.1 (A) and (B). The FT-SPR peak shift associated with a subsequent FGF-2 adsorption step on each of these PEMs is also shown. From our previous work we estimate that a wavenumber shift of -28 cm^{-1} corresponds to about 1 nm in thickness.[36] For PEM_{Hep} we estimate a thickness of about 10 nm, while for PEM_{Chi} we estimate a thickness of about 17 nm. One PEM_{Hep} and one PEM_{Chi} sample were prepared for SPR measurements. From our previous work, the reproducibility in thickness for the buffer condition used in this work is $\pm$ 0.2 nm. Figure 5.1 (C) and (D) show the PM-IRRAS spectra of PEM_{Hep} and PEM_{Chi}, respectively, both before and after FGF-2 adsorption. PEM_{Hep} adsorbs a greater amount of FGF-2 than PEM_{Chi}, as evidenced by the strong FT-SPR peak shift seen in Figure 5.1 (A) compared to the corresponding shift observed in Figure 5.1 (B) for the FGF-2 adsorption steps. Also, amide I

(1650 cm^{-1}) and amide II (1550 cm^{-1}) peaks in the PM-IRRAS spectrum from the PEM$_{Hep}$ shown in Figure 5.1 (C) are larger than their respective counterparts in the PM-IRRAS spectrum from the PEM$_{Chi}$ shown in Figure 5.1 (D).
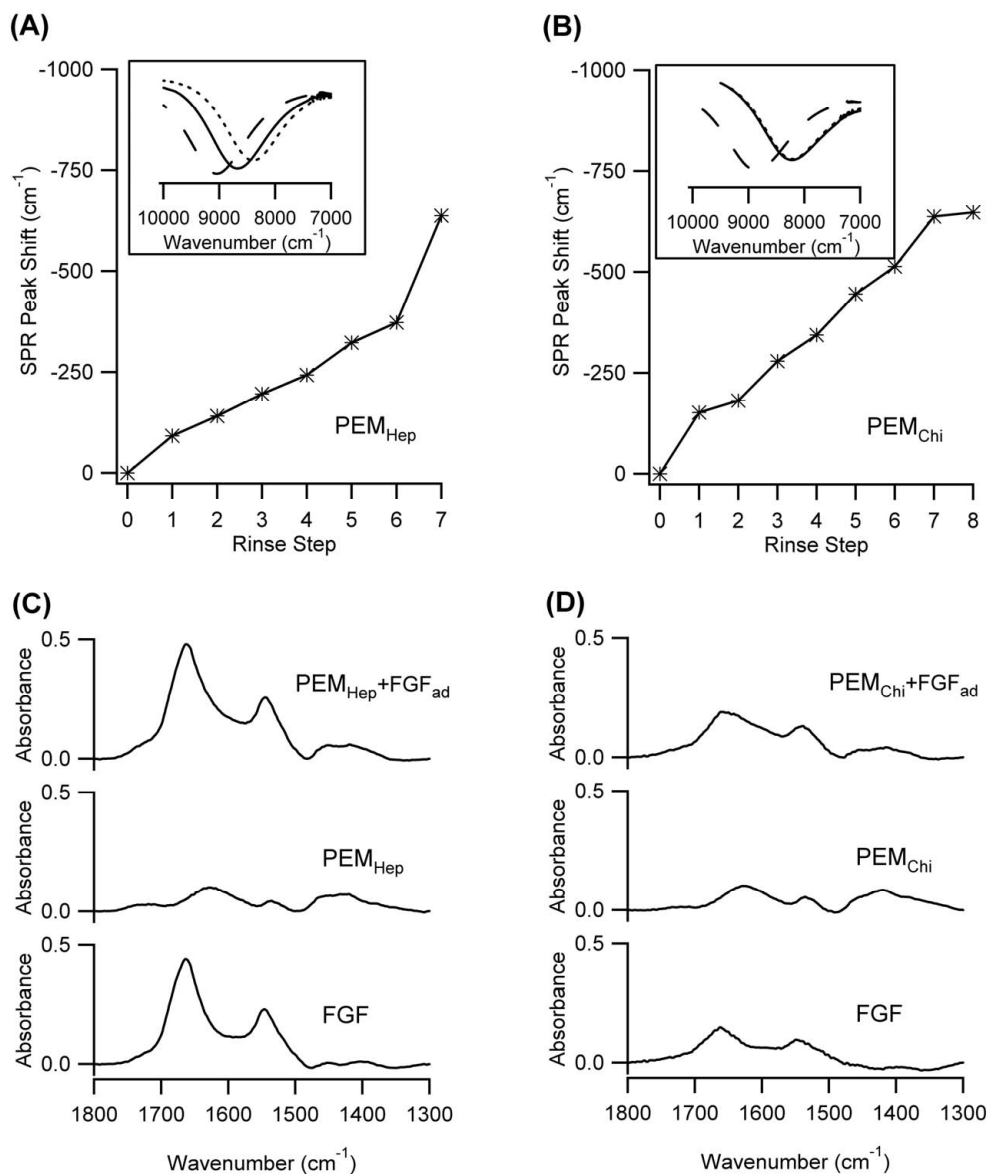
Figure 5.1 FT-SPR peak shift as a function of rinse step for (A) six-layer and (B) seven-layer PEMs on gold. Rinse 0 corresponds to the rinse prior to PEM adsorption. The final rinse step corresponds to the rinse after adsorption of FGF-2 at 100 ng mL^{-1}. Insets show the SPR spectra, in arbitrary reflectance units, of the surface prior to PEM deposition (dashed line, rinse 0), during the rinse immediately prior to protein adsorption (solid line), and during rinse after protein adsorption (dotted line, final rinse). PM-IRRAS spectra for (C) PEM$_{Hep}$ and (D) PEM$_{Chi}$ on gold-coated surfaces. In (C) and (D) spectra of the PEMs (middle) were subtracted from the corresponding spectra of the PEMs with FGF-2 adsorbed (top) to obtain the spectrum of the adsorbed FGF-2 (bottom).

After confirming that FGF-2 adsorbs to PEM_{Hep} and PEM_{Chi}, we translated the PEM assembly procedure to TCPS and titanium. The PEM assembly on these surfaces cannot be readily characterized using FT-SPR, so these were characterized using XPS. Figure 5.2 shows XPS spectra of PEMs on TCPS, and Figure 5.3 shows XPS spectra of PEMs on titanium. In both Figure 5.2 and Figure 5.3, (A) is a survey scan of a five-layer PEM, and (B) shows the relevant peaks for PEMs with different numbers of layers. The increasing nitrogen and sulfur peaks with increasing layer number demonstrate that this procedure results in successful deposition of PEMs on both TCPS and titanium. Furthermore, the attenuation of the titanium peak (Ti2p) with increasing layer number in Figure 5.3 confirms the uniform deposition of PEMs on titanium. The small intensity on the titanium peak for the seven-layer PEM sample (PEM7 in Figure 5.3 (B)) demonstrates that significant and complete surface coverage is achieved with only seven layers of polysaccharide. On TCPS the C1s intensity decreases with addition of PEMs. This is because the atom fraction of carbon in TCPS is higher than the atom fraction of carbon in the polysaccharides. In contrast, the C1s intensity increases as PEMs are added to titanium.
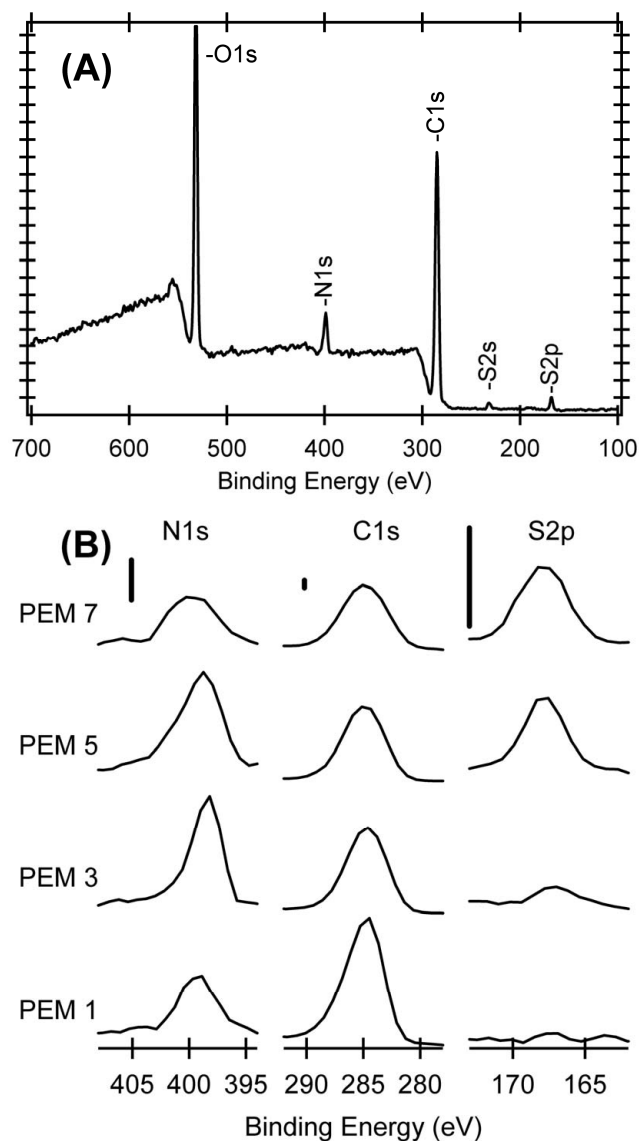
Figure 5.2 (A) XPS spectrum for a five-layer chitosan-terminated PEM constructed on TCPS. (B) N1s, C1s, and S2p envelopes from XPS spectra of chitosan-terminated PEMs constructed on TCPS with different numbers of layers. Increase of the sulfur and nitrogen peaks and partial attenuation of the carbon peak with increasing layer number confirms construction of the PEMs. The scale bars in (B) at the top of each column apply to all spectra in that column, and each scale bar is equal to the distance between tick marks on the ordinate in (A).
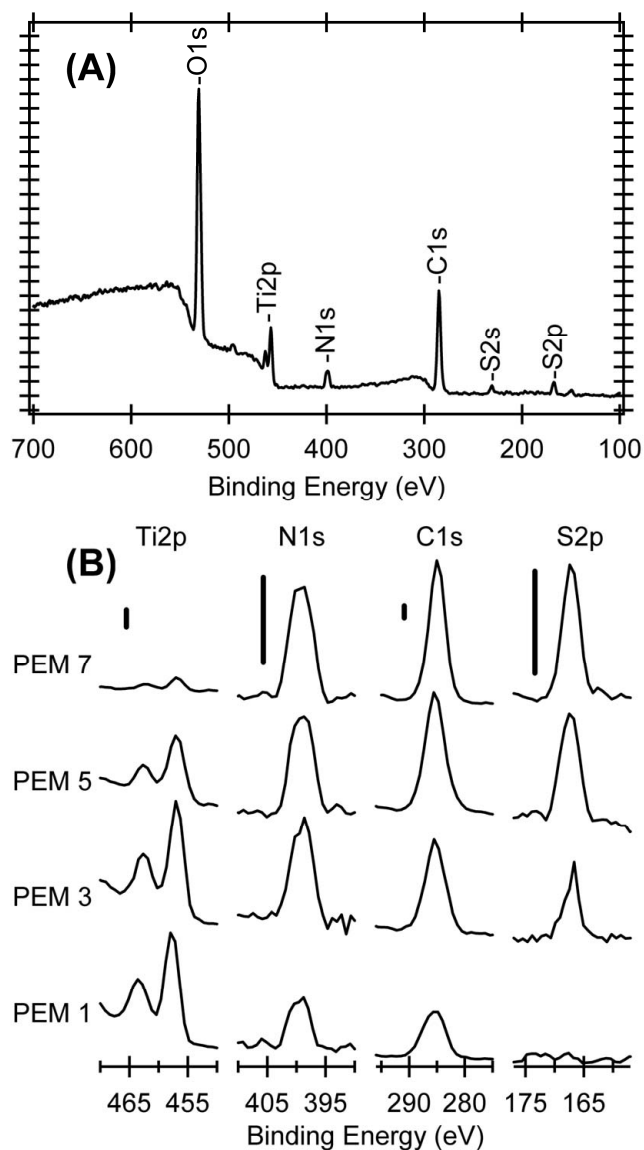
Figure 5.3 (A) XPS spectrum for a five-layer chitosan-terminated PEM constructed on titanium. (B) Ti2p, N1s, C1s, and S2p envelopes from XPS spectra of chitosan-terminated PEMs constructed on titanium with different numbers of layers. Increase of the sulfur, carbon, and nitrogen peaks and attenuation of the titanium peak with increasing layer number confirms construction of the PEMs. The scale bars in (B) at the top of each column apply to all spectra in that column, and each scale bar is equal to the distance between tick marks on the ordinate in (A).

FGF-2 adsorption to PEMs on titanium was evaluated using PM-IRRAS (Figure 5.4). Comparing Figure 5.4 to Figure 5.1 (C) and (D), it appears that the absorption bands associated with both the PEMs and the FGF-2 are weaker on the titanium substrates than on the gold-coated glass. (Note that the ordinate is scaled differently in Figure 5.4 than in

Figure 5.1.) This suggests that the PEMs on the titanium surfaces may not adsorb the same amount of polysaccharides as the gold-coated glass substrates. It also appears that on titanium surfaces, PEM$_{Hep}$ adsorbs a greater amount of FGF-2 than PEM$_{Chi}$ does. This is consistent with the observations of FGF-2 adsorption on PEMs on gold-coated glass (Figure 5.1).
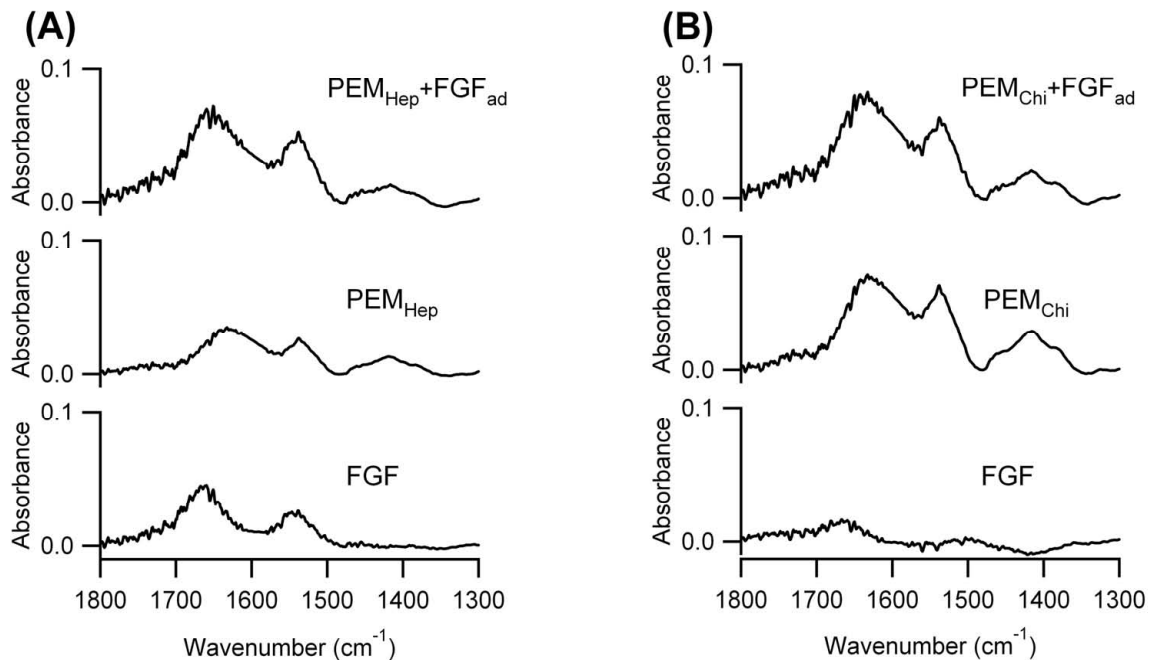
Figure 5.4 PM-IRRAS spectra for (A) PEM$_{Hep}$ and (B) PEM$_{Chi}$ on titanium surfaces. Spectra of the PEMs (middle) were subtracted from the corresponding spectra of the PEMs with FGF-2 adsorbed (top) to obtain the adsorbed FGF-2 (bottom).

5.4.2 MSC dose response to FGF-2 in solution

Figure 5.5 shows the dose response of ovine bone marrow-derived MSCs to FGF-2 in low-serum media (2.5% FBS), on TCPS. For this study, cryopreserved fifth-passage MSCs from three donor animals were used. The initial seeding density was 7000 cells cm^{-2}. A bimodal response is observed, wherein very low and very high concentrations of FGF-2 are not as effective as intermediate doses. At day four, the mean cell density in the 1 ng mL^{-1} and the 10 ng mL^{-1} treatment groups were 2.8 times and 3.0 times the cell density in the

137

negative control group, respectively. Fluorescence microscopy images (Figure 5.5 (B)) show spindle-shaped MSCs cultured on TCPS in low-serum media. MSCs are approaching confluence after 4 days in the cultures with 1 ng mL^{-1} FGF-2. From these dose response experiments, the optimally mitogenic dose of 1 ng mL^{-1} of FGF-2 dissolved in the culture medium was selected as the positive control dose of FGF-2, for evaluation of FGF-2 delivery from PEMs.
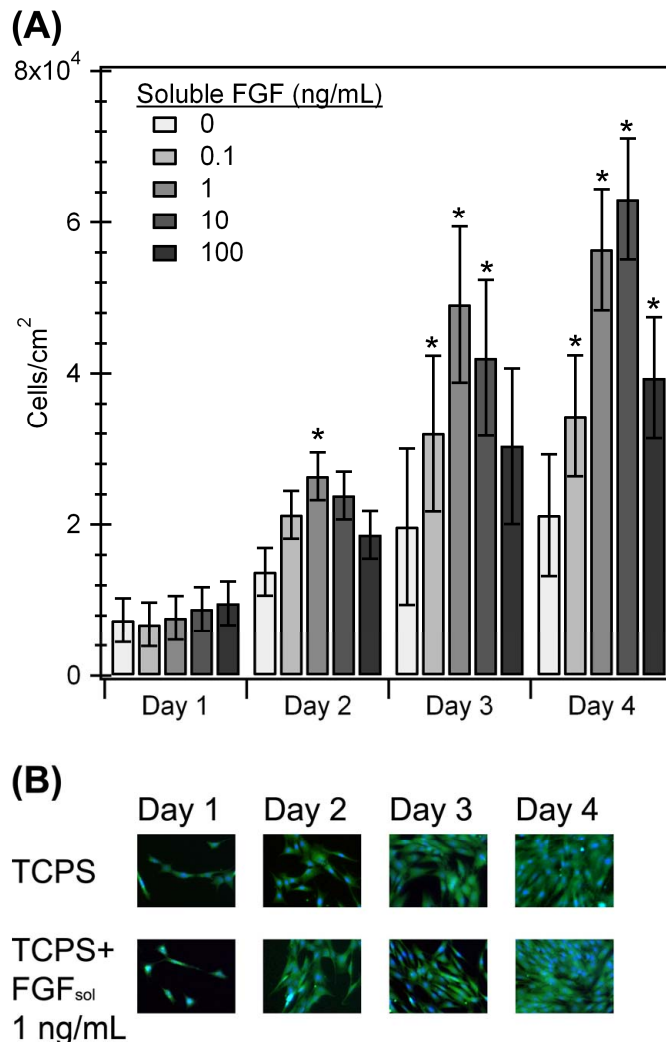
Figure 5.5 (A) MSC dose response to FGF-2 delivered in solution using low-serum media (2.5% FBS) on TCPS over four days. Cells were seeded on day 0 at 7000 cells cm^{-2}. * indicates statistically different from the 0 ng mL^{-1} dose of FGF-2 on the same day ($p < 0.05$). (B) Fluorescence microscopy images of MSCs. Nuclei are stained blue (DAPI) and cytoplasm is stained green (calcein).

5.4.3 MSC adhesion and proliferation on PEM-coated TCPS

The effect of polysaccharide-based PEMs on cell proliferation was investigated on TCPS using two types of surfaces under different conditions (Figure 5.6 and Figure 5.7) in low-serum (2.5% FBS) media. For this study, cryopreserved fifth-passage MSCs from three different animals were used. MSC density on PEM coatings on TCPS with and without soluble FGF-2, adsorbed FGF-2, and adsorbed FN is shown in Figure 5.6 (A) (PEM_{Hep}) and Figure 5.6 (B) (PEM_{Chi}). Representative fluorescence micrographs are shown in Figure 5.7. The notation for these treatment groups is summarized in Table 5.2.
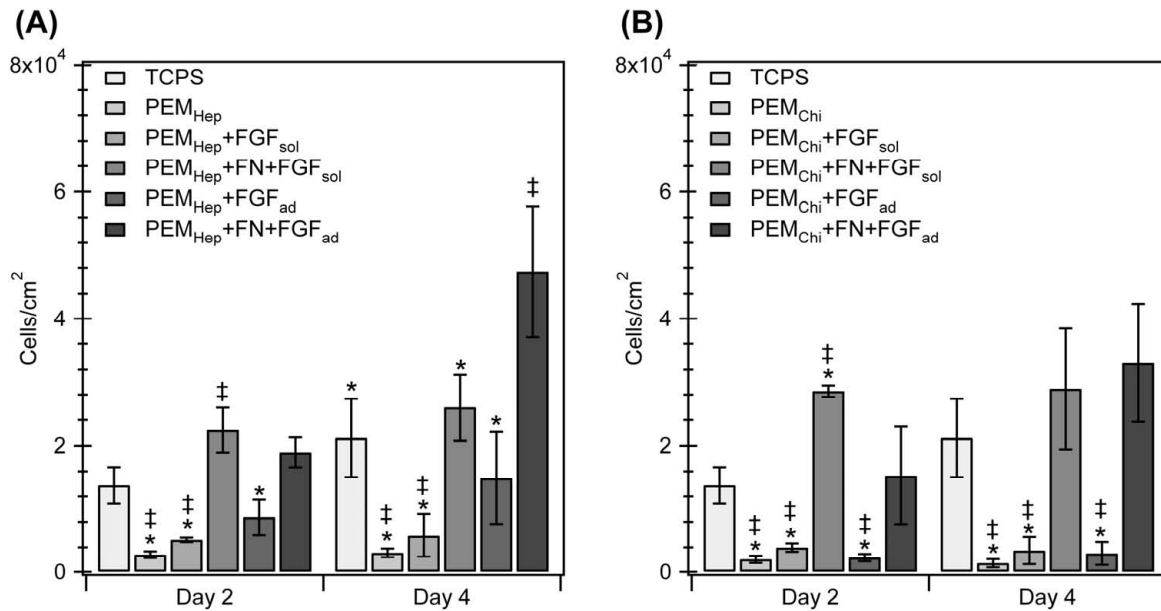
Figure 5.6 MSC density on TCPS coated with (A) PEM_{Hep} and (B) PEM_{Chi} under different culture conditions. Cells were seeded on day 0 at 7000 cells cm^{-2} and cultured in low-serum media. The notation used to indicate the different culture conditions is summarized in Table 5.2. ‡ denotes conditions that are statistically different from TCPS on the same day, and * denotes conditions that are statistically different from PEM+FN+FGF_{ad} on the same day ($p < 0.05$).
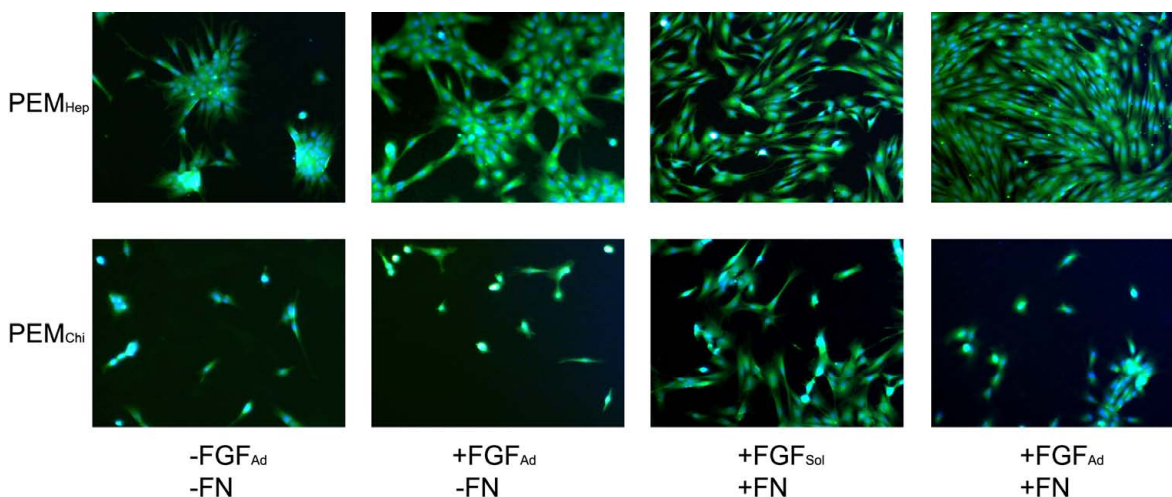
Figure 5.7 Fluorescence microscopy images of MSCs on polysaccharide-based PEMs on day four, corresponding to culture conditions for which MSC density data are reported in Figure 5.6. MSCs form clusters on PEM_{Hep} and are isolated on PEM_{Chi}. When FN is added to PEM_{Hep} surfaces, cells do not form clusters. PEM_{Chi} conditions have fewer cells and a larger fraction of rounded up cells. PEM_{Hep} with FN and FGF-2 adsorbed results in the highest cell density.

The data shown in Figure 5.6 demonstrates that coating the TCPS with polysaccharide-based PEMs with no protein significantly reduces the cell density. This is likely due to decreased initial cell attachment, as the cell density at both day two and day four is lower than the initial seeding density on both PEM_{Hep} and PEM_{Chi}. When FGF-2 was delivered in solution to MSCs on surfaces with adsorbed FN, the cell density at day two was 4.3 times higher on PEM_{Hep} and 6.3 times higher on PEM_{Chi} than when FGF-2 was delivered in solution to MSCs on the same PEMs without FN (Figure 5.6).

Table 5.3 shows the population doubling rate (number of population doublings between days 2 and 4) computed from the cell density data in Figure 5.6. When FGF-2 is delivered in solution to MSCs on either type of PEM, with or without FN, the cells do not proliferate between days two and four, even though additional dissolved FGF-2 was included in the media change on day two. In contrast, when FGF-2 was adsorbed to the PEMs in combination with adsorbed FN, the cells proliferate on both PEM_{Hep} and PEM_{Chi}, between

140

day two and day four. On both $PEM_{Hep}+FN+FGF_{ad}$ and $PEM_{Chi}+FN+FGF_{ad}$ the cells undergo more than one population doubling between days two and four.

Table 5.3 Population doubling rate (number of population doublings between days two and four) for MSCs in low-serum (2.5%FBS) for different treatment groups using TCPS as the substrate.

Sample name	Population doubling rate
TCPS	0.61
PEM_{Hep}	0.14[*]
$PEM_{Hep}+FGF_{sol}$	0.03[*]
$PEM_{Hep}+FN+FGF_{sol}$	0.20
$PEM_{Hep}+FGF_{ad}$	0.66
$PEM_{Hep}+FN+FGF_{ad}$	1.31
PEM_{Chi}	-0.60[‡*]
$PEM_{Chi}+FGF_{sol}$	-0.36[*]
$PEM_{Chi}+FN+FGF_{sol}$	-0.04[*]
$PEM_{Chi}+FGF_{ad}$	0.18
$PEM_{Chi}+FN+FGF_{ad}$	1.19

‡ denotes conditions that are statistically different from TCPS, * denotes conditions that are statistically different from $PEM_{Chi}+FN+FGF_{ad}$ ($p < 0.05$).

Fluorescence microscopy images of MSCs on day four show cells in clusters on PEM_{Hep} and isolated on PEM_{Chi} (Figure 5.7). Figure 5.7 also shows that at day four, the MSCs on the surfaces with adsorbed FN tended to interact more favorably with the surfaces than MSCs on surfaces without adsorbed FN. In general, the PEM_{Hep} surfaces promoted higher MSC density than the PEM_{Chi} surfaces (Figure 5.6 and Figure 5.7).

5.4.4 MSC adhesion and proliferation on PEM-coated titanium

The effect of PEM_{Hep} coatings on cell proliferation was investigated on titanium under different conditions (Figure 5.8) in low-serum (2.5% FBS) media. The initial seeding density was 7000 cells cm^{-2}. For this study, cryopreserved seventh-passage MSCs from three donor animals were used. (MSC proliferation on PUA SAM-modified titanium was also investigated as an additional control surface, and the results are presented in the supporting

information (Appendix).) The effect of PEM$_{Hep}$ alone, PEM$_{Hep}$ with adsorbed FGF-2, and PEM$_{Hep}$ with adsorbed FGF-2 and adsorbed FN were compared to unmodified titanium surfaces, and unmodified titanium with FGF-2 delivered in solution. These conditions are summarized in Table 5.2. The results of the cell proliferation at day two and day four, and representative microscopy images of MSCs on these surfaces at day four are shown in Figure 5.8. The cell proliferation rates are reported in Table 5.4.
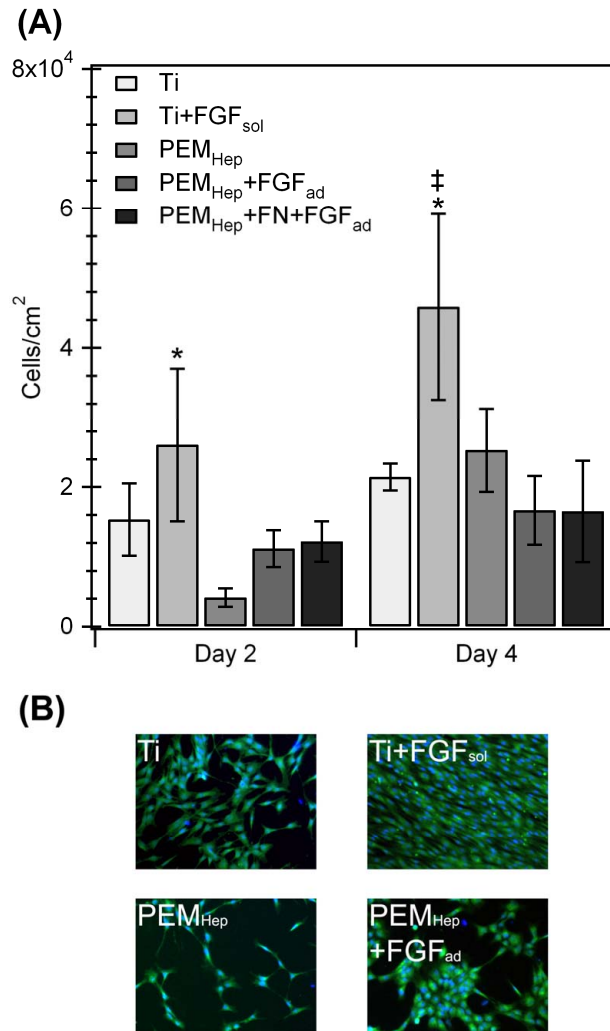
Figure 5.8 (A) MSC density on titanium and titanium modified with PEM$_{Hep}$ under different culture conditions. Cells were seeded on day 0 at 7000 cells cm^{-2} and cultured in low-serum media. The notation used to indicate the different culture conditions is summarized in Table 5.2. ‡ denotes conditions that are statistically different from un-modified titanium on the same day, and * denotes conditions that are statistically different from PEM$_{Hep}$+FN+FGF$_{ad}$ on the same day ($p < 0.05$). (B) Fluorescence microscopy images of MSCs on day 4.

Table 5.4 Population doubling rate (number of population doublings between days two and four) for MSCs in low-serum (2.5 % FBS) for different treatment groups using titanium as the substrate.

Ti	0.53
Ti+FGF$_{sol}$	0.86
PEM$_{Hep}$	1.77‡*
PEM$_{Hep}$+FGF$_{ad}$	0.56
PEM$_{Hep}$+FN+FGF$_{ad}$	0.38

‡ denotes conditions that are statistically different from Ti, and * denotes conditions that are statistically different from PEM$_{Hep}$+FN+FGF$_{ad}$ ($p < 0.05$).

On titanium surfaces MSC density was highest for the FGF$_{sol}$ condition. The addition of the PEM$_{Hep}$ to titanium reduced the cell density, probably by reducing initial cell attachment (Figure 5.8). When FGF-2 was adsorbed to PEM$_{Hep}$ on titanium, the MSC density was improved over that obtained on PEM$_{Hep}$ on day two, but by day four, adsorbed FGF-2 resulted in no significant increase in MSC cell density. The addition of FN to PEM$_{Hep}$ with adsorbed FGF-2 also did not improve cell proliferation. By day four the PEM$_{Hep}$+FN+FGF$_{ad}$ behaved similarly to the PEM$_{Hep}$+FGF$_{ad}$ condition, thus microscopy for only one of these conditions in Figure 5.8 (B).

5.5 Discussion

The relatively low plasma half-life of growth factors such as FGF-2 might be a significant barrier to their therapeutic use for in vivo applications, and motivates the need to develop strategies to stabilize and potentiate their biochemical functions. Both our preliminary data (not shown) and previous investigations have demonstrated that the effect of FGF-2 on MSC proliferation is masked by high FBS concentrations (5% to 10%) using ovine bone marrow-derived[4] and human skin-derived MSCs.[37] Thus, low serum media (2.5% FBS) was used to evaluate the response of MSCs to FGF-2 in this work. Tuning the growth factor dose might also be essential to realizing the desired biochemical activity. FGF-2, for

example, has been previously shown to induce a higher mitogenic response at intermediate doses than at high doses, consistent with our results (Figure 5.5).[3, 38] PEMs might be used to address both of these challenges, by enhancing growth factor stability and tuning the growth factor dose.

PEMs are of interest for the local delivery of therapeutic proteins because this surface coating technique can in principle be translated to many types of materials and to irregular, three dimensional surfaces. PEMs can also be engineered to alter the kinetics and amount of the protein delivered. The delivery of the growth factors BMP-2[33, 39, 40], TGFβ-1[40], and FGF-2[27] has been successfully demonstrated using PEMs that retain or enhance the growth factor activity. DNA-poly(L-lysine) and DNA-poly(allylamine hydrochloride) PEMs were used to deliver BMP-2 to rat bone marrow cells, by van den Bueken et al., demonstrating that the position of the BMP-2 within the PEM could modulate the biological response.[39] Crouzier et al. showed the osteoblast differentiation of myocytes could be modulated by changing the thickness of BMP-2-loaded poly(L-lysine)-hyaluronan PEMs.[33] Dierich et al. demonstrated that PEMs of poly(L-lysine), succinylated poly(L-lysine), and poly(glycolic acid) could be used to deliver combinations of TGFβ-1 and BMP-2 to induce the embryonic stem cell differentiation into both bone and cartilage phenotypes.[40] Tezcaner et al. demonstrated improved photoreceptor cell attachment and differentiation by delivery of FGF-2 from poly(L-lysine)-chondroitin sulfate PEMs.[27]

In the present work, we investigated whether the delivery of FGF-2 from heparin-containing PEMs could stabilize and enhance the growth factor activity, on both TCPS and titanium surfaces. Our results demonstrate the effective delivery of FGF-2 in vitro from polysaccharide-based PEMs, but show that the biological response depends upon both

144

the PEM chemistry and the underlying surface. On both TCPS and titanium, PEM coating reduced cell proliferation, in the absence of FN and FGF-2 (Figure 5.6, Figure 5.7, and Figure 5.8). PEM$_{Hep}$ surfaces on TCPS without FN or FGF-2 yielded higher cell densities by day four than PEM$_{Chi}$ surfaces ($p = 0.04$). Microscopy images show a tendency for cells to form small clusters on PEM$_{Hep}$ and to be more rounded on PEM$_{Chi}$ (Figure 5.7 and Figure 5.8). These differences indicate that the chemistry of the terminal polysaccharide layer of these very thin PEMs influences MSC attachment and proliferation. Mammalian cells have previously been shown to have poor adhesion to polysaccharide-based PEMs unless surface modification is performed. Successful surface modifications have included crosslinking,[26, 41] grafting of RGD peptide,[42, 43] and addition of fibronectin.[24, 41, 44] MSCs and myoblasts show poor adhesion to chitosan/hyaluronan PEMs[41] and poly(L-lysine)/hyaluronan PEMs[26] respectively, unless they are crosslinked. Poly(ethylene imine)/heparin PEMs show poor fibroblast adhesion unless they are pre-coated with serum or FN.[24] In our lab, preliminary studies showed that FN pre-coating of PEMs resulted in higher cell adhesion and proliferation rates than glutaraldehyde crosslinking, glyceraldehyde crosslinking, and unmodified PEMs (data not shown). These findings are in agreement with the results mentioned above using polysaccharide-based PEMs. Nonetheless, neither chitosan nor heparin are considered to be cytotoxic to mammalian cells. In fact, it was recently shown that heparin-coated chitosan membranes showed almost a 5-fold increase in MSC growth compared to TCPS.[45]

The addition of FN greatly improves cell density on both PEM$_{Hep}$ and PEM$_{Chi}$ surfaces on TCPS (Figure 5.6). Fibronectin has an iso-electric point of 5.2[46] making it negatively charged at physiological pH. Thus, based on electrostatic interactions alone, one might expect more

fibronectin to be adsorbed on PEM$_{Chi}$ surfaces than on PEM$_{Hep}$ surfaces. Wittmer et al. demonstrated results using poly(L-lysine)/dextran sulfate PEMs, in which more fibronectin was adsorbed on surfaces terminated with the polycation.[47] However, heparin also contains a specific binding site for fibronectin.[50] In fact, Kan et al. demonstrated that heparin, FGF-1, and fibronectin work synergistically and are essential for endothelial cell growth.[51] On the other hand, Dalton et al. cultured human bone-derived cells on fibronectin surfaces while adding heparin to the medium to investigate whether heparin inhibits cell attachment by blocking the integrin receptor of the heparin region of fibronectin.[52] They found that cell attachment to fibronectin was not affected by the presence of heparin.[52] This study is consistent with our observations, were cell attachment is enhanced with the presence of fibronectin for both heparin-terminated and chitosan-terminated PEMs.

On both gold and titanium surfaces the heparin-terminated PEMs bind more FGF-2 than the chitosan-terminated surfaces (Figure 5.1 and Figure 5.4). The specific binding of FGF-2 to heparin may be the cause of the increased FGF-2 binding to the PEM$_{Hep}$ surfaces over the PEM$_{Chi}$ surfaces observed in Figure 5.1 and Figure 5.4. Also, FGF-2 has an iso-electric point above 7, making it positively charged at the adsorption conditions. This may promote non-specific electrostatic adsorption to the negatively charged PEM$_{Hep}$ surfaces.

On TCPS, adsorbing FGF-2 and FN onto PEMs prior to cell seeding yielded higher cell densities on day 4 than presenting the FGF-2 in solution, even though a media change was performed at day two, replenishing the FGF-2 on the +FGF$_{sol}$ controls. In particular, on TCPS surfaces, PEMs with adsorbed FGF-2 and adsorbed FN resulted in the highest MSC proliferation rate (Table 5.3). In contrast, delivering FGF-2 in solution did not result in significant cell proliferation between days two and day four for MSCs on PEMs or TCPS.

FGF-2 is known to regulate MSC proliferation by binding to the cell surface FGF-2 receptors in the presence of heparin proteoglycans.[22] Binding FGF-2 to heparin also increases its half-life almost six fold.[17] The combined effects of FGF-2 stabilization and FGF-2 activation by heparin binding may contribute to the improved biological activity when FGF-2 was adsorbed to PEM$_{Hep}$ surfaces. It is also possible that the heparin-containing PEMs act as a depot for the sustained release of FGF-2 into the media. However, based on our comparisons to the control experiments in which FGF-2 was delivered in solution, we do not believe that this is the dominant mode of action of the PEMs with respect to promoting FGF-2 activity in these experiments.

In all of the experiments reported above using FGF-2 adsorbed to PEMs, the FGF-2 was adsorbed from solution at a concentration of 50 ng mL^{-1}. However, the dose response study shown in Figure 5.5 demonstrates that the cells may be very sensitive to the amount of FGF-2 delivered. To investigate whether the MSC response can be modulated by altering the amount of FGF-2 adsorbed to the surfaces, MSC proliferation was evaluated on day four on PEM$_{Hep}$+FGF$_{ad}$, PEM$_{Chi}$+FGF$_{ad}$, PEM$_{Hep}$+FN+FGF$_{ad}$, and PEM$_{Chi}$+FN+FGF$_{ad}$ on TCPS prepared with different concentrations of FGF-2 in the adsorption solution (50, 100, 200, and 500 ng mL^{-1}). Figure 5.9 shows cell density data at day four from these experiments. The concentration of FGF-2 in the adsorption solution has no significant effect on final cell densities for all of the surfaces. From these results, we conclude that all of the concentrations evaluated result in saturation of the surfaces with FGF-2.
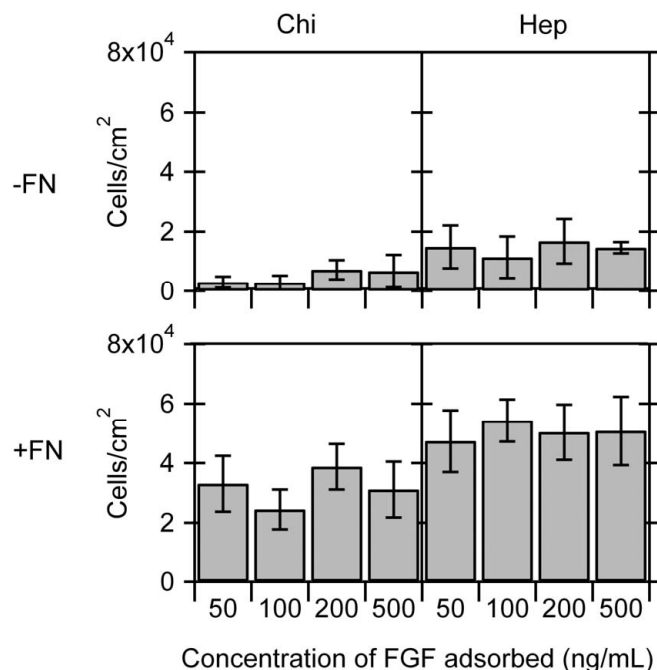
Figure 5.9 MSC density on day 4 on PEM_{Hep} and PEM_{Chi} on TCPS with adsorbed FGF-2, with and without adsorbed FN. Cells were seeded on day 0 at 7000 cells cm^{-2} and cultured in low-serum media. Altering the FGF-2 concentration in the adsorption solution over the range from 50 ng mL^{-1} to 500 ng mL^{-1} did not result in statistically different cell densities within any of the four groups of otherwise similar surfaces.

Our results demonstrate that polysaccharide-based PEMs may be valuable surface coatings for growth factor delivery from biomaterials surfaces. However, in order to engineer PEMs as versatile surface coatings for growth factor delivery, it may be necessary to translate the coating procedure to various types of surfaces. The data in Figure 5.6 (A) and Figure 5.8 (A) show that MSCs respond differently to the FGF-containing PEMs on titanium than they do to the FGF-containing PEMs on TCPS. Interestingly, MSCs cultured on titanium with soluble FGF-2 behaved similarly to cells cultured on TCPS without PEMs. These differences could arise from the relative amount of polysaccharide adsorbed to these surfaces. On titanium PEM_{Hep} coatings alone are sufficient to significantly reduce initial cell attachment (indicated by the day 2 data in Figure 5.8). However, the adsorption of FGF-2 and

FN has no discernable effect on the cell density at day 4. It is also possible that the internal structure of the PEMs on TCPS and titanium are different, resulting in critical differences in the presentation of the FGF-2 to the cell surface FGF-2 receptors, and/or differences in the ability of the cells to remodel or degrade the PEMs. In some experimental reports, heparin or heparan sulfate GAGs have been shown to block FGF-2 signaling by their binding to the FGF-2 receptor.[18] Further work will be done to investigate these effects by quantifying the amount of polysaccharides and protein adsorbed on the different surfaces.

5.6 Conclusions

We have developed surface coatings for the delivery of FGF-2 at therapeutic concentrations using polysaccharide-based PEMs for guided MSC proliferation. Heparin-terminated PEM coatings with adsorbed FGF-2 and adsorbed FN on TCPS were shown to be the best candidate surface coatings for enhancing MSC proliferation in low-serum media. This system represents a promising candidate for the development of surface coatings that can stabilize and potentiate the activity of growth factors for therapeutic applications. However, when the PEM coatings were translated to titanium surfaces, the improvement in MSC proliferation was not observed. Additional work will be necessary to tune the PEM coatings on different surfaces, in order to take advantage of their potential for growth factor delivery.

5.7 Acknowledgments

5.8 References

1. Tessmar, J. K.; Gopferich, A. M., *Advanced Drug Delivery Reviews* **2007**, *59* (4-5), 274-291.
2. De Luca, F.; Baron, J., *Trends in Endocrinology and Metabolism* **1999**, *10* (2), 61-65.
3. Hankemeier, S.; Keus, M.; Zeichen, J.; Jagodzinski, M.; Barkhausen, T.; Bosch, U.; Krettek, C.; Van Griensven, M., *Tissue Engineering* **2005**, *11* (1-2), 41-49.
4. McCarty, R. C.; Gronthos, S.; Zannettino, A. C.; Foster, B. K.; Xian, C. J., *Journal of Cellular Physiology* **2009**, *219* (2), 324-333.
5. Ziegler, J.; Mayr-Wohlfart, U.; Kessler, S.; Breitig, D.; Gunther, K. P., *Journal of Biomedical Materials Research* **2002**, *59* (3), 422-428.
6. Isogai, N.; Morotomi, T.; Hayakawa, S.; Munakata, H.; Tabata, Y.; Ikada, Y.; Kamiishi, H., *Journal of Biomedical Materials Research Part A* **2005**, *74A* (3), 408-418.
7. Huang, X.; Yan, W. Q.; Yang, D. S.; Feng, J.; Feng, Y. B.; Gan, Y. B.; Weng, W. J. In *Bioceramics 18, Pts 1 and 2*, Nakamura, T.; Yamashita, K.; Neo, M., Eds. Trans Tech Publications Ltd: Zurich-Uetikon, 2006; Vol. 309-311, pp 953-956.
8. Keiichi, K.; Mitsunobu, K.; Masafumi, S.; Yutaka, D.; Toshiaki, S., *Clinical Oral Implants Research* **2009**, *20* (6), 560-565.
9. Wenk, E.; Murphy, A. R.; Kaplan, D. L.; Meinel, L.; Merkle, H. P.; Uebersax, L., *Biomaterials* **2010**, *31* (6), 1403-1413.
10. Jeon, O.; Kang, S. W.; Lim, H. W.; Chung, J. H.; Kim, B. S., *Biomaterials* **2006**, *27* (8), 1598-1607.
11. Ma, L.; Zhou, J.; Gao, C. Y.; Shen, J. C., *Journal of Biomedical Materials Research Part B-Applied Biomaterials* **2007**, *83B* (1), 285-292.
12. Nakamura, S.; Kanatani, Y.; Kishimoto, S.; Ohno, C.; Horio, T.; Masanori, F.; Hattori, H.; Tanaka, Y.; Kiyosawa, T.; Maehara, T.; Ishihara, M., *Journal of Biomedical Materials Research Part A* **2009**, *91A* (3), 814-823.
13. Freudenberg, U.; Hermann, A.; Welzel, P. B.; Stirl, K.; Schwarz, S. C.; Grimmer, M.; Zieris, A.; Panyanuwat, W.; Zschoche, S.; Meinhold, D.; Storch, A.; Werner, C., *Biomaterials* **2009**, *30* (28), 5049-5060.

14. Rider, C. C., *Biochemical Society Transactions* **2006**, 34 (3) 458-460.

15. Maccarana, M.; Casu, B.; Lindahl, U., *Journal of Biological Chemistry* **1993**, *268* (32), 23898-23905.

16. McCaffrey, T. A.; Falcone, D. J.; Du, B. H., *Journal of Cellular Physiology* **1992**, *152* (2), 430-440.

17. Damon, D. H.; Lobb, R. R.; Damore, P. A.; Wagner, J. A., *Journal of Cellular Physiology* **1989**, *138* (2), 221-226.

18. Guimond, S.; Maccarana, M.; Olwin, B. B.; Lindahl, U.; Rapraeger, A. C., *Journal of Biological Chemistry* **1993**, *268* (32), 23906-23914.

19. Berry, D.; Kwan, C. P.; Shriver, Z.; Venkataraman, G.; Sasisekharan, R., *Faseb Journal* **2001**, *15* (6), 1422-+.

20. Zamora, P. O.; Tsang, R.; Pena, L. A.; Osaki, S.; Som, P., *Bioconjugate Chemistry* **2002**, *13* (5), 920-926.

21. Vincent, T.; Hermansson, M.; Bolton, M.; Wait, R.; Saklatvala, J., *Proceedings of the National Academy of Sciences of the United States of America* **2002**, *99* (12), 8259-8264.

22. Lee, J. Y.; Choo, J. E.; Choi, Y. S.; Lee, K. Y.; Min, D. S.; Pi, S. H.; Seol, Y. J.; Lee, S. J.; Jo, I. H.; Chung, C. P.; Park, Y. J., *Journal of Biomedical Materials Research Part A* **2007**, *83A* (4), 970-979.

23. Richert, L.; Lavalle, P.; Payan, E.; Shu, X. Z.; Prestwich, G. D.; Stoltz, J. F.; Schaaf, P.; Voegel, J. C.; Picart, C., *Langmuir* **2004**, *20* (2), 448-458.

24. Niepel, M. S.; Peschel, D.; Sisquella, X.; Planell, J. A.; Groth, T., *Biomaterials* **2009**, *30* (28), 4939-4947.

25. Schneider, A.; Vodouhe, C.; Richert, L.; Francius, G.; Le Guen, E.; Schaaf, P.; Voegel, J. C.; Frisch, B.; Picart, C., *Biomacromolecules* **2007**, *8* (1), 139-145.

26. Ren, K. F.; Crouzier, T.; Roy, C.; Picart, C., *Advanced Functional Materials* **2008**, *18* (9), 1378-1389.

27. Tezcaner, A.; Hicks, D.; Boulmedais, F.; Sahel, J.; Schaaf, P.; Voegel, J. C.; Lavalle, P., *Biomacromolecules* **2006**, *7* (1), 86-94.

28. Moby, V.; Kadi, A.; de Isla, N.; Stoltz, J. F.; Menu, P., *Bio-Medical Materials and Engineering* **2008**, *18* (4-5), 199-204.

29. Tsai, W. B.; Chen, R. P. Y.; Wei, K. L.; Tan, S. F.; Lai, J. Y., *Journal of Biomaterials Science-Polymer Edition* **2010**, *21* (3), 377-394.

30. Serizawa, T.; Yamaguchi, M.; Akashi, M., *Biomacromolecules* **2002**, *3* (4), 724-731.

31. Berg, M. C.; Yang, S. Y.; Hammond, P. T.; Rubner, M. F., *Langmuir* **2004**, *20* (4), 1362-1368.

32. Picart, C., *Current Medicinal Chemistry* **2008**, *15* (7), 685-697.

33. Crouzier, T.; Ren, K.; Nicolas, C.; Roy, C.; Picart, C., *Small* **2009**, *5* (5), 598-608.

34. Boddohi, S.; Moore, N.; Johnson, P. A.; Kipper, M. J., *Biomacromolecules* **2009**, *10* (6), 1402-1409.

35. Boddohi, S.; Almodóvar, J.; Zhang, H.; Johnson, P. A.; Kipper, M. J., *Colloids and Surfaces B-Biointerfaces* **2010**, *77* (1), 60-68.

36. Boddohi, S.; Killingsworth, C. E.; Kipper, M. J., *Biomacromolecules* **2008**, *9* (7), 2021-2028.

37. Riekstina, U.; Muceniece, R.; Cakstina, I.; Muiznieks, I.; Ancans, J., *Cytotechnology* **2008**, *58* (3), 153-162.

38. Song, G. B.; Ju, Y.; Soyama, H., *Materials Science & Engineering C-Biomimetic and Supramolecular Systems* **2008**, *28* (8), 1467-1471.
39. van den Beucken, J.; Walboomers, X. F.; Boerman, O. C.; Vos, M. R. J.; Sommerdijk, N.; Hayakawa, T.; Fukushima, T.; Okahata, Y.; Nolte, R. J. M.; Jansen, J. A., *Journal of Controlled Release* **2006**, *113* (1), 63-72.
40. Dierich, A.; Le Guen, E.; Messaddeq, N.; Stoltz, J. F.; Netter, P.; Schaaf, P.; Voegel, J. C.; Benkirane-Jessel, N., *Advanced Materials* **2007**, *19* (5), 693-+.
41. Semenov, O. V.; Malek, A.; Bittermann, A. G.; Voros, J.; Zisch, A. H., *Tissue Engineering Part A* **2009**, *15* (10), 2977-2990.
42. Tsai, W. B.; Chen, R. P. Y.; Wei, K. L.; Chen, Y. R.; Liao, T. Y.; Liu, H. L.; Lai, J. Y., *Acta Biomaterialia* **2009**, *5* (9), 3467-3477.
43. Chua, P. H.; Neoh, K. G.; Kang, E. T.; Wang, W., *Biomaterials* **2008**, *29* (10), 1412-1421.
44. Kirchhof, K.; Hristova, K.; Krasteva, N.; Altankov, G.; Groth, T., *Journal of Materials Science-Materials in Medicine* **2009**, *20* (4), 897-907.
45. Uygun, B. E.; Stojsih, S. E.; Matthew, H. W. T., *Tissue Engineering Part A* **2009**, *15* (11), 3499-3512.
46. Tooney, N. M.; Mosesson, M. W.; Amrani, D. L.; Hainfeld, J. F.; Wall, J. S., *Journal of Cell Biology* **1983**, *97* (6), 1686-1692.
47. Wittmer, C. R.; Phelps, J. A.; Saltzman, W. M.; Van Tassel, P. R., *Biomaterials* **2007**, *28* (5), 851-860.
48. Lavalle, P.; Picart, C.; Mutterer, J.; Gergely, C.; Reiss, H.; Voegel, J. C.; Senger, B.; Schaaf, P., *Journal of Physical Chemistry B* **2004**, *108* (2), 635-648.
49. Crouzier, T.; Picart, C., *Biomacromolecules* **2009**, *10* (2), 433-442.
50. Kan, M. K.; Shi, E. G., *In Vitro Cellular & Developmental Biology* **1990**, *26* (12), 1151-1156.
51. (51) Lee, C. H.; Singla, A.; Lee, Y., *International Journal of Pharmaceutics* **2001**, *221* (1-2), 1-22.
52. Dalton, B. A.; McFarland, C. D.; Underwood, P. A.; Steele, J. G., *Journal of Cell Science* **1995**, *108*, 2083-2092.
53. Boddohi, S.; Kipper, M. J., *Advanced Materials* **2010**, *22*, 2998-3016.
54. Richert, L; Schneider, A.; Vautier, D.; Vodouhe, C.; Jessel , N.; Payan, E.;Schaaf , P.; Voegel, J. C.; Picart, C., *Cell Biochemistry and Biophysics* **2006**, *44*, 273-825.
55. Serizawa, T.; Yamaguchi, M.; Akashi, M., *Biomacromolecules* **2002**, *3*, 724-731.

Chapter 6

Coating Electrospun Chitosan Nanofibers with Polyelectrolyte Multilayers Using the Polysaccharides Heparin and *N,N,N*-Trimethyl Chitosan

6.1 Abstract

A new method is presented for functionalizing electrospun nanofibers with glycosaminoglycans and growth factors by polyelectrolyte multilayer (PEM) deposition. Electrospun chitosan nanofibers, spun from trifluoroacetic acid and dichloromethane, were coated with PEMs, using the polysaccharides heparin and *N,N,N*-trimethyl chitosan. Fibroblast growth factor-2 (FGF-2) was adsorbed on the PEM-coated nanofibers. Nanofiber neutralization, PEM construction, and FGF-2 adsorption were monitored using FT-IR spectroscopy and X-ray photoelectron spectroscopy. Alcian blue staining was used to confirm the presence of heparin. Scanning electron microscopy was used to study nanofiber morphology.

6.2 Introduction

Chitosan electrospun nanofibers have attracted significant interest as nanostructured biomaterials for cell and tissue engineering. Chitosan has desirable biological properties including antimicrobial activity, promotion of wound healing and angiogenesis.[1] Nanoscale surface features may also influence biological response to chitosan materials.[1,2] For example, chitosan biomaterials are commonly functionalized with other molecules to improve mammalian cell adhesion or to introduce additional biological functionality. Common types of functionalization include covalent attachment of peptide adhesion ligands and adsorption of extracellular matrix components. The layer-by-layer (LbL) assembly of polyelectrolyte multilayers (PEMs) is another modification method that has emerged as a simple technique for modifying biomaterials surfaces, enabling one to tune surface chemistry and surface mechanical properties, and to control the presentation and delivery of bioactive compounds from surfaces. We have previously characterized polysaccharide-based PEMs on flat surfaces (gold-coated glass, titanium, and tissue culture polystyrene), and we have used these PEMs to stabilize and deliver basic fibroblast growth factor (FGF-2).[2-5] PEMs might also be used to functionalize chitosan nanofibers. However, functionalization of chitosan nanofibers using aqueous methods presents two practical challenges: the solubility and the mechanical fragility of the nanofibers. These two challenges are particularly troublesome for PEM deposition because the process requires significant manipulation, including repeated exposure to aqueous solutions. Methods of crosslinking chitosan nanofibers to strengthen them and render them insoluble have been reported.[6, 7] But crosslinking consumes amino groups, thereby altering the charge density, reactivity, and biodegradability. This work presents a new method for coating chitosan electrospun nanofibers with PEMs that

overcomes both of the challenges without crosslinking the chitosan. We demonstrate coating of chitosan nanofibers with PEMs using the polysaccharides *N,N,N*-trimethyl chitosan (TMC) and heparin as the polycation and polyanion, respectively. We also demonstrate that these heparin-containing PEM coatings on chitosan nanofibers can bind the growth factor FGF-2.

6.3 Materials and Methods

6.3.1 Materials

Chitosan (80 kDa, 5% acetylated confirmed through ^{1}H NMR, Protosan UP B 90/20) was purchased from Novamatrix (Sandvika, Norway). Heparin sodium (from porcine intestinal mucosa, 14.4 kDa 12.5% sulfur) was purchased from Celsus Laboratories (Cincinnati, OH). Recombinant human FGF basic (FGF-2) 146 aa was purchased from R&D Systems (Minneapolis, MN). Dichloromethane (DCM), trifluoroacetic acid (TFA), and dimethyl sulfate were purchased from Acros Organics (Geel, Belgium). Sodium hydroxide and sodium chloride were purchased from Fisher Scientific (Pittsburgh, PA). Ammonium hydroxide was purchased from Sigma-Aldrich (St. Lois, MO). A Millipore Synthesis water purification unit (Millipore, Billerica, MA) was used to obtain 18.2 MΩ water, used for making all aqueous solutions. TMC was synthesized following the procedure described by de Britto and Assis.[8] A detailed TMC synthesis procedure and its characterization by ^{1}H NMR can be found in the supporting information (Appendix). The degree of quaternization for TMC was calculated to be 22%.

6.3.2 Electrospinning chitosan

Chitosan nanofibers were electrospun following a procedure similar to the one published by Ohkawa et al.[9] Briefly, 7% wt./vol. chitosan solutions were prepared in a TFA:DCM mixture (70:30 by volume). The electrospinning apparatus has been described previously.[10] The collector for these experiments was aluminum foil fastened onto a 0.5 in. thick copper plate (McMaster Carr, Robbinsville, NJ) with vinyl electrical tape. Nanofibers were spun using a volumetric flow rate of 1.0 mL•hr^{-1}, an applied voltage 18 kV, and a horizontal tip-to-collector distance 17.5 cm.

6.3.3 Development of a method for coating electrospun nanofibers with PEMs

Small pieces (~1 cm^2) of the aluminum foil collection electrode were cut using scissors, and nanofiber mat samples were removed using forceps. Although chitosan is insoluble in aqueous solutions above its pK_a (~ 6.4), the nanofibers retained a significant amount of TFA, sufficient to render them soluble in the aqueous solutions used for PEM deposition. Dissolution of the nanofibers was rapid, occurring in less than one minute. This phenomenon has also been observed by Sangsanoh and Supaphol.[11] To extract the TFA, nanofibers were carefully dipped in DCM, ethanol, acetone, or aqueous ammonium hydroxide solutions (0.5 to 5.0 M). After dipping in each of these solvents for 2 minutes, nanofibers were transferred to water to test their solubility. All treated nanofibers rapidly dissolved in the water except for the ones dipped in 5.0 M ammonium hydroxide. TFA removal by 5.0 M ammonium hydroxide treatment was confirmed by XPS and FT-IR.

Four methods were attempted for coating the stabilized nanofibers with heparin-TMC PEMs. In all four methods, TMC and heparin solutions with concentrations of 0.01 M (on a saccharide unit basis) were prepared in water and filtered (0.22 μm PVDF syringe filters,

156

Fisher Scientific) for the polyelectrolyte adsorption steps; water was used for the rinsing steps. Each PEM deposition procedure began with ammonium hydroxide pretreatment, rinsing, and then exposure to solutions following the sequence: (1) heparin, (2) water, (3) TMC, (4) water. This sequence was repeated up to five and a half times to produce 11-layer PEMs. In the first method, the nanofiber mats were dipped in the solutions for two minutes each, using forceps. In the second method, the nanofiber mats were affixed to supports (glass, aluminum, polystyrene, or Parafilm®), and the supports were sequentially dipped in the solutions. In the third method, the nanofiber mats were placed in glass or polystyrene dishes, and the solutions were sequentially applied and removed using a pipette. These first three methods were unsuccessful, as described in the Results section. In the fourth method, the nanofiber mats were gently sandwiched between two filter papers (Whatman 41, 20 μm, ashless, Whatman Inc., Piscataway, NJ) and placed in a Büchner funnel. Solutions were slowly pulled through the filter papers under weak vacuum. This fourth method was successful at maintaining nanofiber integrity. Scanning electron microscopy (SEM) (JSM-6500F JEOL, Tokyo, Japan) was used to observe nanofiber morphology.

6.3.4 Confirmation of PEM coating on electrospun nanofibers

PEM deposition on the chitosan nanofibers was confirmed by XPS (5800 spectrometer, Physical Electronics, Chanhassen, MN), and transmission FT-IR (Nicolet 8700 FT-IR spectrometer, Thermo-Electron, Madison, WI). XPS experiments were performed at a photoelectron takeoff angle of 45 °, and binding energy scales were referenced to the C1s peak (284.7 eV). FT-IR experiments used a DTGS detector (500 scans between 4000-600 cm^{-1} at 8 cm^{-1} resolution). Alcian blue stain (0.1 wt.-% in water, 45 minutes) was used to visually confirm heparin adsorption associated with PEM deposition. FGF-2 was

adsorbed on the PEM-coated nanofibers from solutions of 5 µg•mL^{-1} for 2 hours under gentle agitation, and confirmed by FT-IR.

6.4 Results

Chitosan nanofibers were successfully spun from an approximately 3 mL TFA/DCM solution at 1 mL·hr^{-1}. This yielded nanofiber mats approximately 50 µm thick, measured using a caliper.   As observed by Sangsanoh and Supaphol, the chitosan nanofibers electrospun from TFA-containing solution were water-soluble, even in water with pH above the pKa of the chitosan.[11] In our experiments, when small samples of nanofibers were dipped into 2 mL of water (neutral pH) the pH of the water dropped by 4 to 6 pH units, and the nanofibers rapidly dissolved. This indicates that a significant quantity of TFA, which may form a salt with the amino groups in chitosan,[12] was bound in the untreated nanofibers. The strong F1s intensity in the XPS spectrum of the nanofibers shown in Figure 6.1 (A) confirmed significant retention of TFA, even under high vacuum conditions. Sangsanoh and Supaphol neutralized the TFA in their chitosan nanofibers using high-molarity sodium carbonate. We attempted to extract the bound TFA by soaking the nanofibers in several solvents. Soaking the nanofibers in DCM, ethanol, acetone, or aqueous ammonium hydroxide solutions with concentrations less than 5.0 M was not successful at extracting the TFA. Only nanofibers treated with 5.0 M ammonium hydroxide were insoluble in aqueous solutions. XPS and FT-IR spectra of ammonium hydroxide-treated nanofibers confirmed TFA removal (Figure 6.1 and Figure 6.3).
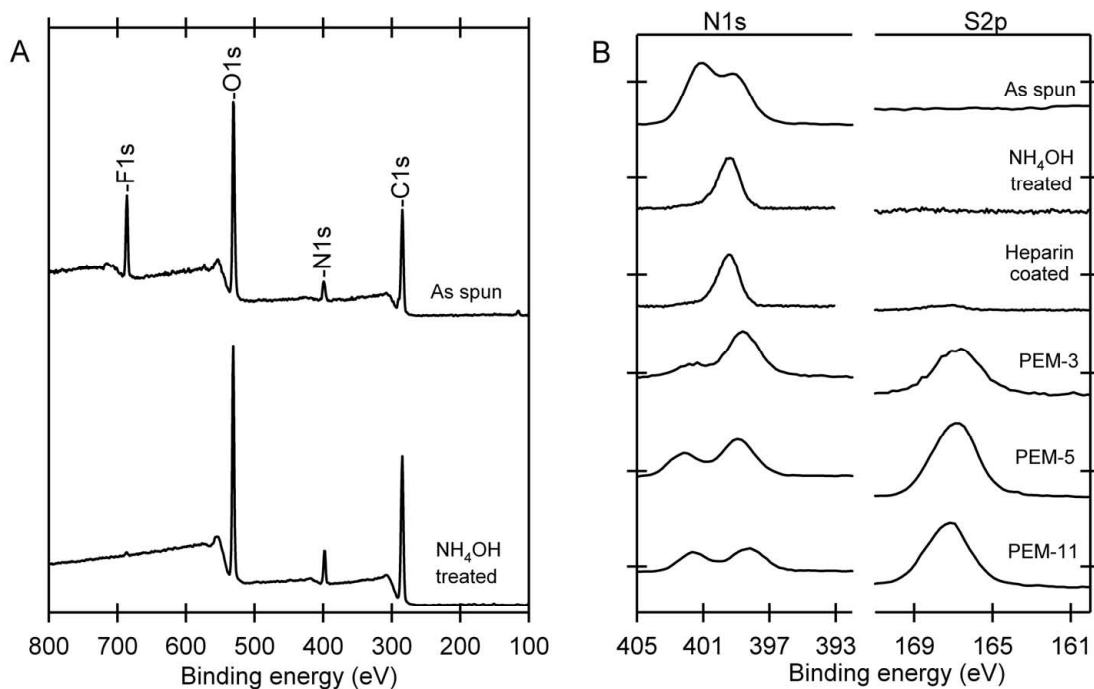
Figure 6.1 (A) XPS spectra of untreated and ammonium hydroxide treated chitosan nanofibers. (B) N1s and S2p envelopes for untreated, ammonium hydroxide-treated, heparin-coated, 3-layer, 5-layer, and 11-layer heparin-TMC PEM-coated chitosan nanofibers.

After stabilization by ammonium hydroxide treatment, the nanofibers were still too fragile to survive the PEM formation when sequentially dipped in several polyelectrolyte and rinse solutions. When dipping into aqueous solutions, the nanofiber mats collapsed, probably due to capillary forces. When removing nanofibers from solutions, the nanofiber mats retained significant quantities of water in their pores, and the weight of this retained water pulled apart the nanofiber mats. Even when small nanofiber samples were handled with great care, after two to five rounds of dipping they lost all structural integrity. This presents a challenge for any aqueous modification of nanofibers, but particularly for PEM assembly involving multiple adsorption and rinsing steps.

Next nanofibers were affixed to several surfaces (glass, aluminum, polystyrene, and Parafilm®) to provide mechanical strength. These supported nanofiber mats were dipped into

159

the solutions, as described above. They were also placed in the bottom of a dish into which the solutions were applied and removed by pipetting. Supporting the nanofibers in this way helped to overcome the problem of the nanofibers being torn apart by the mass of retained water, but the nanofiber mats still collapsed upon repeated exposure to aqueous solutions. Furthermore, after drying, the nanofibers were strongly adhered to all of these surfaces, except for the Parafilm®, and could not be removed without tearing them apart.

Successful manipulation of nanofibers that did not result in collapse or tearing of the nanofiber mats was achieved by gently sandwiching them between two filter papers (Whatman 41, 20 μm, ashless) and placing them in a Büchner funnel. Each solution to be applied was slowly pulled through the filter papers under weak vacuum. Using this method, chitosan nanofibers were neutralized by treatment with 5.0 M ammonium hydroxide solution for 2 minutes, rinsed exhaustively with water (until the rinse water had neutral pH), and modified with PEMs by alternating polyanion and polycation adsorption steps to form up to 11-layer PEMs. Nanofibers were rinsed with water five times between polyelectrolyte adsorption steps. After modification, the nanofibers were easily lifted from the filter paper with forceps.

The N1s and S2p envelopes from the XPS spectra of nanofibers at different stages during this sequence are shown in Figure 6.1 (B). The N1s envelope of the as spun nanofibers contains contributions from protonated amine groups at higher binding energy (401.2 eV) corresponding to ammonium-TFA salt. After ammonium hydroxide treatment and rinsing, only the lower binding energy (398.0 eV) N1s peak remains, corresponding to amine and amide groups in chitosan. Upon subsequent addition of heparin-TMC PEMs, the ammonium peak re-emerges, confirming addition of the quaternary ammonium groups in TMC.[13] The

160

S2p envelope confirms heparin coating of the nanofibers. The intensity of the S2p peak increases with increasing numbers of layers for 1-, 3-, and 5-layer heparin-TMC PEMs. Beyond five layers, XPS is no longer sensitive to additional layers, being a surface technique.

SEM micrographs of untreated and PEM-coated electrospun nanofibers are shown in Figure 6.2. Ammonium hydroxide treatment and PEM coating result in noticeable changes in the nanofiber morphology. In particular, fewer of the smallest diameter nanofibers are visible in the PEM-modified nanofibers. The PEM-modified nanofibers also appear to be fused together at the junctions, but the nanofiber mats remain porous, with uniform and featureless surfaces.
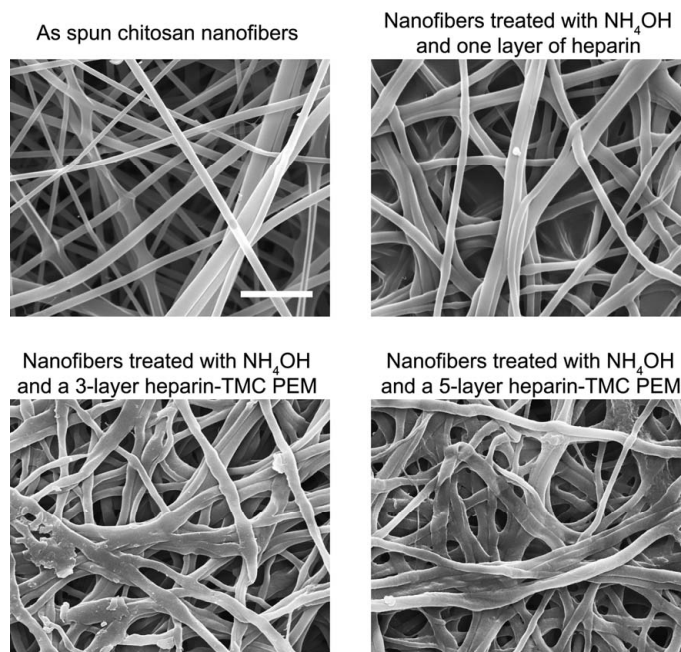
Figure 6.2 SEM micrographs of untreated chitosan nanofibers and nanofibers coated with heparin-TMC PEMs. Scale bar in the upper left image is 3 μm and applies to all four images.

The FT-IR spectrum of the as spun nanofibers shows amine stretching vibrations (3250 and 3400 cm^{-1}), protonated amine vibrations (1675 and 1530 cm^{-1}), a carboxylate stretch (1200 cm^{-1}, vertical line in Figure 6.3), and three absorption bands between 850 and

720 cm^{-1} (Figure 6.3). The carboxylate absorption and the three absorption bands in the lower wavenumber region are from bound TFA.[11] After ammonium hydroxide treatment, the protonated amine (1675 and 1530 cm^{-1}) peaks are reduced, and the intensity of the N-H stretching vibrations (3300 to 3450 cm^{-1}) is increased. The NH$_2$ scissors at 1590 cm^{-1} also appears after treatment. TFA removal is confirmed by loss of the carboxylate (1200 cm^{-1}, vertical line in Figure 6.3) absorption and the absorptions between 850 and 720 cm^{-1}.
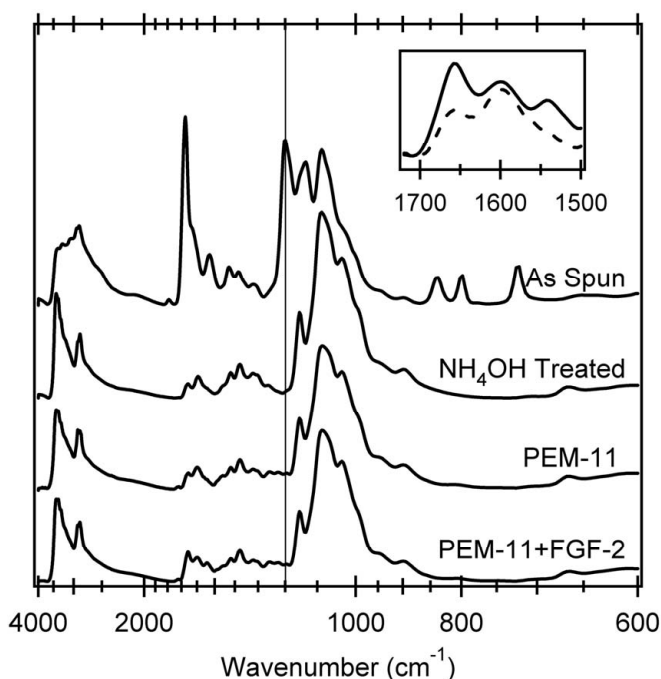
Figure 6.3 Transmission FT-IR spectra of chitosan nanofibers with different modifications. The absorption band at 1200 cm^{-1} is marked by the vertical line, for clarity. Inset shows spectra of 11-layer PEM-coated nanofibers with (solid line) and without (broken line) adsorbed FGF-2 in the region of the amide I (1650 cm^{-1}) and amide II (1550 cm^{-1}) absorption bands.

To further confirm addition of heparin to the nanofibers, ammonium hydroxide-treated and heparin-coated nanofibers were stained with alcian blue, which binds to sulfated glycosaminoglycans, such as heparin. After staining and rinsing, the nanofibers were, photographed and imaged by optical microscopy. Images of stained nanofibers are shown in Figure 6.4. Only the heparin-coated nanofibers bind the alcian blue, and the alcian blue staining is uniform, indicating effective coating of the nanofibers with heparin.

162
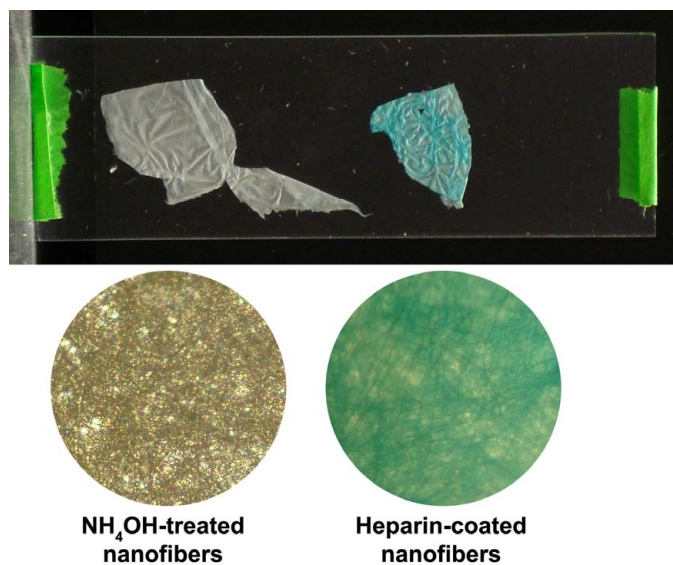
Figure 6.4 Ammonium hydroxide-treated and heparin-coated chitosan nanofibers stained with alcian blue. Only the heparin-coated nanofibers stain blue, confirming the presence of heparin.

Finally, FGF-2 was adsorbed to the PEM-coated nanofibers. The IR spectrum of PEM-coated FGF-2-treated nanofibers exhibits stronger amide I and II peaks located near 1650 (carbonyl stretch) and 1550 cm^{-1} (N-H in-plane bend), respectively, compared to the same nanofibers without FGF-2 (Figure 6.3 inset). Our previous work demonstrates the ability of heparin-chitosan PEMs to enhance FGF-2 delivery to mesenchymal stem cells.[2] In our previous work, FGF-2 adsorption was monitored using in situ surface plasmon resonance and polarization modulation infrared reflection absorption spectroscopy.[2] FGF-2 adsorbs in significant amounts on heparin- terminated PEMs.[2] This result suggests that PEM-modified nanofibers might also be used for the delivery of therapeutic growth factors for cell and tissue engineering.

6.5 Discussion

Sulfated glycosaminoglycans (GAGs) such as heparin are of particular interest as biomaterials because they are capable of binding and stabilizing important therapeutic growth factors.[1] However reports of electrospinning the sulfated GAGs are scarce in literature. Likely, they are difficult to electrospin because their low molecular weight and high charge density prevent sufficient entanglement formation, even at relatively high concentrations. Several reports in which heparin was electrospun as a blend with other natural and synthetic polymers can be found. Viswanathan et al. electrospun a blend of cellulose and heparin using room-temperature ionic liquids as the solvent.[14] They demonstrated that the heparin-containing microfibers could reduce coagulation time of human whole blood.[14] Heparin has also been electrospun in blends of poly(ε-caprolactone) and poly(L-lactide-co-ε-caprolactone),[15, 16] and attached to nanofibers via both covalent coupling and electrostatic adsorption.[17, 18] Casper et al. covalently bound heparin to collagen and gelatin microfibers to deliver FGF-2.[18] The methods developed here provide for the facile and reproducible functionalization of chitosan electrospun nanofibers with heparin-containing PEMs. We demonstrate that the amount of heparin on the surface can be tuned by altering the number of layers and that the heparin maintains its biochemical activity with respect to FGF-2 binding.

6.6 Conclusions

Electrospun chitosan nanofibers were successfully coated with PEMs using the polysaccharides heparin and *N,N,N*-trimethyl chitosan. PEM coating was confirmed with XPS and alcian staining. FGF-2 was successfully adsorbed on the PEM-coated nanofibers. This method will enable the aqueous modification of chitosan nanofibers with many types of bioactive moieties via the LbL assembly of PEMs. For example, this method could be further developed for the stabilization of therapeutic growth factors for delivery in vitro and in vivo.

6.7 Acknowledgement

6.8 References

1. S. Boddohi, M. J. Kipper, *Adv. Mater.* **2010,** 22, 2998.
2. J. Almodóvar, S. Bacon, J. Gogolski, J. D. Kisiday, M. J. Kipper, *Biomacromolecules* **2010,** 11, 2629 .
3. S. Boddohi, J. Almodóvar, H. Zhang, P. A. Johnson, M. J. Kipper, *Colloids Surf., B* **2010**, *77*, 60.
4. S. Boddohi, C. E. Killingsworth, M. J. Kipper, *Biomacromolecules* **2008**, *9*, 2021.
5. S. Boddohi, S. Yonemura, M. J. Kipper, *Polymer Preprints* **2009**, *50*, 331.
6. J. D. Schiffman, C. L. Schauer, *Biomacromolecules* **2007**, *8*, 2665.
7. J. D. Schiffman, C. L. Schauer, *Biomacromolecules* **2007**, *8*, 594.
8. D. de Britto, O. B. G. Assis, *Carbohydr. Polym.* **2007**, *69*, 305.
9. K. Ohkawa, D. I. Cha, H. Kim, A. Nishida, H. Yamamoto, *Macromol. Rapid Comm.* **2004**, *25*, 1600.
10. T. T. Ruckh, K. Kumar, M. J. Kipper, K. C. Popat, *Acta Biomater.* **2010**, *6*, 2949.
11. P. Sangsanoh, P. Supaphol, *Biomacromolecules* **2006**, *7*, 2710.
12. H. Makoto, I. Akira, O. Fumihiko, U. Makoto, *J. Appl. Polym. Sci.* **1992**, *45*, 1857.
13. C. Yao, X. S. Li, K. G. Neoh, Z. L. Shi, E. T. Kang, *Journal of Membrane Science* **2008**, *320*, 259.
14. G. Viswanathan, S. Murugesan, V. Pushparaj, O. Nalamasu, P. M. Ajayan, R. J. Linhardt, *Biomacromolecules* **2006**, *7*, 415.
15. E. Luong-Van, L. Grondahl, K. N. Chua, K. W. Leong, V. Nurcombe, S. M. Cool, *Biomaterials* **2006**, *27*, 2042.
16. I. K. Kwon, T. Matsuda, *Biomacromolecules* **2005**, *6*, 2096.
17. Y. Lu, H. L. Jiang, K. H. Tu, L. Q. Wang, *Acta Biomaterialia* **2009**, *5*, 1562.
18. C. L. Casper, W. D. Yang, M. C. Farach-Carson, J. F. Rabolt, *Biomacromolecules* **2007**, *8*, 1116.

Chapter 7

Controlled Released of Bioactive FGF-2 From Electrospun Chitosan Nanofibers Using Polysaccharide-Based Nanostructures

- Volpato F.Z., Almodóvar J., Erickson K., Popat K., Migliaresi C.; Kipper M.J., "Controlled release of bioactive FGF-2 from electrospun chitosan nanofibers using polysaccharide-based nanostructures", (In Preparation)

7.1 Abstract

Here we demonstrate the controlled release of the growth factor FGF-2 from electrospun chitosan nanofiber mats. FGF-2 is loaded onto heparin-chitosan polyelectrolyte complex nanoparticles (PCNs). These PCNs are then electrostatically adsorbed to chitosan nanofibers, and released from the nanofibers with zero-order kinetics over a period of 27 days. When the nanofibers are further modified with a single bilayer of polysaccharide-based polyelectrolyte multilayer (PEM, composed of *N,N,N*-trimethyl chitosan and heparin), the release is completely prevented, and the FGF-2/PCN complexes are retained on the fibers for the duration of the release experiment (27 days). The mitogenic activity of the FGF-2/PCN complexes is also evaluated, with respect to the proliferation of ovine bone-marrow derived mesenchymal stem cells (MSCs). FGF-2/PCN complexes exhibit mitogenic activity in a 4-day MSC proliferation experiment even after being incubated for 27 days at 37 °C in solution. Interestingly, when the FGF-2/PCN complexes are adsorbed to chitosan and coated with PEMs, the mitogenic activity of the FGF-2 steadily decreases with increasing incubation

time. This work demonstrates a new system for stabilizing and controlling the delivery of heparin-binding growth factors, using polysaccharide-based nanomaterials.

7.2 Introduction

In recent years growth factor therapy has become very attractive as a means to induce faster and "better" tissue growth.[1] Growth factors are involved in many signaling pathways that regulate healing, cell processes, and maintenance of healthy tissue. Growth factors, including members from the fibroblast growth factor (FGF) family, affect mesenchymal stem cell (MSC) attachment, migration, and differentiation. Specifically, FGF-2 is involved in osteogenesis,[2, 3] chondrogenesis[4] and angiogenesis.[5] However, over the time scales associated with these biological responses, growth factor delivery poses a challenge. When delivered with out protection they are susceptible to degradation. FGF-2, for example, has plasma half-life of 1.5 min.[7] A recent study investigated the release of growth factors from scaffolds for bone repair, and noticed that the bioactivity significantly decreases after only 24 hours of incubation.[6] Some biomaterials have been developed for the delivery of growth factors but fail to protect them from degradation. One study demonstrated controlled release of FGF-2 from ceramic materials but was degraded after the second day.[8] Growth factors delivered in solution are susceptible to proteolytic degradation as soon as they enter the body. Thus biomaterials that can protect growth factors from degradation have potential to vastly improve the efficiency and economics of growth factor-based therapies.

Sulfated glycosaminoglycans (GAGs), found in the extracellular matrix of mammalian tissues, are involved in the protection of growth factors. Heparin, in particular, has been implicated in the protection and modulation of FGF-2.[9] Heparin-bound FGF has a six fold increase in its plasma half life.[10] Thus sulfated GAGs, including heparin, are ideal for growth

factor delivery. Indeed, multiple studies have been performed for the delivery of FGF-2 using heparin-containing materials.[11-13] Recently, our lab demonstrated that heparin-containing polyelectrolyte multilayers (PEMs) enhance MSC response to adsorbed FGF-2.[13] MSCs displayed higher proliferation rates when cultured in heparin-terminated PEMs with adsorbed FGF-2 compared to FGF-2 delivered in solution at optimal doses.[13]

We have previously presented the deposition of PEM and their characterization on both chitosan electrospun nanofibers and flat surfaces.[14-16] In this work, we demonstrate a novel system, using polysaccharide-based materials, for the delivery of bioactive FGF-2. FGF-2 is loaded onto heparin/chitosan polyelectrolyte complex nanoparticles (PCNs) with heparin in excess. Electrospun chitosan nanofibers are then modified with FGF-2 containing PCNs or FGF-2 containing PCNs covered with a polyelectrolyte multilayer (*N,N,N*-trimethyl chitosan/heparin) bilayer. FGF-2 release is assayed for a period of 27 days through fluorescence readings. The bioactivity of the released FGF-2 is assessed by measuring proliferation of ovine bone marrow-derived mesenchymal stem cells.

7.3 Materials and Methods

7.3.1 Materials

Highly purified chitosan (80 kDa, 5% acetylated as determined by ^{1}H NMR, Protasan UP B 90/20) was supplied by NovaMatrix (Sandvika, Norway). Rhodamine-modified chitosan was prepared by dissolving 100 mg of chitosan in 10 mL of 0.1 M acetic acid, adding 10 mL of methanol to the solution, followed by the addition of 3.25 mL of 2 mg/mL rhodamine B isothiocyanate (Sigma; St Lois, MO) in methanol, and allowing the solution to react overnight. Rhodamine-modified chitosan was purified via dialysis, freeze dried, and stored at 4°C protected from light until use. Heparin sodium (from porcine intestinal mucosa, 12.5%

sulfur) was purchased from Celsus Laboratories (Cincinnati,OH). *N,N,N*-Trimethyl chitosan (TMC) was synthesized following a procedure described by de Britto and Assis.[17] Recombinant human basic fibroblast growth factor (FGF-2) 146 aa was purchased from R&D Systems (Minneapolis, MN). 5(6)-Carboxyfluorescein *N*-hydroxysuccinimide ester was purchased from Sigma-Aldrich (St. Lois, MO). Sodium bicarbonate and dimethyl sulfoxide (DMSO) were supplied by Fisher Scientific (Pittsburgh, PA). Trifluoracetic acid (TFA), dichloromethane (DCM), ammonium hydroxide, dimethyl sulfate, sodium hydroxide and sodium chloride were purchased from Acros Organics (Geel, Belgium). The following were purchased from HyClone (Logan, UT): fetal bovine serum (FBS), 0.25 % trypsin with EDTA, low glucose Dulbecco's modified Eagle's medium (D-MEM), minimum essential medium alpha (α-MEM) (supplemented with L-glutamine, ribonucleosides, and deoxyribonucleosides), and Dulbecco's phosphate buffered saline (DPBS) without Ca^{2+} and Mg^{2+}. The following were purchased from Gibco (Grand Island, NY): antibiotic-antimycotic (anti/anti), 1 M HEPES buffer solution, and Dulbecco's phosphate buffered saline with Ca^{2+} and Mg^{2+}. Calcein-AM in DMSO (4 mM) was purchased from Invitrogen (Eugene, OR). 4'6-Diamidino-2-phenylindole-2HCl (DAPI) was purchased from Thermo Fisher Scientific (Rockford, IL). Human fibronectin was purchased from BD Biosciences (Bedford, MA). All of the polymers, growth factor and solvents were used without further purification. All aqueous solutions were prepared using ultrapure, 18.2 MΩ, water (DI water).

7.3.2 Electrospinning process

The electrospinning apparatus consisted of a high-voltage (1–30kV) direct current power supply (GAMMA High Voltage Instruments, ES30P-10W/DAM); a syringe pump (Harvard Apparatus) set at 0.5 mL/h flux rate; and a rectangular brass collector, covered with

aluminum foil. The metal needle of the syringe, connected to the power supply, and the collection target were kept at a distance of 18 cm. Chitosan was dissolved in TFA:DCM (7:3) overnight at 7 wt%, at room temperature. The condition was selected after preliminary analysis of conductivity and viscosity as well as evaluations on the stability and homogeneity of the solutions. The optimized electrospinning voltage was defined as 18 kV. Although chitosan is an insoluble polycation in aqueous solution, the presence of residual solvent render the electrospun mats soluble in water. In order to eliminate residual solvent, a procedure for network stabilization has been developed by Almodóvar and Kipper.[14] Briefly, the mats were gently sandwiched between two filter papers (Whatman 41, 20 µm, ashless, Whatman, Inc, USA) and placed in a Büchner funnel. Then, a 5 M solution of ammonium hydroxide was slowly pulled through the filter papers under weak vacuum, maintaining the fibers integrity. Four liters of DI water were then flushed to removed trapped ammonium hydroxide and ensure that the pH of the fibers was near 7.

7.3.3 Polyelectrolyte complex nanoparticle (PCN) production

The production of PCN has been previously described by Boddohi et al.[18] The yield of particles, zeta potential, and hydrodynamic radius were determined as a function of charge mixing ratio. Briefly, pure polymer solutions (0.9 mg/mL for chitosan and 0.95 mg/mL for heparin) were prepared in 0.1M, pH 5.0 acetate buffer. At pH 5.0 chitosan has sufficient protonated amines to form complexes with sulfate and carboxylate groups of heparin. The solutions were filtered using 0.22 µm polyvinylidene fluoride syringe filters (PVDF, Fisher Scientific). PCNs were prepared at room temperature by a one-shot addition using heparin as the starting solution for the production of anionic particles. The ratio of 4:1 (heparin:chitosan, saccharide basis) was chosen taking into account the previous studies.[15]

171

Vigorous stirring for 3 h was maintained during the complex formation. After 3 h of stirring, the solution was allowed to settle overnight to remove aggregated particles. After settling, the solution containing dissolved PCNs was decanted, followed by centrifugation at $4500 \times g$ for 15 min to separate the particles from uncomplexed polymer using an Eppendorf 5804 centrifuge (Eppendorf, Westbury, NY). After centrifugation, the supernatant was disposed of, leaving behind only the particles. The particles were then resuspended in DI water. PCN diameter was measured using dynamic light scattering (DLS). DLS was performed using a DynaPro Titan (WyattTechnologies, Santa Barbara, CA) instrument using an 830 nm laser. All measurements consisted of 10 acquisitions, performed at a fixed angle of 90° at 25 °C.

7.3.4 Basic fibroblast growth factor (FGF-2) labeling

The supplied FGF-2 was dissolved in 0.1 M $NaHCO_3$ (pH 8) at a concentration of 25 µg/mL. The solution was vigorously stirred in an ice bath to avoid protein denaturation. The dye solution was prepared by the dissolution of 5(6)-carboxyfluorescein *N*-hydroxysuccinimidyl ester in DMSO at a concentration of 10 mg/mL. 10 µL of the dye solution was slowly added to 1 mL of protein solution and allowed to react for 4 hours with vigorous stirring in an ice bath. The unreacted dye was removed by the dialysis of the labeled-protein solution in PBS (pH 7.4) for 24 hours, using 3 kDa molecular weight cut-off (MWCO) dialysis cassettes (Slide-A-Lyzer, Thermo Scientific). A fluorescence microplate reader (FLUOstar Omega, BMG Labtech, Durham, NC) was used to confirm labeling of the FGF-2 and to determine the calibration curve used to quantify labeled FGF-2 in solution, with excitation and emission wavelengths of 485 and 520 nm, respectively.

7.3.5 Growth factor adsorption on PCNs

The labeled FGF-2 (FGF-2^{LB}) was adsorbed on the PCN surface exploiting the ability that FGF-2 has to bind sulfated glycosaminoglycans, such as heparin. A saturated solution of FGF-2^{LB} with a concentration of 600 ng/mg of PCN was prepared in order to allow most of the sulfate sites in heparin to bind to the FGF-2^{LB}. The solution was gently mixed for 30 minutes to allow the reaction. The unreacted FGF-2^{LB} was removed by the dialysis of the FGF-2^{LB}/PCN solution in DI water for 48 hours using 20 kDa MWCO dialysis cassettes (Slide-A-Lyzer, Thermo Scientific). The concentrated FGF-2^{LB}/PCN was diluted in DI water at the necessary concentrations depending on the experiment. FGF-2^{LB} adsorption on PCNs and entrapment efficiency was confirmed using the fluorescence microplate reader mentioned above.

7.3.6 Modification of nanofiber mats with PCNs and polyelectrolyte multilayers (PEM)

Chitosan nanofibers were modified with FGF-2^{LB}/PCN complexes and some samples were also subsequently modified with TMC-heparin PEMs (one bilayer). Modification of nanofibers was achieved using a procedure similar to the one used for stabilizing the mats. First, a 250 mL aqueous suspension of FGF-2^{LB}/PCN, at a concentration of 0.5 mg/mL, was slowly pulled through a 3 cm^2 sample of fibers sandwiched between filter papers, under weak vacuum. The FGF-2^{LB}/PCN complexes were electrostatically adsorbed on the chitosan nanofibers. Next, some of these samples were further modified with a single bilayer of TMC-heparin PEM. Briefly, TMC and heparin solutions with concentration of 0.01M (on a saccharide basis) were prepared in DI water and filtered using 0.22 μm PVDF syringe filters (Fisher Scientific). DI water was used as rinsing steps. 250 mL of each solution was pulled through the samples once, in the following sequence: (a) heparin, (b) water, (c) TMC and (d)

water. Almodóvar and Kipper have previously demonstrated the efficacy of this procedure for modifying chitosan nanofibers with polysaccharide-based PEMs.[14]

7.3.7 Morphology of the electrospun networks

Scanning electron microscopy (SEM) (Supra 40, Zeiss; JSM-6500F, Jeol) was used to evaluate the morphology of the produced networks. Preceding observation, the samples were gold sputtered. Chitosan nanofiber mats were imaged using SEM before and after NH_4OH treatment, after modification with FGF-2/PCN complexes, and after modification with PEMs. SEM was also conducted on samples after FGF-2 release experiments (described below).

7.3.8 Networks fluorescence characterization

Qualitative analysis of the modification of chitosan nanofibers was performed using confocal laser microscopy (A1, Nikon). Modification with FGF-2[LB]/PCN complexes was performed on a nanofiber mat made from rhodamine-modified chitosan. An image for the rhodamine fibers was obtained at λ ex 540 nm and λ em 625 nm. Afterwards, an image for the FGF-2[LB]/PCN was obtained at the same location and both images were converged into one. For all other experiments, unmodified chitosan was used, and the fluorescence of the FGF-2[LB] was observed at λ ex 492 nm and λ em 517 nm. The samples were imaged before and after the release experiments (described below) to assess the presence of FGF-2[LB]. Images were taken using a Zeiss LSM510 confocal microscope using a 63× and a 20× objective.

7.3.9 Release of PCN-FGF-2[LB] from nanofibers with and without PEM

Release of FGF-2[LB]/PCN complexes from nanofibers was determined by fluorescence spectroscopy of the supernatant. Samples (3 cm^2) were placed in a petri dish with 10 mL of

174

DI water and incubated at 37°C under continuous agitation (at ~10 rpm). At regular intervals, 300 μL of solution were collected, stored frozen, and a similar amount of fresh DI water was added to the release medium. At the end of the release study all samples were thawed and the concentration of FGF-2 in the supernatant was measured using the fluorescence microplate reader as described above. The fluorescence data was correlated to a calibration curve to report the amount of FGF-2^{LB} in solution. The cumulative mass of FGF-2^{LB} was determined by correcting for the sampling and supernatant replacement. The experimental conditions studied are summarized in Table 7.1. Each condition was studied in triplicate.

Table 7.1 Sample nomenclature for FGF-2 release kinetics experiments.

Sample Name	Condition
Fibers only	Fiber samples without PCNs or PEMs.
FGF-2/PCN	FGF-2^{LB}/PCN complexes adsorbed onto fibers
FGF-2/PCN+PEM	FGF-2^{LB}/PCN complexes adsorbed onto fibers further modified with one bi-layer of PEM

7.3.10 Harvest and culture expansion of ovine mesenchymal stem cells (MSCs)

MSCs were harvested and cultured following the methods by Almodóvar et al.[13] Briefly, bone marrow aspirates were obtained from female sheep (4-7 years old). Nucleated cells were separated from the bone marrow aspirate via centrifugation, and these cells were seeded on culture flasks. The non-adherent cells were removed and MSC colonies were allowed to develop for at least 7 days. The MSCs were then cryo preserved (in FBS with 5 % DMSO) in liquid nitrogen until further use.

7.3.11 Preservation of FGF-2 activity

The mitogenic activity of the FGF-2 was evaluated using MSCs. FGF-2 is a potent mitogen for ovine MSCs, when delivered at the appropriate concentration in solution. We have also previously shown that the mitogenic activity of FGF-2 can be enhanced when it is

delivered to ovine MSCs by incorporating it into heparin-containing PEMs.[13] To evaluate whether the FGF-2 activity is preserved under the conditions studied above, FGF-2/PCN complexes were incubated for 1, 9, 18 and 27 days at 37°C in DI water, both in solution and in TMC-heparin PEMs. Negative control conditions were also studied. For these negative control conditions, PCNs without FGF-2 were also incubated for 1, 9, 18 and 27 days, both in solution and in TMC-HEP PEMs. These conditions are summarized in Table 7.2. For these experiments unlabeled FGF-2 was used, to avoid any effects of the dye.

Table 7.2 Sample nomenclature for FGF-2 activity assay

Sample name	Condition
PCN	PCN were incubated for 1, 9, 18, or 27 days, and then were added to MSC cultures on fibronectin-coated TCPS.
FGF-2/PCN	FGF-2/PCN complexes were incubated for 1, 9, 18 or 27 days and then were added to MSC cultures on fibronectin-coated TCPS to evaluate the FGF-2 activity.
PCN+PEM	PCN adsorbed on chitosan-coated TCPS, further modified with one bilayer of PEM, were incubated for 1, 9, 18, or 27 days. Surfaces were then coated with fibronectin and MSCs were added after the incubation period.
FGF-2/PCN+PEM	FGF-2/PCN complexes adsorbed on chitosan-coated TCPS, further modified with one bilayer of PEM, were incubated for 1, 9, 18, or 27 days. Surfaces were then coated with fibronectin and MSCs were added after the incubation period to evaluate the FGF-2 activity.

Referring to the entries in Table 7.2, to prepare the PCN (and FGF-2/PCN) conditions, PCNs (and FGF-2/PCN complexes) were incubated at 37°C in DI water for either 1, 9, 18, or 27 days. To prepare PCN+PEM (and FGF-2/PCN+PEM) samples, chitosan was first adsorbed to the surfaces of 24-well tissue culture polystyrene (TCPS) plates. These chitosan-modified surfaces were then modified with PCNs (or FGF-2/PCN complexes), and coated with TMC-heparin PEMs (one bilayer), according to methods we have previously

described.[15] Eight of each type of sample were prepared and were incubated at 37°C in DI water for either 1, 9, 18, or 27 days (duplicate samples were prepared for each of four time points) under mild agitation.

MSC proliferation experiments were used to test the FGF-2 activity of these incubated samples. In all of these experiments, MSCs were cultured in the wells of 24-well TCPS plates, coated with fibronectin (from 10 μg/mL solutions). For the PCN and FGF-2/PCN conditions, PCN or FGF-2/PCN complexes that had been previously incubated for 1, 9, 18 or 27 days were added to the cultures (MSCs on fibronectin-coated TCPS) at a concentration equivalent to about 0.2 ng/mL FGF-2. This concentration is not near the optimally mitogenic dose determined from our previous work. However, it is hypothesized that the presence of heparin in the PCN will enhance FGF-2 activity and thus lower concentrations will be sufficient. For the PCN+PEM and the FGF-2/PCN+PEM samples, the fibronectin coating was applied on top of the previously incubated PEMs. For all experiments, MSCs were seeded at 7000 cells per cm^2. These cells were cultured for four days using low-serum media (α-MEM with 2.5 % FBS, 1 % anti/anti, 2.5 % HEPES 1 M) at 37°C and 5% CO_2. After the 4 days of culture the MSCs were stained with calcein, fixed with glutaraldehyde, and counter stained with DAPI.[13] The proliferation of untreated MSCs and MSCs exposed to uncomplexed FGF-2 in solution were also evaluated. For these experiments, MSCs were seeded at 7000 cells per cm^2 on fibronectin-coated TCPS, and cultured for 4 days at the same conditions as indicated above.

For each experiment, fluorescence microscopy images were obtained using an Olympus IX70 epifluorescence microscope (Center Valley, PA) equipped with a QImaging Micropublisher camera and a filter wheel, with the wide ultraviolet (WU) and narrow blue

(NB) filter for DAPI and calcein-AM, respectively. Images for cell counting were obtained using a 4× objective. Both green and blue channel images were collected from five fields of view from each well of the 24-well plates, representing approximately 25 % of the total surface area. These images were processed using the ImageJ 1.41o software (National Institutes of Health, USA) to count the nuclei (DAPI stained).

7.3.12 Statistical Analysis

All values were expressed as mean ± standard deviation. Comparisons between groups were performed via analysis of variance (ANOVA) models with Tukey's multiple comparison tests. Differences with $p < 0.05$ were considered statistically significant.

7.4 Results

7.4.1 Electrospinning of chitosan and modification of fibers with PCN and PEM

Chitosan was successfully electrospun from TFA/DCM. Scanning electron micrographs of the electrospun chitosan mats are shown in Figure 7.1 (A) before and (B) after NH_4OH treatment. The stabilization treatment modifies the fiber morphology in terms of homogeneity and fiber cross section. We speculate that these changes are related to the increase of local pH, due to the release of residual TFA. Despite these changes, the fiber mats maintain a high surface area and open porosity, allowing PCN adsorption. Figure 7.1 (C) shows a high-magnification SEM image of a fiber mat after NH_4OH treatment to show the smooth surface of the fibers.
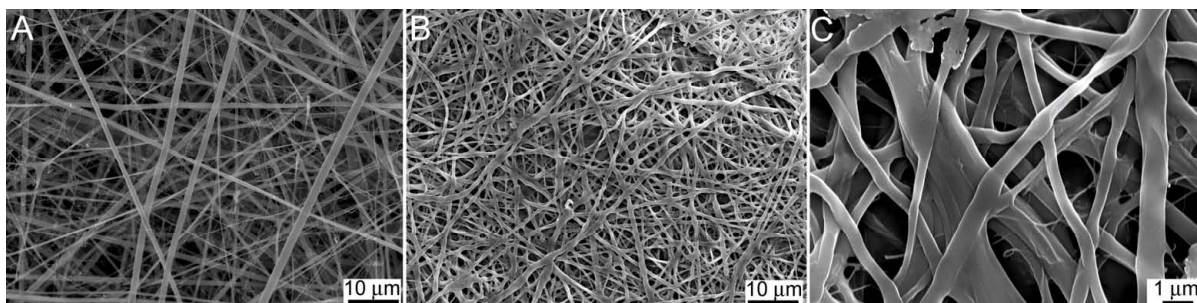
Figure 7.1 Mat morphology (A) as prepared and after NH$_4$OH treatment at (B) low and (C) high magnification.

PCN production and characterization has been previously performed in our lab.[18] DLS was performed before and after FGF-2^{LB} adsorption and radii of 270 and 302 nm were obtained for PCN and FGF-2^{LB}/PCN respectively. FGF-2^{LB}/PCN complexes were electrostatically adsorbed to the nanofiber mats. High-magnification scanning electron micrographs of the fiber surfaces are presented in Figure 7.2. The adsorbed FGF-2^{LB}/PCN complexes can be seen on the surfaces of the fibers in Figure 7.2 (A). These appear as small (< 100 nm diameter) circular features on the surfaces of the fibers. The apparent diameter of the complexes is smaller when they are adsorbed to the nanofibers and dried for SEM imaging, compared to the hydrodynamic radius that is observed by DLS when they are hydrated in aqueous solutions, as we have noted in previous reports.[15] After PEM deposition, these features are not visible in the SEM image shown in Figure 7.2 (B). We note in Figure 7.2 (A) that PCN are able to penetrate into the fiber mat, and are not restricted to fibers very near the surface of the mat. Figures 7.2 (C) and (D) show the fiber mats after 27 days of incubation at 37°C in DI water. Figure 7.2 (C) is a fiber mat modified with FGF-2^{LB}/PCN complexes, and Figure 7.2 (D) is a fiber mat modified with the complexes and one PEM bilayer. After incubation, the largest fibers (those with diameter > 1 μm) remain, and the fiber mats maintain their mechanical integrity,

179
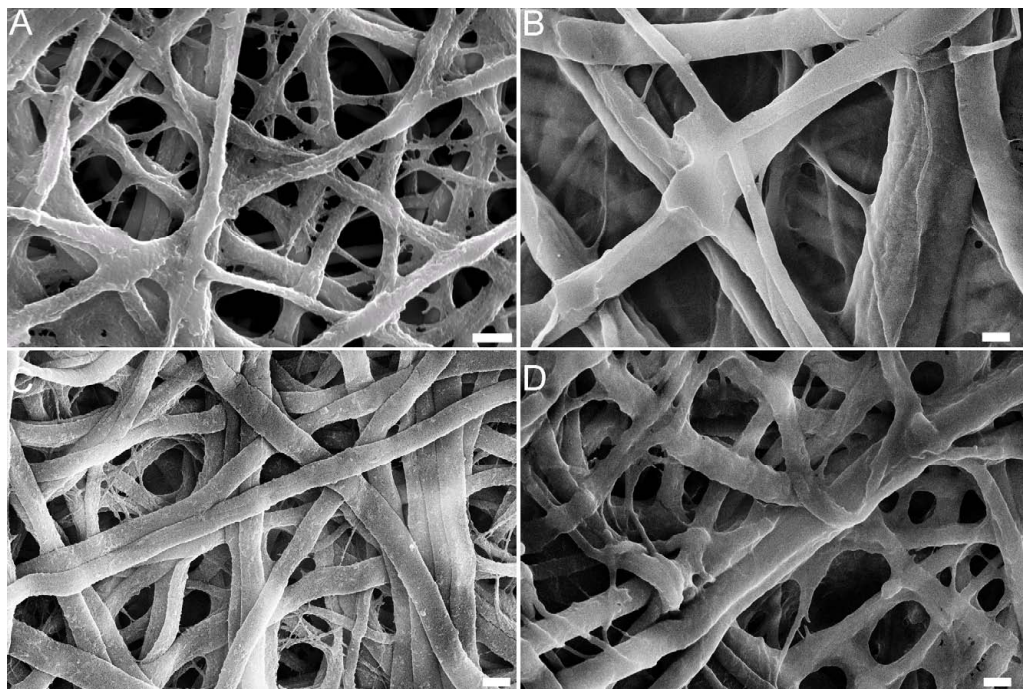
Figure 7.2 High magnification SEM images depicting fiber roughness before release experiments (A) PCN and (B) PCN+PEM, and after release experiments (C) PCN and (D) PCN+PEM. All scale bars are 1 μm.

Figure 7.3 shows a confocal micrograph of FGF-2^{LB}/PCN complexes adsorbed onto rhodamine-modified chitosan fibers. The FGF-2^{LB}/PCN complexes penetrate the fiber network and adsorb well on the fibers further confirming what was observed in the SEM images.
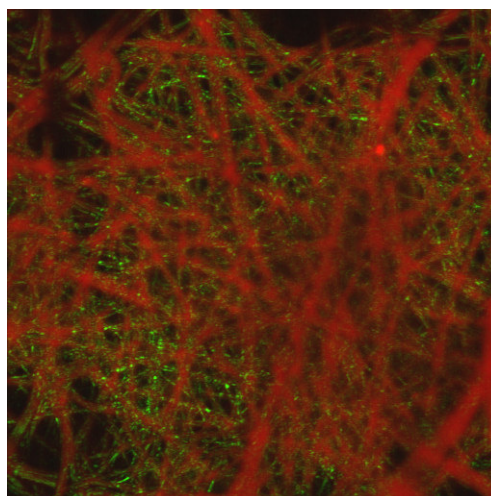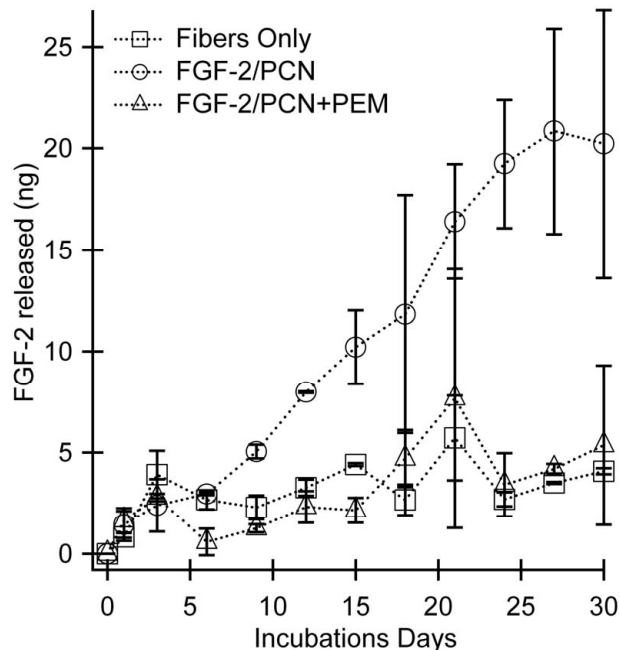

Figure 7.3 Confocal microscopy image of rhodamine-modified chitosan nanofiber mat with FGF-2^{LB}/PCN complexes adsorbed.

7.4.2 Release of FGF-2^{LB}/PCN complexes from chitosan nanofibers with and without PEM

To evaluate the release the FGF-2^{LB}/PCN, a 30-day release study was conducted. The cumulative release of FGF-2^{LB} from the nanofibers is shown in Figure 7.4. When the FGF-2^{LB}/PCN complexes are adsorbed to the nanofiber mats in the absence of additional PEM coatings, the complexes are released from the nanofibers over a course of at least 27 days, with apparent zero-order release kinetics. However, when a single bilayer of TMC-heparin PEM is adsorbed to on top of the PCN, there is no discernable release of FGF-2^{LB} into the supernatant. The presence of the heparin-containing PEM effectively traps the FGF-2^{LB}, preventing its release into solution. The PCN+PEM nanofibers did exhibit some non-zero fluorescence readings that tended to increase during the course of the release study, but these readings were no different than the readings from control samples containing no FGF-2^{LB}. Following the 30-day release study, the nanofiber mats were imaged by confocal microscopy to assess the presence of remaining FGF-2^{LB}. Figure 7.5 (A) shows a PCN-modified nanofiber mat after 27 days of release, and Figure 7.5 (B) shows a FGF-2/PCN+PEM-modified nanofiber mat after 27 days of release. These images confirm the release results shown in Figure 7.4. The image of the FGF-2/PCN sample without PEMs exhibits very little fluorescence after 27 days of incubation (Figure 7.5 (A)), indicating that the FGF-2^{LB} has been completely released into the supernatant. However, the nanofiber mat with the PEM (Figure 7.5 (B)) exhibits significant fluorescence after the 27-day incubation indicating that the PEM inhibits the release of the FGF-2^{LB} into solution.

Figure 7.4 Cumulative release of FGF-2^{LB} from the nanofibers.
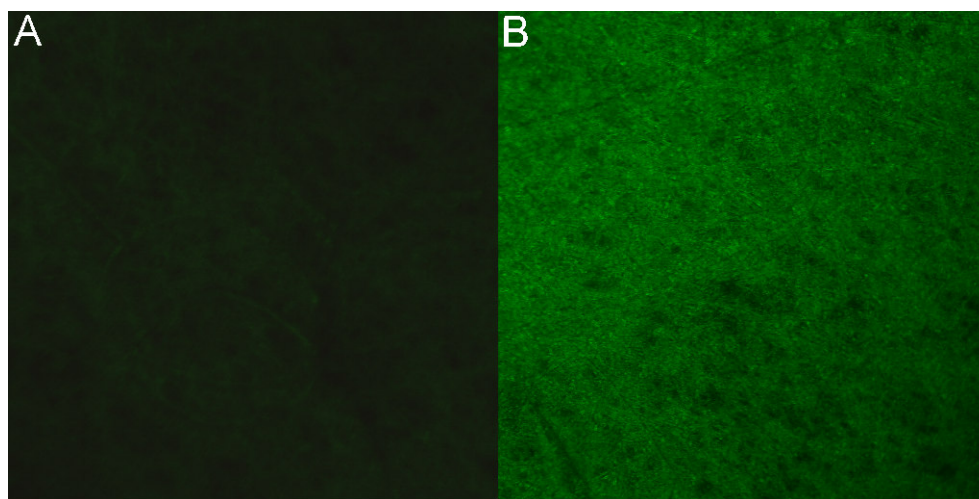
Figure 7.5 Confocal microscopy images of (A) FGF-2/PCN and (B) FGF-2/PCN+PEM modified nanofiber mats after 30-day release experiments.

7.4.3 Biological activity of released of FGF-2/PCN complexes

FGF-2^{LB} entrapment efficiency on PCN was calculated by measuring the fluorescence of FGF-2^{LB}/PCN samples shortly after production and purification through dialysis. A standard curve was prepared using known concentrations of FGF-2^{LB}. We find that the entrapment efficiency is 6.3 % yielding a final ratio of FGF-2^{LB}/PCN of 37.5 ng/mg. The concentration

to evaluate the bioactivity of FGF-2/PCN was calculated, using the above yield, to be 0.2 ng/mL. This concentration is below, but within a responsive dose, the optimal dose for ovine MSCs proliferation response in low-serum media.[13] However, we have previously seen that heparin enhances the activity of FGF-2 thus we believe that a lower concentration of FGF-2, in the presence of heparin, would have a strong activity. Indeed, as seen below, when evaluating the bioactivity of FGF-2 using ovine MSCs we observe that it is preserved, even at such a low dose.

The biological activity of the FGF-2/PCN complexes adsorbed in TMC-heparin PEMs and released from chitosan nanofibers was evaluated by measuring MSC proliferation. We have previously demonstrated that FGF-2 increases ovine MSCs proliferation under low-serum conditions, while the absence of FGF-2 under low-serum conditions hinders proliferation.[13] In the current work, to discern the biological activity of FGF-2/PCN complexes, MSCs were cultured on fibronectin-coated 24-well TCPS plates for 4 days, and the mitogenic activity was evaluated by counting cells in fluorescence micrographs.

Figure 7.6 shows cell density after 4 days of culture for all of the experimental conditions listed in Table 7.2. The cell density numbers are all normalized to MSCs grown on bare TCPS for 4 days. After 4 days the bare TCPS displayed a fairly low cell density (4×10^4 cells/cm^2) compared to the soluble FGF-2 condition, which had a cell density of 1.4×10^5 cells/cm^2.
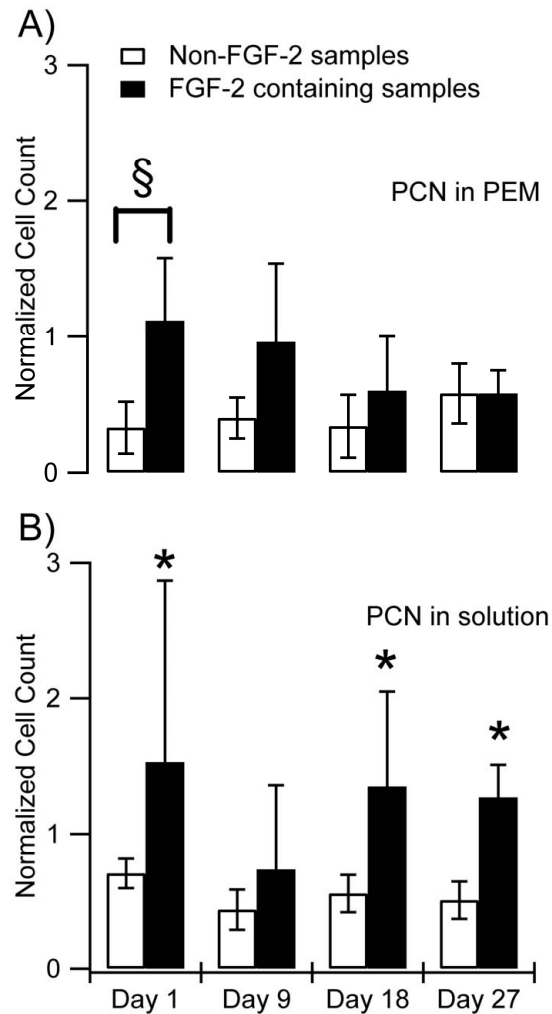
Figure 7.6 MSC density for all experimental conditions listed in Table 2. Cells were seeded at 7000 cells cm^{-2} and cultured in low-serum media for four days. Different days indicate the amount of days that the tested samples were incubated before cell seeding. (A) Cells cultured on TCPS coated with chitosan, PCNs (or FGF-2/PCN complexes), one bilayer of TMC-heparin PEM, and fibronectin. (B) Cells cultured on TCPS with PCN (or FGF-2/PCN complexes) delivered in solution. * in B indicates that this condition is statistically different from the other three conditions with the same incubation time. § in A indicates statistically different results for the two experiments at 1 day incubation time. ($n = 3$, $p < 0.05$)

Figure 7.7 shows representative epifluorescence micrographs of the MSCs cultured for 4 days under each of the experimental conditions, from which the cell density data in Figure 7.6 were determined. TCPS coated with PCN and PEMs showed poor cell growth in the absence of FGF-2, which is in agreement with our previous work, even though the PEMs are

coated with the adhesive protein fibronectin (Figure 7.6 (A)). FGF-2/PCN complexes beneath the PEM layer did increase the proliferation; however, this difference was only statistically significant for the PEMs incubated for 1 day. In fact, the difference in cell density between the cells cultured on PEMs and PEMs with FGF-2/PCN complexes is reduced as the incubation time increases. This suggests that either the FGF-2 in these samples is slowly being released from the PEMs (which was not discerned in the release experiments) or that the FGF-2 in these conditions is losing its biological activity as the incubation time is extended.
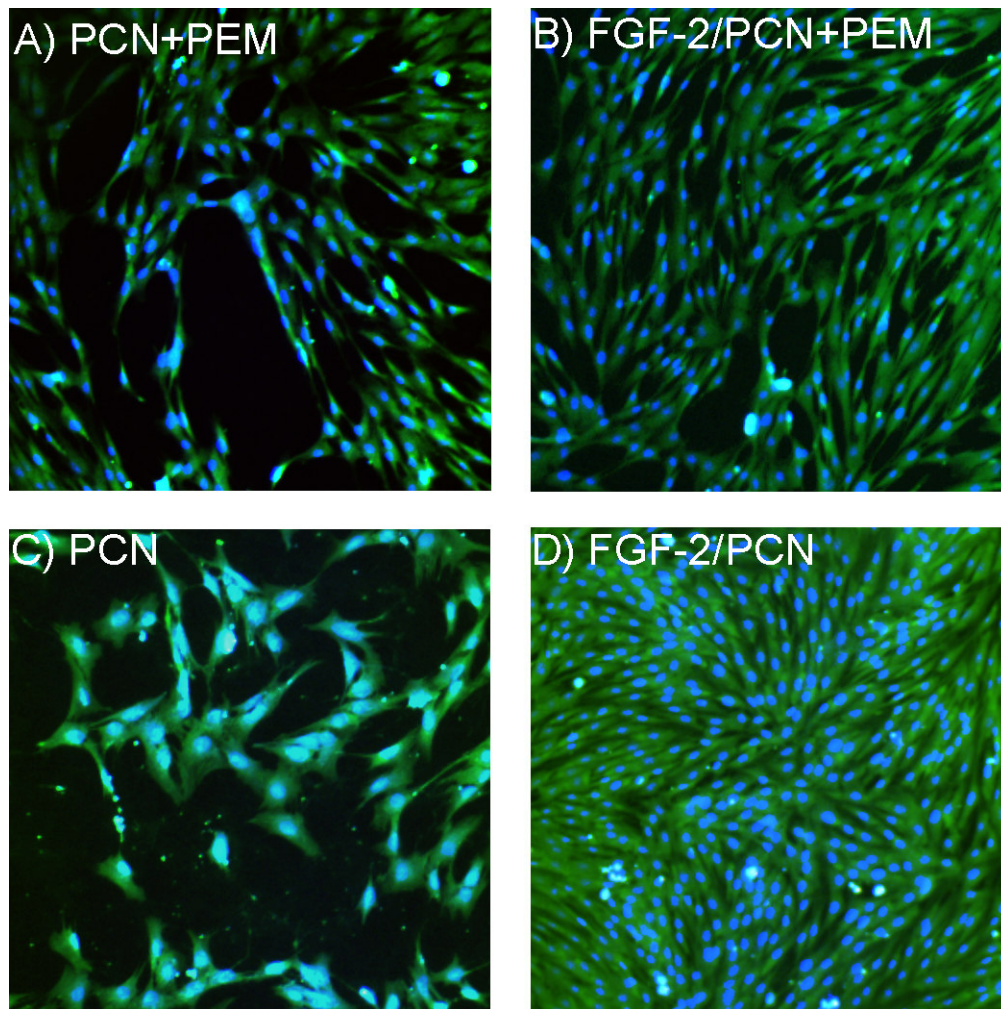
Figure 7.7 Representative fluorescence microscopy images of MSCs stained with DAPI (nuclei) and calcein-AM (cytoplasm). MSCs were cultured for 4 days on FGF-2/PEM+PCN or PEM+PCN or exposed to PCN or FGF-2/PCN all four which were incubated for 9 days.

When PCN (without FGF-2) are added to the MSC cultures, poor cell proliferation is observed (Figure 7.6 (B) and Figure 7.7 (C)). However, when FGF-2/PCN complexes are delivered in solution, FGF-2 retains its activity over 30 days (27 days of incubation + 4 days of cell culture) (Figure 7.6 (B)). The MSCs cultured at this condition are nearly confluent in the image shown in Figure 7.7 (D).

7.5 Discussion

PCN can be continuously released from nanofibers over a period of 27 days and they preserve the activity of the FGF-2. As demonstrated previously by McCaffrey et al.[19] and Damon et al.,[10] heparin was confirmed to protect FGF-2 from proteolytic and chemical inactivation. Figure 7.7 shows representative fluorescence microscopy images to complement the proliferation data in Figure 7.6. It confirms that confluent monolayers of MSCs are formed with the FGF-2/PCN. Higher cell density is observed on the FGF-2/PCN+PEM as compared to the similar sample without FGF-2. In fact, both images without FGF-2 show poor cell density. The large error bar on FGF-2/PCN data for day 1 is actually because one sample became so confluent that cells began to lift off. Cells that lifted from the surface were not counted.

Other biomaterials developed for the delivery of FGF-2 include sulfonated silk fibroin,[11] chitosan/hydroxyapatite scaffolds,[20] heparin conjugated fibrin gels,[12] and GAG containing polyelectrolyte multilayers.[13, 21] Some of these studies demonstrate control release of FGF-2 but do not attempt to investigate whether the protein retains its activity.[20] Some of these studies show very promising results in the delivery of FGF-2 by using sulfated synthetic or natural materials.[11-13, 21] Sulfated molecules, such as heparin and chondroitin sulfate, are very

186

promising as biomaterials because they protect growth factor from degradation and enhance their activity.

Indeed, we have demonstrated in this work that heparin-containing PCN preserve the activity of FGF-2 over a period of 27 days. Moreover, we can either release or retain FGF-2-containing nanoparticles from nanofibers by simply adding a bilayer of PEM. A similar study was also performed by Kim et al. using electrospun poly(ε–caprolactone)/gelatin blends containing heparin.[22] They were also able to release bioactive FGF-2 for a period of 30 days, using human umbilical vascular endothelial cells to test the bioactivity.[22] In the absence of heparin they noticed a burst release, and the FGF-2 quickly became inactive.[22] It is known that heparin protects FGF-2 from degradation, but its interactions with the growth factor also allows its controlled released. Recently, Chu et al. investigated FGF-2 release and bioactivity using polyelectrolyte complexes created from heparin and poly(ethylene argininylaspartate diglyceride).[23] Bioactivity was assessed by measuring the proliferation of human aortic endothelial cells.[23] They noticed a controlled release of bioactive FGF-2 for a period of 40 days.[23]

The exact mechanism of FGF-2[LB] release from the nanofibers is unknown. However, we assume that the complexes are desorbing from the fibers and dissolving into the supernatant, rather than that the FGF-2[LB] is dissolving. When FGF-2[LB] binds to heparin-containing PCNs by electrostatic interaction with the sulfate groups in heparin, the overall charge density of the PCN complexes should be reduced. This, in turn reduces the number of charged groups on the FGF-2[LB]/PCN complexes that can electrostatically bind to the amine groups presented on the surfaces of the chitosan nanofibers, permitting their slow dissolution into the supernatant.

7.6 Conclusion

In this work we have developed an electrospun system for delivery of basic fibroblast growth factor. Polysaccharide-based PCN were successfully applied to deliver and stabilize the FGF-2 from denaturation and inactivation up to 30 days of incubation. While, the distinctive properties of PEMs were exploited to inhibit the PCN/FGF-2 release. We demonstrated the tuning of the delivery system, where the growth factor can be released along 30 days if the PCN are in the surface or its conservation beneath the surface if PEM are deposited for longer than 30 days. The biological evaluation established that the FGF-2 is still active after 30 days of incubation, which contributed to a higher proliferation of MSCs. The ability of the system to load PCN independently and at different layers transforms the electrospun networks an important method that might be applied for the stabilization and delivery of therapeutic growth factors in vivo.

7.7 Acknowledgements

7.8 References

1. Li, R. H.; Wozney, J. M., *Trends in Biotechnology* **2001,** *19* (7), 255-265.
2. Hanada, K.; Dennis, J. E.; Caplan, A. I., *Journal of Bone and Mineral Research* **1997,** *12* (10), 1606-1614.
3. Lee, J. Y.; Choo, J. E.; Choi, Y. S.; Lee, K. Y.; Min, D. S.; Pi, S. H.; Seol, Y. J.; Lee, S. J.; Jo, I. H.; Chung, C. P.; Park, Y. J., *Journal of Biomedical Materials Research Part A* **2007,** *83A* (4), 970-979.
4. Vincent, T.; Hermansson, M.; Bolton, M.; Wait, R.; Saklatvala, J., *Proceedings of the National Academy of Sciences of the United States of America* **2002,** *99* (12), 8259-8264.

5. Zamora, P. O.; Tsang, R.; Pena, L. A.; Osaki, S.; Som, P., *Bioconjugate Chemistry* **2002,** *13* (5), 920-926.

6. Ziegler, J.; Anger, D.; Krummenauer, F.; Breitig, D.; Fickert, S.; Guenther, K. P., *Journal of Biomedical Materials Research Part A* **2008,** *86A* (1), 89-97.

7. Tessmar, J. K.; Gopferich, A. M., *Advanced Drug Delivery Reviews* **2007,** *59* (4-5), 274-291.

8. Ziegler, J.; Mayr-Wohlfart, U.; Kessler, S.; Breitig, D.; Gunther, K. P., *Journal of Biomedical Materials Research* **2002,** *59* (3), 422-428.

9. Salmivirta, M.; Lidholt, K.; Lindahl, U., *Faseb Journal* **1996,** *10* (11), 1270-1279.

10. Damon, D. H.; Lobb, R. R.; Damore, P. A.; Wagner, J. A., *Journal of Cellular Physiology* **1989,** *138* (2), 221-226.

11. Wenk, E.; Murphy, A. R.; Kaplan, D. L.; Meinel, L.; Merkle, H. P.; Uebersax, L., *Biomaterials* **2010,** *31* (6), 1403-1413.

12. Jeon, O.; Kang, S. W.; Lim, H. W.; Chung, J. H.; Kim, B. S., *Biomaterials* **2006,** *27* (8), 1598-1607.

13. Almodóvar, J.; Bacon, S.; Gogolski, J.; Kisiday, J. D.; Kipper, M. J., *Biomacromolecules* **2010,** *11* (10), 2629-2639.

14. Almodóvar, J.; Kipper, M. J., *Macromolecular Bioscience* **2011,** *11* (1), 72-76.

15. Boddohi, S.; Almodóvar, J.; Zhang, H.; Johnson, P. A.; Kipper, M. J., *Colloids and Surfaces B-Biointerfaces* **2010,** *77* (1), 60-68.

16. Boddohi, S.; Killingsworth, C. E.; Kipper, M. J., *Biomacromolecules* **2008,** *9* (7), 2021-2028.

17. de Britto, D.; Assis, O. B. G., *Carbohydrate Polymers* **2007,** *69* (2), 305-310.

18. Boddohi, S.; Moore, N.; Johnson, P. A.; Kipper, M. J., *Biomacromolecules* **2009,** *10* (6), 1402-1409.

19. McCaffrey, T. A.; Falcone, D. J.; Du, B. H., *Journal of Cellular Physiology* **1992,** *152* (2), 430-440.

20. Tigli, R. S.; Akman, A. C.; Gumusderelioglu, M.; Nohutcu, R. M., *Journal of Biomaterials Science-Polymer Edition* **2009,** *20* (13), 1899-1914.

21. Macdonald, M. L.; Rodriguez, N. M.; Shah, N. J.; Hammond, P. T., *Biomacromolecules* **2010,** *11* (8), 2053-2059.

22. Kim, M. S.; Shin, Y. M.; Lee, J. H.; Kim, S. I.; Nam, Y. S.; Shin, C. S.; Shin, H., *Macromolecular Bioscience* **2011,** *11* (1), 122-130.

23. Chu, H. H.; Johnson, N. R.; Mason, N. S.; Wang, Y. D., *Journal of Controlled Release* **2011,** *150* (2), 157-163.

Chapter 8

Osteogenic Ovine and Equine Mesenchymal Stem Cell

Differentiation on Electrospun Chitosan Nanofibers With and

Without Dexamethasone

Portions of this chapter appear in the following:
- Samantha Bacon, <u>Jorge Almodóvar</u>, John D. Kisiday, Matt J. Kipper; "Osteogenic Ovine and Equine Mesenchymal Stem Cells Differentiation on Electrospun Chitosan Nanofibers With and Without Dexamethasone", Colorado State University Honors Thesis (Fort Collins, CO), May 2011

8.1 Abstract

Both chemical and topographical cues have been shown to affect bone marrow-derived mesenchymal stem cells (MSC) differentiation. Moreover, MSC differentiation also behaves differently depending on the species from which bone marrow is harvested. In this study we investigate the effect on osteogenic differentiation of MSCs seeded on electrospun chitosan nanofibers and flat tissue-culture polystyrene. MSCs were obtained from both equine (eMSCs) and ovine (oMSCs) bone marrow, and parallel experiments were performed. The effect of dexamethasone on osteogenic differentiation was also investigated. Adherence of ovine MSCs to the nanofibers was investigated after 8 days by fluorescence and scanning electron microscopy (SEM). Alkaline phosphatase (ALP) activity was measured for oMSCs after 10, 20 and 30 days while eMSCs were tested after 6, 12, and 18 days for osteogenic differentiation. Calcium and phosphate deposition were investigated using energy-dispersive

190

X-ray spectroscopy (EDX) and alizarin red staining. We find that we can successfully grow and maintain both eMSCs and oMSCs on electrospun chitosan nanofibers. ALP production is higher for MSCs (both equine and ovine) seeded on nanofibers than TCPS, even in the absence of dexamethasone. However, eMSCs exhibit almost 400 times more ALP than oMSCs. Both eMSCs and oMSCs exhibit calcium deposition on both TCPS and nanofibers.

8.2 Introduction

The ability of mesenchymal stem cells (MSCs) to differentiate towards different lineages makes them attractive for tissue engineering applications. Bone marrow-derived MSCs have been demonstrated to differentiate into bone, cartilage, muscle, fat, marrow, and tendon cells as well as other connective tissues.[1, 2] Cell differentiation has been shown to be affected by soluble cues, scaffold material and properties, and external physical cues.[3] Properties of scaffolds which affect differentiation include, porosity, stiffness, and the size of 2-D and 3-D surface and chemical features.[3] Thus, biomaterials engineers have to take into consideration all of these properties when designing scaffolds for regenerative medicine. An ideal scaffold for tissue engineering would be one that resembles native tissue or tissue components such as the extracellular matrix (ECM). Native ECM is generally composed of multiple proteins and polysaccharides which are hierarchically organized in dimensions spanning from the nano- to macro-scale. One technique widely used to create ECM mimetic scaffolds is electrospinning.

In recent years, electrospinning has been become a popular technique for creating nanostructured scaffolds for tissue engineering.[4] The technique consists of a syringe filled with a polymer solution connected to a pump and a power supply. A polymer solution is dispensed through a capillary and a high voltage is applied between the capillary tip and a

grounded collector.[4] The solvent evaporates as the polymer jet travels in air, following the electric field path, and it is eventually deposited in a grounded collector. Electrospun nanofibers have been created for mammalian cell growth using both naturally derived polymers[5-7] and synthetic polymers.[8-11] Badami et al. investigated the effect of fiber diameter on MC3T3-E1 osteoprgenitor cells spreading, proliferation, and differentiation on electrospun poly(lactic acid) substrates.[7] They observed that cell density increases with fiber diameter (between 0.14-2.1 μm) but it did not have a strong effect in differentiation.[7] Christopherson et al. also investigated the effect on fiber diameter on rat neural stem cell differentiation and proliferation on electrospun polyethersulfone.[11] They noticed that differentiation was heavily influenced by fiber diameter; small fibers (283 nm) showed an increase in differentiation compared to large (749 nm) fibers.[11] Mammalian cell proliferation seems to be enhanced when cultured on nanofibers versus flat surfaces.[7, 9, 11] In some instances, MSCs show higher differentiation activity on nanofibers versus flat surfaces.[9, 11] Electrospun scaffolds can also be use to deliver soluble differentiation cues, such as dexamethasone.[10] Electrospun scaffolds are promising as ECM mimetic materials, and polysaccharide-based electrospun scaffolds might provide additional features (e.g. chemistry) that mimic native ECM.

Electrospining of chitosan has been difficult due to its limited solubility in organic solvents and the high viscosity of aqueous solutions, which are above the necessary electrospinning concentration.[12] Nonetheless, chitosan has been successfully electrospun in our lab[13] and in others[14] using a mixture of trifluoroacetic acid and dichloromethane (70:30 v/v). There is a lack of literature of mammalian cell culture on electrospun chitosan nanofibers. Sangsanoh et al. investigated the biocompatibility of solvent-cast chitosan and

electrospun chitosan nanofibers using Schwann, osteoblast, keratinocyte and fibroblast cells.[5] Electrospun and solvent-cast chitosan supported the viability of keratinocytes and Schwann cells while it did not support the viability of osteoblasts and fibroblasts.[5] Duan et al. created hybrid poly(lactic-*co*-glycolic acid) (PLGA) chitosan nanofibers by electrospinning solutions of each polymer onto the same collector.[15] They noticed that the viability of human embryo skin fibroblast increases with the addition of chitosan compared to pure PLGA.[15]

While many studies in the literature have investigated the osteogenic differentiation of various species of bone marrow-derived MSCs including human, equine, and rat, few studies have attempted to characterize the differentiation of ovine MSCs (oMSCs) into osteoprogenitor cells in vitro. The use of oMSCs is potentially valuable for the orthopedic tissue engineering field because of the similarities in a sheep's weight bearing, anatomy, and size to those of a human.[16] Large mammals, including sheep and horses, are widely use in a clinical setting to evaluate possible orthopedic implants.[17]

In this work, the osteogenic differentiation potential of both ovine and equine MSCs will be evaluated using tissue-culture polystyrene (TCPS) and electrospun chitosan nanofibers. To investigate wether the nanoscale features of electrospun chitosan are sufficient to induce differentiation, conditions will be investigated with and without the soluble cue dexamethasone. Cell viability will be assessed using fluorescence and scanning electron microscopy. Osteogenic differentiation will be evaluated by measuring alkaline phosphatase (ALP) activity and calcium mineralization using both alizarin red and energy-dispersive X-ray spectroscopy. This work will expand the literature on ovine MSCs characterization in vitro.

8.3 Experimental Section

8.3.1 Materials

The following were purchased from HyClone (Logan, UT): fetal bovine serum (FBS), 0.25% trypsin with EDTA, low-glucose Dulbecco's modified Eagle's medium (D-MEM-LG), high-glucose Dulbecco's Eagle's medium (D-MEM-HG), minimum essential medium alpha (α MEM; supplemented with L-glutamine, ribonucleosides, and deoxyribonucleosides), and Dulbecco's phosphate buffered saline (DPBS) without Ca^{2+} and Mg^{2+}. The following were purchased from Gibco (Grand Island, NY): antibiotic-antimycotic (anti/anti), 1 M HEPES buffer solution, and Dulbecco's phosphate buffered saline with Ca^{2+} and Mg^{2+}. Four mM calcein-AM in dimethyl sulfoxide (DMSO) was purchased from Invitrogen (Eugene, OR). Bicinchoninic acid (BCA) total protein assay and 4'6-diamidino-2-phenylindole•2HCl (DAPI) were purchased from Thermo-Scientific (Rockford, Il). Chitosan (poly(β-(1,4)-D-glucosamine-co-N-acetyl-D-glucosamine); 5% acetylated, determined by ^{1}H NMR) was purchased from Novamatrix (Sandvika, Norway). Recombinant human FGF basic (FGF-2) 146 aa was purchased from R&D Systems (Minneapolis, MN). Human fibronectin was purchased from BD Biosciences (Bedford, MA). DMSO was purchased from Fisher Scientific (Pittsburgh, PA). Glutaraldehyde, ethanol (200 proof, 99.5%), dichloromethane (DCM), trifluoroacetic acid (TFA) and hexamethyldisilazane (HDMS) were purchased from Acros Organics (Geel, Belgium). Ammonium Hydroxide, L-ascorbic acid, alizarin red, β-glycerol phosphate disodium salt pentahydrate and dexamethasone were purchased from Sigma-Aldrich (St. Louis, MO). Vectashield mounting medium for fluorescence with DAPI was purchased from Vector Laboratories, Inc. (Burlingame, CA). Alkaline phosphatase (ALP) assay was purchased from AnaSpec-Eurogentec Group (Freemont, CA). A Millipore

194

Synthesis water purification unit (Millipore, Billerica, MA) was used to obtain ultrapure, 18.2 MΩ water (DI water), used for making all protein solutions.

8.3.2 Electrospun chitosan nanofiber fabrication

Chitosan was electrospun at 1.11 kV/cm from a 7% w/v solution in TFA/DCM (70:30 by volume) following the previously published method from our lab.[13] The prepared solution was placed in a 5 mL glass syringe with a 20-gauge blunt-tip catheter connected to a syringe pump. A flow rate of 1 mL/hr was initially used, but after fine tuning a 0.25 mL/hr flow rate was found to produce better, constant fiber mats. The fibers were collected on aluminum foil surrounding a copper plate placed approximately 18 cm perpendicularly from the end of the catheter tip for approximately 6 nonconsecutive hours until the desired fiber thickness was achieved upon gross examination.

8.3.3 Mesenchymal stem cell isolation and proliferation

Ovine MCSs (oMSCs) were harvested and isolated following the procedure found in reference.[18] Briefly, bone marrow aspirates were obtained from the iliac crest of euthanized 4-year old female sheep. The MSCs were isolated from the bone marrow by centrifugation, culture-expanded for at least 8 days and cryogenically frozen in freezing media (95% FBS, 5% DMSO) in a Mr. Frosty (Fisher) at -80° C, and then stored in liquid nitrogen until further use. After thawing for use, the cells were seeded in ovine expansion media (α-MEM with 10% FBS, 2.5% HEPES 1M, and 1% anti/anti) at 10000 cells/cm^2 in tissue culture flasks and reseeded every 2 days (at approximately 80% confluence) until enough cells were available for experimentation. EMSCs were donated by Dr. John Kisiday from the Department of Clinical Sciences at Colorado State University. After arrival, the cells were cryogenically frozen and stored in liquid nitrogen following the same procedure used for oMSCs. After

thawing for use, the eMSCs were seeded in equine expansion media (α-MEM with 10% FBS, 2.5% HEPES 1M, 1% anti/anti, and 4 ng/mL FGF-2). The media was changed every 2 days until enough cells were present for experimentation.

8.3.4 Nanofibers preparation for MSCs

The chitosan nanofibers were neutralized with 5M ammonium hydroxide to remove the excess TFA left from the fabrication process following the procedure described by Almodóvar and Kipper.[13] NH_4OH solution was pulled through the fibers sandwiched between two Whatman #2 filter papers by applying a weak vacuum using a Büchner funnel. The NH_4OH was removed by filtration of 2 L of diH_2O until the nanofibers reached the pH of the water. The nanofibers were sterilized by either exposing them to UV light for 30 minutes or soaking in 70% ethanol for 15 minutes followed by soaking in PBS for 10, 5 and 1 minute progressively. Preliminary investigations showed that UV decreases the integrity of the fibers, thus ethanol sterilization was used for all MSCs experiments. The fibers were then treated with fibronectin (FN) by allowing a 10 µg/mL solution absorb to the fibers for 1 hour followed by a PBS rinse. Sterile fibers containing FN were stored at 4°C until further use. Immediately before use, the fibers were cut into 8 mm diameter circles with a biopsy punch. To seed MSCs on the nanofibers, the 8 mm circle of fibers was placed in a hydrophobic petri dish to discourage the MSCs from adhering to the wrong surface. Media (no more than 50 µL) containing the desired cell concentration was then dropped onto the fibers and left to absorb for 30 minutes at room temperature. To ensure the cells did not dry out during the absorption process, about 25 µL of media was added as needed. After the 30 minute period the nanofibers containing MSCs were carefully transferred to a well of a 24-well plate containing the appropriate media using sterile tweezers.

8.3.5 MSCs response to chitosan nanofibers

OMSCs proliferated on nanofibers for 8 days in expansion media with media changes every 2 days. As a control, oMSCs were also grown on flat TCPS concurrently. To determine the cellular response to the fibers, the fibers containing cells were examined with fluorescence and scanning electron microscopy (SEM). Samples were prepared for fluorescence microscopy by staining live cells using calcein-AM (2 µg/mL) for 50 minutes at 37°C. The cells were then fixed using a 2% glutaraldehyde solution in DPBS with Ca^{2+} and Mg^{2+} for 40 minutes at 4°C, followed by nuclei counter staining using either DAPI in DPBS (1 µg/mL) with Ca^{2+} and Mg^{2+} for 15 minutes at room temperature or DAPI in Vectashield mounting medium. Samples for SEM were dehydrated by soaking them progressively in 30%, 50%, 70% and 100% ethanol (200 proof) in water in 10 minute intervals, followed by a 10-minute soak in HMDS. The samples were then dried and stored in a desiccator until further use. For SEM imaging, the nanofibers were mounted on an aluminum stub using double-sided copper tape and grounded using colloidal graphite. The samples were then coated with 10 nm of gold or graphite and visualized using a JSM-6500F JEOL (Tokyo, Japan) SEM.

8.3.6 MSCs osteogenic differentiation design of experiments

Because few previous studies have investigated or characterized the differentiation of oMSCs, several culture conditions were preliminarily investigated (Table 8.1). First we began by seeding cells at concentrations of 10000, 20000, 30000 and 40000 cells/cm^2 in α-MEM osteogenic differentiation media (α-MEM media, 10% FBS, 1% anti-anti, 2.5% HEPES, 10^{-8} M dexamethasone, 50 mM ascorbic acid, and 8 mM β-glycerol phosphate) for 15 days. Subsequent studies used much lower concentrations including 500, 1000, 2000,

4000, 6000, 8000 and 10000 cells/cm^2 in α-MEM and low-glucose D-MEM osteogenic differentiation media for 21-28 days. On all initial studies the oMSCs became too confluent in osteogenic media and they began to lift off the flat surfaces. The final differentiation study involved oMSCs seeded at 1000 cells/cm^2 on both fibers and flat TCPS for 10, 20 and 30 days. While one set of samples was placed in high-glucose D-MEM osteogenic differentiation media with dexamethasone, the other set was placed in the same media excluding dexamethasone to investigate the differentiation potential of the fibers alone. EMSCs were also investigated concurrently at 20,000 cells/cm^2 with the same media and scaffold conditions for 6, 12 and 18 days as a comparison since equine differentiation has been better characterized. Duplicates were made for each condition.

Table 8.1. Preliminary investigations on oMSCs osteogenic differentiation

Study	Media‡	Surface	Dexamethasone (10^{-8} M)	Days of Culture	Cell Density (cells/cm^2)	Results
1	α-MEM	Nanofibers & TCPS	All Samples	15	10000, 20000, 30000, 40000	oMSCs became too confluent and started to lift off the flat surfaces.
2	α-MEM	Nanofibers & TCPS	All Samples	21-28	500, 1000, 2000, 4000, 6000, 10000	oMSCs were still becoming too confluent. Some ALP activity is noted.
3	α-MEM & D-MEM-LG	TCPS	All Samples TCPS	24	500, 1000, 2000	oMSCs were still becoming too confluent. Some alizarin red staining is noted.
4	D-MEM-HG	Nanofibers & TCPS	Some Samples	10, 20, 30	1000	See results section bellow (8.4)

‡All media contained: 10% FBS, 1% Anti/Anti, 2.5% Hepes, 50 mM Ascorbic Acid, and 8mM β-glycerol phosphate

*8.3.7 Detection of MSCs osteogenic differentiation*

Alizarin red staining was used on samples on TCPS to detect extracellular calcium. The MSCs were fixed with 2% glutaraldehyde in water for 40 minutes at 4°C. After rinsing, 500 µL of alizarin red (2% w/v in water, pH 4.2 adjusted with NaOH and HCl) was added to

each sample and incubated at room temperature for 30 minutes then rinsed with DPBS without Ca^{2+} and Mg^{2+}. This method was not used for samples on fibers because the negative control stained red, indicating the fibers themselves stain for alizarin and not just the deposited calcium. Both flat samples and samples with nanofibers were tested for alkaline phosphatase activity using an ALP colorimetric assay kit following the manufacturer's protocol. Briefly, MSCs on flat surfaces were scratched off while nanofibers samples were manually homogenized. The MSCs were then incubated in buffer containing triton X-100 for 30 minutes to lyse them. The lysate was recuperated via centrifugation, and 50 μL of lysate was added to each well of a 96-well plate. 50 μL of *p*-nitrophenyl phosphate was added to each sample and the plate was incubated at 36ºC reacting for a period of 30 minutes. Total protein content was also measured using a BCA assay, by exposing 25 μL of lysate to 200 μL of the BCA reagents as directed by the manufacturer and incubating at 36ºC and reacting for 30 minutes. An ALP standard curve was performed using known concentrations of calf intestine ALP. A BCA standard curve was performed using known concentrations of bovine serum albumin. The buffers for both assays were ensured to be the same in order to avoid deviations from different buffers. After the reaction period, the optical densities for both ALP (405 nm) and BCA (570 nm) were measured using a spectrophotometer (FLUOstar Omega, BMG Labtech, Durham,NC). Duplicate readings were performed for each of the duplicate samples (total of 4 readings per condition). Amounts of ALP were normalized to total protein content in order to avoid difference in readings due to differences in cell number. Calcium and phosphate deposition was measured using energy-dispersive X-ray spectroscopy (EDX). Samples for EDX were coated using carbon in order to avoid the overlapping peaks of phosphorus and gold.

8.4. Results

8.4.1 Chitosan nanofiber scaffold fabrication and preparation

Chitosan nanofibers were successfully electrospun until they formed a consistent layer of approximately 50 µm thick (Figure 8.1 (A)). Neutralization of the nanofibers resulted in a slight change of fiber morphology as previously seen.[13] However, there are enough pores and fibers to allow MSCs infiltration (Figure 8.2 (B)). As part of this study, a technique needed to be found to effectively create a sterilized environment for the MSCs without disrupting the integrity of the fibers. Two sterilization techniques were tested, exposure to UV light for 30 minutes and exposure to a solution of 70 % ethanol in water for 15 minutes followed by rinsing using sterile PBS. SEM micrographs showed that fibers treated with UV light for 30 minutes appeared to have melted losing their porosity. However, the nanofibers treated with 70 % ethanol were comparable to the ammonium hydroxide treated nanofibers (Figures 8.1 (B) and (C)) in terms of porosity and fiber integrity. Thus, ethanol treatment was used to sterilize the fibers for all in vitro experiments.
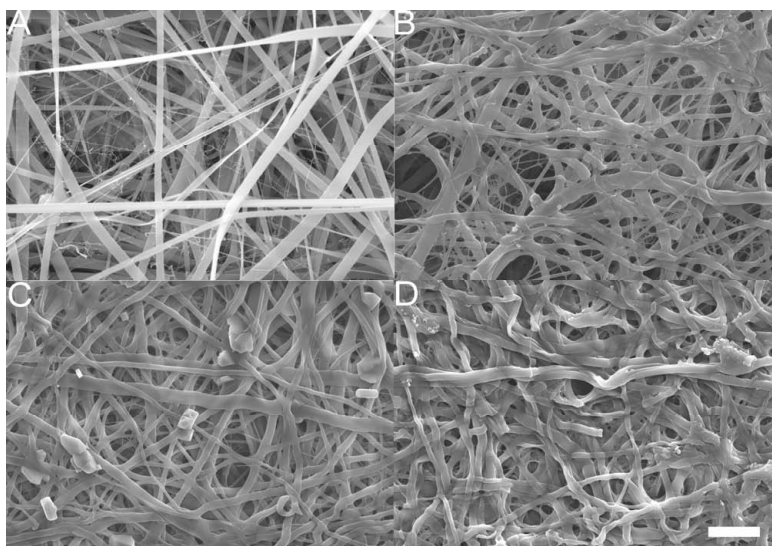
Figure 8.1 SEM micrographs of: (A) As spun chitosan nanofibers. (B) NH$_4$OH treated chitosan nanofibers. (C) NH$_4$OH treated chitosan nanofibers sterilized using 70% ethanol for 15 minutes and extensively rinse with PBS. (D) NH$_4$OH treated chitosan nanofibers sterilized by exposing them for 30 minutes in UV light. Scale bar in panel D is 5 µm and corresponds to all panels.

8.4.2 MSCs response to chitosan nanofibers

Ovine MSCs' ability to survive on the chitosan nanofibers was determined by microscopy. Eight days after seeding the cells on the fibers in expansion media, some samples were fixed and stained with DAPI, and/or calcein-AM to be visualized using fluorescence microscopy while others were dehydrated to be visualized through SEM. The SEM images shown in Figure 8.2 demonstrate the adherence of oMSCs to the fibers. The morphology of oMSC on nanofibers, shown on Figure 8.2 (C), might resemble that of native tissue; where the cell spreads out and extends portions of its membrane to interact with the topography of its surroundings. In this case, the cells are seen reaching for various fibers. Figure 8.2 (A) also shows that a large amount of oMSCs adhered and expanded on the chitosan nanofibers.
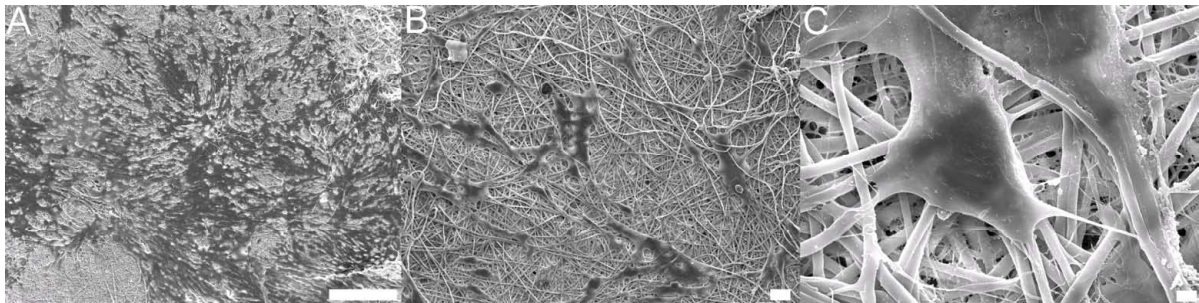
Figure 8.2 SEM micrographs of ovine MSCs seeded on fibronectin coated chitosan nanofibers. (A) ×100 magnification 200 µm scale bar. (B) ×300 magnification 20 µm scale bar. (C) ×3000 magnification 2 µm scale bar.

The large amount of oMSCs on the chitosan nanofibers are readily seen on Figures 8.3 and 8.4. Figure 8.3 (A) shows nuclei stained (DAPI) oMSCs seeded on chitosan nanofibers while Figure 8.3 (B) shows a bright field image of the nanofibers with oMSCs. Both images are from the same location. A large amount of cells can be observed through their stained nuclei. Also, individual nuclei are observed meaning that oMSCs are not becoming multinucleated and dying.
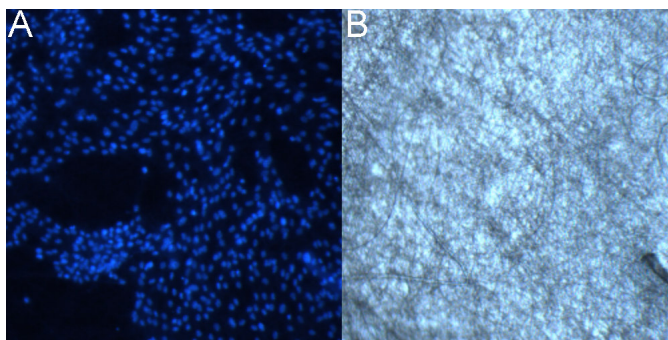
Figure 8.3 (A) Fluorescence microscopy image of DAPI (nuclei) stained ovine MSCs seeded on fibronectin coated chitosan nanofibers. (B) Bright field microscopy image of chitosan nanofiber mat. Both images were obtained from the same location of the same sample.

Figure 8.4 shows oMSCs seeded on chitosan nanofibers with both their cytoplasm (calcein-AM) and nuclei (DAPI) stained. The individual cytoplasm of an oMSCs can not be distinguished because of the large amount of cells growing on the nanofibers. Collectively, the images in Figures 8.2, 8.3, and 8.4 indicate that the cells successfully adhered and proliferated on the fibers. All of these nanofibers samples had fibronectin adsorbed because without it we observed poor MSC attachment (data not shown). This observation is consistent to our previous results of oMSCs seeded on polysaccharide-based surface coatings.[18] It was also observed that some of the fibers tend to ball up after several days of culture. We believe that this happens because the number of MSCs is so large that the cells contract the fibers. We also observe MSCs at the bottom of the wells containing fibers indicating that some cells fell from the fibers and continue growing on the TCPS.

Figure 8.4. Fluoresences microscopy images of oMSCs seeded on chitosan nanofibers. The cytoplasm of the MSCs is stained green with calcein (A) while the nuclei is stained blue using Vectashield containing DAPI (B). Overlapping calcein and DAPI (C).

8.4.3 MSCs osteogenic differentiation on nanofibers and flat surfaces

Throughout the entire period of these studies the fibers seemed to remain viable. No visible degradation or delamination was observed, even after 30 days of culture. Samples with oMSCs were tested for differentiation on days 10, 20 and 30 while eMSCs samples were tested on days 6, 12 and 18 by measuring produced ALP, and calcium deposition using alizarin red, and EDX. Figures 8.6 and 8.7 shows ALP activity for eMSCs and oMSCs respectively, seeded on both TCPS and nanofibers. Expressed ALP was normalized to total protein content in order to avoid deviations due to difference in cell number. We find that the eMSCs exhibit higher ALP activity on the nanofibers compared to the flat TCPS after 18 days of culture. On day 6 little ALP activity is noted on all conditions. On day 12 eMSCs on nanofibers produced a similar amount of ALP regarding of the presence of dexamethasone. This amount is similar to the amount of ALP produced on flat surfaces with dexamethasone on the same day. The presence of dexamethasone increases ALP production on eMSCs seeded on nanofibers after 18 days and on flat TCPS after 12 days.
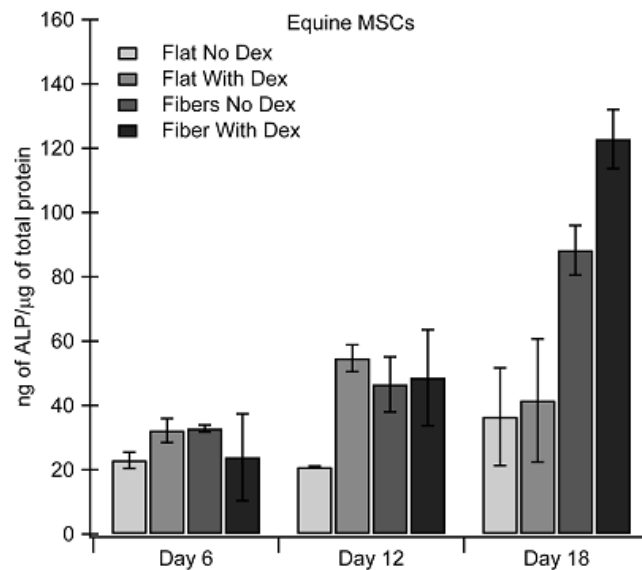
Figure 8.5 Amount (ng) of expressed alkaline phosphatase normalized to total protein content (μg) for equine MSCs seeded on either flat TCPS or chitosan nanofibers with and without dexamethasone. Error bars represent the range of two samples (n=2)

ALP activity for oMSCs is over 400 times lower than eMSCs (Figure 8.6). This expression was close to the lower limit of detection of the assay. ALP expression for oMSCs increases throughout the 30 days of culture. Similar to eMSCs, oMSCs express higher ALP activity when seeded on nanofibers.
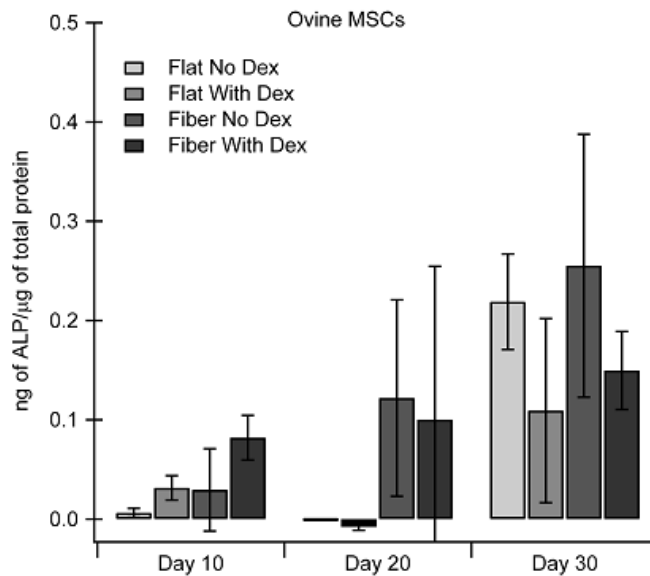
Figure 8.6 Amount (ng) of expressed alkaline phosphatase normalized to total protein content (μg) for ovine MSCs seeded on either flat TCPS or chitosan nanofibers with and without dexamethasone. Error bars represent the range of two samples (n=2).

Alizarin red was used to detect deposition of calcium due to matrix mineralization. Alizarin was not used on the nanofibers because they stain positive in the absence of MSCs. Figure 8.7 show photographs of the bottom of an Alizarin stained well from a 24-well plate. We find that eMSCs, which stain positive with Alizarin, showed a deeper red color compared to positive oMSCs samples (Figure 8.7) indicating that eMSCs have higher calcium deposition. For Figure 8.7, oMSCs were cultured for 10, 20, and 30 days with and without dexamethasone. Ovine MSCs deposit comparable amounts of calcium with and without dexamethasone, although calcium deposition seems to increase throughout the days of culture. However, eMSCs, cultured for 6, 12, and 18 days, exhibit very different calcium

deposition depending on the presence of dexamethasone. At day 18, when dexamethasone is present eMSC produce a noticeable amount of calcium, but when dexamethasonse is absent calcium deposition is undetectable. The opposite is true at day 12. On day 6, no calcium was detected of eMSCs with and without dexamethasone.
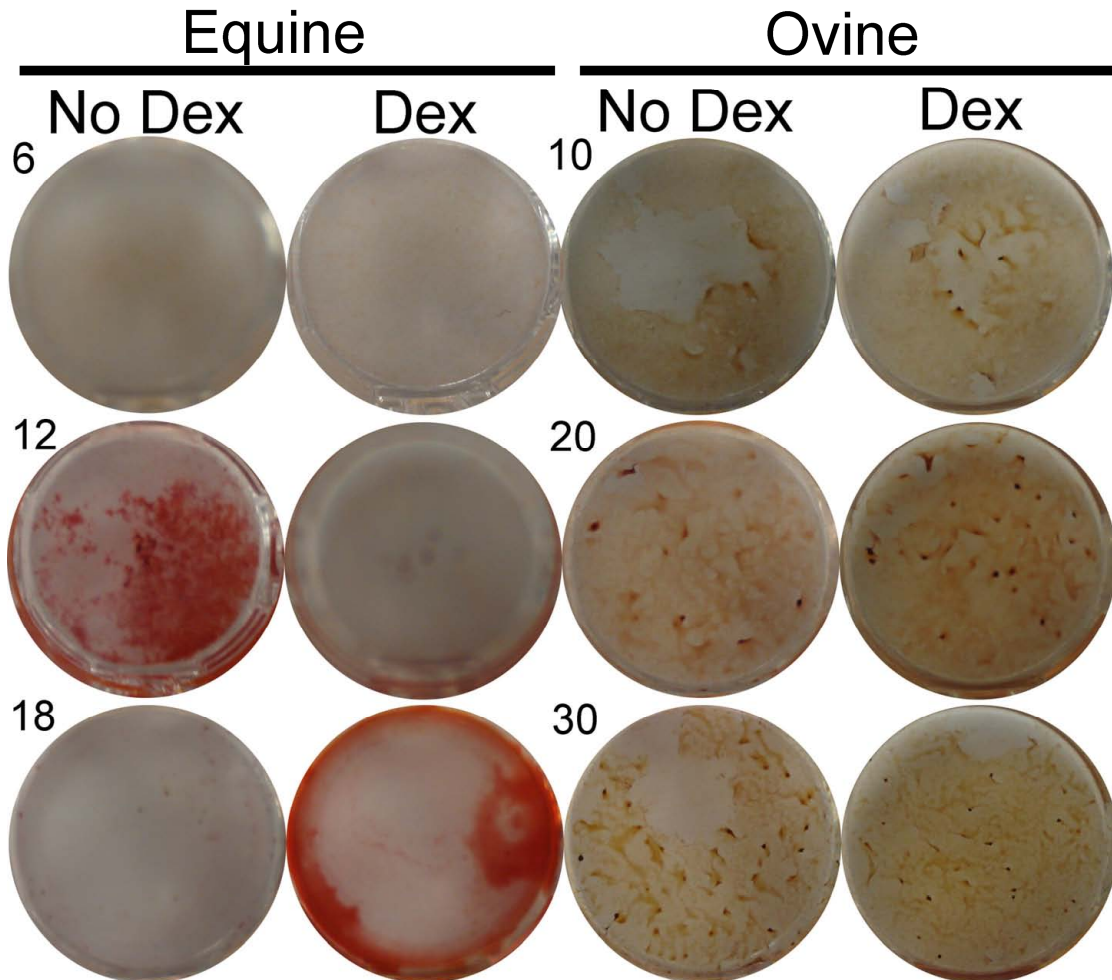
Figure 8.7 Alizarin red stained MSCs cultured on flat TCPS. Equine MSCs, first two columns, were cultured for 6, 12, and 18 days with and without dexamethasone. Ovine MSCs, last two columns, were cultured for 10, 20, and 30 days with and without dexamethasone.

Energy dispersive X-ray spectroscopy confirms calcium and phosphorus deposition of eMSCs cultured for 12 days on nanofibers with dexamethasone. Figure 8.8 (A) shows a bone-like granule, that when scanned with EDX exhibits considerable amounts of calcium and phosphate (Figure 8.8 (B)). We observe a Ca:P ratio of 1.29 for the sample in Figure 8.8. This ratio is similar to the expected ratio of octacalcium phosphate (1.33) and important precursor of hydroxylapatite.[19, 20]
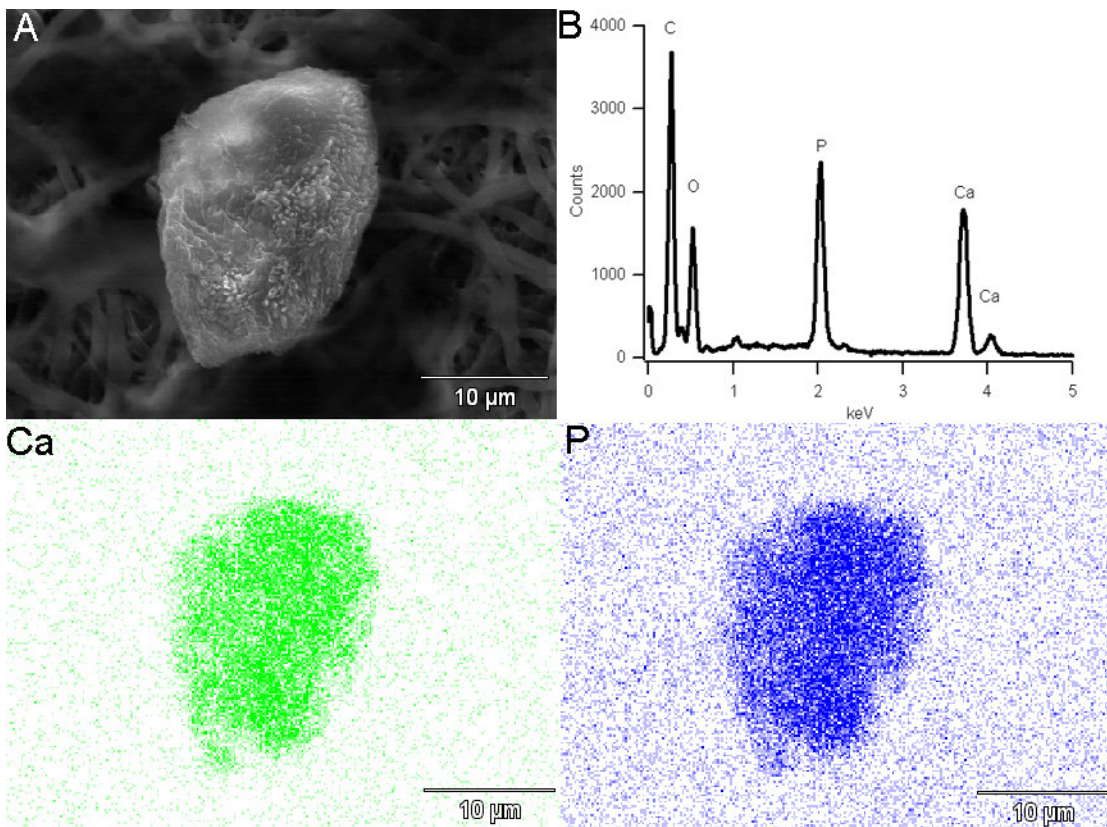
Figure 8.8 EDX compilation of data for equine MSCs on nanofibers with dexamethasone cultured for 12 days. (A) SEM image that was scanned. (B) EDX spectrum of the granule feature in image (A) corresponding to the Ca and P map shown on the bottom two panels.

Figure 8.9 shows three representative SEM micrographs at different magnifications of eMSCs cultured for 12 days on osteogenic media containing dexamethasone. Mineralized matrix deposition can be seen in Figure 8.9 as well as healthy-looking MSCs. The fibers also are visible in this figure, displaying no signs of degradation.
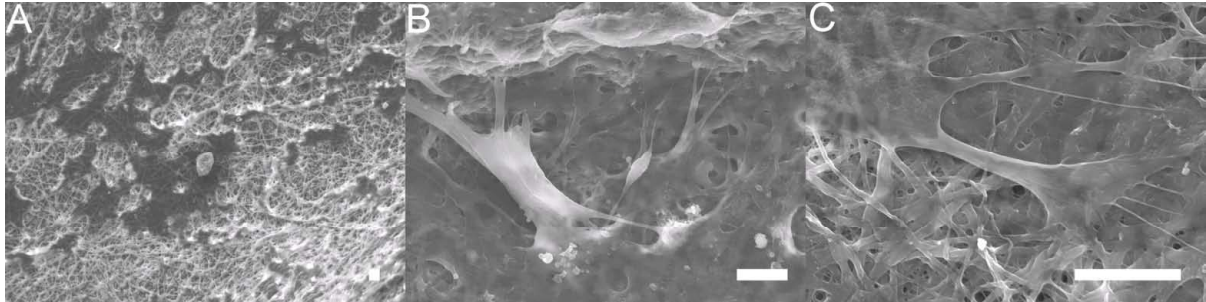
Figure 8.9. SEM micrographs of equine MSCs cultured for 12 days on osteogenic media with dexamethasone seeded on fibronectin coated chitosan nanofibers. (A) ×300 magnification. (B) ×1000 magnification. (C) ×3000 magnification. All scale bars are 10 μm.

Figures 8.10 and 8.11 shows EDX data for ovine cultured for 20 days under osteogenic media with (Figure 8.10) and without (Figure 8.11) dexamethasone. Both figures exhibits calcium, phosphate, oxygen, chlorine, and sulfur peaks. Two strong peaks for aluminum and silicon are also observed in Figure 8.10. They appear because the mounting stub is made of aluminum and double-sided carbon tape was used to attached the sample to the stub. The sulfur peaks might be due to sulfonated matrix deposition. When dexamethasone is present higher amounts of calcium are detected. Interestingly ovine MSCs seem to deposit small amounts of phosphorus as compared to equine MSCs, to the point were Ca:P ratio does not correlate to any of the naturally available calcium phosphates.

Figure 8.10 EDX compilation of data for ovine MSCs on nanofibers with dexamethasone cultured for 20 days. (A) SEM image that was scanned. (B) EDX spectrum of the granule feature in image (A) corresponding to the Ca and P map shown on the bottom two panels.
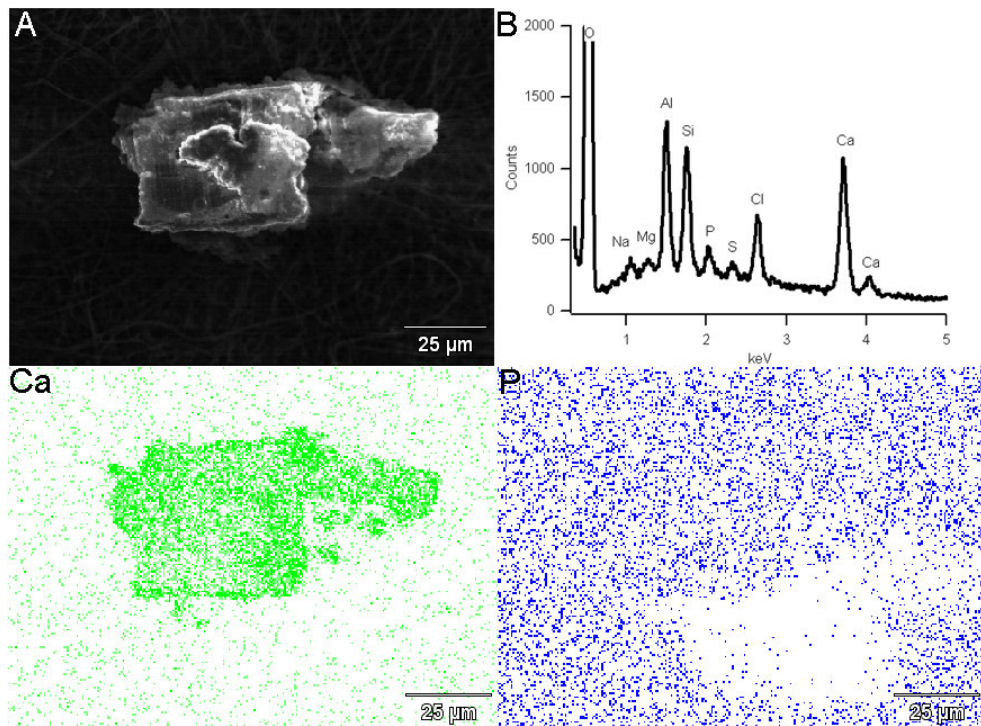

Figure 8.11 EDX compilation of data for ovine MSCs on nanofibers without dexamethasone cultured for 20 days. (A) SEM image that was scanned. (B) EDX spectrum of the granule feature in image (A) corresponding to the Ca and P map shown on the bottom two panels.

Figure 8.12 shows six representative SEM micrographs at different magnifications of oMSCs cultured for 20 days on osteogenic media with (D-F) and without (A-C) dexamethasone. Mineralized matrix deposition can be seen in Figure 8.12 as well as healthy looking MSCs. The fibers also are visible in this figure, displaying no signs of degradation after 20 days of culture.
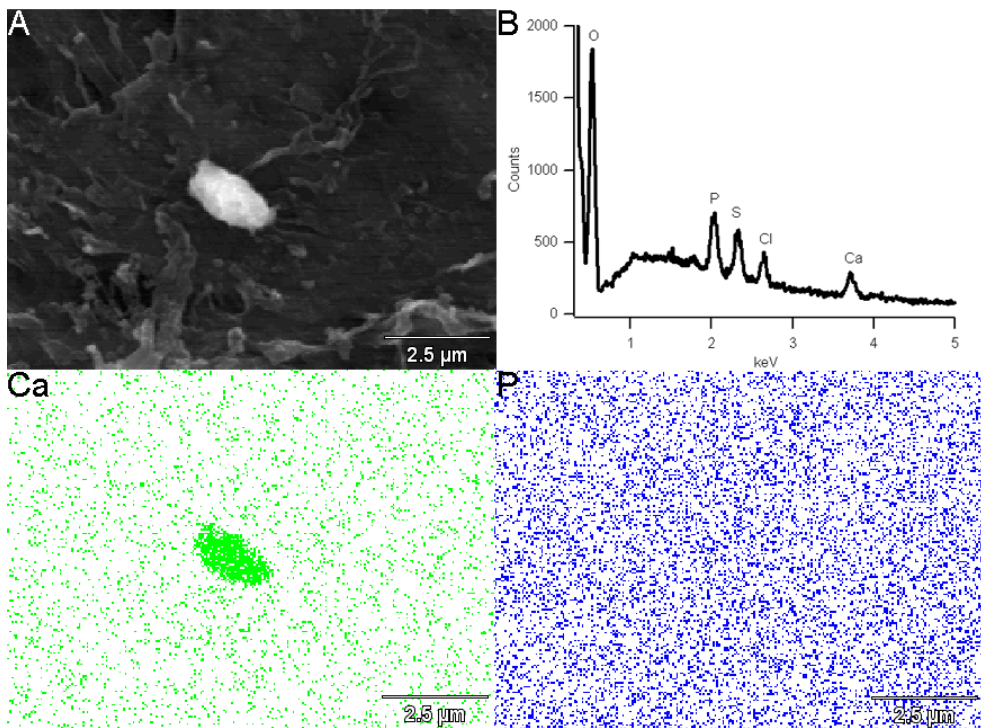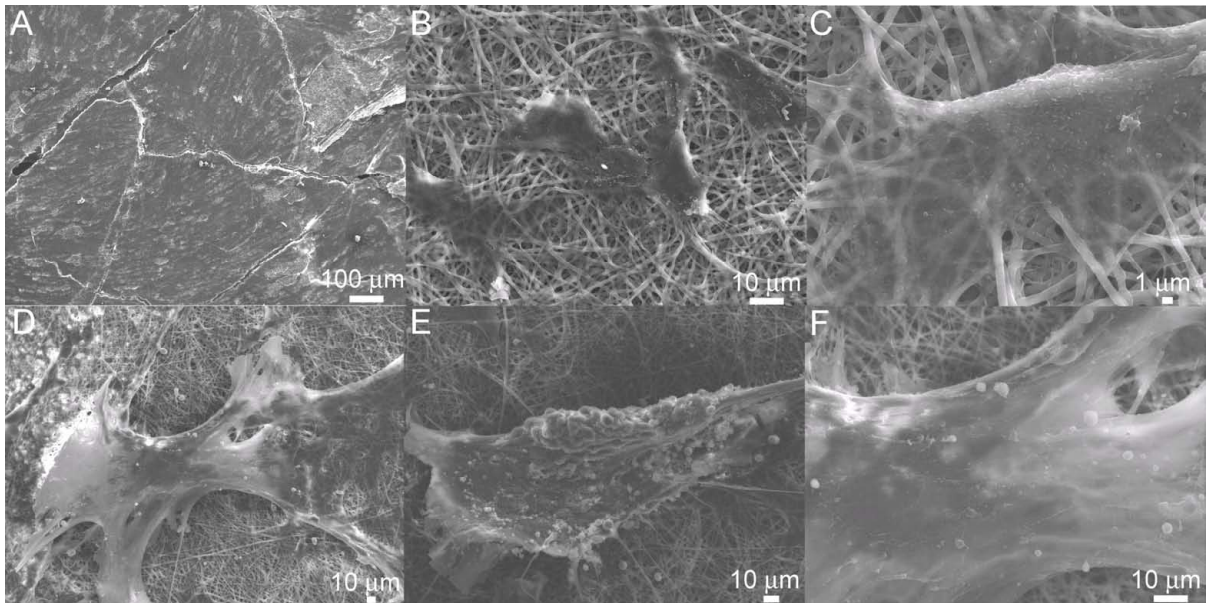

Figure 8.12 SEM micrographs of ovine MSCs cultured for 20 days on osteogenic media without (A-C) and with (D-F) dexamethasone seeded on fibronectin coated chitosan nanofibers. (A) ×100 magnification. (B) ×1000 magnification. (C) ×3000 magnification. (D) ×300 magnification. (E) ×450 magnification. (F) ×1000 magnification

8.5 Discussion

The ability to provide a three dimensional, portable scaffold conducive to cell adhesion and proliferation is significant because of its potential clinical applications. The results indicate that MSCs proliferated favorably on the chitosan nanofibers. Macroscopically, the fibers with cells would curl in on themselves around day 10, indicating that not only had the cells successfully adhered, but they could even pull on the fibers without tearing them.

209

Microscopically, SEM showed that the cells could grip and extend on the fibers, as shown in Figure 8.2. Therefore, electrospun chitosan nanofibers are a viable scaffold for MSC growth and survival.

Sheep are an ideal model for musculoskeletal tissue engineering because their anatomy and weight bearing resemble that of a human.[16] The osteogenic potential of ovine bone marrow-derived MSCs has been previously demonstrated both in vitro and in vivo.[16, 21-23] Zannettino et al. investigated the osteoconductivity of several inorganic scaffolds, in vivo, loaded with either ovine or human MSCs.[21] The MSCs-containing scaffolds were implanted subcutaneously in the dorsal surface of mice.[21] Interestingly, they observed that ovine MSCs displayed the capacity to form bone in 7 of the 8 scaffolds tested; whereas, human MSCs exhibited considerable bone formation only on 4 of the scaffolds.[21] They propose that this could be because ovine MSCs have a higher proliferation rate and exhibit 20% longer life span that human MSCs in vitro.[21] We also observe large proliferation rate of ovine MSCs. Ovine MSCs grew very rapidly, even when using osteogenic media, on flat TCPS regardless of the initial seeding density (500-40000 cells/cm^2). Ovine MSCs, on flat TCPS, would begin lifting around day 8 and they would appear balled up by day 10 when using osteogenic media. In our previous work, in order to observe the effect of FGF-2 had on oMSC proliferation, we had to use low-serum media (2.5% FBS) to decrease the proliferation rate typically observed under standard culture conditions (10% FBS).[18] In contrast, equine MSCs can not be culture-expanded unless they are grown with 10% serum and FGF-2. The fast proliferation rate of ovine MSCs certainly provides a challenge for their in vitro characterization which has been addressed by either using low-serum[18] or serum-deprived media.[24]

Niemeyer et al. cultured either ovine or human MSCs in mineralized collagen and implanted them into a critical-size defects on the tibia of sheep.[22] They noticed significant bone formation from the defects containing ovine MCS and poor bone formation from the human MSCs.[22] Recently, ovine MSCs were characterized by Rentsch et al. for their osteogenic potential on TCPS and embroidered polycaprolactone-*co*-lactide scaffolds.[16] On TCPS, they observe that under osteogenic conditions the MSCs get flatter and broader and begin forming colonies.[16] The colonies formed sheets that detached easily from the TCPS.[16] We observe this similar behaviour. On their scaffolds they quantified osteogenic differentiation using both the o-cresolphthalein complexone colorimetric assay and Von Kossa staining.[16] Interestingly, they mentioned that ALP activity could not be detected in ovine MSCs.[16] The absence of ALP from ovine MSCs cultured in vitro has also been observed by Kon et al.[25] Martin et al. observed this similar behaviour using bone marrow-derived feline MSCs.[26] They hypothesized that the absence of ALP in feline MSCs might be due to the short half-life of the protein in that species.[26] A recent report by Korda et al. is the only one found were ovine MSCs express reasonable amount of ALP after 7 and 14 days of culture on TCPS and osteogenic media.[23] Our results show low, but detectable, amounts of ALP for oMSCs grown under osteogenic conditions for both TCPS and flat surfaces.

The native production of ALP under expansion media (i.e. no osteogenic additives) was recorded for both equine and ovine MSCs cultured for 5 days in nanofibers and TCPS (Figure 8.9). We observe that native ALP production is low in TCPS for both equine and ovine MSCs, while the presence of the chitosan nanofibers upregulates native ALP production for both species.
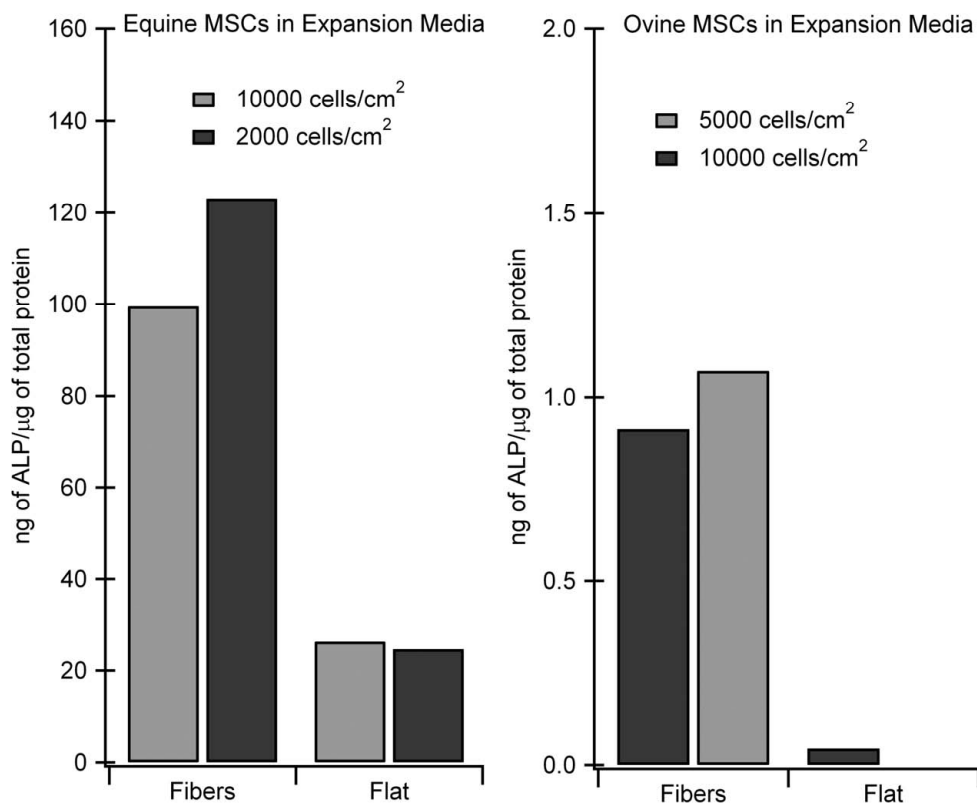
Figure 8.9 Amount (ng) of expressed alkaline phosphatase normalized to total protein content (µg) for equine MSCs seeded on either flat (TCPS) or chitosan nanofibers (A) and ovine MSCs seeded on either flat (TCPS) or chitosan nanofibers (B). MSCs were seeded using expansion media without dexamethasone, β-glycerol phosphate, or ascorbic acid.

These preliminary results are indicative that the differentiation of MSCs can be modulated via nanosturctures alone. Interestingly, ovine MSCs exhibited the highest ALP production when cultured for 5 days in expansion media compared to the conditions in Figure 8.6. These results might indicate that indeed ovine ALP has a much shorter half-life that equine ALP, or that it is expressed at much earlier time points. The role of ALP is to signal cells to accumulate phosphate ions from solution and deposit it into collagen fibrils.[23] ALP expression peaks at earlier time points and then decreases.[23] The fact that ovine MSCs express small amounts of ALP and phosphorus (as evidenced by EDX) might suggest that the mechanism of bone formation for ovine MSCs is different than that of equine. Nonetheless, the nanostructure of the chitosan fibers promotes osteogenesis for both ovine and equine

MSCs. The effect of nanostructured topography on MSCs osteogenic differentiation has been demonstrated on both hard[27] and soft[28] surfaces. Popat et al. reported an increase in ALP activity of mice marrow stromal cells when seeded on nanoporous alumina substrates versus amorphous alumina substrate.[27] Dalby et al. demonstrated that human MSCs produced bone mineral in the absence of dexamethasone when they are cultured on polymethylmethacrylate surfaces containing nanofeatures (nanopits) with different symmetry and disorder.[28] The samples with higher disorder exhibited an increase in osteogenic differentiation.[28] Thus the use of randomly distributed nanofibers might be beneficial to promote osteogenic differentiation.

8.6 Conclusions

This work demonstrates the potential of electrospun chitosan nanofibers as possible scaffolds for bone tissue engineering. Ovine and equine MSCs were successfully cultured in fibronectin-coated chitosan nanofibers. The chitosan nanofibers remained viable even after 30 days of culture. Both ovine and equine MSCs exhibited higher ALP activity on chitosan nanofibers when compared to flat TCPS. Albeit, equine ALP activity was roughly 400 times higher than ovine for all conditions. Alizarin red and EDX confirm mineralization of calcium on flat surfaces and nanofibers respectively. This work demonstrates further characterization of ovine MSCs in vitro, and the ability of soft nanostructured materials to dictate cell behaviour.

8.7 References

1. Caplan, A. I., *Journal of Orthopaedic Research* **1991,** *9* (5), 641-650.
2. Lanza, R. P.; Langer, R.; Vacanti, J., *Principles of Tissue Engineering*. Second ed.; Academic Press: San Diego, 2000; p 697-708.
3. Goldberg, M.; Langer, R.; Jia, X. Q., *Journal of Biomaterials Science-Polymer Edition* **2007,** *18* (3), 241-268.
4. Sill, T. J.; von Recum, H. A., *Biomaterials* **2008,** *29* (13), 1989-2006.
5. Sangsanoh, P.; Suwantong, O.; Neamnark, A.; Cheepsunthorn, P.; Pavasant, P.; Supaphol, P., *European Polymer Journal* **2010,** *46* (3), 428-440.
6. Sangsanoh, P.; Waleetorncheepsawat, S.; Suwantong, O.; Wutticharoenmongkol, P.; Weeranantanapan, O.; Chuenjitbuntaworn, B.; Cheepsunthorn, P.; Pavasant, P.; Supaphol, P., *Biomacromolecules* **2007,** *8* (5), 1587-1594.
7. Badami, A. S.; Kreke, M. R.; Thompson, M. S.; Riffle, J. S.; Goldstein, A. S., *Biomaterials* **2006,** *27* (4), 596-606.
8. Li, W. J.; Danielson, K. G.; Alexander, P. G.; Tuan, R. S., *Journal of Biomedical Materials Research Part A* **2003,** *67A* (4), 1105-1114.
9. Ruckh, T. T.; Kumar, K.; Kipper, M. J.; Popat, K. C., *Acta Biomaterialia* **2010,** *6* (8), 2949-2959.
10. Martins, A.; Duarte, A. R. C.; Faria, S.; Marques, A. P.; Reis, R. L.; Neves, N. M., *Biomaterials* **2010,** *31* (22), 5875-5885.
11. Christopherson, G. T.; Song, H.; Mao, H. Q., *Biomaterials* **2009,** *30* (4), 556-564.
12. Boddohi, S.; Kipper, M. J., *Advanced Materials* **2010,** *22* (28), 2998-3016.
13. Almodóvar, J.; Kipper, M. J., *Macromolecular Bioscience* **2011,** *11* (1), 72-76.
14. Sangsanoh, P.; Supaphol, P., *Biomacromolecules* **2006,** *7* (10), 2710-2714.
15. Duan, B.; Wu, L. L.; Yuan, X. Y.; Hu, Z.; Li, X. L.; Zhang, Y.; Yao, K. D.; Wang, M., *Journal of Biomedical Materials Research Part A* **2007,** *83A* (3), 868-878.
16. Rentsch, C.; Hess, R.; Rentsch, B.; Hofmann, A.; Manthey, S.; Scharnweber, D.; Biewener, A.; Zwipp, H., *In Vitro Cellular & Developmental Biology-Animal* **2010,** *46* (7), 624-634.
17. Frisbie, D. D.; Smith, R. K. W., *Equine Veterinary Journal* **2010,** *42* (1), 86-89.
18. Almodóvar, J.; Bacon, S.; Gogolski, J.; Kisiday, J. D.; Kipper, M. J., *Biomacromolecules* **2010,** *11* (10), 2629-2639.
19. Varma, H. K.; Yokogawa, Y.; Espinosa, F. F.; Kawamoto, Y.; Nishizawa, K.; Nagata, F.; Kameyama, T., *Biomaterials* **1999,** *20* (9), 879-884.
20. Fan, Y. W.; Duan, K.; Wang, R. Z., *Biomaterials* **2005,** *26* (14), 1623-1632.
21. Zannettino, A. C. W.; Paton, S.; Itescu, S.; Gronthos, S., *Tissue Engineering Part A* **2010,** *16* (12), 3579-3587.
22. Niemeyer, P.; Schonberger, T. S.; Hahn, J.; Kasten, P.; Fellenberg, J.; Suedkamp, N.; Mehlhorn, A. T.; Milz, S.; Pearce, S., *Tissue Engineering Part A* **2010,** *16* (1), 33-43.
23. Korda, M.; Hua, J.; Little, N. J.; Heidari, N.; Blunn, G. W., *Tissue Engineering Part A* **2010,** *16* (2), 675-683.
24. McCarty, R. C.; Gronthos, S.; Zannettino, A. C.; Foster, B. K.; Xian, C. J., *Journal of Cellular Physiology* **2009,** *219* (2), 324-333.

25. Kon, E.; Muraglia, A.; Corsi, A.; Bianco, P.; Marcacci, M.; Martin, I.; Boyde, A.; Ruspantini, I.; Chistolini, P.; Rocca, M.; Giardino, R.; Cancedda, R.; Quarto, R., *Journal of Biomedical Materials Research* **2000,** *49* (3), 328-337.
26. Martin, D. R.; Cox, N. R.; Hathcock, T. L.; Niemeyer, G. P.; Baker, H. J., *Experimental Hematology* **2002,** *30* (8), 879-886.
27. Popat, K. C.; Chatvanichkul, K. I.; Barnes, G. L.; Latempa, T. J.; Grimes, C. A.; Desai, T. A., *Journal of Biomedical Materials Research Part A* **2007,** *80A* (4), 955-964.
28. Dalby, M. J.; Gadegaard, N.; Tare, R.; Andar, A.; Riehle, M. O.; Herzyk, P.; Wilkinson, C. D. W.; Oreffo, R. O. C., *Nature Materials* **2007,** *6* (12), 997-1003.

Chapter 9

Conclusions and Future Work

9.1 Conclusions

The work presented in this thesis demonstrates the potential of polysaccharide-based nanostructured materials for growth factor delivery and mesenchymal stem cell activation (MSC). Polysaccharide-based polyelectrolyte multilayers (PEMs) were constructed from the polycations chitosan and *N,N,N*-trimethyl chitosan and the polyanions hyaluronan, chondroitin sulfate, and heparin on gold-coated glass. Their hydrophilicity, composition, and ion pairing were investigated using a number of spectroscopic tools. Construction of PEMs on tissue-culture polystyrene and titanium was also investigated. Protein loading, release, and stability were investigated on these PEM-modified flat surfaces, spectroscopically, using model proteins and basic fibroblast growth factor (FGF-2). The bioactivity of the loaded growth factor on polysaccharide-based PEMs was assessed using bone marrow-derived ovine MSCs.

Furthermore, electrospun chitosan nanofibers were constructed and modified with polysaccharide-based PEMs and polyelectrolyte complex nanoparticles (PCNs). FGF-2, complexed to PCN, was successfully loaded and released from the chitosan nanofibers, retaining their bioactivity, for over a period of 27 days. Finally, the ability of the chitosan fibers to support and promote osteogenic potential of MSCs was investigated.

The specific aims for this thesis were accomplished in the following manner:

I. *Investigate, spectroscopically, the layer-by-layer assembly of polysaccharide-based multilayers using chitosan and N,N,N-trimethyl chitosan as polycations and hyaluronan, chondroitin sulfate and heparin as the polyanions.*

This specific aim is addressed in chapter 3. This work was the first to provide composition details of PEMs based on *N,N,N*-trimethyl chitosan (TMC) and glycosaminoglycans. The polysaccharide-based PEMs formed from the polycations chitosan (CHI) and TMC, and the polyanions hyaluronan (HA), chondroitin sulfate (CS), and heparin (HEP) are compared. Using a combination of spectroscopic techniques that measure the wet and dry thickness [Fourier transform-surface plasmon resonance (FT-SPR) and spectroscopic ellipsometry, respectively] and the PEM chemistry [polarization modulation-infrared reflection absorption spectroscopy (PM-IRRAS) and X-ray photoelectron spectroscopy (XPS)] and water contact angle measurements, this work provides an understanding of how the charge density on the polysaccharides affects their hydrophilicity and swelling. By comparison of water contact angle and thickness measurements, we found that the most hydrophilic PEMs were formed from the weak polycation-weak polyanion (i.e. the CHI-HA PEMs) and strong polycation-strong polyanion pairs (i.e. TMC-CS and TMC-HEP PEMs); the most hydrophobic PEMs were formed when one polyelectrolyte was strong and the other was weak (i.e. CHI-CS, CHI-HEP, and TMC-HA PEMs). PM-IRRAS and XPS provided details of the PEM composition that allow us to make conjectures that explain these observations. When both polyelectrolytes are weak, there is reduced ion pairing, enabling the PEMs to swell. When a strong polyelectrolyte is combined with a weak polyelectrolyte, the strong polyelectrolyte controls the charge density on the weak polyelectrolyte, effectively enforcing

increased ion pairing that compacts the PEM and reduces the swelling. Finally, when both polyelectrolytes are strong, the TMC only has a fraction of strong cationic groups at fixed locations along the polymer chain. Thus the strong polyanions do not as readily influence the charge density on TMC, and instead pair with some small molecular weight counterions. This increases the osmotic pressure in the PEMs, causing them to swell. This work demonstrates how PEM behaviour is affected by polysaccharide pair selection.

II. *Investigate how polysaccharide based surfaces affect the structure and stability of proteins using IR spectroscopy.*

This specific aim is addressed in chapter 4. The adsorption and stability of model proteins onto polyelectrolyte multilayers prepared from naturally derived polysaccharides was investigated in chapter 4. It was confirmed via Fourier transform infrared (FT-IR) spectroscopy that both negatively and positively charged proteins adsorb onto both negatively charged and neutral PEMs. Both lysozyme and bovine serum albumin (BSA) undergo changes in their secondary structures when adsorbed to PEM, characterized by loss of α-helical content and increases in β-sheet structures. For lysozyme, the secondary structure is more stable when it is adsorbed from dilute solution. For BSA, the β-sheet structures that are formed during adsorption are apparently strongly H-bonded, as they undergo a reduced degree of hydrogen-deuterium exchange (HDX) compared to the protein in solution. FT-SPR, PM-IRRAS, and transmission FT-IR along with HDX are shown to be powerful tools for investigating protein adsorption, release, and stability on polysaccharide-based PEMs. Chapter 4 demonstrates with multiple tools for investigating protein stability which can be applied to relevant proteins in tissue engineering such as growth factors.

III. *Demonstrate the ability of polysaccharide-based PEMs to stabilize the growth factor FGF-2 and therefore enhance MSC proliferation on flat surfaces.*

This specific aim is addressed in chapter 5. In chapter 5, surface coatings were developed for the delivery of FGF-2 at therapeutic concentrations using polysaccharide-based PEMs for guided MSC proliferation. PEMs were constructed on both TCPS and titanium. Heparin-terminated PEM coatings with adsorbed FGF-2 and adsorbed fibronectin on TCPS were shown to be the best candidate surface coatings for enhancing MSC proliferation in low-serum media. This system represents a promising candidate for the development of surface coatings that can stabilize and potentiate the activity of growth factors for therapeutic applications. However, when the PEM coatings were translated to titanium surfaces, the improvement in MSC proliferation was not observed. Additional work will be necessary to tune the PEM coatings on different surfaces, in order to take advantage of their potential for growth factor delivery.

IV. *Develop methods for the coating of electrospun chitosan nanofibers using PEMs, and use them as a substrate for the adsorption and controled release of FGF-2.*

This specific aim is addressed on both chapters 6 and 7. In chapter 6, electrospun chitosan nanofibers were successfully coated with PEMs using the polysaccharides heparin and *N,N,N*-trimethyl chitosan. PEM coating was confirmed with XPS and Alcian blue staining. FGF-2 was successfully adsorbed on the PEM-coated nanofibers. This method will enable the aqueous modification of chitosan nanofibers with many types of bioactive moieties via the layer-by-layer assembly of PEMs. In chapter 7, an electrospun system was developed for the delivery of FGF-2. Polysaccharide-based PCNs were successfully applied to deliver and stabilize FGF-2 from denaturation and inactivation up to 27 days of incubation. While, the

distinctive properties of PEMs were exploited to inhibit the PCN/FGF-2 release. We demonstrated the tuning of the delivery system, where the growth factor can be either released, with zero-order kinetics, or retained for a period of 27 days, simply by the addition of a PEM. The biological evaluation established that the FGF-2 is still active after 27 days of incubation, which contributed to a higher proliferation of MSCs. The ability of the system to load FGF-2 independently and at different layers transforms the electrospun networks into an important method that might be applied for the stabilization and delivery of therapeutic growth factors in vivo.

v. *Demonstrate, the ability of the electrospun chitosan nanofibers to support MSC growth and investigate how nanoscale features affect osteogenic differentiation.*

This specific aim is addressed in chapter 8. This work demonstrates the potential of electrospun chitosan nanofibers as possible scaffolds for bone tissue engineering. Ovine and equine MSCs were successfully cultured in fibronectin-coated chitosan nanofibers. The chitosan nanofibers remained viable even after 30 days of culture. Both ovine and equine MSCs exhibited higher alkaline phosphatase (ALP) activity on chitosan nanofibers when compared to flat TCPS. Albeit, equine ALP activity was roughly 400 times higher than ovine for all conditions. Alizarin red and EDX confirm mineralization of calcium on flat surfaces and nanofibers respectively. This work demonstrates further characterization of ovine MSCs in vitro, and the ability of soft nanostructured materials to dictate cell behaviour.

9.2 Future Work

While extensive work has been presented in this thesis, future studies must be performed in order to fully understand and optimize these systems. Regarding PEM constructions, more investigations should be performed in creating "hybrid" PEMs, meaning PEMs with more than two types of polysaccharides. For example, we know that the CHI-HA system yields the thickest of the PEMs, which might be desirable in some cases. However, HA does not contain the specific binding sites for important growth factors which heparin has. Thus, hybrid CHI-HA/HEP films could be constructed to obtain thicker films with heparin functionality. Hydrophilicity, composition, and ion pairing studies can be performed on these films. Other PEM properties that should be investigated which affect cell behavior include: film stiffness, roughness, degradation, and diffusion. Investigations to address these properties could be performed on polysaccharide-based PEMs. Most of the extensive characterization of PEMs was performed on gold-coated glass. However, gold-coated glass is not a representative biomaterial. Further extensive characterization of PEMs constructed on titanium should be performed in order to modulate cell response on titanium. As it is presented in chapter 5, the underlying substrate upon which PEMs are deposited affects cell response. Finally, models which predict PEM behavior can be applied to polysaccharide-based PEMs in order to predict certain properties.

Chapter 4 of this thesis demonstrates the potential of different FT-IR techniques, along with HDX, to elucidate protein loading, release, and stability. In particular, these techniques allow the study of protein-PEM interactions. Validation was performed with model proteins, but other biologically relevant proteins can also be used. Future IR studies on protein loading, release, and stability can be performed with fibronectin, and growth factors such as

FGF-2 and transforming growth factor beta 1 (TGF-β1). We can investigate the structural stability of the proteins and correlate that to the in vitro bioactivity both in solution and adsorbed to the PEMs. Moreover, thermal and enzymatic degradation of the proteins can be evaluated using these techniques, which will then allow fine tuning of PEMs to avoid degradation.

Cell response to adsorbed growth factors on polysaccharide-based PEMs as surface coatings should be expanded in order to evaluate through which mechanism the cells respond to the FGF-2 adsorbed onto PEMs. We proposed three different mechanisms to explain these phenomena: (1) the PEM acts as a depot for the sustained release of FGF-2, (2) heparin binding stabilizes FGF-2 with respect to degradation, and (3) heparin mediates FGF-2/FGF-2 receptor interaction on MSCs. Future work should be performed to investigate which, if any, of these mechanisms match the experimental results. Proper understanding of growth factor-PEM interaction will open the door for investigating other heparin-binding growth factors which affect MSCs differentiation such as TGF-β1 and bone morphonogenic proteins. Finally, other cell types should be investigated including human and equine MSCs.

Very little work has been published on electrospinning of chitosan, modification of electrospun chitosan nanofibers, and cell response to electrospun chitosan nanofibers. Optimization on the electrospinning process, regarding solvent, voltage, tip-to-collector distance, etc. should be performed in order to better control the fiber diameter and the porosity of the fiber mat. Fiber alignment could be controlled using rotating collectors which would yield chitosan nanofibers of interesting geometries. Optimization of the nanofibers neutralization using ammonium hydroxide should be performed to minimize the change in fiber morphology. Coating of the nanofibers with polysaccharides can be expanded to other

polysaccharides depending on the application. The nanostructured scaffold presented in chapter 7, combining PCN, PEM, and nanofibers, has plenty of room for optimization. PCN loading on nanofibers was very small, as noticed by the small amounts of released FGF-2. The bioactivity of the released FGF-2 from the nanofibers samples should be evaluated by seeding cells on the nanofibers.

The potential for chitosan nanofibers as scaffolds for osteogenic differentiation must be further evaluated. First, different markers for osteogenic differentiation could be used including osteocalcin and osteopotin. Particularly since ALP activity is difficult to measure on ovine MSCs. These other proteins can be evaluated using immunofluorescence techniques or gene expression techniques such as polymerase chain reaction. Modification of the nanofibers with PEM and PCN in combination with growth factor loading could be investigated to developed materials for osteogenesis. Selection of growth factors could also lead to development of biomaterials for chondrogenesis. Human MSCs should also be evaluated with these systems. Finally, in vivo testing should be performed for all of these systems in order to validate them as potential biomaterials.

This thesis presented some characterization of bone marrow-derived ovine MSCs. Currently there is a lack of in vitro characterization of ovine MSCs, yet sheep are routinely used for in vivo investigations. They certainly behave differently compared to bone marrow-derived MSCs of other large mammals, such as equine and human. Future extensive evaluation of ovine MSCs should be performed. These studies could include flow-cytometry investigations, differentiation of the different MSCs lineages, gene expression, proteomics, and others. These studies could elucidate the mechanism of bone formation in sheep.

The applications of polysaccharide-based PEMs, PCNs, nanofibers, and different combinations thereof for the modification of biomaterials are limitless. Biomaterials such as hydrogels, titanium or titanium alloy implants, and demineralized tissue (such as bone) are a few of the many biomaterials which can be modified with the polysaccharide-based nanostructures presented in this work in order to improve their biocompatibility or for the delivery of stable growth factors.

Appendix

A.1 Supporting Information for Chapter 3. Layer-by-Layer Assembly of Polysaccharide-Based Multilayers: A Spectroscopic Study of Hydrophilicity, Composition, and Ion Pairing

A.1.1 Synthesis of N,N,N-trimethyl chitosan (TMC)

TMC was synthesized following the procedure described by de Britto and Assis.[1] Briefly 0.25 g (0.0016 mol) of chitosan was reacted with 5 mL (0.05 mol) of dimethyl sulfate containing 1 mL of DI water, 0.2 g (0.005 mol) of sodium hydroxide, and 0.3 g (0.005 mol) of sodium chloride at room temperature for 6 hours. The products were dialyzed, using tubing cellulose membrane (Sigma Aldrich; St. Louis, MO) with a molecular weight cutoff of 12,000 Da, against solutions of NaCl and NaOH of decreasing ionic strength (0.5 M, 0.25 M, and 0.1 M of both NaOH and NaCl) over a period of 3 days. TMC was precipitated from solution using acetone and dried in a vacuum desiccator.

The ^{1}H NMR spectra of chitosan and TMC were collected using a 400 MHz (n = 2, d = 5 s) spectrometer (Varian Inova; Palo Alto, CA). Samples were dissolved in D$_2$O/HCl 100/1 v/v and D$_2$O respectively at 5 g L^{-1}. ^{1}H NMR spectra confirm successful methylation of chitosan. Figure A.1.1 shows the ^{1}H NMR spectra of chitosan (top) and TMC (bottom). The chitosan has degree of acetylation 5 %. The methylation to form TMC results

in some *O*-methylation and some *N,N*-dimethyl amino and *N,N,N*-trimethyl amino groups. Degree of *N,N,N*-trimethyl substitution (DQ), *N,N*-dimethyl substitution (DM), and *O*-methyl substitution (DOM) were calculated to be 18%, 45 %, and 38 % respectively, using the equations described previously:[2]

$$DQ = \frac{[N(CH_3)_3]}{[H]} \times \frac{1}{9} \times 100\% \qquad \text{E1}$$

$$DM = \frac{[N(CH_3)_2]}{[H]} \times \frac{1}{6} \times 100\% \qquad \text{E2}$$

$$DOM = \frac{[O(CH_3)_2]}{[H]} \times \frac{1}{3} \times 100\% \qquad \text{E3}$$

were $[N(CH_3)_3]$ is the integral of the signal intensity of hydrogens of the trimethylated amino group at 3.3 ppm, $[N(CH_3)_2]$ is the integral of the signal intensity of hydrogens of the dimethylated amino group at 2.9 ppm, $[O(CH_3)_2]$ is the integral of the signal intensity of hydrogens of the *O*-methyl groups at 3.5 ppm and [H] is the integral of the signal intensity of the hydrogens on the saccharide C-1 carbon between 4.7 – 5.7 ppm. For the TMC used in chapter 6 we calculated degree of susbstitution for DQ, DM, and DOM to be 22 %, 66 %, and 54 % respectively, using equations E1, E2, and E3.
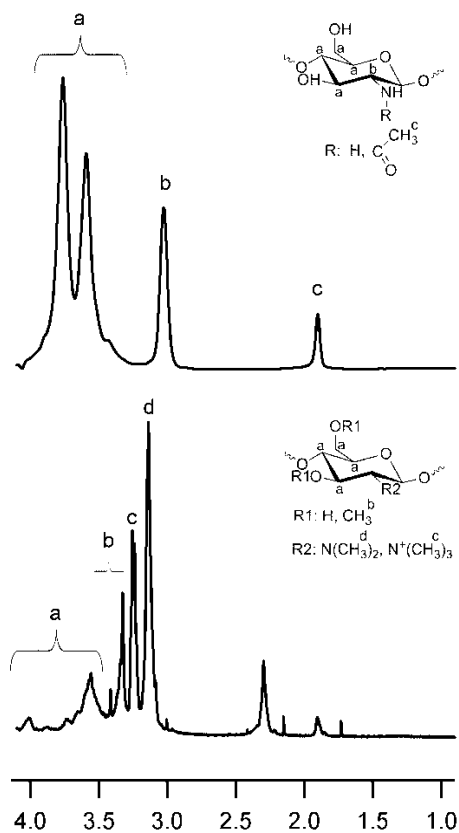
Figure A.1.1 ^{1}H NMR spectra of chitosan (top) and TMC (bottom).

A.1.2 Fitting ellipsometry and FT-SPR data

Thick (30- or 20- layer) and thin (10-layer) PEMs were constructed on gold-coated, MUA-SAM-modified SF-10 glass for all six possible polycation-polyanion combinations. Ellipsometry data was obtained for both thick and thin PEMs at two angles.

It was not possible to obtain reliable fits to the ellipsometry data on the 10-layer PEMs with both the thickness and the optical properties as fit parameters. However, the optical properties and thickness could be obtained from the ellipsometry data from the thick PEMs. The wavelength dependence of the refractive index, *n* of each PEM pair was modeled using the Cauchy equation (E4).

$$n = A + \frac{B}{\lambda^2} + \frac{C}{\lambda^4}$$

E4

The MUA-SAM and the PEM were modeled as a single Cauchy layer. Table A.1.1 shows the Cauchy parameters for all PEM combinations obtained through ellipsometry.

Table A.1.1 Cauchy Parameters for all PEM pairs and water

Component	A	B (nm^2)	C (nm^4)
Water[*]	1.328	2100	6.7×10^7
CHI-HEP	1.454	10518	0
CHI-CS	1.492	0	3.1182×10^9
CHI-HA	1.424	2812.1	0
TMC-HEP	1.484	4613.9	0
TMC-CS	1.413	0	6.4285×10^8
TMC-HA	1.474	69326	0

[*] Parameters obtained from reference 3.

For predicting the FT-SPR curves a macro was written in the software IgorPro that uses the Fresnel equations to predict the FT-SPR curve. The Fresnel calculations were adapted from a script created by Prof. Robert Corn from the University of California, Irvine.[4] The FT-SPR curve prediction requires the refractive index and thickness of all of the layers involved. A typical FT-SPR experiment consists of four layers: the prism and glass medium (all of the same refractive index), the gold film, the deposited layer, and the solvent. Both the solvent and prism/glass are considered to be infinitely thick. The gold thickness and refractive index are known and the solvent (water) refractive index is also known. The PEM thickness can then be estimated if the refractive index is known (Table A.1.2). The refractive index of the film can be calculated by using equation E4 and the parameters in Table A.1.1. A script was written that uses the Fresnel equations and calculates a FT-SPR peak for an array of thicknesses. The FT-SPR peak is calculated over a range of wavelength, thus the script was also modified to take into account the change of refractive index of both water and

the PEM by implementing the Cauchy equation. It was noted that when taking the dependence on wavelength of the refractive index of water into account the calculated thickness of the PEMs varies, while the wavelength dependence of the PEM refractive index PEM has little effect on the calculated thickness.

Table A.1.2 Thicknesses and contact angle data for different PEM pairs. Thicknesses were predicted using both FT-SPR and Ellipsometry.

| PEM	SPR (nm)	Ellipsometry (nm)	Contact Angle (deg)
CHI-HEP	10.5 ± 1.5	6.8 ± 0.4	54.1 ± 8.0
CHI-CS	11.9 ± 2.9	11.6 ± 1.1	52.4 ± 9.0
CHI-HA	28.2 ± 1.1	15.0 ± 0.7	35.0 ± 3.8
TMC-HEP	9.1 ± 1.2	2.7 ± 0.7	40.4 ± 0.4
TMC-CS	10.0 ± 1.9	4.0 ± 0.2	41.2 ± 2.4
TMC-HA	12.1 ± 0.7	6.8 ± 0.4	56.9 ± 8.7

A.1.3 High-resolution XPS of the C1s, N1s, O1s, and S2p envelopes of all PEMs and pure components

High-resolution XPS spectra for oxygen (O1s), nitrogen (N1s), carbon (C1s) and sulfur (S2p) were obtained for the pure polysaccharides and all of the thick PEMs. These are shown in Figures A.1.2, A.1.3, and A.1.4. Both heparin and chondroitin sulfate polysaccharides and PEMs exhibit the expected sulfur peak at 169.2 ev from the sulfate in both polysaccharides, heparin exhibiting a stronger peak. The oxygen peaks contain many contributions (hydroxyl, carboxylic acid carbonyl, glycosidic bond, ether, amide carbonyl, and sulfate), which makes unambiguous peak assignments difficult, thus none are displayed. Some assignments can be done in the carbon peak. Most samples show a peak around 288 eV, which is due to the 1-carbon from the saccharide ring. Carbons bonded to a hydroxyl produce a peak at 286.5 eV. Assignment for the components of the N1s peak can be found in Chapter 3.
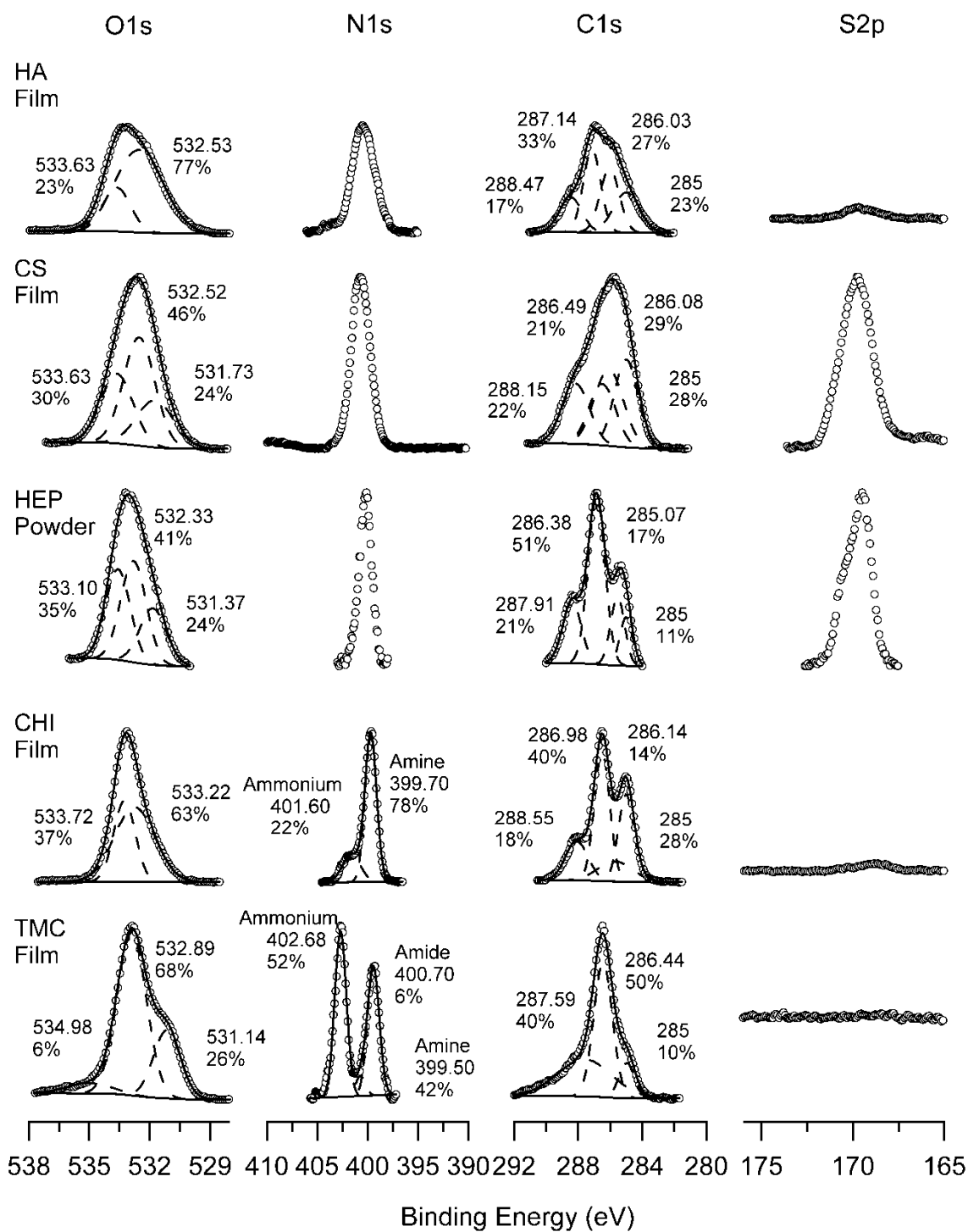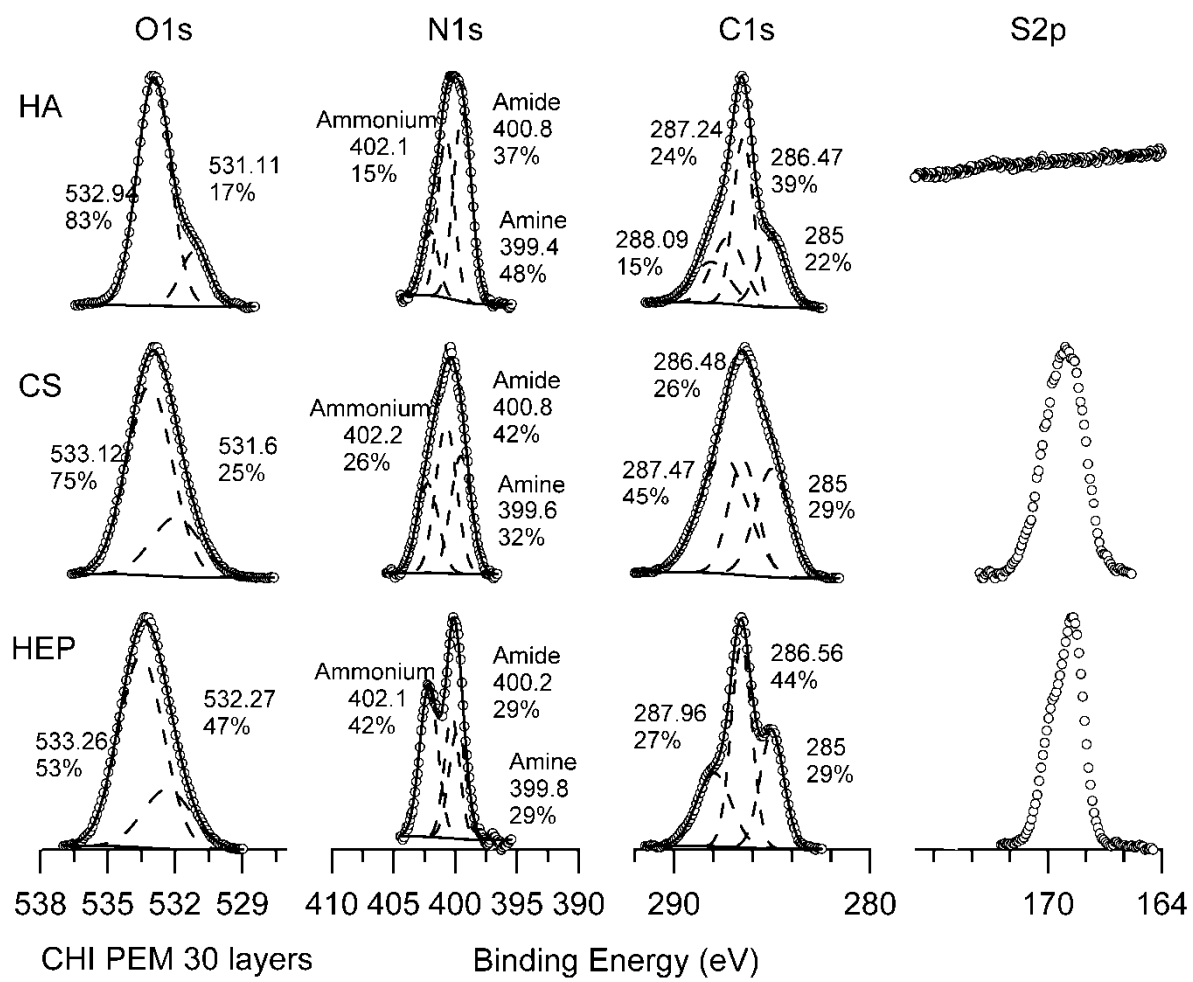
Figure A.1.2 High-resolution O1s, N1s, C1s, and S2p XPS spectra for all of the pure polysaccharides used in this study.
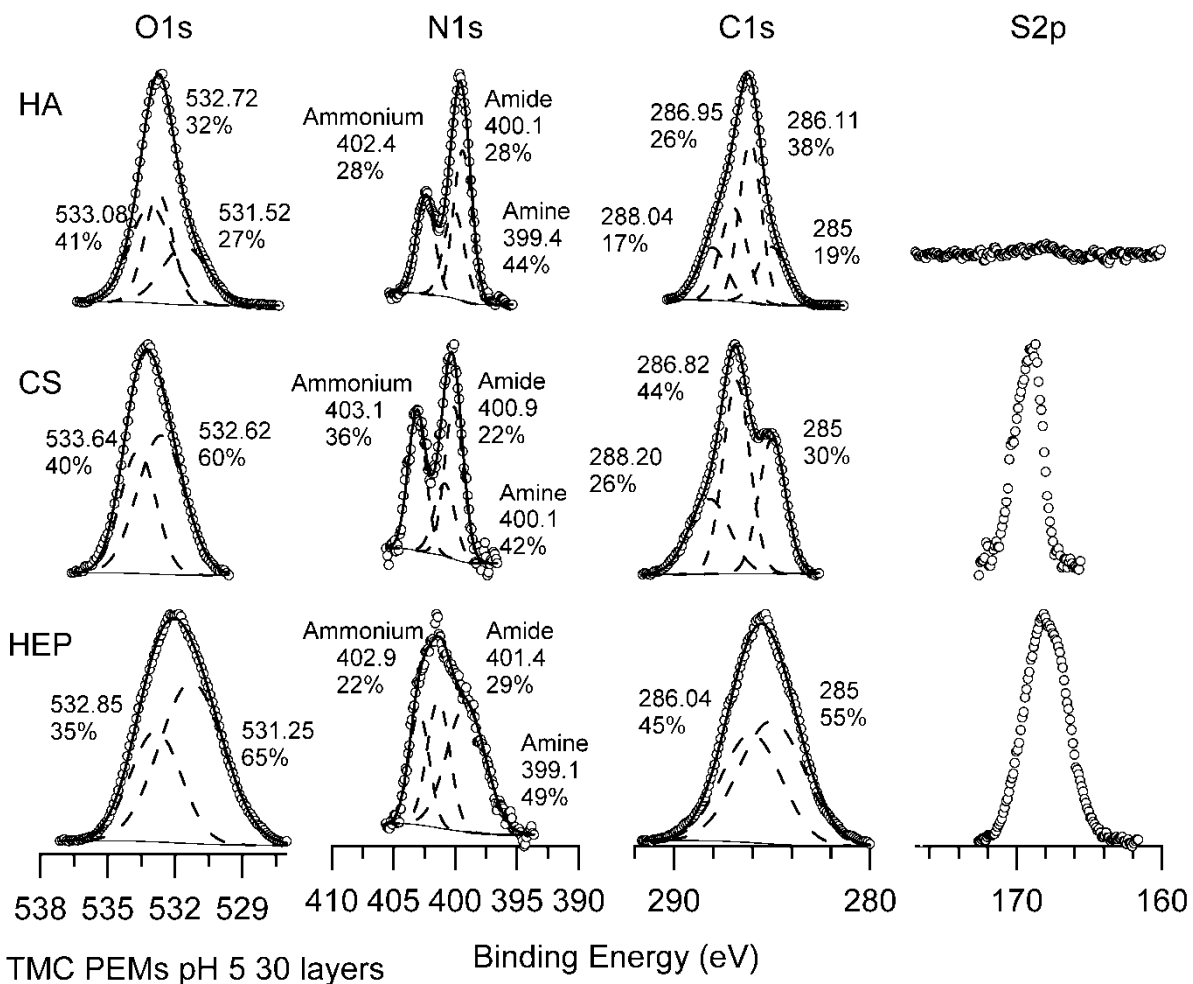
Figure A.1.3 High-resolution O1s, N1s, C1s, and S2p XPS spectra for the PEMs with TMC as the polycation.

Figure A.1.4 Hi-resolution O1s, N1s, C1s, and S2p XPS spectra for the PEMs with CHI as the polycation.

A.2 Supporting Information for Chapter 5. Polysaccharide-Based Polyelectrolyte Multilayer Surface Coatings can Enhance Mesenchymal Stem Cell (MSC) Response to Adsorbed Growth Factors

A.2.1 Polyelectrolyte multilayer (PEM) assembly on titanium

Construction of polyelectrolyte multilayers (PEM) was translated to titanium, which is a widely used metal for biomedical applications. Titanium foil was cut, using a water saw, into either 20 mm × 20 mm square chips or disks of 13 mm in diameter and polished using silicone carbide paper of increasing grit size (1000, 1200, 1500, 2000, 4000) using water to clean between each grit increment. The titanium chips were cleaned and acid-etched by exposing them for 30 minutes to piranha solution (70 % sulfuric acid, 30 % hydrogen peroxide) under sonication, followed by a ten-minute water sonication step and 10 minutes in a Tegal Plasmaline (Petaluma,Ca) air plasma chamber set at 50 W and 0.5 torr. **Caution**: **piranha solution reacts violently with many organic materials and should be handled with care.** Self assembled monolayer (SAM) of 11-phosphonoundecanoic acid (PUA) was deposited on the titanium substrate by adsorption from a 10 mM solution in DMSO. Other organic solvents were evaluated to dissolve PUA including: ethanol, methanol, and hexane. However, DMSO resulted in a solution with the least amount of un-dissolved PUA (confirmed visually). PUA was selected due to its ability to form SAM on oxides of titanium, as well as its structural similarity with 11-mercaptoundecanoic acid which is used on gold coated glass slides. Construction of PEMs and protein adsorption was performed by placing the titanium surfaces in the wells of multi-well plates, and following the protocol used for PEM construction on TCPS. Six-layer PEMs (PEM$_{Hep}$) were prepared with and without

adsorbed FGF-2, and were subsequently also modified with fibronectin. PM-IRRAS and XPS were used to characterize construction of PEMs on titanium.

The formation of the PUA-SAM on titanium is heavily dependent on how much the titanium is oxidized. When the titanium substrates were exposed for longer times to sonicated piranha solution stronger IR adsorption peaks were noted after assembly of PEM. Less polysaccharide is adsorbed on titanium substrates than gold as confirmed by PM-IRRAS. This could be due because a less dense PUA-SAM is formed when compared to the MUA-SAM on gold. However, a PUA-SAM is successfully deposited as confirmed by the phosphorus peak on XPS (Figure A.2.1).

MSC proliferation does not seem to be significantly reduced on titanium modified with the SAM-PUA on day 2 (Figure A.2.2) in the presence of FGF-2.
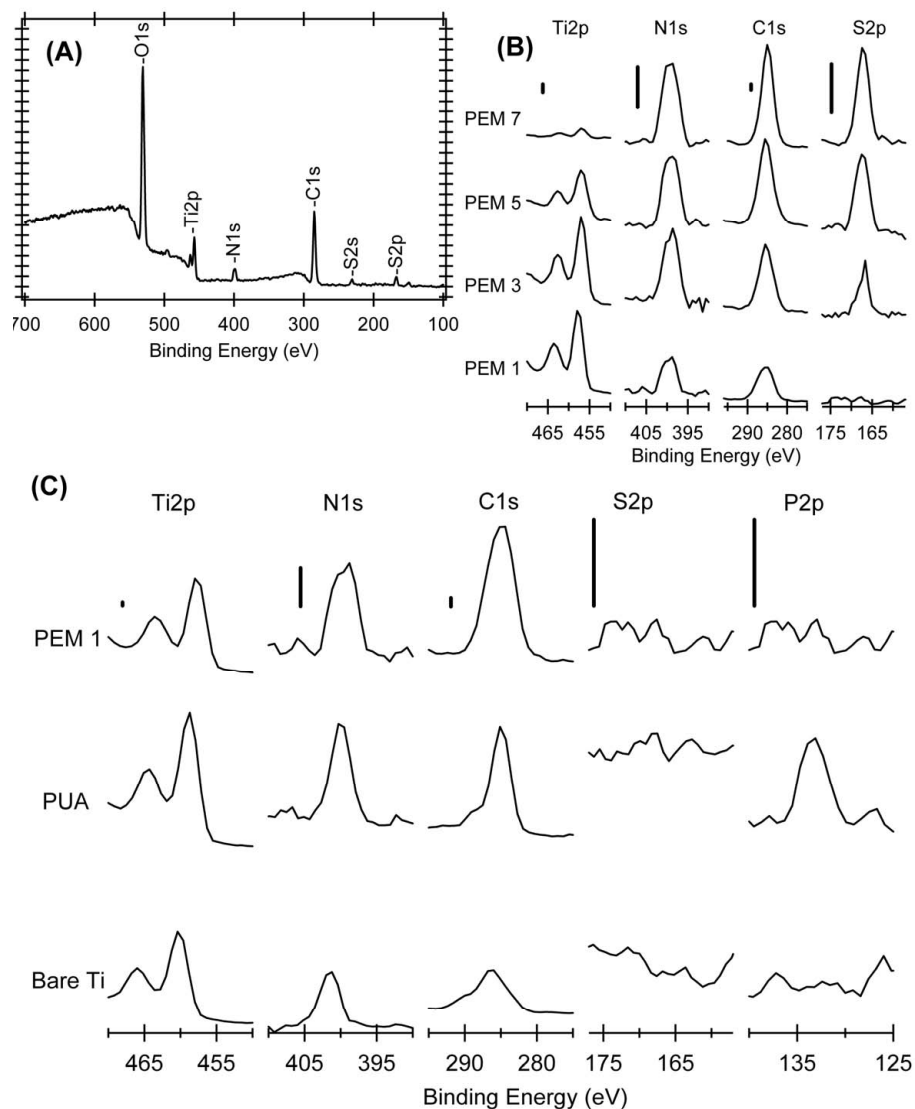
Figure A.2.1 XPS survey spectrum for a 5 layer chitosan terminated PEM constructed on titanium (A). Zoom in region of survey spectra of the titanium, nitrogen, carbon, and sulfur regions of odd number chitosan terminated PEM constructed on titanium (B). Zoom in region of survey spectra of the titanium, nitrogen, carbon, sulfur, and phosphorus regions of bare titanium, titanium modified with a SAM-PUA, and a one layer chitosan terminated PEM constructed on titanium (C). Increase of the sulfur, carbon, and nitrogen peak and attenuation of the titanium peak as more polysaccharide is adsorbed confirms construction of multilayer. Vertical tick marks for (A) correspond to 3000 c/s, all scale bars for (B) correspond to 2000 c/s, and all scale bars for (C) correspond to 1000 c/s.
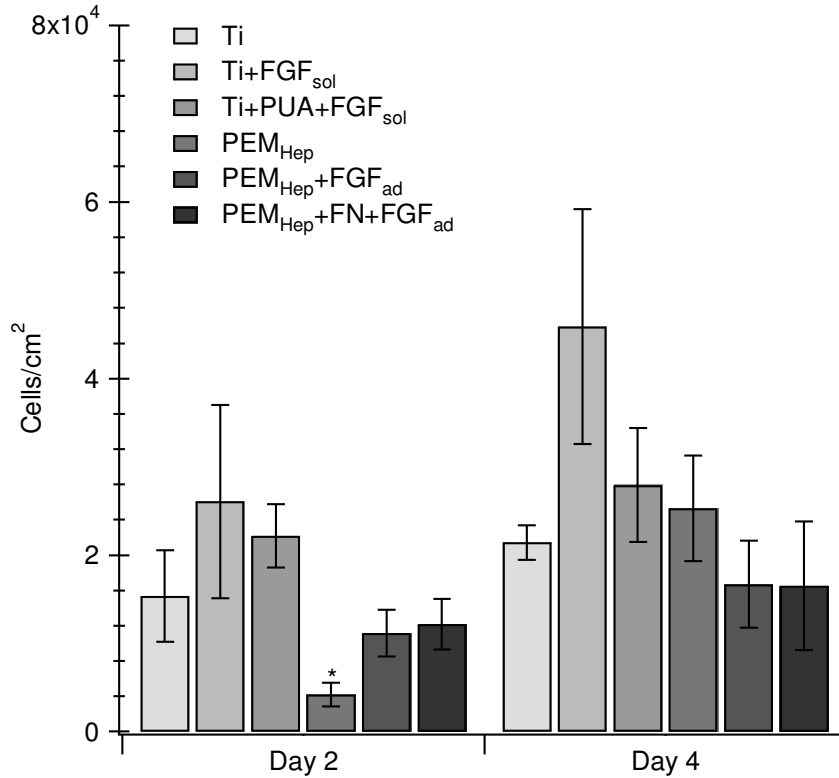
Figure A.2.2 MSC number on titanium coated with polysaccharide based PEM which are heparin terminated (A). Sol denotes FGF delivered in solution at 1 ng/mL. Ad denotes FGF adsorbed from an initial concentration of 50 ng/mL. * $p < 0.05$ when compared to bare titanium. Fluorescence microscopy images using DAPI (blue) and calcein (green) fluorescence markers for MSCs on PEM coated Ti at day 4 (B).

A.3 References

1. D. de Britto, O. B. G. Assis, Carbohydr. Polym. 2007, 69, 305.
2. R. J. Verheul, M. Amidi, M. J. van Steenbergen, E. van Riet, W. Jiskoot, W. E. Hennink, Biomaterials 2009, 30, 3129.
3. http://www.rit.edu/kgcoe/microsystems/lithography/research/fluids/Refractive_index _results.pdf
4. http://corninfo.ps.uci.edu/writings/Ref4txt.html

CURRICULUM VITAE

Jorge L. Almodóvar

Ph.D. Candidate, Dr. Matt Kipper's Lab
Department of Chemical and Biological Engineering
Colorado State University
Fort Collins, CO
Home: 4408 John F Kennedy Parkway, Apt. F305.
Fort Collins, CO 80525
Cel. 787-469-5450
Email: jorgealmodovar@gmail.com

EDUCATION

- **Ph.D. in Chemical Engineering,** August, 2011
Colorado State University, Department of Chemical and Biological Engineering
Thesis adviser: Dr. Matt Kipper
Dissertation title: *Polysaccharide-based nanostructures for growth factor delivery and mesenchymal stem cell activation*

- **B.S. in Chemical Engineering,** May 2007
Iowa State University
GPA: 3.46/4.00
Honors: Omega Chi Epsilon 2006-2007

- **University of Oviedo**, Spain, Summer 2007
Study abroad program: International Summer Course in Chemical Engineering

PROFESSIONAL EXPERIENCE

- **Graduate Research Assistant,** August 2007 – Present
Colorado State University, Department of Chemical and Biological Engineering

- **Research Intern,** May 2009 – August 2009
Empirical Labs (Fort Collins, CO)
Developed methods for the production and characterization of liposomes for the encapsulation of vitamin-C. Gained R&D experience in the nutraceutical field.

- **Undergraduate Research Assistant**, January 2006 – May 2007
Iowa State University, Department of Chemical and Biological Engineering
  - Teamed with graduate student in a research project involving differentiation of adult neural progenitor cells.
  - Involved in research project titled, *Cobalt Ferrite Nanocrystals: Out-Performing Magnetotactic Bacteria.*

RESEARCH SKILLS

Knowledgeable in sample preparation techniques for biomedical applications including: layer-by-layer assembly of polyelectrolyte multilayers on gold, titanium and polystyrene substrates, polyelectrolyte complex nanoparticles, and electrospun nanofibers. Worked extensively with the polysaccharides chitosan, *N,N,N*-trimethyl chitosan, heparin, hyaluronic acid and chondroitin sulfate. Synthesized *N,N,N*-trimethyl chitosan.

Trained in techniques and equipment including: Fourier transform infrared spectroscopy (Transmission FTIR, FT-SPR, PMIRRAS, ATR-FTIR), X-ray photoelectron spectroscopy, variable angle spectroscopic ellipsometry, scanning electron microscopy, quartz crystal microbalance, thermal evaporation deposition, gel-permeation chromatography, atomic force spectroscopy, confocal microscopy, freeze-drying, dynamic light scattering, water contact angle, and nuclear magnetic resonance spectroscopy.

Experienced in cell culture and biomolecular techniques including: sterile techniques, bone marrow cell harvest, cell expansion, cell counting, colorimetric assays, fluorescence imaging, ELISA, and gel electrophoresis. Worked with bone marrow-derived equine and ovine mesenchymal stem cells.

Fluent in both English and Spanish. Extensive knowledge of the Igor Pro spectral analysis software, Microsoft office, and MATLAB.

AWARDS AND SCHOLARSHIPS

Whitaker International Fellowship	April 2011 - present
Colorado State University Graduate Assistantship	August 2007 - present
Colorado Graduate Grant	August 2007 - present
Gates Millennium Scholar	August 2003 - May 2009
Bridge to the Doctorate Fellowship	August 2007 - May 2008
McNair Fellowship	August 2007 - May 2008
American Chemical Society Scholar	August 2003 - May 2007
Cargill Oviedo Scholar	May 2006 - July 2006
Boy Scouts of America, Eagle Scout	November 2001

MEMBERSHIP IN PROFESSIONAL SOCIETIES

American Association for the Advancement of Science	February 2009 - present
American Institute of Chemical Engineers	August 2008 - present
American Chemical Society	August 2003 - present
Biomedical Engineering Society	August 2010 - Present

SCIENTIFIC PUBLICATIONS (peer reviewed)

1. Bacon S., <u>Almodóvar J.,</u> Kisiday J.D., Kipper M.J.; "Osteogenic Ovine and Equine Mesenchymal Stem Cell Differentiation on Electrospun Chitosan Nanofibers with and without Dexamethasone", (In Preparation)

2. Volpato F.Z., <u>Almodóvar J.,</u> Erickson K., Popat K., Migliaresi C.; Kipper M.J., "Controlled release of bioactive FGF-2 from electrospun chitosan nanofibers using polysaccharide-based nanostructures", (In Preparation)

3. <u>Almodóvar J.,</u> Place L.W., Gogolski J., Erickson K., Kipper M.J.; "Layer-by-Layer Assembly of Polysaccharide-Based Multilayers: A Spectroscopic Study of Hydrophilicity, Composition, and Ion Pairing"; *Biomacromolecules*, (2011), In Press**.** DOI: 10.1021/bm200519y

4. <u>Almodóvar J.,</u> Kipper M.J.; "Coating electrospun chitosan nanofibers with polyelectrolyte multilayers using the polysaccharides heparin and *N,N,N*-trimethyl chitosan", *Macromolecular Biosciences*, 11 (2011) 72-76

5. Kisiday, J.D., Hale, B.W., Lee, C.M., <u>Almodóvar, J.,</u> Kipper, M.J., McIlwraith, C.W., Frisbie, D.D; "Expansion of mesenchymal stem cells on fibrinogen-rich protein surfaces derived from blood plasma", *Journal of Tissue Engineering and Regenerative Medicine*, (In press, 2010) DOI: 10.1002/term.352

6. <u>Almodóvar J.,</u> Bacon S., Gogolski J., Kisiday J.D., Kipper M.J.; "Polysaccharide-based polyelectrolyte multilayer surface coatings can enhance mesenchymal stem cell (MSC) response to adsorbed growth factors", *Biomacromolecules*, 11 (2010) 2629-2639

7. Boddohi S., <u>Almodóvar J.</u> Zhang H. Johnson P. Kipper M; "Layer-by-layer assembly of polysaccharide based nanostructured surfaces containing polyelectrolyte complex nanoparticles", *Colloids and Surfaces B:Biointerfaces*, 77 (2010) 60-68

CONFERENCE PROCEEDINGS

1. <u>Jorge Almodóvar</u>, Matt J. Kipper; "Tailoring Polysaccharide-Based Nanostructured Biomaterials for Guided Mesenchymal Stem Cell (MSC) Response", *Annual Biochemical Engineering Symposium* (Fort Collins, CO), May 2009

2. <u>Jorge Almodóvar</u>, Laura Dempsy, Matt J. Kipper; "FT-IR Studies on Stability of Proteins Adsorbed to Polysaccharide-Based Polyelectrolyte Multilayers", *Annual Biochemical Engineering Symposium* (Ames, IA), April 2008

BOOK CHAPTER

1. Kipper M., <u>Almodóvar J.</u> "Engineering Soft Nanostructures for Guided Cell Response" in *Nanotechnology in Tissue Engineering and Regenerative Medicine,* Ed. Popat K., Boca Raton, FL: CRC, 2011. Print.

PRESENTATIONS AT NATIONAL AND REGIONAL MEETINGS (*denotes speaker)

1. Almodóvar J.*, Bacon S., Gogolski J., Kisiday J.D., Kipper M.J.; "Polysaccharide-based polyelectrolyte multilayer surface coatings can enhance mesenchymal stem cell (MSC) response to adsorbed growth factors." Paper presented at the American Institute of Chemical Engineers annual meeting in Salt Lake City, UT. April 2010.

2. Almodóvar J.*, Bacon S., Gogolski J., Kisiday J.D., Kipper M.J.; "Polysaccharide-based polyelectrolyte multilayer surface coatings can enhance mesenchymal stem cell (MSC) response to adsorbed growth factors." Poster presented at the Biomedical Engineering Society annual meeting in Austin, TX. October 2010.

3. Volpato F.Z., Almodóvar J.*, Kipper M.J., Migliaresi C.; "Functionalization of Chitosan Electrospun Networks by Polyelectrolyte Multilayer and Nanoparticle Adsorption." Paper presented at the Materials Research Society Functionalized Nanobiomaterials for Medical Applications meeting in Denver, CO. October 2010.

4. Almodóvar J.*, Bacon S., Gogolski J., Kisiday J.D., Kipper M.J.; "Polysaccharide-based polyelectrolyte multilayer surface coatings can enhance mesenchymal stem cell (MSC) response to adsorbed growth factors." Poster presented at the Nanotechnology Symposium in Fort Collins, CO. April 2010.

5. Gogolski J.*, Almodóvar J., Kipper M.J.; "Surface modification of titanium using polysaccharide based polyelectrolyte multilayer." Paper presented at the American Institute of Chemical Engineers Regional Meeting, Rocky Mountain Region in Albuquerque, NM. April 2010.

6. Almodóvar J.*, Kipper M.J.; Tailoring Polysaccharide-Based Nanostructured Biomaterials for Guided Mesenchymal Stem Cell (MSC) Response. Paper presented at the American Institute of Chemical Engineers Annual meeting in Nashville, TN. November 2009.

7. Boddohi S. *, Almodóvar J., Johnson P.A., and Kipper M.J., "Nanostructured Polysaccharide Based Surface Coatings: Tailored Morphology and Chemistry." Paper presented at the American Institute of Chemical Engineers Annual meeting in Nashville, TN. November 2009.

8. Almodóvar J.*, Kipper M.J.; "Tailoring Polysaccharide-Based Nanostructured Biomaterials for Guided Mesenchymal Stem Cell (MSC) Response." Poster presented at the Annual Biochemical Engineering Symposium in Pringree Park, CO. May 2009.

9. Almodóvar J.*, Kipper M.J.; "FT-IR Studies on Stability of Proteins Adsorbed to Polysaccharide-Based Polyelectrolyte Multilayers." Paper presented at the American Institute of Chemical Engineers Annual meeting in Philadelphia, PA. November 2008.

10. Almodóvar J.*, Gogolski J., Kipper M.J.; "Nanostructured polysaccharide-based surface for MSC differentiation." Poster presented at the American Institute of Chemical Engineers Annual meeting in Philadelphia, PA. November 2008.

11. Almodóvar J.*, Kipper M.J.; "FT-IR Studies on Stability of Proteins Adsorbed to Polysaccharide-Based Polyelectrolyte Multilayers." Paper presented at the Annual Biochemical Engineering Symposium in Ames, IA. April 2008.

SERVICE

- Involved in the formation of the Colorado State University chapter of the Biomedical Engineering Society in the 2010-2011 academic year. Held graduate student adviser position.
- Served as advisor for an undergraduate honor's thesis student at Colorado State University.
- Teaching Assistant:
  - **Chemical and Biological Engineering II (CBE102),** Department of Chemical and Biological Engineering, Colorado State University, Spring 2008, Spring 2009, Spring 2010, Spring 2011
  - **Computational Methods in Chemical Engineering (ChE310),** Department of Chemical and Biological Engineering, Iowa State University, Fall 2006
- Reviewer:
  - Book proposal for Wiley Books publishing house
  - Journals: Journal of Tissue Engineering and Regenerative Medicine; International Polymer

PROFESSIONAL REFERENCES

- Dr. Matt J. Kipper (Ph.D. Advisor)
  Assistant Professor
  Colorado State University
  Department of Chemical and Biological Engineering &
  School of Biomedical Engineering
  1370 Campus Delivery
  100 Glover Building, Fort Collins, CO 80523-1370
  Fort Collins, CO 80523-1370
  Tel. (970) 491-0870
  Fax. (970) 491-7369
  matthew.kipper@colostate.edu

- Dr. John D. Kisiday (Collaborator at CSU)
  Assistant Professor
  Colorado State University
  Department of Clinical Sciences &
  School of Biomedical Engineering
  161678 Campus Delivery
  Fort Collins, CO 80523-1678
  Tel. (970) 297-5071
  john.kisiday@colostate.edu

- Dr. Travis Bailey (Collaborator at CSU)
  Assistant Professor
  Colorado State University
  Department of Chemical and Biological Engineering &
  Department of Chemistry
  1370 Campus Delivery
  100 Glover Building, Fort Collins, CO 80523-1370
  Tel. (970) 491-4648
  Fax. (970) 491-7369
  travis.bailey@colostate.edu

- Dr. Surya Mallapragada (Undergraduate Research Advisor)
  Department Chair and Stanley Chair in Interdisciplinary Engineering
  Iowa State University
  Department of Chemical and Biological Engineering
  2114 Sweeney Hall
  Ames, IA 50011-2230
  Tel. (515)294-7407
  Fax. (515)294-2689
  suryakm@iastate.edu